Quantum statistical approach to optical properties in dense plasmas
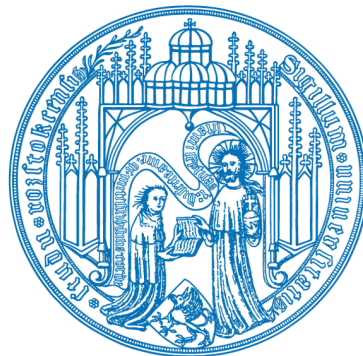
vorgelegt von Chengliang Lin
Oktober 2017

CONTENTS

1. INTRODUCTION

A commonly used physical term is *isolated system*, which means that there are no energy and matter exchange between the investigated system and its surrounding environment. The isolated system is an idealized concept and a rough approximation that works only for macroscopic objects in classical mechanics. In reality, the quantum system under study can not be isolated from its surrounding environment. The trivial surrounding environment is the vacuum where the creation and annihilation of virtual particles are allowed according to Heisenberg's uncertainty principle. In other non-trivial surroundings, e.g. plasmas, the physical problem, that we tackle for a real quantum system, is a many-body problem, where a statistical description is always indispensable. Moreover, a quantitative change of a system can lead to a qualitative change of the system, since new physical phenomena can arise from the correlations of many particles [Wen86], such as collective excitations [HM86, Zim87], screening effects [KKER86, KSKB05], localization [JZK+03], modifications of the spectral lines [Gri97], and Rydberg blockades [LFC+01].

Among all many-body systems in nature, plasma plays a fundamental role. Matter in plasma states covers a wide range of physical regimes, as shown in the temperature-density plane for plasmas (see Fig. 1.1). More than 90% of visible matter in the universe is in the plasma state [KSKB05]. A plasma is an ionized neutral gas consisting of a large number of charged particles, i.e. electrons ans ions, as well as the force carrier for the electromagnetic interaction between the charged particles, i.e. photons. Generally, the plasma is characterized by density, temperature, and its chemical composition. To describe the geometrical or the dynamical properties of the plasma system, some useful parameters can be introduced to quantify the plasma system. The following parameters are introduced to characterize the dynamical properties of a plasma: the Landau length l_L, the thermal de Broglie wavelength λ_th, and the Debye screening length λ_D [KKER86, Red13],

$$l_\mathrm{L}^c = \frac{z_c^2\, e^2}{4\pi\varepsilon_0 k_\mathrm{B}\, T}, \quad \lambda_\mathrm{th}^c = \sqrt{\frac{2\pi\hbar^2}{m_c k_\mathrm{B}\, T}}, \quad \lambda_\mathrm{D}^{-1} = \sqrt{\sum_c \frac{z_c^2 e^2\, n_c}{\varepsilon_0 k_\mathrm{B}\, T}}, \tag{1.1}$$

where the index c denotes the particle species with the corresponding mass m_c, charge number z_c and density n_c. Further plasma parameters are the average distance a_c between particles of species c (also known as Wigner-Seitz radius) and the Thomas-Fermi radius R_TF [Sal98]:

$$a_c = \left(\frac{3}{4\pi\, n_c}\right)^{1/3}, \quad R_\mathrm{TF}^c = \frac{1}{2}\left(\frac{3\pi}{4}\right)^{2/3} \frac{a_\mathrm{B}}{z_c^{1/3}} \tag{1.2}$$

with the Bohr radius $a_\mathrm{B} = 4\pi\varepsilon_0\hbar^2/(m_\mathrm{e}\, e^2)$.

From these parameters, the plasma coupling parameter Γ_c and the degeneracy parameter θ_c can be defined. Due to the long-range nature of the Coulomb interaction, the plasma particles interact simultaneously with each other. In other words, the motion of particles in plasma is correlated with the motion of nearby particles. The strength of this correlation can

be represented via a dimensionless parameter Γ_c, which is taken as the ratio of the average potential energy and the thermodynamic kinetic energy

$$\Gamma_c = \frac{l_{\mathrm{L}}^c}{a_c} = \frac{z_c^2\, e^2}{4\pi\varepsilon_0 a_c k_{\mathrm{B}}\, T} \sim T^{-1} \cdot n_{\mathrm{e}}^{1/3}. \tag{1.3}$$

For the last relation, the charge neutrality condition $\sum_c z_c n_c = n_{\mathrm{e}}$ is used. According to the point of view of scattering theory, the plasma coupling parameter can also be interpreted as follows: with respect to the Coulomb collisions, the Landau length l_{L} describes the critical collision, in which the particle is deflected by $90°$ [DKMS05]. If the distance of two charged particles a_c is larger than the Landau length l_{L}, the deflection angle after the collision must be smaller than $90°$. In this case, the investigated particle is less affected by the neighboring particles and the plasma can be regarded as weakly coupled ($\Gamma_c < 1$). In the opposite case, a strongly coupled plasma system is established ($\Gamma_c > 1$).
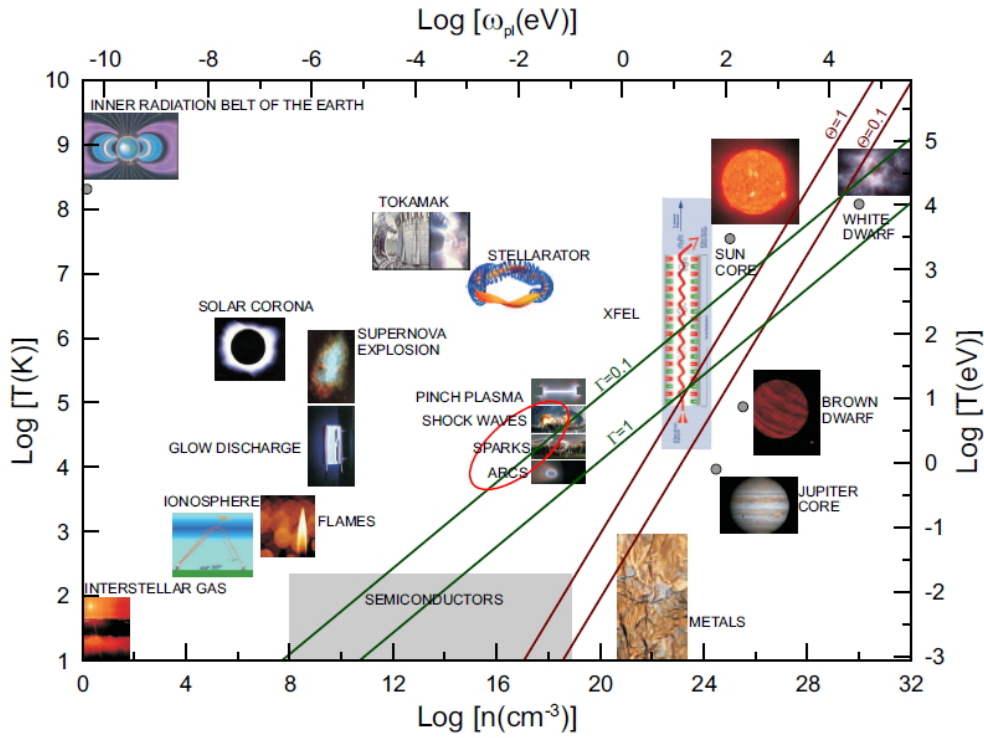
Abb. 1.1: The density-temperature plane of plasmas (taken from [Oma07]).

The degeneracy parameter θ_c is defined via the ratio of the thermodynamic kinetic energy $k_{\mathrm{B}}T$ and the Fermi energy $E_{\mathrm{F}}^c = \hbar^2\,(3\pi^2 n_c)^{2/3}/(2m_c)$. Due to their large masses, ions can generally be treated classically, which means the ionic subsystem is weakly degenerate. Therefore, one is always interested in the degeneracy for the electron subsystem, i.e. θ_{e}, which reads as

$$\theta_{\mathrm{e}} = \frac{k_{\mathrm{B}}T}{E_{\mathrm{F}}^e} \sim T \cdot n_{\mathrm{e}}^{-2/3}. \tag{1.4}$$

Approaching the low temperature limit, the quantification for plasmas discussed above is complicated by degeneracy effects and strong coupling effects (ion lattice effects). Due to

their different thermal wavelengths compared to the average interparticle distance, the degeneracy and coupling strength for electrons and ions should be treated independently [GGL06, GRH$^+$07]. To account for these effects in the low temperature limit, more appropriate concepts of effective temperatures in plasmas can be introduced. For free electrons in plasmas, the effective temperature can be introduced as [GGL06, GRH$^+$07]

$$T_{\mathrm{e}}^{\mathrm{eff}} = \left(T_{\mathrm{q}}^2 + T_{\mathrm{e}}^2\right)^{1/2} \tag{1.5}$$

with temperature $T_{\mathrm{q}} = T_{\mathrm{F}}/(1.3251 - 0.1779\sqrt{r_s})$ related to the Fermi temperature $T_{\mathrm{F}} = E_{\mathrm{F}}^e/k_{\mathrm{B}}$ and the Brünckner parameter $r_s = a_{\mathrm{e}}/a_0$ with the Bohr radius a_0. Then the effective degeneracy parameter for electron system can be written as

$$\theta_{\mathrm{e}}^{\mathrm{eff}} = \frac{k_{\mathrm{B}}\,T_{\mathrm{e}}^{\mathrm{eff}}}{E_{\mathrm{F}}^e}. \tag{1.6}$$

Similarly, as the ion temperature is decreased, the ionic system becomes more strongly coupled and trends to crystallize. The ions can still oscillate around their lattice sites and the collective excitation modes, i.e. phonons, are generated. In this case, the following effective temperature for ions can be defined [GGL06]

$$T_{\mathrm{i}}^{\mathrm{eff}} = \left(\gamma_0\,T_{\mathrm{D}}^2 + T_{\mathrm{i}}^2\right)^{1/2} \tag{1.7}$$

with $\gamma_0 = 3/(2\pi^2)$. The Debye temperature T_{D} accounts for the ion lattice effects and screening of ions by free electrons and is expressed as

$$T_{\mathrm{D}} = \frac{\hbar}{k_{\mathrm{B}}} \cdot \frac{\omega_{\mathrm{pi}}}{1 + \kappa_{\mathrm{e}}^2/k^2} \tag{1.8}$$

with the ion plasma frequency $\omega_{\mathrm{pi}} = \sqrt{z_i^2 n_i\,e^2/\left(\varepsilon_0 m_{\mathrm{i}}\right)}$ and $k = (2/z_i)^{1/3}\left(3\pi^2 n_e\right)^{1/3}$. The inverse screening length for electrons can be represented as

$$\kappa_{\mathrm{e}} = \frac{n_e\,e^2}{\varepsilon_0 k_{\mathrm{B}} T_{\mathrm{e}}^{\mathrm{eff}}}. \tag{1.9}$$

This expression interpolates the inverse Debye screening length and the inverse Thomas-Fermi length for electron systems. Consequently, the effective ion coupling parameter can be rewritten as

$$\Gamma_{\mathrm{i}}^{\mathrm{eff}} = \frac{z_i^2 e^2}{4\pi\varepsilon_0\,k_{\mathrm{B}} T_{\mathrm{i}}^{\mathrm{eff}}\,a_{\mathrm{i}}}. \tag{1.10}$$

To determine these parameters and therefore to reveal the physical essence of the many-body systems (plasmas), information of density, temperature, and their spatial distributions are necessary. Therefore, special diagnostic techniques are needed to infer these conditions in a plasma. One of the most important diagnostic techniques is the optical spectroscopy, more explicitly speaking, the emission spectrum, because it carries a wealth of information about the local instantaneous plasma density and temperature conditions surrounding the emitter [Sal98, Fuj05, KSKB05]. In particular, for short lifetime plasmas generated by nanosecond or femtosecond laser pulses or particle beams, the emission spectral lines may be the only reliable method for studying the dynamical properties of these plasmas [Sal98].

The intensity, shift, and broadening of the emitted spectra carry a wealth of information to describe the many particle plasma system. When talking about spectral lines, one distinguishes the continuous spectrum (i.e. the bremsstrahlung and inverse bremsstrahlung) and spectra emitted from discrete bound levels (for instance, bound-bound transition and photo-ionization).
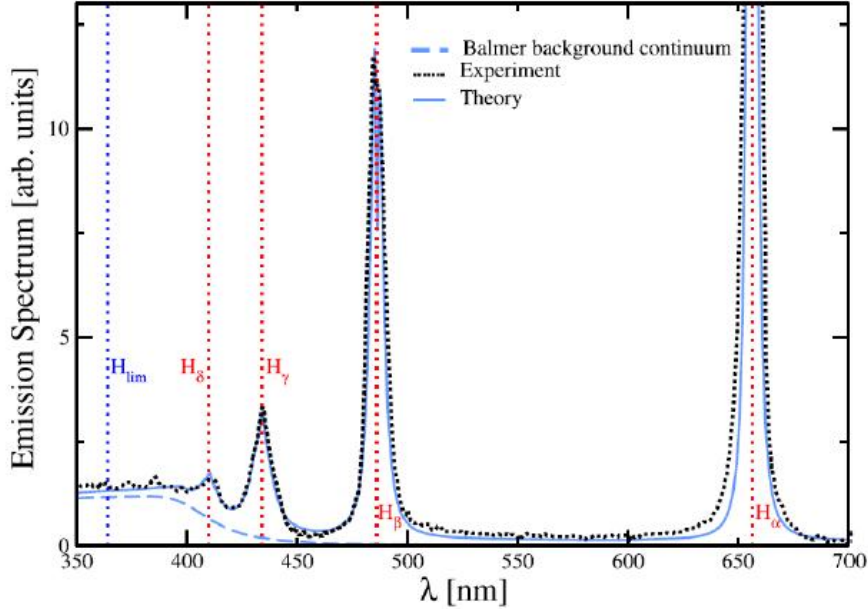
Abb. 1.2: Emission spectra in a hydrogen plasma at $T_e = 16000\,\mathrm{K}$ and $n_e = 1.9 \cdot 10^{17}\,\mathrm{cm}^{-3}$ [OWR11]. The continuum background, the emission from the low-lying levels and from the Rydberg states near the continuum edge are shown, where no discontinuity between the bound and free states is observed.

As shown in Fig. 1.2 for a hydrogen plasma, the total emission spectrum can be divided into three regimes with respect to the wavelength λ: bound-bound transitions in the range of $420 - 700$ nm, free-free transitions in the range of $350 - 380$ nm, and the bound-free related regime in the range of $380 - 420$ nm. Two important features can be clearly seen from this figure: 1) there is no abrupt jump in the bound-free transition regime (in the range of $380 - 420$ nm); 2) the position of the continuum edge is shifted in contrast to the isolated case H_{lim}.

Among all the emission mechanisms, transitions from Rydberg states (including bound-free and bound-bound transitions), which are energetically near to the continuum of scattering states, are of particular interest. The correct treatment of the Rydberg states which are near the continuum edge is a longstanding problem in plasma spectroscopy [EKKR85, GR06, GR07, LGRR16]. In contrast to the low-lying bound states, the Rydberg states are more sensitive to the influence of the surrounding plasmas. As we know, the screening of a given ion by the free electrons and neighboring ions in a plasma results in the reduction of the ionization potential and line broadening of eigenenergy levels of the given atom. Consequently, the bound states should be truncated up to some main quantum number. This phenomenon is well known in calculating the partition function, for example as in the description of Planck-Larkin partition function [KKER86, KSKB05]. One should note that,

from the experimental measurements of spectral lines, no discontinuity for bound-bound and bound-free transitions is observed, see Fig. 1.2. This fact is extensively discussed by different authors [WKP72, HZ82, RGS86, NMG$^+$98, D'y98, OWR11, D'y16]. For the Rydberg states near the continuum edge, it may be quite difficult to rigorously distinguish the borderline between the real continuum edge and bound states. On one hand, the real continuum edge is lowered because of the screening of the plasma particles. Consequently, some bound levels are dissolved or, equivalently, are shifted into continuous states. This phenomenon is termed in the literature as pressure ionization, or continuum lowering, or ionization potential depression (IPD) [KKER86, Sal98, Gri97, Fuj05, KSKB05]. On the other hand, the bound states are broadened due to the fluctuating micro-field experienced by the bound electrons. If the broadening (or width) of the bound states is larger than half of the energy difference to the adjacent levels, a quasi-continuum state could be established. This effect is knows as Inglis-Teller (IT) effect [IT39]. To distinguish and better understand the IPD and IT effect, a more accurate theory is necessary.

In addition to plasma physics, Rydberg states play an important role in other research fields of physics, such as in quantum information [LBMW03, ASSR13, And15], in understanding the basic concepts of quantum mechanics [LFC$^+$01, Sch07, GAH$^+$16], in astrophysics [GMI$^+$09], in semiconductor physics [KFS$^+$14, GAH$^+$16], and so on [Gal94]. Because of their macroscopic characters and long lifetimes, the Rydberg atoms may be regarded as an outstanding example demonstrating both macroscopic classical and microscopic quantum behavior. The appearance of the classicality in a quantum system due to localization, i.e., the loss of quantum information of a quantum system, can be described by decoherence resulting from the interaction of an open quantum system with its surroundings [JZK$^+$03].

In the context of new experimental facilities exploring confined neutral atoms, warm dense matter (WDM), and materials in the high-energy density regime with the newly developed laser techniques, a detailed theoretical investigation of thermodynamic, transport, and optical properties of strongly coupled and nearly degenerate Coulomb systems becomes of emerging interest. For example, the emission spectra for carbon plasmas were measured [NMG$^+$98], where the influence of the IPD and IT effect was discussed. Traditional expressions for the IPD given by Ecker and Kröll (EK) [EK63] or Stewart and Pyatt (SP) [SPJ66] are commonly applied in different simulation codes for understanding the experimental results. More recently, using intense short-pulse laser irradiation to produce highly excited plasmas at condensed matter densities, different measurements related to the IPD were performed [Ve12, CVC$^+$12, HAJ$^+$13a, FKP$^+$14, Ct16, KCK$^+$16], for example, measurements on the ionization energy of the K-shell in aluminum and the subsequent K$_\alpha$ lines by Ciricosta *et al.* [Ve12, CVC$^+$12, Ct16], Ly- and He-lines for ions Al^{11+} and Al^{12+} by Hoarty *et al.* [HAJ$^+$13a], and the Thomson scattering spectrum for CH mixtures [FKP$^+$14, KCK$^+$16].

Various approaches can be used to calculate the spectral line profiles in a plasma environment, for instance, unified theory or quantum mechanical scattering theory. Using the thermodynamic Green's function technique, a systematic quantum statistical approach has been developed [RSK81, HRSZ86, Gün95]. This approach has been successfully applied to calculate the line profiles of hydrogen, H-like ions, and helium in plasma environments [Gün95, Oma07, Lor14]. Generally, the electrons are considered in the impact approximation, while the ions are treated quasi-statically by the microfield distribution [Gün95, Dem10, SM10]. In this investigation, we introduce the ionic structure factor to account for ionic correlations.

Motivated by these exciting perspectives, we study the optical properties of a radiating particle surrounded by a warm dense plasma environments. Obviously, the accurate atomic

structures of this radiating particle are evidently modified by the surrounding plasma due to their interactions. We concentrate on the following questions in the present investigation:

- What is the most suitable description for Rydberg states in a plasma?

- How can we describe the spectral lines within the theory of open quantum systems?

- What is the reasonable quantum statistical description for the shift of the continuum edge and for the ionization potential depression in plasmas?

- What are the differences and the connections between the ionization potential depression and the Inglis-Teller effect?

In attempt to answer these questions, this thesis is organized as following. In chapter 2, general descriptions of the Green's function technique and open quantum system are reviewed. The Green's function technique is a powerful tool for both equilibrium and non-equilibrium many-body system. The modifications of the accurate atomic properties by the plasma surroundings are described via the self-energy. In particular, the fundamental theory about the single- and two-particle GF under the so-called cluster decomposition is presented. In contrast to GF theory, where the time evolution is described by the operators, we take into account the time-dependence through the density operator (or statistical operator). The equation of motion for the relevant density operator is derived in Born-Markov approximation.

Chapter 3 presents the study of a test particle interacting through collisions with a low-density plasma background by using the quantum master equation approach. The influence of the plasma on the dynamics of the atom is determined by the dynamical structure factor of the surrounding plasma. To describe transition rates of the Rydberg states, a Gaussian wave packet description is introduced. The optimized Gaussian wave packet which is most stable under collisions with plasma particle is denoted as robust state which is characterized by a special width in the Gaussian distribution. Additionally, the application of the quantum master equation approach to calculate the profiles of spectral lines is also presented.

In chapter 4, we return to the Green's function theory, with which the ionization potential depression in plasmas is investigated. We take into account the ionic correlation effects by introducing the dynamical structure factor within the framework of the quantum statistical theory. A general expression for the IPD is obtained. Different experimental measurements, for instance, via the K-shell ionization energy, via the dissolution of spectral lines, and via the Thomson scattering, are analyzed. The calculated IPD values under different experimental conditions are illustrated and discussed.

Subsequently, spectral properties of the Green's function approach to spectral line shapes of non-ideal plasmas are described in chapter 5. Finally, conclusions and future prospects are given in chapter 6.

2. THEORIES FOR OPTICAL PROPERTIES IN PLASMAS

In this chapter, we will discuss two theoretical approaches to investigate the properties, in particular the optical properties, within plasmas. The first approach is the Green's function (GF) technique, which is an effective theory in the language of the quasi-particle concept. The influence of the surroundings on the investigated system is accounted for by the self-energy. The other approach, the quantum master equation (QME) approach, is based on the theory of open quantum systems, where a reduced density operator, acting only on the Hilbert space of the system under study, is introduced by taking the average over the degrees of freedom of the surrounding environment. The optical transitions in the electrodynamic field are determined by the solution of the QME.

2.1 Quantum description for a quantum system

2.1.1 Operators, states, and their evolution equations

The fundamental elements to describe a quantum system in quantum mechanics are the state vectors $|\Psi(t)\rangle$ and the operators $\hat{O}(t)$ that act on the quantum states. The time evolution of the quantum system can be described in different pictures, i.e., the Schrödinger picture (indicated by an index S), the Heisenberg picture (denoted by an index H) or the interaction picture which is also known as the Dirac picture (signified by an index D). More details about those fundamental concepts can be found in textbooks, for example, see Refs. [Sch68, Nol17].

In the Schrödinger picture, the equation of motion of the quantum system is described by the time evolution of the state vectors $|\Psi_{\mathrm{S}}(t)\rangle$ while the operator $\hat{O}_{\mathrm{S}}(t) \equiv \hat{O}_{\mathrm{S}}(t_0) := \hat{O}_{\mathrm{S}}$ are constant with respect to time t. The state vectors $|\Psi_{\mathrm{S}}(t)\rangle$ evolve in time according to the Schrödinger equation (SE),

$$i\hbar\frac{\partial}{\partial t}|\Psi_{\mathrm{S}}(t)\rangle = \hat{H}_{\mathrm{S}}|\Psi_{\mathrm{S}}(t)\rangle, \tag{2.1}$$

with the Hamiltonian $\hat{H}_{\mathrm{S}}$. Introducing the time evolution operator $\hat{U}(t, t_0)$, the transform of a state $|\Psi_{\mathrm{S}}(t_0)\rangle$ at the initial time t_0 to another state $|\Psi_{\mathrm{S}}(t)\rangle$ at the time t can be written as

$$|\Psi_{\mathrm{S}}(t)\rangle = \hat{U}(t, t_0)|\Psi_{\mathrm{S}}(t_0)\rangle. \tag{2.2}$$

In general, the time evolution operator $\hat{U}(t, t_0)$ is an unitary operator which fulfills the relation $\hat{U}^{\dagger}(t, t_0)\hat{U}(t, t_0) = \hat{U}(t, t_0)\hat{U}^{\dagger}(t, t_0) = \hat{\mathcal{I}}$ with the identity operator $\hat{\mathcal{I}}$. Here the superscript "$\dagger$" denotes the Hermitian conjugate of an operator. Inserting the expression (2.2) into the SE (2.1), we find the time evolution operator obeys the following equation

$$i\hbar\frac{\partial}{\partial t}\hat{U}(t, t_0) = \hat{H}_{\mathrm{S}}\,\hat{U}(t, t_0) \tag{2.3}$$

with the initial condition

$$\hat{U}(t_0, t_0) = \hat{\mathcal{I}}. \tag{2.4}$$

Note that in the Schrödinger picture, an operator, for instance, the Hamiltonian $\hat{H}_\mathrm{S}$, can also have an explicate dependence on the time t, if there exists an external driving, for example, by a laser field. More generally, if the Hamiltonians at different times do not commute, then the time evolution operator can be expressed as a time-ordered exponential

$$\hat{U}(t, t_0) = \mathrm{T} \exp\left(-\frac{i}{\hbar} \int_{t_0}^{t} \hat{H}_\mathrm{S}(\tau)\, d\tau\right), \tag{2.5}$$

where T is the chronological time-ordering operator which arranges the products of time-dependent operators such that the operators will be ordered from left to right in descending order of time t.

   Another useful physical quantity in quantum mechanics is the statistical operator or the density operator. It is given in the Schrödinger picture as

$$\hat{\rho}_\mathrm{S}(t) = |\Psi_\mathrm{S}(t)\rangle\langle\Psi_\mathrm{S}(t)| = \sum_{m,n} a_m(t) a_n^*(t) \cdot |\psi_{\mathrm{S},m}\rangle\langle\psi_{\mathrm{S},n}| = \hat{U}(t, t_0)\, \hat{\rho}_\mathrm{S}(t_0)\, \hat{U}^\dagger(t, t_0), \tag{2.6}$$

where we have use the possibility to express the state $|\Psi_\mathrm{S}(t)\rangle$ as a superposition of basis states $|\psi_{\mathrm{S},m}\rangle$ with the corresponding coefficient $a_m(t)$. Differentiating the Eq. (2.6) with respect to time with the help of the SE, we obtain the equation of motion for the density matrix

$$i\hbar\frac{\partial}{\partial t}\hat{\rho}_\mathrm{S}(t) = \left[\hat{H}_\mathrm{S}(t), \hat{\rho}_\mathrm{S}(t)\right]_-, \tag{2.7}$$

which is commonly referred to as the von Neumann or Liouville-von Neumann equation. Here $\left[\hat{A}, \hat{B}\right]_- := \hat{A}\hat{B} - \hat{B}\hat{A}$ denotes the commutator of two operators. It can be seen that once the state vector $|\Psi_\mathrm{S}(t)\rangle$ is determined by solving the SE, the density operator $\hat{\rho}_\mathrm{S}(t)$ is also totally determined.

   In contast to the Schrödinger picture, in the Heisenberg picture the time evolution of the system is incorporated in the operator $\hat{O}_\mathrm{H}(t)$, while the state vector is time-independent, i.e., $|\Psi_\mathrm{H}(t)\rangle \equiv |\Psi_\mathrm{H}(t_0)\rangle$ for arbitrary time t. Consequently, the statistical operator in the Heisenberg picture $\hat{\rho}_\mathrm{H}(t) = \hat{\rho}_\mathrm{H}(t_0)$ is also a constant of time. Assuming that at the initial time t_0 the quantum states in both picture coincide, i.e., $\hat{\Psi}_\mathrm{H}(t_0) = \hat{\Psi}_\mathrm{S}(t_0)$, $\hat{\rho}_\mathrm{H}(t_0) = \hat{\rho}_\mathrm{S}(t_0)$, and $\hat{O}_\mathrm{H}(t_0) = \hat{O}_\mathrm{S}(t_0)$, then the operators in the Heisenberg picture are related to those in the Schrödinger picture through the canonical transformation

$$\hat{O}_\mathrm{H}(t) = \hat{U}^\dagger(t, t_0)\, \hat{O}_\mathrm{S}(t)\, \hat{U}(t, t_0). \tag{2.8}$$

The equation of motion for operators in the Heisenberg picture is described by

$$\frac{d}{dt}\hat{O}_\mathrm{H}(t) = \frac{i}{\hbar}\left[\hat{H}_\mathrm{H}(t), \hat{O}_\mathrm{H}(t)\right]_- + \frac{\partial}{\partial t}\hat{O}_\mathrm{H}(t), \tag{2.9}$$

In this equation, d/dt denotes the total time derivative, while $\partial/\partial t$ is the partial derivative with respect to the explicit time dependence of the operators in the Schrödinger picture. In the case that the operator in the Schrödinger picture does not explicitly depend on time, the Eq. (2.9) reduces to the form

$$\frac{d}{dt}\hat{O}_\mathrm{H}(t) = \frac{i}{\hbar}\left[\hat{H}_\mathrm{H}(t), \hat{O}_\mathrm{H}(t)\right]_-. \tag{2.10}$$

representation / time evolution	Schrödinger picture	Heisenberg picture	Dirac picture
state vectors $|\Psi(t)\rangle$	time-dependent	constant	time-dependent
operators $\hat{O}(t)$	constant	time-dependent	time-dependent
density matrix $\hat{\rho}(t)$	time-dependent	constant	time-dependent

Tab. 2.1: Time-dependence in different formulations of quantum mechanics for a quantum system.

The interaction picture is an intermediate representation between the Schrödinger picture and the Heisenberg pictures. In other words, the Schrödinger and the Heisenberg picture are the limiting cases of the interaction picture. To transform into the interaction representation, we separate the Hamiltonian $\hat{H}_{\mathrm{S}}(t)$ into two parts

$$\hat{H}_{\mathrm{S}}(t) = \hat{H}_{\mathrm{S}}^0 + \hat{H}_{\mathrm{S}}^{\mathrm{int}}(t), \tag{2.11}$$

and define the unperturbed time evolution operator

$$\hat{U}_0(t) = \exp\left(-i\hat{H}_{\mathrm{S}}^0\, t/\hbar\right). \tag{2.12}$$

The selection of the part $\hat{H}_{\mathrm{S}}^0$, which is usually time-independent, depends on the particular physical situation under study. A general principle for this seperation is to ensure the simplified problem under study with the Hamiltonian $\hat{H}_{\mathrm{S}}^0$ solvable and to treat the time-dependent part with Hamiltonian $\hat{H}_{\mathrm{int}}^{\mathrm{S}}(t)$ as a perturbation to the system under investigation [Wik17]. The state vector and the operator in the interaction picture are then defined via

$$|\hat{\Psi}_{\mathrm{I}}(t)\rangle = e^{i\hat{H}_{\mathrm{S}}^0\, t/\hbar}\,|\hat{\Psi}_{\mathrm{S}}(t)\rangle, \qquad \hat{O}_{\mathrm{I}}(t) = \exp\left(i\hat{H}_{\mathrm{S}}^0\, t/\hbar\right)\hat{O}_{\mathrm{S}}(t)\exp\left(-i\hat{H}_{\mathrm{S}}^0\, t/\hbar\right). \tag{2.13}$$

Using these definitions, we have for the Hamiltonian and the density operator

$$\hat{H}_{\mathrm{I}}^0(t) = \exp\left(i\hat{H}_{\mathrm{S}}^0\, t/\hbar\right)\cdot\hat{H}_{\mathrm{S}}^0(t)\cdot\exp\left(-i\hat{H}_{\mathrm{S}}^0\, t/\hbar\right) = \hat{H}_{\mathrm{S}}^0, \tag{2.14}$$

$$\hat{H}_{\mathrm{I}}^{\mathrm{int}}(t) = \exp\left(i\hat{H}_{\mathrm{S}}^0\cdot t/\hbar\right)\cdot\hat{H}_{\mathrm{S}}^{\mathrm{int}}(t)\cdot\exp\left(-i\hat{H}_{\mathrm{S}}^0\, t/\hbar\right), \tag{2.15}$$

$$\hat{\rho}_{\mathrm{I}}(t) = \exp\left(i\hat{H}_{\mathrm{S}}^0\cdot t/\hbar\right)\hat{\rho}_{\mathrm{S}}(t)\cdot\exp\left(-i\hat{H}_{\mathrm{S}}^0\, t/\hbar\right). \tag{2.16}$$

Transforming the SE for the state vector and the von Neumann equation for the density operator from the Schrödinger picture to the interaction picture gives

$$i\hbar\frac{d}{dt}\hat{\Psi}_{\mathrm{I}}(t) = \hat{H}_{\mathrm{I}}^{\mathrm{int}}(t)\cdot\hat{\Psi}_{\mathrm{I}}(t), \tag{2.17}$$

$$i\hbar\frac{d}{dt}\hat{\rho}_{\mathrm{I}}(t) = \left[\hat{H}_{\mathrm{I}}^{\mathrm{int}}(t), \hat{\rho}_{\mathrm{I}}(t)\right]_{-}. \tag{2.18}$$

A summary of formulations of quantum mechanics in the different pictures is given in Tab. 2.1. In addition to these three representations for quantum mechanics, Feynman introduced a path integral formulation of quantum mechanics based on a semiclasscial picture. The path integral is a particular representation of the law of superposition in quantum mechanics, and is an attempt to describe the quantum world in terms of the pictures of corresponding classical systems [Wen86]. For further details on this approach, the textbook by Feynman and Hibbs [FH65] is recommended.

2.1.2 Average for observables: pure state and statistical mixture

The expectation value of an operator is given by

$$O(t) = \langle \Phi(t) | \hat{O}(t) | \Phi(t) \rangle = \text{Tr} \left\{ \hat{\rho}(t) \hat{O}(t) \right\}. \tag{2.19}$$

For a pure state, the density operator is described by $\hat{\rho}(t) = |\Psi(t)\rangle\langle\Psi(t)|$ and the trace procedure is represented via $\text{Tr} \{\cdots\} = \langle \Phi(t)| \cdots |\Phi(t)\rangle$. The physical equivalence of the three pictures in Tab. 2.1 is shown evidently by the fact that the expectation value of an observable $\hat{O}(t)$ is the same in all pictures

$$O(t) := \langle \hat{O}(t) \rangle = \langle \hat{O}_{\text{S}}(t) \rangle = \langle \hat{O}_{\text{H}}(t) \rangle = \langle \hat{O}_{\text{I}}(t) \rangle, \tag{2.20}$$

where the average is taken over the degree of freedom of the quantum system and is defined in the different pictures as

$$\langle \hat{O}_{\text{S}}(t) \rangle = \text{Tr} \left\{ \hat{\rho}_{\text{S}}(t) \hat{O}_{\text{S}}(t) \right\} = \text{Tr} \left\{ \hat{\rho}_{\text{S}}(t) \hat{O}_{\text{S}}(t_0) \right\}, \tag{2.21}$$

$$\langle \hat{O}_{\text{H}}(t) \rangle = \text{Tr} \left\{ \hat{\rho}_{\text{H}}(t) \hat{O}_{\text{H}}(t) \right\} = \text{Tr} \left\{ \hat{\rho}_{\text{H}}(t_0) \hat{O}_{\text{H}}(t) \right\}, \tag{2.22}$$

$$\langle \hat{O}_{\text{I}}(t) \rangle = \text{Tr} \left\{ \hat{\rho}_{\text{I}}(t) \hat{O}_{\text{I}}(t) \right\}. \tag{2.23}$$

Here we assume that the quantum system is not driven by any external field, i.e., the Hamiltonian $\hat{H}_{\text{S}}$ and other operators in the Schrödinger picture have no explicit time dependence.

Working in the Heisenberg picture, the time-dependent average can be expressed as [ZMR97, SL13]

$$O(t) = \text{Tr} \left\{ \hat{\rho}_{\text{H}}(t_0) \hat{O}_{\text{H}}(t) \right\} = \langle \Psi_0 | \hat{U}(t_0, t) \hat{O}(t) \hat{U}(t, t_0) | \Psi_0 \rangle. \tag{2.24}$$

This relation can be interpreted as that the time-dependent average of an observable is the overlap between the initial state described by the bra $\langle \Psi_0 |$ and a ket obtained by transforming $|\Psi_0\rangle$ from some initial time t_0 to t, after which an action is carried out via an operator $\hat{O}(t)$, and then evolving the resulting ket backward from t to t_0. Therefore, the expression (2.24) can be more distinctly depicted as in the following figure, which is denoted as the *Keldysh contour* γ^{K}, also known as *Schwinger-Keldysh contour* [ZMR97, SL13].
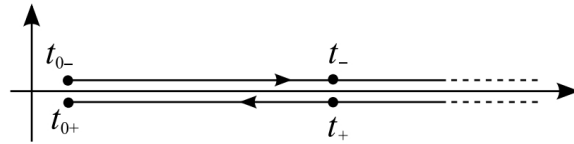
Abb. 2.1: The Schwinger-Keldysh contour $\gamma^{\text{K}} = \gamma^- + \gamma^+$ [SL13] includes a forward (upper) γ^- and a backward (lower) branch γ^+ between t_0 and t. The final time t can be extended to ∞ without influence on the real physical dynamics.

Generally, it is not possible to completely isolate a quantum system from its surrounding environment. The trivial environment is the vacuum which may have only negligible influence on the test system. Because of the complicate interactions between the quantum system and its environment, the complete information on the state of the system at a particular time is not perfectly known. Within the framework of quantum statistical physics, this incomplete

information about a quantum system due to system-environment interaction is described by assigning a probability $p_n \in [0, 1]$ to a corresponding state $|\phi_n\rangle$ with $\sum_n p_n = 1$ [SL13, Röp13]. In other words, the essential idea here is to describe the total quantum system (system + environment) in terms of a statistical mixture of isolated systems, and to account for the system-environment coupling via the probability p_n that is completely determined by the features of the environment. Obviously, the pure isolated state is described by setting the probabilities $p_n = 0$ for all states $|\phi_n\rangle$ except for one single state $|\phi_m\rangle$ $(m \neq n)$ with $p_m = 1$.

The probabilities p_n can be time-dependent for the non-equilibrium case. In the equilibrium case, the probabilities are related to the *partition function* and the macroscopic quantities are connected to the ensemble average (no dependence on time t). In this work, we use the grand-canonical ensemble, where the statistical operator [ZMR97, SL13, Röp13]

$$\hat{\rho}_{\text{grand}} = \frac{\exp\left(-\beta \hat{H}^{\text{M}}\right)}{\mathcal{Z}_{\text{grand}}} = \sum_n \frac{e^{-\beta E_n^{\text{M}}}}{\mathcal{Z}_{\text{grand}}} |\phi_n\rangle\langle\phi_n| \tag{2.25}$$

describes the thermodynamical equilibrium of a system at a given temperature T and the chemical potential μ with the partition function

$$\mathcal{Z}_{\text{grand}} = \text{Tr}\left\{\exp\left(-\beta \hat{H}^{\text{M}}\right)\right\} = \sum_n \exp\left(-\beta E_n^{\text{M}}\right), \tag{2.26}$$

where E_n^{M} is related to the eigenenergy E_n via the relation $E_n^{\text{M}} = E_n - \mu N$ with the particle number N. Correspondingly, the average of any macroscopic quantity is determined via

$$O^{\text{M}} = \text{Tr}\left\{\hat{\rho}_{\text{grand}}\hat{O}^{\text{M}}\right\} = \sum_m \langle\phi_m| \hat{\rho}_{\text{grand}}\hat{O}^{\text{M}} |\phi_m\rangle. \tag{2.27}$$

The temperature-dependence in the exponential $\exp\left(-\beta \hat{H}^{\text{M}}\right)$ can be also expressed as a time evolution operator $e^{-i\hat{H}t/\hbar}$, if we regard the parameter β as an imaginary time [SL13],

$$\beta \cdot \hbar \rightarrow e^{i\theta} t \rightarrow it, \tag{2.28}$$

where we continuously change θ from 0 to $\pi/2$. This replacement is known as *analytic continuation*, also known in field theory as *Wick rotation*. Then the ensemble average can also be graphically described by a contour which is known as the *Matsubara contour* γ^{M} [ZMR97, SL13] in the thermodynamic GF techniques.
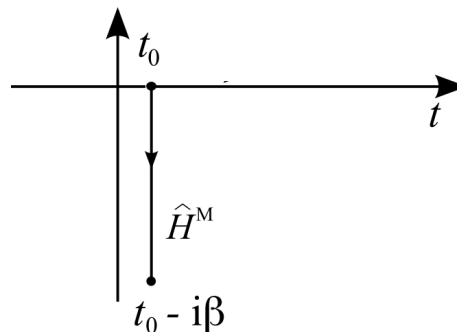

Abb. 2.2: The Matsubara contour γ^{M} [SL13]: the time evolves along the negative axis from t_0 to $t_0 - i\beta$.

For operators along the contour γ^{M}, we have the following definitions

$$\hat{H}^{\mathrm{M}} \equiv \hat{H}(z \in \gamma^{\mathrm{M}}) := \hat{H}(t_0) - \mu \hat{N} \qquad \text{for the Hamiltonian ;} \qquad (2.29)$$

$$\hat{O}^{\mathrm{M}} \equiv \hat{O}(z \in \gamma^{\mathrm{M}}) := \hat{O}(t_0) \qquad \text{for any other operator.} \qquad (2.30)$$
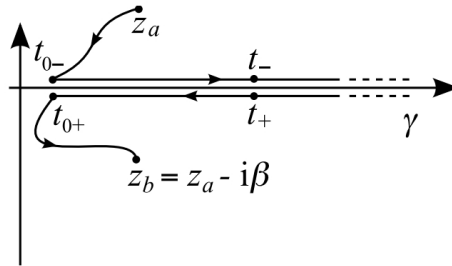

Abb. 2.3: Konstantinov-Perel's contour $\gamma = \gamma^{\mathrm{K}} \oplus \gamma^{\mathrm{M}}$ [SL13]: the time ordering is indicated by the arrow along the contour, i.e., any time point between z_a and t_{0-} (t_{0+} and z_b) is earlier (later) than a point in the Keldysh contour γ^{K}.

The analytic continuation allow us to describe the real time evolution and the ensemble average in a consistent way. Introducing a more general contour $\gamma = \gamma^{\mathrm{K}} \oplus \gamma^{\mathrm{M}}$, as depicted in Fig. 2.3, then we have for the average along the contour

$$O(z) = \frac{\mathrm{Tr}\left[\mathcal{T} \left\{ e^{-i \int_\gamma d\bar{z}\, \hat{H}(\bar{z})} \, \hat{O}(\bar{z}) \right\} \right]}{\mathrm{Tr}\left[\mathcal{T} \left\{ e^{-i \int_\gamma d\bar{z}\, \hat{H}(\bar{z})} \right\} \right]}, \qquad (2.31)$$

where the operator $\mathcal{T}$ is the extended time-ordered operator. The contour introduced above is known as the *Konstantinov-Perel's contour* [ZMR97, SL13]. The physical meaning of the Konstantinov-Perel's contour can be explained as following: the system is initially prepared in equilibrium at some time t_0 and then evolves out of equilibrium because of the perturbation of an external field. After the external perturbation is turned off, the system will relax into the equilibrium once again. Based on this contour idea, both the equilibrium and the non-equilibrium properties of a system can be described in a systematic theory [ZMR97, Wei99, SL13, Röp13].

To acquire the time-dependent average of an observable (including both real-time average and imaginary-time average), the corresponding equation of motion for the observable should be solved under some boundary conditions. The equation of motion for the observable $\langle \hat{O}(t) \rangle$ can be obtained by differentiating it with respect to time t. As we discussed at the beginning of this chapter, the time-dependence is described by the state vector and the corresponding density operator in the Schödinger picture or can be assigned to the operator in the Heisenberg picture [ZMR97]. This fact indicates that we can have different methods to access the dynamical properties of a system. The first approach, constructed from the equation of motion for the density operator in the Schödinger picture, i.e., the quantum Liouville-von Neumann equation, is well known in the research field of dissipative quantum systems [BP07, JZK$^+$03, Wei99, Röp13, ZMR97]. In this case, the concept of the so-called reduced density operator has to be introduced. We will describe this method in detail in the last section of this chapter. In the following section, we introduce an alternative to the

method based on the Liouville-von Neumann equation, i.e., the Green's function formalism in terms of the quasi-particle concept [Röp13, ZMR97, KKER86, KSKB05, SL13], which is an approach based on the equations of motion for field operators given in the Heisenberg picture.

2.1.3 Correlation functions and their relation to physical properties of a system

To study properties of a physical system, one experimentally perturbs the system and see how it responds to this perturbation [Wen86]. However, the experimental observations can not be described by a simple and universally valid theory. To develop a theory for a system, one has to find out the corresponding physical quantities related to the special problem under question [Gün95, KSKB05, Röp13]. For instance, measurements of conductivity, emission spectrum, structure factor and many other physical properties can be performed [Wen86, Röp13]. Theoretically, the force-force (current-current) correlation function is used to described the conductivity [Rei05, KSKB05], while we use dipole-dipole correlation functions for the emission spectrum [KKER86, Gün95] and density-density correlation functions for structure factors [GR09]. Evidently, theorists always tend to find the corresponding correlation functions to describe the desired properties of a physical system.

The correlation functions can be expressed in a general form of time-ordered strings of operators

$$\hat{k}(z_1, \cdots, z_n) = \mathrm{T}\left\{\hat{O}_1(z_1) \cdots \hat{O}_n(z_n)\right\} \tag{2.32}$$

with the time-order operator T. Physically observed quantities are then determined via

$$k(z_1, \cdots, z_n) = \mathrm{Tr}\left\{\hat{k}(z_1, \cdots, z_n)\right\}, \tag{2.33}$$

where the trace is taken over certain relevant degrees of freedom. In fact, all physical observables should be described by the corresponding operators. For example, the density operator is given in terms of creation and annihilation field operators at equal time [KKER86, KSKB05, SL13]

$$\hat{n}(z) = \hat{\phi}^\dagger(z)\,\hat{\phi}(z). \tag{2.34}$$

Another special series of important operators are constructed by an equal number of creation and annihilation field operators [SL13]

$$\hat{G}_n(1, \cdots, n; 1', \cdots, n') = \frac{1}{i^n}\mathcal{T}\left\{\hat{\phi}_{\mathrm{H}}(1) \cdots \hat{\phi}_{\mathrm{H}}(n)\,\hat{\phi}_{\mathrm{H}}^\dagger(n') \cdots \hat{\phi}_{\mathrm{H}}^\dagger(1')\right\}, \tag{2.35}$$

from which the Green's functions can be defined. An important feature of this series of correlation operators is hidden in their corresponding equations of motion. It is found that the equation of motion for $\hat{G}_n$, given by the derivative of $\hat{G}_n$, is expressed in terms of $\hat{G}_{n-1}$ and $\hat{G}_{n+1}$, which is known as BBGKY hierarchy [KSKB05, Röp13, SL13]. This means that we have to solve an infinite hierarchy of coupled differential equations, if we attempt to obtain the exact knowledge of the $n-$th correlation operator $\hat{G}_n$. This renders these equations practically unsolvable. Moreover, in most cases one is only interested in the properties of $\hat{G}_n$. Consequently, the system of coupled differential equations should be truncated under some assumptions or approximations. This simplification results in the quasi-particle concept and the definition of self-energy within the framework of the Green's function approach [KKER86, Gün95, KSKB05, Röp13, SL13].

2.2   Green's function technique

As mentioned above, the ensemble average includes the interaction between the system and the environment via the statistical weight p_n, which can be described by a modified Hamiltonian related to the quasi-particle concept. In this section, we introduce the thermodynamic (or Matsubara) Green's function and the quasi-particle concept [KSKB05, Röp13, SL13]. Using these definitions, we will discuss the relations between the Green's function and the continuum lowering as well as the spectral lines.

From the $n-$th order correlation operator $\hat{G}_n$

$$\hat{G}_n(1, \cdots, n; 1', \cdots, n') = \frac{1}{i^n} \mathcal{T} \left\{ \hat{\phi}_{\mathrm{H}}(1) \cdots \hat{\phi}_{\mathrm{H}}(n) \, \hat{\phi}_{\mathrm{H}}^{\dagger}(n') \cdots \hat{\phi}_{\mathrm{H}}^{\dagger}(1') \right\}, \qquad (2.36)$$

the thermodynamical $n-$particle GF G_n is defined as [SL13]

$$G^{\mathrm{M}}(1, \cdots, n; 1', \cdots, n') = \frac{\mathrm{Tr}\left\{ \exp\left(-\beta\,\hat{H}^{\mathrm{M}}\right)\,\hat{G}_n(1, \cdots, n; 1', \cdots, n') \right\}}{\mathrm{Tr}\left\{ \exp\left(-\beta\,\hat{H}^{\mathrm{M}}\right) \right\}}. \qquad (2.37)$$

In the following, we are merely interested in the single- and two-particle Green's functions. The generalization to a $n-$particle GF, for example the 4-particle GF for α particles [RSSN98], is straightforward.

2.2.1   Single-particle Green's function and continuum lowering

2.2.2.1 Single-particle Green's function

In this and the following subsections we discuss the general properties of the one-particle and the two-particle GFs in equilibrium denoted by the superscript "M" (short hand notation for "Matsubara") following the notations in Ref. [SL13]. The one-particle GF G_1 represents the propagation of an additionally created particle inserted in a many-body environment at some initial time τ_2 and at the position $\mathbf{x}_2$ to an other time point τ_1 and position $\mathbf{x}_1$. The general informations contained in the single-particle GF G_1 are the one-particle energy and its lifetime. Obviously, the GF can also be represented in another basis, for example, in the momentum space $|\mathbf{p}\rangle$. Therefore, it is more convenient to work with the GF operator (i.e., the GF correlator) which is invariant with respect to the basis. In thermodynamic equilibrium, the GF operator $\hat{G}_1$ only depends on the time τ_1 and τ_2 via their difference, i.e., $\tau_1 - \tau_2$ in the form [KKER86, Röp13, SL13]

$$\hat{G}_1^{\mathrm{M}}(\tau_1, \tau_2) = \hat{G}_1^{\mathrm{M}}(\tau_1 - \tau_2) = \frac{1}{-i\beta} \sum_{\nu} e^{-i\,\omega_\nu\,(\tau_1 - \tau_2)}\,\hat{G}_1^{\mathrm{M}}(\omega_\nu), \qquad (2.38)$$

with the *Matsubara frequencies* containing the statistical information on temperature

$$\omega_\nu = \begin{cases} \frac{\pi\nu}{\beta} & \nu = 0, \pm 2, \pm 4 \cdots \qquad \text{for bosons} \\ \frac{\pi\nu}{\beta} & \nu = \pm 1, \pm 3, \pm 5 \cdots \qquad \text{for fermions} \end{cases} \qquad (2.39)$$

and where the Matsubara GF operator in ω_ν space is defined by

$$\hat{G}_1^{\mathrm{M}}(i\,\omega_\nu) = \frac{1}{i\,\omega_\nu - \hat{h}^{\mathrm{M}}}. \qquad (2.40)$$

Here, the chemical potential is included in the one-particle Hamiltonian $\hat{h}^{\mathrm{M}} = \hat{h} - \mu$. Alternatively, we can also assign the chemical potential in the definition of the Matsubara frequencies [Röp13]. To investigate the properties of plasma, the homogeneity of space and time is generally assumed because of the momentum and energy conservation. Consequently, the Hamiltonian is diagonal in the single-particle quantum numbers $c = \{\mathbf{p}_c, s_c\}$ with the momentum $\mathbf{p}_c$ and the spin s_c of the particle species c. Working in momentum space, we have

$$G^{\mathrm{M}}_{1,0}(c, i\,\omega^c_\nu) = \frac{1}{i\,\omega^c_\nu - \epsilon_c}. \tag{2.41}$$

The free GF $G^{\mathrm{M}}_{1,0}(c, i\,\omega^c_\nu)$ is only valid for a non-interacting system. In reality, the interactions between different particles in a physical system must be taken into account. Generally, during the propagation, the test particle can interact with its surrounding particles and also dynamically interact with itself. The latter process is known as re-absorption of a photon, i.e., the test particle emits a photon which will move freely in the plasma and then will be absorbed again by this test particle. For the interacting system, the full (dressed) GF $G^{\mathrm{M}}_1(c, i\,\omega^c_\nu)$ incorporating the influence of the plasma environment can be expressed in terms of the free GF $G^{\mathrm{M}}_{1,0}(c, i\,\omega^c_\nu)$ and the "self-energy" $\Sigma_1(c, i\,\omega^c_\nu)$ as follows

 $\tag{2.42}$

$$G^{\mathrm{M}}_1(c, i\,\omega^c_\nu) = G^{\mathrm{M}}_{1,0}(c, i\,\omega^c_\nu) + G^{\mathrm{M}}_{1,0}(c, i\,\omega^c_\nu) \cdot \Sigma_1(c, i\,\omega^c_\nu) \cdot G^{\mathrm{M}}_1(c, i\,\omega^c_\nu) \tag{2.43}$$

$$= \frac{1}{\left\{ G^{\mathrm{M}}_{1,0}(c, i\,\omega^c_\nu) \right\}^{-1} - \Sigma_1(c, i\,\omega^c_\nu)}.$$

This equation is known as *Dyson equation* [KKER86, KSKB05, SL13, Röp13]. The self-energy appears in the denominator and can be formally regarded as an energy shift. However, the self-energy is in general a complex quantity and frequency-dependent. We will discuss this point in more details later. The self-energy $\Sigma_1(c, i\,\omega^c_\nu)$ originates from the fact that we wish to construct an effective theory for the investigated system by embedding all the irrelevant degrees of freedom into one effective quantity [ZMR97, SL13, Röp13].

2.2.2.2 Screened potential

Similar to the modification of the free GF by the plasma environment, the bare Coulomb potential is also changed in plasmas. More accurately, the long range Coulomb potential of the test particle is shielded by the plasma particles [KKER86, KSKB05, SL13, Röp13]. In the basic equations of quantum statistical theory, the binary interaction of charged particles of a plasma is characterized via the Coulomb potential which is a long range potential in the form of $\sim 1/r$. A shortcoming of the bare Coulomb interaction is that this long range potential leads to divergences in the calculation of relevant physical quantities [KSKB05]. Additionally, such long range potential allows the charged particles in the plasma to interact with each other simultaneously which leads to a collective motion of the charged particles. Because of the simultaneity and instantaneity of the mutual interaction, the interaction between two test particles is modified by the surrounding particles. This phenomenon is known as the dynamical screening of the Coulomb potential, which is an important and fundamental quantity for all many-body systems [KKER86, KSKB05].

In the language of the GF technique, the dynamically screened potential is given in the diagrammatic representation as [Röp13]
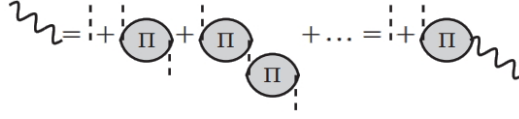
and, correspondingly, in the mathematical form via

$$V_{ab}^{\text{scr}}(\mathbf{q},\omega) = V_{ab}(\mathbf{q}) + \sum_{cd} V_{ac}(\mathbf{q})\,\Pi_{cd}(\mathbf{q},\omega)\,V_{db}^{\text{scr}}(\mathbf{q},\omega). \tag{2.44}$$

This expression, known as screening equation, can be further simplified by reordering and rejoining the charges e_a, e_b, e_c, e_d. The the following expression is obtained

$$V_{ab}^{\text{scr}}(\mathbf{q},\omega) = \frac{V_{ab}(\mathbf{q})}{1 - \sum_{cd} V_{cd}(\mathbf{q})\,\Pi_{cd}(\mathbf{q},\omega)} := \frac{V_{ab}(\mathbf{q})}{\varepsilon(\mathbf{q},\omega)} \tag{2.45}$$

with the dielectric function that is defined via the polarization function $\Pi_{cd}(\mathbf{q},\omega)$

$$\varepsilon(\mathbf{q},\omega) = 1 - \sum_{cd} V_{cd}(\mathbf{q})\,\Pi_{cd}(\mathbf{q},\omega). \tag{2.46}$$

The quantity (2.45) is the Fourier transform of the Coulomb potential modified by the dielectric function. This modification may be explained as follows: a charged test particle immersed in plasma polarizes its surrounding particles, so that any other particle experiences the test particle and its screening cloud at the same time. The dielectric function (2.46) is a complex quantity whose real and imaginary part satisfy the Kramers-Kronig relation. Then Eq. (2.45) can be rewritten in the spectral representation in the following form

$$V_{ab}^{\text{scr}}(\mathbf{q},\omega) = V_{ab}(\mathbf{q}) \cdot \left\{ 1 + \int_{-\infty}^{\infty} \frac{d\omega'}{\pi} \cdot \frac{\operatorname{Im}\varepsilon^{-1}(\mathbf{q},\omega'-i\eta)}{\omega-\omega'} \right\}. \tag{2.47}$$

The simplest approximation for the polarization function $\Pi_{cd}(\mathbf{q},\omega)$ and, correspondingly, for the dielectric function $\varepsilon(\mathbf{q},\omega)$ is the so-called *random-phase approximation* (RPA)

$$\Pi_{cc}^{\text{RPA}}(\mathbf{q},\omega) = \quad\bigcirc\quad = \frac{2s_c+1}{\Omega_0} \sum_{\mathbf{p}} \frac{f_c(\epsilon_{\mathbf{p}-\mathbf{q}}) - f_c(\epsilon_{\mathbf{p}})}{\omega + \epsilon_{\mathbf{p}-\mathbf{q}} - \epsilon_{\mathbf{p}}} \tag{2.48}$$

where the polarization functions are assumed to be diagonal in the particle species. Inserting this expression into Eq. (2.46), the dielectric function in RPA is obtained

$$\varepsilon^{\text{RPA}}(\mathbf{q},\omega) = 1 - \sum_{c} V_{cc}(\mathbf{q})\,\Pi_{cc}^{\text{RPA}}(\mathbf{q},\omega)$$

$$= 1 - \sum_{c,\mathbf{p}} \frac{2s_c+1}{\Omega_0} \cdot V_{cc}(\mathbf{q}) \cdot \frac{f_c(\epsilon_{\mathbf{p}-\mathbf{q}}) - f_c(\epsilon_{\mathbf{p}})}{\omega + \epsilon_{\mathbf{p}-\mathbf{q}} - \epsilon_{\mathbf{p}}}. \tag{2.49}$$

The dielectric function in RPA includes profound information of the properties of the plasma and is valid for arbitrary degeneracy and can be evaluated in different limits. For example, collective oscillation, described by the plasma frequency (plasmon resonance), appears in

the long-wavelength limit ($\mathbf{q} \to 0$). Additionally, the well-known Debye screening for a non-degenerate plasma can be derived in the static limit ($\omega \to 0$), while the Thomas-Fermi screening for a strongly degenerate plasma is recovered in the low-temperature limit ($T \to 0$).

The consequences of the screening effects in plasma are the following: 1) the continuum edges that describe the eigenenergies of free particles are changed; 2) the bound state energies of the composite ions are modified. Consequently, the transition energies for bound-bound and bound-free transitions are different from those in the case of isolated ions.

2.2.2.3 Self-energy and continuum lowering

After the introduction of the screened potential and the dressed GF, we follow the ideas in Ref. [KKER86] and can now discuss the single-particle self-energy $\Sigma_1(\mathbf{p}, z)$ in more detail. The simplest approximation for the single-particle self-energy is the Hartree-Fock (HF) approximation, which is constructed by the free GF for the single-particle and the bare Coulomb potential

$$\Sigma_1^{\mathrm{HF}}(\mathbf{p}, z) = \overset{\frown}{\bullet \rightarrow \bullet} = \sum_{\mathbf{q}, \omega} G_1^0(\mathbf{p} - \mathbf{q}, z - \omega) \cdot V(\mathbf{q}). \tag{2.50}$$

The first contribution, known as Hartree term, generally vanishes for a homogeneous system because of charge neutrality. The second contribution, i.e., the Fock term, is related to the statistical correlation because of the Pauli principle [KKER86]. Unless otherwise stated, we concentrate only on the Fock term (but still name this approximation as HF approximation) and the corresponding improvements based on the Fock term.

In contrast, the full consideration for the single-particle self-energy is described by the $GW\Gamma$-approximation, where G denotes the dressed GF, $W = V^{\mathrm{scr}}$ signifies the screened potential, and Γ indicates the vertex correction "▲" to the interaction vertex " ● ".

$$\Sigma_1^{\mathrm{GW\Gamma}}(\mathbf{p}, z) = \overset{\frown}{\blacktriangle \rightarrow \blacktriangle} = \sum_{\mathbf{q}, \omega} G_1(\mathbf{p} - \mathbf{q}, z - \omega) \cdot V^{\mathrm{scr}}(\mathbf{q}, \omega). \tag{2.51}$$

To evaluate the self-energy and other quantities according to the perturbation theroy within the $GW\Gamma$-approximation, special care must be taken in order to avoid double counting throughout the different diagram classes. Moreover, the diagrams included in this approach result in an infinite hierarchy of equations which is impossible to be solved. Therefore, a further simplification is to truncate this infinite hierarchy of equations on a certain level for practical calculation. One possibility for the truncation is the GW-approximation by ignoring the vertex correction Γ.

In a next step to the HF approximation, the GW^0-approximation (or the self-consistent HF approximation) is obtained using the full GF instead of the free GF in the orginal HF approximation,

$$\Sigma_1^{\mathrm{GW^0}}(\mathbf{p}, z) = \overset{\frown}{\bullet \rightarrow \bullet} = \sum_{\mathbf{q}, \omega} G_1(\mathbf{p} - \mathbf{q}, z - \omega) \cdot V(\mathbf{q}, \omega). \tag{2.52}$$

A further important approximation is the Montroll-Ward (MW) approximation obtained by replacing the bare Coulomb potential $V(\mathbf{q})$ by the screened potential $V^{\mathrm{scr}}(\mathbf{q}, \omega)$. Hence, the MW approximation is also known as V^{s}- or $G_0 V^{\mathrm{s}}$-approximation,

$$\Sigma_1^{\mathrm{MW}}(\mathbf{p}, z) = \overset{\displaystyle\frown}{\underset{\displaystyle\longrightarrow}{\qquad}} = \sum_{\mathbf{q},\omega} G_1^0(\mathbf{p} - \mathbf{q}, z - \omega) \cdot V^{\mathrm{scr}}(\mathbf{q}, \omega). \tag{2.53}$$

Based on the self-energy $\Sigma_1(c, z)$, a new concept "quasi-particle" can be introduced, where the particle mass is renormalized in order to restore the orginal free particle's propagator structure [RM09]

$$\frac{1}{m_{\mathrm{eff}}^c} = \frac{\partial^2}{\partial (\hbar\mathbf{p})^2} \, E_{1,c}^{\mathrm{qu.}}(\mathbf{q}) \quad \text{with} \quad E_{1,c}^{\mathrm{qu.}}(\mathbf{q}) = \epsilon_c + \mathrm{Re}\,\{\Sigma_1(c, \omega)\}\,|_{\omega = E_{1,c}^{\mathrm{qu.}}(\mathbf{q})}. \tag{2.54}$$

Obviously, the quasi-particle energy $E_{1,c}^{\mathrm{qu.}}(\mathbf{q})$ includes the energy shift in addition to the kinetic energy of the free particle. The energy shift is usually negative, so that the threshold value for the definition of continuum states is not given by $\mathbf{p} = 0$ any more but from some negative value [KKER86, KSKB05]. In other words, it seems that the continuum edge is lowered. This phenomenon is connected to the ionization potential depression in plasma and will be discussed in detail in terms of the single-particle self energy in MW approximation and the structure factor in Chapter 4.

2.2.2.4 Evaluation of Self-energy

As an example, we calculate the self-energy within the G_0V^{s}- (or MW) approximation, i.e. Eq. (2.53). The needed elements are the free GF of single-particle $G_{1,0}^{\mathrm{M}}(c, i\omega_\nu^c)$ and the dynamically screened potential $V_{ab}^{\mathrm{scr}}(\mathbf{q}, \omega)$. We repeat the corresponding expressions

$$G_{1,0}^{\mathrm{M}}(c, z_\nu^c) = \frac{1}{z_\nu^c - \epsilon_c}, \tag{2.55}$$

$$V_{cc}^{\mathrm{scr}}(\mathbf{q}, \omega) = V_{cc}(\mathbf{q}) \cdot \left\{ 1 + \int_{-\infty}^{\infty} \frac{d\omega'}{\pi} \cdot \frac{\mathrm{Im}\varepsilon^{-1}(\mathbf{q}, \omega')}{\omega - \omega'} \right\}. \tag{2.56}$$

Writing out the screening potential $V_{cc}^{\mathrm{scr}}(\mathbf{q}, \omega)$, the self-energy in MW approximation $\Sigma_{1,c}^{\mathrm{MW}}$ can be expressed as

$$\Sigma_{1,c}^{\mathrm{MW}}(\mathbf{p}, z) = \sum_{\mathbf{q},\omega} G_1^0(\mathbf{p} - \mathbf{q}, z - \omega) \cdot V^{\mathrm{scr}}(\mathbf{q}, \omega) = \Sigma_c^{\mathrm{HF}}(\mathbf{p}, z) + \Sigma_c^{\mathrm{corr}}(\mathbf{p}, z) \tag{2.57}$$

with the Hartree-Fock (HF) contribution for the self-energy [KKER86]

$$\Sigma_c^{\mathrm{HF}}(\mathbf{p}) = i \sum_{\mathbf{k}} V_{cc}(\mathbf{k}) \, G_{1,0}^{\mathrm{M}}(c, z_\nu^c) = -\int \frac{d^3\mathbf{k}}{(2\pi)^3} V_{cc}(k) \, f_c(\mathbf{p} - \mathbf{k}) \tag{2.58}$$

and the correlation contribution due to the influence of the plasma environment

$$\Sigma_c^{\mathrm{corr}}(\mathbf{p}, z_\nu^c) = \sum_{\mathbf{q},\omega} \int_{-\infty}^{\infty} \frac{d\omega'}{\pi} \, \frac{\mathrm{Im}\varepsilon^{-1}(\mathbf{q}, \omega')}{\omega - \omega'} \cdot \frac{1}{z_\nu^c - \omega - \epsilon_{c,\mathbf{p}-\mathbf{q}}}. \tag{2.59}$$

Using the Matsubara frequency summation rule for bosons [KKER86, RM09, Röp13]

$$\frac{i}{\beta} \sum_{\nu} \frac{1}{\omega_\nu - \omega_1} \cdot \frac{1}{\omega_\nu - \omega_2 + \omega_\lambda} = \frac{n_{\mathrm{B}}(\omega_1) - n_{\mathrm{B}}(\omega_2)}{\omega_1 - \omega_2 + \omega_\lambda}, \tag{2.60}$$

we arrive at the following expression

$$\Sigma_c^{\mathrm{corr}}(\mathbf{p}, z_\nu^c) = -\sum_{\mathbf{q}} \int_{-\infty}^{\infty} \frac{d\omega'}{\pi} \, \mathrm{Im}\varepsilon^{-1}(\mathbf{q}, \omega') \cdot \frac{n_{\mathrm{B}}(\omega) - n_{\mathrm{B}}(z_\nu^c - \epsilon_{c,\mathbf{p}-\mathbf{q}})}{z_\nu^c - \epsilon_{c,\mathbf{p}-\mathbf{q}} - \omega'}. \qquad (2.61)$$

Because of $z_\nu^c = \pi \nu_c / \beta$ with $\nu_c = 0, \pm 2, \cdots$ for bosons and $\nu_c = \pm 1, \pm 3, \cdots$ for fermions, and thus $e^{i\beta z_\nu^c} = (-1)^{2s_c}$ depending on the spin s_c of the particle, we have

$$n_{\mathrm{B}}(z_\nu^c - \epsilon_{c,\mathbf{p}-\mathbf{q}}) = \frac{1}{\exp\left(i\beta z_\nu^c - \beta\epsilon_{c,\mathbf{p}-\mathbf{q}}\right) - 1} = 1 + (-1)^{2s_c} f_c(\mathbf{p} - \mathbf{q}), \qquad (2.62)$$

where $f_c(\mathbf{p} - \mathbf{q})$ is the Bose distribution for bosons with integer spins and the Fermi distribution for fermions with half-integer spins, respectively. Inserting this relation into Eq. (2.61), we obtain

$$\Sigma_c^{\mathrm{corr}}(\mathbf{p}, z_\nu^c) = -\sum_{\mathbf{q}} \int_{-\infty}^{\infty} \frac{d\omega'}{\pi} \, \mathrm{Im}\varepsilon^{-1}(\mathbf{q}, \omega') \cdot \frac{n_{\mathrm{B}}(\omega) + 1 + (-1)^{2s_c} f_c(\mathbf{p} - \mathbf{q})}{z_\nu^c - \epsilon_{c,\mathbf{p}-\mathbf{q}} - \omega'}. \qquad (2.63)$$

This expression is of essential importance in investigating the continuum lowering, i.e., the ionization potential depression, since it describes modifications of atomic properties in a plasma environment. We will discuss this expression in detail in Chapter 4.

2.2.2 Two-particle Green's function and spectral lines

2.2.3.1 Two-particle Green's function

Similar to the one-particle GF, the two-particle GF describes the propagation of a two-particle system which initially locates in $(\mathbf{x}_1', \mathbf{x}_2')$ to another position $(\mathbf{x}_1, \mathbf{x}_2)$, during which this two-particle system may interact with each other and with its surroundings. The aim of introducing the two-particle GF in our case is to describe bound states which can be regarded as a new particle species in the chemical picture [KKER86, RM09, SL13, Röp13].

To acquire the information about the two-particle system, a system of coupled equations for the GFs should be solved, which in practice can never be achieved due to the huge numbers of degree of freedom. We must find reasonable approximations for G_2. According to the definition Eq. (2.37), the GF should fulfill a general symmetry property. The approximate two-particle GF has also to obey this condition [SL13]

$$G_2^{\mathrm{M}}(1, 2; 1^+, 2^+) = G_2^{\mathrm{M}}(2, 1; 2^+, 1^+). \qquad (2.64)$$

Another condition for the approximate GFs is that they should satisfy the same conservation laws as the original exact GFs. This condition is reflected in the fact that the approximate GFs follow the same boundary conditions as the exact GFs.

The simplest approximation for the two-particle GF is the Hartree approximation by neglecting the direct interaction between the two particles and the symmetry or anti-symmetry in the case of two identical particles [RM09, SL13, Röp13]. Taking into account the identity of the particles, the Hartree-Fock approximation can be obtained [Röp13]

The " $+$ " describes the quantum statistical properties of bosons and " $-$ " of fermions. In our case for the spectral lines, we introduce the so-called ladder approximation for the two-particle GF [Röp13]

This diagram is the starting point for evaluating the atomic polarization function for spectral lines within the framework of Green's function technique.

2.2.3.2 Spectral lines: electron and ion dynamics

The emission and absorption of light in WDM is considered within perturbation theory, the photons are coupled to the dipole-dipole correlation function. The line profile is given by the Fourier transform of the dipole autocorrelation function [Duf69, Gün95, Dem10]

$$I(\omega) = \frac{1}{\pi} \text{Re} \int e^{i\omega t} \text{Tr}\{\hat{\rho}_{\text{eq}} \hat{\mathbf{d}}(0) \hat{\mathbf{d}}(t)\}, \tag{2.65}$$

where $\hat{\rho}_{\text{eq}}$ is the equilibrium statistical operator, $\hat{\mathbf{d}}$ the dipole operator of the emitting radiator and the time dependence is given within the Heisenberg picture. In a more general version the dipole moment is determined by the entire plasma. Also higher multi-pole moments of the charge density can be considered. Such relations between a dissipative property like absorption of light and fluctuations in equilibrium (fluctuation-dissipation theorem) are obtained from linear response theory. The relation (2.65) is a special form, equivalent relations are the dielectric function which is related to the polarization function. Furthermore, the polarization function can be expressed as correlation function of (charge) density fluctuations in equilibrium. Similar relations for the emission and absorption of light are obtained from quantum master equations as shown in Ref. [LGRR16] and will be discussed in detail in next chapter. The evaluation of equilibrium correlation functions like the dipole autocorrelation function (2.65) and the density-density correlations can be performed using different approaches: path integral methods, MD simulations, perturbation expansion and Feynman diagrams which will be considered here. In the general form, the polarization function is presented by the sum of all irreducible diagrams with incoming and outgoing particle-hole lines as shown in the following.

To calculating the spectral lines in plasmas, the ions and electrons are in general treated separately because of their large difference of masses and hence significant distinction of their thermodynamic mobility. The average over the degrees of freedom of plasma can be performed in two stages: first over the fast moving electrons and then over the slow ions [GHR91, Dem10, Duf69, SM10]

$$\langle \cdots \rangle_{\text{plasma}} = \langle \langle \cdots \rangle_{\text{electrons}} \rangle_{\text{ions}}. \tag{2.66}$$

While evaluating the average over electrons, the ions produce a slowly varying electric field F, if the ions are assumed to be essentially stationary. The free electrons collide with the radiator and result in the so-called pressure broadening of the spectra, which has a Lorentzian

shape [GHR91, SM10]

$$\langle \cdots \rangle_{\text{electrons}} \to \frac{1}{\omega - \Delta(F) - i\Gamma(F)}. \tag{2.67}$$

Here $\Delta(F)$ and $\Gamma(F)$ are related to the shift and broadening of the spectral lines, respectively. On the other hand, the ions are randomly distributed in plasmas. Different ion configurations near the perturbed atom or ion lead to different field strength F. To account for all possible ionic distributions, we introduce the microfield distribution $W(F)$ and express the average over ions as [GHR91, SM10]

$$\langle \cdots \rangle_{\text{ions}} \to \int_0^\infty dF\, W(F) \cdot \langle \cdots \rangle_{\text{electrons}}. \tag{2.68}$$

The influence of the plasma ions on the emitter is usually quantitatively described by the linear and quadratic Stark effect [LL85, Gün95, Dem10, SM10], which is determined by the field strength F. For non-interacting ions, the probability distribution $W(F)$ of the field strength F is given by the Holtsmark distribution [Hol19]. To include the correlation effects, Hopper's tables for the low frequency microfield [Hoo68], the APEX approach [IRS$^+$00], and the fit formula by Potekhin *et al.* [PCG02] can be used.

Depending on the plasma parameters, the ion dynamics might become important and can not be neglected any more. Generally, line wings can be treated statically and the line center is affected by ion-dynamics. Based on the quasi-static approximation of the microfield, two different methods are commonly used to include ion-dynamics into the line profile calculation, i.e., the model microfield method and the reformulation of the frequency fluctuation model [Dem10, Lor14].

2.2.3.2 Spectral lines in terms of Green's function approach

Within the framework of the quantum statistical approach [Gün95, KKER86], the optical properties of a plasma system, i.e., the absorption coefficient $\alpha(\omega)$ and the refraction index $n(\omega)$, are determined by the transversal dielectric function $\epsilon_{\text{tr}}(\mathbf{q}, \omega)$ via the relation [Gün95, KKER86, Oma07, Lor14]

$$n(\omega) + ic\,\alpha(\omega)/\omega = \lim_{q \to 0} \sqrt{\epsilon_{\text{tr}}(\mathbf{q}, \omega)}, \tag{2.69}$$

with c denoting the speed of light in vacuum. In the long wavelength limit, both the transversal and longitudinal part of the dielectric function $\epsilon(\mathbf{q}, \omega)$ are identical, i.e. $\epsilon_{\text{tr}}(\mathbf{q}, \omega) = \epsilon_{\text{long}}(\mathbf{q}, \omega)$. The longitudinal dielectric function $\epsilon_{\text{long}}(\mathbf{q}, \omega)$ is further related to the polarization function $\Pi(\mathbf{q}, \omega)$ as

$$\epsilon_{\text{long}}(\mathbf{q}, \omega) = 1 - V(q)\,\Pi(\mathbf{q}, \omega), \tag{2.70}$$

in which the polarization function $\Pi(\mathbf{q}, \omega)$ can be evaluated systematically by using thermodynamic Green's functions and Feymann's diagrams. This means, a cluster decomposition of the polarization function with consideration of all the irreducible diagrams can be performed. In order to obtain the spectral line shapes, the bound states, described by the second order term of the cluster decomposition in the chemical picture, have to be take into account [Gün95]

$$\Pi(\mathbf{q}, \omega) = \Pi_{\text{RPA}}(\mathbf{q}, \omega) + \Pi_{\text{atom}}(\mathbf{q}, \omega). \tag{2.71}$$

The atomic polarization function $\Pi_{\mathrm{atom}}(\mathbf{q}, \omega)$ can be described diagrammatically as [Oma07]

$$G_2(n_1, \mathbf{P}, \Omega_\lambda)$$
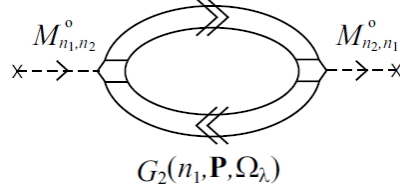
with the dressed GF G_2 and the unperturbed transition matrix $M^0_{n_1 n_2}(\mathbf{q})$ expressed via

$$M^0_{n_1 n_2}(\mathbf{q}) = i \left\{ Z \delta_{n_1 n_2} - \int d^3\mathbf{r} \phi^*_{n_1}(\mathbf{r}) e^{-i\mathbf{q}\cdot\mathbf{r}} \phi_{n_2}(\mathbf{r}) \right\}. \tag{2.72}$$

The spectral line shapes are determined by the imaginary part of the atomic polarization function $\Pi_{\mathrm{atom}}(\mathbf{q}, \omega)$. The full spectral line profile $I(\omega)$, called the Voigt profile, is obtained as a convolution of the Doppler-broadened line profile with the pressure-broadened line profile $I_{\mathrm{pr}}(\omega)$ [Gün95, Lor14]

$$I(\omega) \sim \int_{-\infty}^{\infty} \frac{d\omega'}{\omega'} \exp\left[-\frac{m_{\mathrm{A}} c^2}{2 k_{\mathrm{B}} T} \left(\frac{\omega - \omega'}{\omega'} \right)^2 \right] \cdot I_{\mathrm{pr}}(\omega). \tag{2.73}$$

The contribution of the pressure broadening is expressed as

$$I_{\mathrm{pr}}(\omega) = \mathrm{Im} \left\{ \sum_{ii'ff'} I^{f,f'}_{i,i'}(\omega) \cdot \langle i | \langle f | U(\omega) | f' \rangle | i' \rangle \right\} \tag{2.74}$$

with

$$\sum_{ii'ff'} I^{f,f'}_{i,i'}(\omega) = \langle i | \mathbf{r} | f \rangle \langle f' | \mathbf{r} | i' \rangle \cdot \frac{\omega^4}{8\pi^3 c^3} \cdot e^{-\hbar\omega/(k_{\mathrm{B}} T)}. \tag{2.75}$$

The evolution operator $U(\omega)$ is of essential importance for determining the spectral line shapes and can be taken in different approximations. For example, in the quasistatic approximation it is described by

$$U_{\mathrm{st}}(\omega) = \int_0^{\infty} d\beta \, P(\beta) \, L^{-1}(\omega, \beta) \tag{2.76}$$

with

$$L(\omega, \beta) = \hbar\omega - (E_i(\beta) - E_f(\beta)) + \mathrm{Re}\,(\Sigma_i - \Sigma_f) + i\mathrm{Im}\,(\Sigma_i + \Sigma_f) + i\Gamma^{\mathrm{V}}_{if} \tag{2.77}$$

The shift of the spectral lines is determined by the difference of the self-energies of the upper and lower level and there is no vertex contribution for the level shift. The displacement of the level energy accounting for the influence of the microfield is given by [GHR91]

$$E_i(\beta) = E^0_i + C(\beta), \tag{2.78}$$

where the energy shift $C(\beta)$ depends on the detailed microfield models. The electron and ion subsystems are assumed to be decoupled. Consequently, the self energy can be decomposed into a β-dependent ionic part and a frequency-dependent electronic part

$$\Sigma_{\nu\nu'}(\omega, \beta) = \Sigma^{\mathrm{el}}_{\nu\nu'}(\omega, \beta) + \Sigma^{\mathrm{ion}}_{\nu\nu'}(\beta). \tag{2.79}$$

In dynamically screened Born approximation, the electronic self-energy is given by [Gün95]

$$\Sigma_\nu^{\text{el}} = -\frac{1}{e^2} \int \frac{d^3\mathbf{q}}{(2\pi\hbar)^3} V(q) \sum_{\nu'} |M_{\nu\nu'}(\mathbf{q})|^2 \int_{-\infty}^{\infty} \frac{d\omega}{\pi} \left[1 + n_{\text{B}}(\omega)\right] \frac{\text{Im}\,\epsilon^{-1}(\mathbf{q}, \omega + i0)}{E_\nu - E_{\nu'} - (\hbar\omega + i0)}, \quad (2.80)$$

where $V(\mathbf{q})$ is the interaction potential between the transition electron in eigenstate E_ν and the plasma electrons with the momentum transfer $\mathbf{q}$. $n_{\text{B}}(\omega)$ and $\epsilon(\mathbf{q}, \omega + i0)$ are the Bose-Einstein distribution and the dielectric function, respectively. The calculations of spectral lines using the GF techniques will be discussed in detail in chapter 5.

2.3 Theory of open quantum systems

As we discussed in last Sec. 2.2, it is usually impossible to analytically determine the time evolution of the global system-environment combination. Therefore, a system + environment model is introduced in order to acquire the information of the system of interest and to describe the influence of the environment on investigated system. Alternative to the Green's function approach, the exact global dynamics of the combined system and the approximate evolution of the reduced system can also be described by the so-called quantum master equations in the theory of open quantum systems [Wei99, BP07, Röp13]. In this section, we review some fundamental concepts in the theory of open quantum systems and the general formalism of quantum master equations. More details can be found in Refs. [Sch07, BP07, Röp13].

2.3.1 System-environment coupling: quantum master equation

We consider a quantum subsystem ($\mathcal{S}$) with Hamiltonian $\hat{H}_{\text{sys}}(t)$. This subsystem is interacting with its surrounding environment ($\mathcal{E}$) whose Hamiltonian is $\hat{H}_{\text{en}}(t)$. The interaction potential between the subsystem and environment is described by $\hat{H}_{\text{int}}(t)$. Then the Hamiltonian of the total quantum system, which is generally assumed to be a closed system, reads

$$\hat{H}_{\text{total}}(t) = \hat{H}_{\text{sys}}(t) + \hat{H}_{\text{en}}(t) + \hat{H}_{\text{int}}(t). \quad (2.81)$$

Assumed that the Hamiltonian has no explicit time-dependence, then we have $\hat{H}_{\text{total}}(t) = \hat{H}_{\text{total}}$. The dynamics of the combined system can be described by the Liouville-von Neumann equation for the total density operator $\hat{\rho}(t)$

$$\frac{\partial}{\partial t}\hat{\rho}(t) - \frac{1}{i\hbar}\left[\hat{H}_{\text{total}}, \hat{\rho}(t)\right]_- = 0 \quad (2.82)$$

Generally, it is more convenient to work in the interaction picture for deriving the quantum master equation. Introducing the noninteracting Hamiltonian $\hat{H}_0(t)$ of the combined system, i.e., $\hat{H}_0(t) = \hat{H}_{\text{sys}}(t) + \hat{H}_{\text{en}}(t)$ we have

$$\hat{H}_{\text{int}}^{\text{I}}(t) = \exp\left(i\frac{\hat{H}_0}{\hbar}t\right)\hat{H}_{\text{int}}\exp\left(-i\frac{\hat{H}_0}{\hbar}t\right). \quad (2.83)$$

Then the Liouville-von Neumann equation (2.82) can be rewritten as

$$\frac{\partial}{\partial t}\hat{\rho}^{\text{I}}(t) = \frac{1}{i\hbar}\left[\hat{H}_{\text{int}}^{\text{I}}(t), \hat{\rho}^{\text{I}}(t)\right]_-. \quad (2.84)$$

Because only the properties of the subsystem $\mathcal{S}$ are relevant and of essential interest, we should transform this expression to a closed equation of motion for the reduced system. To accomplish this goal, the first step is to construct the density operator for the reduced system from the total density operator. This can be done by the so-called Nakajima-Zwanzig projection operator technique [BP07]. The corresponding reduced statistical operator for the subsystem $\mathcal{S}$ reads

$$\hat{\rho}_{\text{sys}}^{\text{I}}(t) \equiv \text{Tr}_{\text{en}}\,\hat{\rho}(t). \tag{2.85}$$

Then, the average value of any observable $\hat{\mathcal{S}}$ of the subsystem $\mathcal{S}$ is calculated as $\langle\hat{\mathcal{S}}\rangle^t \equiv \text{Tr}\{\hat{\mathcal{S}}\,\hat{\rho}(t)\} = \text{Tr}_{\text{sys}}\{\hat{\mathcal{S}}\,\hat{\rho}_{\text{sys}}(t)\}$. Formally integrating the Eq. (2.84) we arrive at

$$\hat{\rho}_{\text{sys}}^{\text{I}}(t) = \hat{\rho}_{\text{sys}}^{\text{I}}(0) - i\int_0^t dt'\left[\hat{H}_{\text{int}}^{\text{I}}(t'),\hat{\rho}^{\text{I}}(t')\right]_-. \tag{2.86}$$

Reinserting this resulting expression back into the Eq. (2.84), and performing the trace over all bath variables, the following expression can be obtained

$$\frac{\partial}{\partial t}\hat{\rho}_{\text{sys}}^{\text{I}}(t) = -\int_0^t dt'\,\text{Tr}_{\text{en}}\left[\hat{H}_{\text{int}}^{\text{I}}(t),\left[\hat{H}_{\text{int}}^{\text{I}}(t'),\hat{\rho}^{\text{I}}(t')\right]_-\right]_-. \tag{2.87}$$

The right side of Eq. (2.87), also known as influence term $\mathcal{L}[\hat{\rho}_{\text{sys}}^{\text{I}}(t)]$, can be generally divided into two parts [Sch07]

$$\mathcal{L}[\hat{\rho}_{\text{sys}}^{\text{I}}(t)] = -i\left[\hat{H}_{\text{sys}}'^{\text{I}}(t),\hat{\rho}^{\text{I}}(t)\right]_- + \mathcal{D}[\hat{\rho}_{\text{sys}}^{\text{I}}(t)]. \tag{2.88}$$

The first term is an unitary part describing the reformulation of the energy levels of the reduced system. The second term represents the decoherence and dissipation of the reduced system due to the environment. Generally, this term is of essential interest to us because most physical informations are contained in this term.

In deriving the expression (2.87), we have assumed

$$\text{Tr}_{\text{en}}\left[\hat{H}_{\text{sys}}^{\text{I}}(t),\hat{\rho}^{\text{I}}(0)\right]_- = 0. \tag{2.89}$$

This assumption can always be achieved, if necessary, by a formal redefinition of the Hamiltonians $\hat{H}_0^{\text{I}}$ and $\hat{H}_{\text{sys}}^{\text{I}}(t)$ [Sch07, Goc07, Röp13]. The expression (2.87) is exact and no approximations have been performed in the derivation. Evidently, equation (2.87) has no closed form, since the dynamics of the reduced system still depends on the total density operator $\hat{\rho}^{\text{I}}(t')$. Furthermore, equation (2.87) is non-local in time t because of the dependence on all previous times t' in the total density operator $\hat{\rho}^{\text{I}}(t')$. To obtain a closed quantum master equation that is local in time and is determined entirely by the reduced density operator $\hat{\rho}_{\text{sys}}^{\text{I}}$, some assumptions about the system-environment states and dynamics have to be introduced. This goal can be achieved by imposing the Born-Markov approximation, which is motivated from assumptions of weak system-environment couplings and of an environment that is large compared to the size of the system [Sch07, BP07].

Under the assumption of weak coupling between the system and its environment, a perturbative expansion can be carried out with respect to the interaction strength. In Born approximation, this expansion is truncated up to the second order of the system-environment coupling. Moreover, the combined density operator $\hat{\rho}^{\text{I}}(t)$ is assumed to be expressed in an approximate product form at all times

$$\hat{\rho}^{\text{I}}(t) \approx \hat{\rho}_{\text{sys}}^{\text{I}}(t) \otimes \hat{\rho}_{\text{en}}^{\text{I}}(t_0). \tag{2.90}$$

The environment is assumed to be in equilibrium with $\hat{\rho}_{\rm en}^{\rm I}(t) = \hat{\rho}_{\rm en}^{\rm I}(t_0) = \hat{\rho}_{\rm en}^{\rm I}$. Actually, performing the Born approximation is equivalent to construct a relevant statistical operator $\hat{\rho}_{\rm rel}(t) = \hat{\rho}_{\rm sys}(t)\hat{\rho}_{\rm en}$ that is fulfilling the condition of the maximum of information entropy for given constraints. The relevant statistical operator $\hat{\rho}_{\rm rel}(t)$ obeys the renormalization condition $\operatorname{Tr}\hat{\rho}_{\rm rel}(t) = 1$ and the self-consistency condition $\hat{\rho}_{\rm sys}(t) = \operatorname{Tr}_{\rm en}\hat{\rho}_{\rm rel}(t) = \operatorname{Tr}_{\rm en}\hat{\rho}(t)$ [Röp13].

The Markov approximation means that the memory effects on dynamical correlations of the environment are negligible [BP07, Sch07, Wei99, Röp13]. In other words, the dynamical corrections in the environment are destroyed so quickly that the reduced system is not aware of any changes of the environment at all previous times. Therefore, the dynamics of the relevant reduced system depends merely on the properties of the environment at the present time. Consequently, the density operator of the composite system $\hat{\rho}^{\rm I}(t')$ at a certain previous time t' can be replaced by $\hat{\rho}^{\rm I}(t)$, and the limit of the integration on the right-hand side of Eq. (2.87) can be extended to ∞. Taking these simplification into account, the Born-Markov master equation is obtained

$$\frac{\partial}{\partial t}\hat{\rho}_{\rm sys}^{\rm I}(t) = -\int_0^t dt'\, \operatorname{Tr}_{\rm en}\left[\hat{H}_{\rm int}^{\rm I}(t), \left[\hat{H}_{\rm int}^{\rm I}(t'), \hat{\rho}_{\rm sys}^{\rm I}(t)\,\hat{\rho}_{\rm en}^{\rm I}\right]_-\right]_-. \tag{2.91}$$

The interaction Hamiltonian is assumed to be in a diagonal and bilinear form with respect to the system operator $\mathcal{S}_\alpha$ and the environment operator $\mathcal{E}_\alpha$ [BP07, Sch07]

$$\hat{H}_{\rm int} = \sum_\alpha \mathcal{S}_\alpha \otimes \mathcal{E}_\alpha. \tag{2.92}$$

Inserting this expression into the Born-Markov master equation (2.91), a more explicit expression can be obtained [Sch07]

$$\frac{\partial}{\partial t}\hat{\rho}_{\rm sys}^{\rm I}(t) = -\int_0^\infty d\tau \sum_{\alpha\beta}\left\{\mathcal{C}_{\alpha\beta}(\tau)\cdot\left[\hat{\mathcal{S}}_\alpha(t)\,\hat{\mathcal{S}}_\alpha(t-\tau)\,\hat{\rho}_{\rm sys}^{\rm I}(t) - \hat{\mathcal{S}}_\alpha(t-\tau)\,\hat{\rho}_{\rm sys}^{\rm I}(t)\,\hat{\mathcal{S}}_\alpha(t)\right]\right.$$
$$\left. + \mathcal{C}_{\beta\alpha}(-\tau)\cdot\left[\hat{\rho}_{\rm sys}^{\rm I}(t)\,\hat{\mathcal{S}}_\beta(t-\tau)\,\hat{\mathcal{S}}_\alpha(t) - \hat{\mathcal{S}}_\alpha(t)\,\hat{\rho}_{\rm sys}^{\rm I}(t)\,\hat{\mathcal{S}}_\beta(t-\tau)\right]\right\}, \tag{2.93}$$

where $\mathcal{C}_{\alpha\beta}(\tau)$ is the spectral correlation tensor and is defined as

$$\mathcal{C}_{\alpha\beta}(\tau) = \langle\,\mathcal{E}_\alpha(\tau)\,\mathcal{E}_\beta\,\rangle_{\rm en}. \tag{2.94}$$

The expressions (2.91), (2.92) and (2.93) are the starting point for our study on the Rydberg states in plasmas in Chapter III.

To analyze the dynamical behavior of the reduced system under the influence of the environment, two different special system-environment couplings are usually preferred, i.e. the *Rotating-Wave coupling* and the *Feynman-Vernon coupling* [IMM03, BP07]. The Feynman-Vernon coupling is given in terms of the creation and annihilation operators of the reduced system $(\hat{a}, \hat{a}^\dagger)$ and of the environment $(\hat{b}_i, \hat{b}_i^\dagger)$

$$\hat{H}_{\rm int} = \sum_i (\hat{a} + \hat{a}^\dagger)\cdot(g_i\,\hat{b}_i + g_i^*\hat{b}_i^\dagger) \tag{2.95}$$

with the coupling strength g_i to the corresponding mode i of the environment. By neglecting the counter rotating terms $\hat{a}\,\hat{b}_i$ and $\hat{a}^\dagger\,\hat{b}_i^\dagger$ (rotating wave approximation), the Rotating-Wave coupling can be obtained

$$\hat{H}_{\rm int} = \sum_i (g_i^*\,\hat{a}\,\hat{b}_i^\dagger + g_i\,\hat{a}^\dagger\,\hat{b}_i). \tag{2.96}$$

This simplification leads different problems in corresponding special cases [IMM03, LGRR16], for examples, incorrect value for environmentally induced frequency shifts, and reduction of non-Markovianity in non-Markovian regime, see Ref. [LGRR16] and other references therein. We will return to this discussion in next Chapter and show that if the rotating wave approximation is carried out prematurely, it will be inappropriate to describe the dissipative properties of the relevant atomic system and results in erroneous transition rates [LGRR16].

2.3.2 Decoherence and localization

Due to the system-environment coupling, entanglements are generated between the system and environment, and therefore, a coherent state is formed. With time evolution, the coherence decay because of the scattering of the environment particles off the investigated particle. This process is known quantum decoherence [JZK$^+$03, BP07, Goc07]. When speaking of scattering off a macroscopic object, this process is generally denoted as localization and can be well described by the quantum Brownian motion [JZK$^+$03]. For simplicity, we only consider the motion in one space dimension with the corresponding equation of motion [JZK$^+$03]

$$i\frac{\partial}{\partial t}\hat{\rho}_{\text{sys}}(t) = \left[\hat{H}_{\text{sys}}, \hat{\rho}_{\text{sys}}(t)\right]_- - i\Lambda\left[\hat{x}, [\hat{x}, \hat{\rho}_{\text{sys}}(t)]_-\right]_-, \tag{2.97}$$

where Λ is the localization rate (also denoted as decoherence rate in a more general case) characterizing how fast the destruction of coherence between different positions is. Within the Caldeira-Leggett model [Wei99, BP07, Goc07], the localization rate $\Lambda = \gamma/\lambda_{\text{th}}^2$ depends on the thermal wavelength of the macroscopic object λ_{th} and the relaxation rate γ which is related to the effective scattering cross section contributing to the destruction of entanglement [DBD77, DBD79, SVY81, BP07]. The solution of the equation for Brownian motion of a free particle can be described by the following ansatz [JZK$^+$03]

$$\rho_{\text{sys}}(x, y, t) = \exp\Big\{ -A(t)\,(x-y)^2 + iB(t)\,(x+y)(x-y) + C(t)\,(x+y)^2$$
$$+ iK(t)\,(x-y) + L(t)\,(x+y) + D(t)\Big\}. \tag{2.98}$$

We consider a simplified but more explicit version of this ansatz

$$\rho_{\text{sys}}(x, y, t) = \rho_{\text{sys}}(x, y, 0) \cdot e^{-\Lambda\, t\, (x-y)^2}. \tag{2.99}$$

To get a feeling of the magnitude of the localization rate Λ, we show some examples for this quantity in the following table.

	$a = 10^{-5}\,\text{m}$	$a = 10^{-7}\,\text{m}$	$a = 10^{-8}\,\text{m}$
Cosmic background radiation	10^6	10^{-6}	10^{-12}
300 K photons	10^{19}	10^{12}	10^6
Sunlight on earth	10^{21}	10^{17}	10^{13}
Air molecules	10^{36}	10^{32}	10^{30}

Tab. 2.2: Localization rate Λ in unit of $\text{cm}^{-1}\text{s}^{-1}$ for a dust particle with spatial size a under different types of scattering environment [JZK$^+$03]

As an example, we consider a coupling system formed by four linearly distributed dust particles with width $\sigma = \sqrt{0.5}\,\mu\text{m}$ located in position $x_1 = -9\,\mu\text{m}$, $x_1 = -3\,\mu\text{m}$, $x_1 = 3\,\mu\text{m}$,

and $x_1 = 9\,\mu$m, respectively. Each spatially separated component can be described by a Gaussian wave packet

$$\psi_i(x) = \exp\left\{-\frac{(x-x_i)^2}{2\sigma^2}\right\}. \tag{2.100}$$

As an illustration of coherence and decoherence, we take a superposition of four Gaussian wave packets following the idea in Ref. [JZK$^+$03].

$$\Psi_{\text{wp}}(x) = \sum_{i=1}^{4} \psi_i(x) \tag{2.101}$$

with the density matrix in the position representation at the initial time $t_0 = 0$

$$\rho_{\text{sys}}(x,y,0) = \Psi_{\text{wp}}(x)\,\Psi_{\text{wp}}(y). \tag{2.102}$$
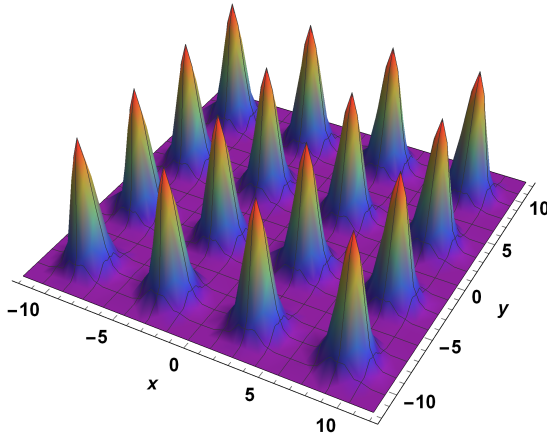
(a) Density matrix distribution $\rho_{\text{sys}}(x,y,t=0)$ (b) Density matrix distribution $\rho_{\text{sys}}(x,y,0.5\,\mu\text{s})$
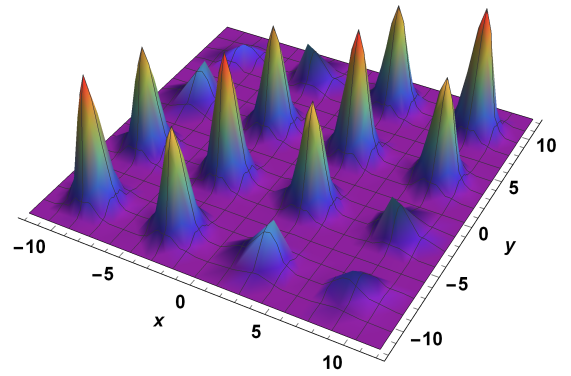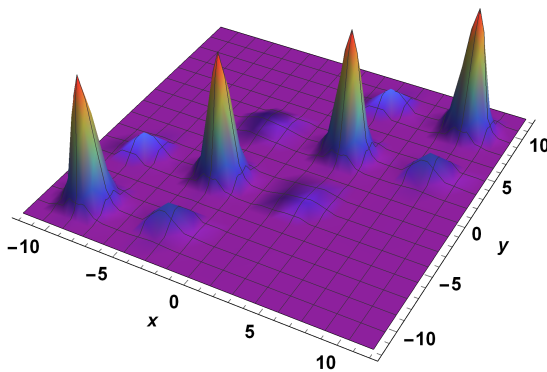
(c) Density matrix distribution $\rho_{\text{sys}}(x,y,5\,\mu\text{s})$ (d) Density matrix distribution $\rho_{\text{sys}}(x,y,15\,\mu\text{s})$

Abb. 2.4: Time evolution of the density matrix $\rho_{\text{sys}}(x,y,t)$ for the coupled system (2.101), where the positions x and y are in unit of μm.

Assumed that this coupling system is scattered by 300 K photons with the localization rate $10^{12}\,\mathrm{cm}^{-1}\mathrm{s}^{-1}$, see Tab. 2.2, the time evolution of the density matrix for this system can be depicted, as shown in Fig. 2.4. It can be seen that, the nondiagnol elements of the density matrix describing the system-environment entanglement disappear very fast because of the scattering with the thermal photons. In the viewpoint of quantum mechanis, the quantum feature of this coupled system is destroyed, and therefore, it can be treated as a classical system. This phenomenon, known as "appearance of a classical world in quantum theory" [JZK+03, Sch07], is universal for all microscopic and macroscopic objects, such as body cells, dust particle in air, astronomical objects and so on.

In contrast to the wave packet description for a free particle moving in a special environment, we will show in Chapter 3 that a wave packet description can also be formed for the bound Rydberg electron in an atom. The Rydberg electron undergoes frequent scattering with its surrounding particles which leads to a strong localization due to the weak coupling with the ion core. Consequently, the Rydberg electron can be described quasi-classically. Such a quasi-classical description turns out to be more appropriate to calculate the transition rates in plasmas.

2.3.3 Emission and absorption

Another famous application of the quantum master equation is in the investigation of the interaction of matter with electromagnetic field, where the transition rates induced by photons, the Lamb shift, the mass renormalization, and many other interest properties can be derived. Here we consider an atom coupled to the electromagnetic field [BP07, Röp13], which is studied in detail in my master thesis [Lin14]. The relevant system in this case is the atomic system with the Hamiltonian $\hat{H}_{\mathrm{sys}}$ including the kinetic energy of the electrons and the nuclei as well as the Coulomb coupling between them. The Hamiltonian of the bath $\hat{H}_{\mathrm{en}}$, i.e. of the electromagnetic field, is given by

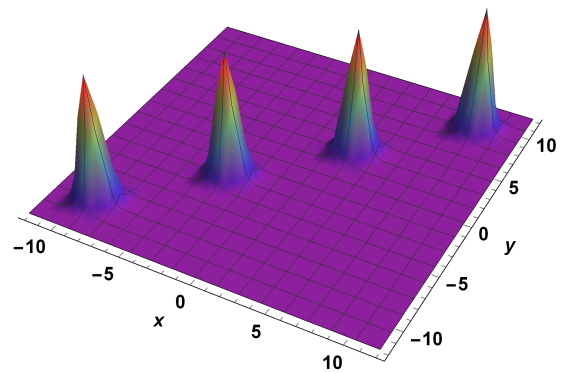$$\hat{H}_{\mathrm{en}} = \sum_{\mathbf{k}} \sum_{\lambda=1,2} \hbar\omega_{\mathbf{k}}\, \hat{b}_\lambda^\dagger(\mathbf{k})\hat{b}_\lambda(\mathbf{k}), \tag{2.103}$$

where $\hat{b}_\lambda^\dagger(\mathbf{k})$ and $\hat{b}_\lambda(\mathbf{k})$ are the creation and annihilation operator for the photon in the polarization mode $\mathbf{e}_\lambda(\mathbf{k})$ with energy $\hbar\omega_{\mathbf{k}}$. The interaction Hamiltonian can be represented as

$$\hat{H}_{\mathrm{int}}(t) = -\int_{-\infty}^{\infty} \frac{d\omega}{2\pi}\, e^{-i\omega t}\hat{\mathbf{D}}(\omega) \cdot \hat{\mathbf{E}}(t) \tag{2.104}$$

with the dipole operator in the spectral representation [Röp13]

$$\hat{\mathbf{D}}(\omega) = e\pi\hbar \sum_{n,n'} |\phi_n\rangle\langle\phi_n|\,\hat{\mathbf{r}}\,|\phi_{n'}\rangle\langle\phi_{n'}| \cdot \delta(E_n - E_{n'} + \hbar\omega) \tag{2.105}$$

and the vector for the electric field

$$\hat{\mathbf{E}}(t) = i \sum_{\mathbf{k}} \sum_{\lambda=1,2} \left(\frac{2\pi\hbar\omega_{\mathbf{k}}}{\Omega_0}\right)^{1/2} \mathbf{e}_\lambda(\mathbf{k}) \cdot \left\{\hat{b}_\lambda(\mathbf{k})\, e^{-i\omega_{\mathbf{k}}t} - \hat{b}_\lambda^\dagger(\mathbf{k})\, e^{i\omega_{\mathbf{k}}t}\right\}. \tag{2.106}$$

Inserting the interaction Hamiltonian into the Born-Markov QME, the so-called quantum optical master equation can be obtained [Röp13]

$$\frac{\partial}{\partial t}\hat{\rho}_{\mathrm{sys}}(t) - \frac{1}{i\hbar}\left[\hat{H}_{\mathrm{sys}}, \hat{\rho}_{\mathrm{sys}}(t)\right]_- - \frac{1}{i\hbar}\left[\hat{H}_{\mathrm{infl}}, \hat{\rho}_{\mathrm{sys}}(t)\right]_- = \mathcal{D}[\hat{\rho}_{\mathrm{sys}}(t)] \tag{2.107}$$

with the influence Hamiltonian describing the mass renormalization of the system

$$\hat{H}_{\text{infl}} = \int_{-\infty}^{\infty} \frac{d\omega}{2\pi} \, \hbar S(\omega) \, \hat{\mathbf{D}}^{\dagger}(\omega) \cdot \hat{\mathbf{D}}(\omega), \tag{2.108}$$

and the dissipation term containing information of the transition rates

$$\mathcal{D}[\hat{\rho}_{\text{sys}}(t)] = \int_{0}^{\infty} \frac{d\omega}{2\pi} \frac{4\omega^3}{3\hbar c^3} \cdot [1 + n_{\text{B}}(\omega)] \cdot \left\{ \hat{\mathbf{D}}(\omega) \, \hat{\rho}_{\text{sys}}(t) \, \hat{\mathbf{D}}^{\dagger}(\omega) - \frac{1}{2} \left\{ \hat{\mathbf{D}}^{\dagger}(\omega) \cdot \hat{\mathbf{D}}(\omega), \hat{\rho}_{\text{sys}}(t) \right\}_{+} \right\}$$
$$+ \int_{0}^{\infty} \frac{d\omega}{2\pi} \frac{4\omega^3}{3\hbar c^3} \cdot n_{\text{B}}(\omega) \cdot \left\{ \hat{\mathbf{D}}^{\dagger}(\omega) \, \hat{\rho}_{\text{sys}}(t) \, \hat{\mathbf{D}}(\omega) - \frac{1}{2} \left\{ \hat{\mathbf{D}}(\omega) \cdot \hat{\mathbf{D}}^{\dagger}(\omega), \hat{\rho}_{\text{sys}}(t) \right\}_{+} \right\}, \tag{2.109}$$

where $S(\omega)$ is the spectral function of the bath and reads

$$S(\omega) = \frac{2}{3\pi\hbar c^3} \mathcal{P} \int_{0}^{\infty} d\omega_k \, \omega_k^3 \cdot \left\{ \frac{1 + n_{\text{B}}(\omega)}{\omega - \omega_k} + \frac{n_{\text{B}}(\omega)}{\omega + \omega_k} \right\}, \tag{2.110}$$

where $\mathcal{P}$ denotes the principle value and c is the speed of light.

The first line of Eq. (2.109) describes the emission process in the electromagnetic field, where both the spontaneous emission and the thermal emission of photons are included. The second line of Eq. (2.109) gives the transition rate for the absorption of photons. As we can see here, the Einstein $A-$ and $B-$coefficients, which are expressed via the transition rates, are fulfilling.

2.4 Some open questions

We have reviewed the fundamental description of the Green's function technique and the open quantum system. Some well known applications are given. As discussed in Chapter 1, we devote ourselves to the optical properties in a plasma in the present investigation. Therefore, we collect some open questions that we will concentrate on in the rest part of this dissertation and in future researches.

1) Besides the interaction with the radiation field, the atom/ion immersed in a plasma is also influenced by Coulomb collision with other charged and neutral particles. This may be the most important interaction mechanism in plasmas, which results in a number of effects, for example, transition rates induced by charge carriers, pressure broadening of spectral lines, localization of particles, screening effects, conductivity, formation of bound states, and so on. Then an interesting and important question arises from this Coulomb interaction: how can we include the influence of a plasma environment?

2) What are robust states, in particular, for Rydberg states?

3) How does the atomic potential modified in a plasma in contrast to in the isolated case?

4) Which rules should we obey when defining a relevant system? What is the borderline between the relevant system and the irrelevant environment?

5) How can we go beyond the Born-Markov approximation?

3. TRANSITION RATES AND RYDBERG STATES IN PLASMAS

In this chapter, we derive a quantum master equation for an atom coupled to a heat bath represented by a charged particle many-body environment. In the Born-Markov approximation, the influence of the plasma environment on the reduced system is described by the dynamical structure factor. Wave packets are introduced as robust states allowing for a quasiclassical description of Rydberg electrons. Transition rates for highly excited Rydberg levels are investigated. A circular-orbit wave-packet approach has been applied in order to describe the localization of electrons within Rydberg states. The calculated transition rates are in a good agreement with experimental data and Monte-Carlo simulations. Based on the quantum master equation, expressions for the spectral lines are derived, where the photons are turned out to be relevant degrees of freedom in comparison with the case for deriving the Pauli equation. The main results of this chapter are published in Phys. Rev. A 93, 042711 (2016).

3.1 Pauli equation for population number of bound states

3.1.1 Physical system and Hamiltonians

We investigate the reduced system of a Rydberg atom (A) embedded in a bath (B) consisting of charged particles c , electrons ($c = e$) and (singly) charged ions ($c = i$), charge e_c, mass m_c, particle density n_c and temperature T. The microscopic model under consideration is a hydrogen atom coupled to a surrounding charge-neutral plasma, $\sum_c e_c n_c = 0$. In the bath, in general, the formation of bound states such as atoms is also possible. Furthermore, the interaction of the atom is mediated by the Maxwell field which contains, besides the Coulomb interaction with the charged particles, also single-particle states, the photons. The total system is then described by the Hamiltonian

$$\hat{H} = \hat{H}_{\mathrm{A}} + \hat{H}_{\mathrm{B}} + \hat{H}_{\mathrm{int}}. \tag{3.1}$$

In a plasma environment the Hamiltonian $\hat{H}_{\mathrm{B}}$ includes both the kinetic energy and the Coulomb interactions of charged particles $\hat{H}_{\mathrm{Coul}}$ (see Eq. (3.2) below) as well as the degrees of freedom of the photonic field $\hat{H}_{\mathrm{photon}}^{\perp}$ describing the transversal Maxwell field of the plasma environment, i.e. $\hat{H}_{\mathrm{B}} = \hat{H}_{\mathrm{Coul}} + \hat{H}_{\mathrm{photon}}^{\perp}$.

For the plasma, surrounding the radiating atom, the Hamiltonian containing both the kinetic energy and the pairwise Coulomb interaction is described by

$$\hat{H}_{\mathrm{Coul}} = \sum_{c,p} \frac{\hbar^2 p^2}{2 m_c} \hat{c}_p^{\dagger} \hat{c}_p + \frac{1}{2} \sum_{c,d,p_1 p_2, p_1' p_2'} \frac{e_c e_d}{\epsilon_0 \Omega_0 |\mathbf{p}_1' - \mathbf{p}_1|^2} \delta_{\mathbf{p}_1 + \mathbf{p}_2, \mathbf{p}_1' + \mathbf{p}_2'} \delta_{\sigma_1, \sigma_1'} \delta_{\sigma_2, \sigma_2'} \hat{c}_{p_1}^{\dagger} \hat{d}_{p_2}^{\dagger} \hat{d}_{p_2'} \hat{c}_{p_1'} \tag{3.2}$$

where we used second quantization $\hat{c}_p, \hat{c}_p^\dagger$ for free particle states $|p\rangle = |\mathbf{p}, \sigma\rangle$ (wave vector and spin) of charge c. The grand canonical equilibrium (3.10) contains also the particle number operator $\hat{N}_c = \sum_p \hat{c}_p^\dagger \hat{c}_p$. The macroscopic state of the bath is fixed by the Lagrange multipliers μ_c and T. Ω_0 is the volume of the total system. Because of charge neutrality $\sum_c e_c \hat{N}_c \equiv 0$ both μ_e, μ_i are related.

The transversal Maxwell field

$$\hat{H}_{\text{photon}}^\perp = \sum_{\mathbf{k},s} \hbar \omega_{\mathbf{k},s} \hat{n}_{\mathbf{k},s} \tag{3.3}$$

is quantized and denoted by the photon modes $|\mathbf{k}, s\rangle$. The frequency $\omega_{\mathbf{k}} = c|\mathbf{k}| = 2\pi c/\lambda$ is the dispersion relation for the frequency as a function of the wave number $\mathbf{k}$. $\hat{n}_{\mathbf{k},s} = \hat{b}_{\mathbf{k},s}^\dagger \hat{b}_{\mathbf{k},s}$ is the occupation number with the polarization $s = 1, 2$.

The atomic Hamiltonian reads in the non-relativistic case

$$\hat{H}_{\text{A}} = \frac{\hat{\mathbf{P}}^2}{2M} + \frac{\hat{\mathbf{p}}^2}{2m} - \frac{e^2}{4\pi\varepsilon_0 |\hat{\mathbf{r}}|} , \tag{3.4}$$

where the center-of-mass (c.o.m.) motion is described by the total mass $M = m_e + m_i$ and the variables $\hat{\mathbf{R}}, \hat{\mathbf{P}}$, the relative motion by the reduced mass m and the relative variables $\hat{\mathbf{r}}, \hat{\mathbf{p}}$. The eigenstates $|\Psi_{n,\mathbf{P}}\rangle$ of the isolated hydrogen atom are the solutions of the Schrödinger equation $\hat{H}_A |\Psi_{n,\mathbf{P}}\rangle = E_{n,\mathbf{P}} |\Psi_{n,\mathbf{P}}\rangle$ with the eigenenergy $E_{n,\mathbf{P}} = \mathbf{P}^2/(2M) + E_n$. The quantum number $n = \{\bar{n}, l, m, m_s\}$ describes the internal state for bound states $E_n < 0$ and $n = \{\mathbf{p}, m_s\}$ for scattering states $E_{\mathbf{p}} = \mathbf{p}^2/(2m) > 0$. For the bound states, the wave function $\Psi(\mathbf{R}, \mathbf{r}) = \langle \mathbf{R}, \mathbf{r} | \Psi_{n,\mathbf{P}} \rangle = \Psi_{\mathbf{P}}(\mathbf{R}) \psi_n(\mathbf{r})$ contains the eigenstates $\psi_n(\mathbf{r})$ of the hydrogen atom. The c.o.m. motion $\Psi_{\mathbf{P}}(\mathbf{R})$ is given by a plane wave. In this work we concentrate on the internal degrees of freedom of the bound states. The c.o.m motion, which, e.g., determines the Doppler broadening of the spectral line profile, will not be discussed here in detail. In most cases it will be dropped considering the adiabatic limit.

The interaction between the atomic electron and the plasma environment is given by the coupling of the atomic current operator to the electromagnetic field of the bath

$$\hat{H}_{\text{int}}(t) = \int d^3\mathbf{r} \hat{j}_{\text{A}}^\mu(x) \hat{A}_{\mu,\text{B}}(x) \tag{3.5}$$

with $x^\mu = \{ct, \mathbf{r}\}$. Introducing the creation $(\hat{\psi}^\dagger(x))$ and annihilation $(\hat{\psi}(x))$ operator for the atomic electron, the current operator of the atomic subsystem $\hat{j}_{\text{A}}^\mu(x) = \{c\hat{\varrho}_{\text{A}}(x), \hat{\mathbf{j}}_{\text{A}}(x)\}$ can be explicitly written as $\hat{\varrho}_{\text{A}}(x) = -e\hat{\psi}^\dagger(x)\hat{\psi}(x)$ for the electron probability density and $\hat{\mathbf{j}}_{\text{A}}(x) = \frac{ie\hbar}{2m_e}\left[\hat{\psi}^\dagger(x)\frac{\partial}{\partial\mathbf{r}}\hat{\psi}(x) - \left(\frac{\partial}{\partial\mathbf{r}}\hat{\psi}^\dagger(x)\right)\hat{\psi}(x)\right]$ for the electric current density of the electron (non-relativistic limit). The time-dependence in these operators are given in Heisenberg picture.

The source of the electromagnetic field of the bath $\hat{A}_{\text{B}}^\mu(x) = (\hat{U}_{\text{B}}(x), \hat{\mathbf{A}}_{\text{B}}(x))$ is the current density $\hat{j}_{\text{B}}^\mu(x)$ of all charge carriers in the plasma. In the present work the Coulomb gauge $\nabla \times \hat{\mathbf{A}}_{\text{B}}(x) = 0$ is used. The Fourier transform

$$\hat{\mathbf{j}}_{\mathbf{q},\text{B}}(\omega) = \int_{\Omega_0} d^3\mathbf{r} \int_{-\infty}^{\infty} dt e^{i\omega t - i\mathbf{q}\cdot\mathbf{r}} \hat{\mathbf{j}}_{\text{B}}(t, \mathbf{r}) \tag{3.6}$$

of the electrical current in the surrounding plasma can be decomposed into a transverse component $\sum_c \hat{\mathbf{j}}_{\mathbf{q},\text{B}}^{\perp,c}(\omega)$ coupled only to the vector potential $\hat{\mathbf{A}}_{\mathbf{q},\text{B}}(\omega)$ and a longitudinal one

$\sum_c \hat{j}^{||,c}_{\mathbf{q},\mathrm{B}}(\omega)\mathbf{q}/q$ which is related only to the Coulomb potential. Because of the continuity equation, the relation $\mathbf{q} \cdot \hat{\mathbf{j}}_{\mathbf{q},\mathrm{B}}(\omega) = q\hat{j}^{||}_{\mathbf{q},\mathrm{B}}(\omega) = \omega\hat{\varrho}_{\mathbf{q},\mathrm{B}}(\omega)$

$$\mathbf{q} \cdot \mathbf{j}_{\mathbf{q},\mathrm{B}}(\omega) = qj^{||}_{\mathbf{q},\mathrm{B}}(\omega) = \omega n_{\mathbf{q},\mathrm{B}}(\omega) \tag{3.7}$$

holds, where $\hat{\varrho}_{\mathbf{q}}(\omega)$ is the Fourier transform of the corresponding charge density operator $\hat{\varrho}(x)$.

The general form of the interaction (3.5) includes the Coulomb interaction via the longitudinal component of the currents, and the coupling of the transverse component of the currents with the radiation field. We do not investigate the radiation interaction connected with the transverse component. The radiative field of the plasma determines the natural broadening which has already been extensively discussed in [BP07, Röp13] by using the quantum master equation approach. However we focus on the Coulomb interaction of the hydrogen atom with its surrounding charged particles in this work. In this case, the distribution and the motion of the charge carriers in the plasma produce a scalar potential which is given in terms of the longitudinal current [Rei05]:

$$\hat{U}_{\mathbf{q},\mathrm{B}}(\omega) = \sum_c \frac{\hat{\varrho}^c_{\mathbf{q},\mathrm{B}}(\omega)}{\epsilon_0 \mathbf{q}^2} = \sum_c \frac{\hat{j}^{||,c}_{\mathbf{q},\mathrm{B}}(\omega)}{\epsilon_0 \omega q}. \tag{3.8}$$

This results in the pressure broadening of the spectral lines as shown in Sec. 3.3.

3.1.2 General quantum master equation

The state of the total system is described by the statistical operator $\hat{\rho}(t)$. We assume that the observables $\hat{A}$ of the subsystem A commute with the observables $\hat{B}$ of the bath B. If only the properties of the subsystem A are relevant, we can consider the corresponding statistical operator

$$\hat{\rho}_\mathrm{A}(t) \equiv \mathrm{Tr}_\mathrm{B}\, \hat{\rho}(t) \tag{3.9}$$

performing the trace over all bath variables. Then, the average value of any observable $\hat{A}$ of the subsystem A is calculated as $\langle\hat{A}\rangle^t \equiv \mathrm{Tr}\{\hat{A}\,\hat{\rho}(t)\} = \mathrm{Tr}_\mathrm{A}\{\hat{A}\,\hat{\rho}_\mathrm{A}(t)\}$. The equilibrium state $\hat{\rho}_\mathrm{B}$ of the bath B is assumed as the grand canonical distribution

$$\hat{\rho}_\mathrm{B} = \frac{1}{Z_\mathrm{B}}\exp\left[-\frac{\hat{H}_\mathrm{B} - \sum_c \mu_c \hat{N}_c}{k_B T}\right], \qquad Z_\mathrm{B} = \mathrm{Tr}_\mathrm{B}\exp\left[-\frac{\hat{H}_\mathrm{B} - \sum_c \mu_c \hat{N}_c}{k_B T}\right] \tag{3.10}$$

with the chemical potentials μ_c of the species c.

If the bath is assumed to have short memory in the sense that the correlation in the bath decays very quickly in comparison to the time evolution of the reduced system (Markov approximation), and the dynamics of the reduced system is considered only in second order with respect to $\hat{H}_\mathrm{int}$ (Born approximation), a closed equation of motion can be derived for the reduced statistical operator $\hat{\rho}_\mathrm{A}(t)$ of the subsystem A by performing the average with respect to the bath in (2.82), i.e., the Born-Markov master equation [Röp13], as discussed in the last chapter,

$$\frac{\partial}{\partial t}\hat{\rho}_\mathrm{A}(t) - \frac{1}{i\hbar}[\hat{H}_\mathrm{A}, \hat{\rho}_\mathrm{A}(t)] = \mathcal{D}[\hat{\rho}_\mathrm{A}(t)] \tag{3.11}$$

with the influence term

$$\mathcal{D}[\hat{\rho}_\mathrm{A}(t)] = -\frac{1}{\hbar^2}\int_{-\infty}^0 d\tau\, e^{\varepsilon\tau}\, \mathrm{Tr}_\mathrm{B}\left[\hat{H}_\mathrm{int}, \left[\hat{H}_\mathrm{int}(\tau), \hat{\rho}_\mathrm{A}(t)\hat{\rho}_\mathrm{B}\right]\right]. \tag{3.12}$$

This is the quantum master equation (QME) in Born-Markov approximation. To go beyond the Born approximation, a more general solution has been given in [ZMR97].

Born approximation indicates that higher orders of the interaction Hamiltonian in the time evolution of the operator " $\exp\left\{-i\left(\hat{H}_0 + \hat{H}_{\text{int}}\right) t\right\}$ " can be dropped. Consequently, the time dependence in Born approximation is given by the interaction picture

$$\hat{O}^{\text{I}}(t, t_0) = e^{i(\hat{H}_{\text{A}} + \hat{H}_{\text{B}})(t-t_0)/\hbar} \, \hat{O} \, e^{-i(\hat{H}_{\text{A}} + \hat{H}_{\text{B}})(t-t_0)/\hbar}. \tag{3.13}$$

At $t = t_0$, the interaction picture coincides with the Schrödinger picture. Note that the time of reference t_0 is often taken as zero. In interaction picture, the QME in Born-Markov approximation reads

$$\frac{\partial}{\partial t} \hat{\rho}^{\text{I}}_{\text{A}}(t, t_0) = \mathcal{D}^{\text{I}}(t, t_0), \tag{3.14}$$

i.e., only the perturbation determines the time evolution of $\hat{\rho}^{\text{I}}_{\text{A}}(t, t_0)$ (note that $\hat{H}_{\text{B}}$ commutes with $\hat{\rho}_{\text{A}}(t)$). The influence term in interaction representation follows as

$$\mathcal{D}^{\text{I}}(t, t_0) = -\frac{1}{\hbar^2} \int_{-\infty}^{0} d\tau \, e^{\varepsilon\tau} \, \text{Tr}_{\text{B}} \left[\hat{H}^{\text{I}}_{int}(t, t_0), \left[\hat{H}^{\text{I}}_{int}(t+\tau, t_0), \hat{\rho}^{\text{I}}_{\text{A}}(t, t_0)\hat{\rho}_{\text{B}} \right] \right]. \tag{3.15}$$

In zeroth order with respect to the perturbation, $\hat{\rho}^{\text{I}}_{\text{A}}(t, t_0)$ is constant, therefore not changing with time t.

3.1.3 Atomic quantum master equation and Pauli equation

In this section the master equation for the reduced statistical operator (3.14) shall be applied to atomic bound states in a many-particle plasma environment. However, most of the discussion is valid for a much more general case.

The photonic field $\hat{H}^{\perp}_{\text{photon}}$ is not relevant in our present consideration for the Pauli equation in this section. We focuss on the Coulomb interaction with the charged particles of the bath. The longitudinal part of the interaction Hamiltonian can be extracted from the general form $\hat{H}_{\text{int}}$ (3.5) by using the expression (3.8) and performing the Fourier transform with respect to the time for the atomic charge density operator

$$\hat{\varrho}^{\text{I}}_{\mathbf{q},\text{A}}(t, t_0) = \int_{-\infty}^{\infty} \frac{d\omega}{2\pi} \, e^{-i\omega(t-t_0)} \, \hat{\varrho}^{\text{I}}_{\mathbf{q},\text{A}}(\omega) \tag{3.16}$$

so that

$$\hat{H}^{\text{I},\,\|}_{\text{int}}(t, t_0) = \sum_{\mathbf{q}} \frac{1}{\epsilon_0 q^2 \Omega_0} \int \frac{d\omega}{2\pi} \, e^{-i\omega(t-t_0)} \, \hat{\varrho}^{\text{I}}_{\mathbf{q},\text{A}}(\omega) \hat{\varrho}^{\text{I}}_{-\mathbf{q},\text{B}}(t, t_0) \tag{3.17}$$

with $\hat{\varrho}_{\mathbf{q},\text{B}} = \sum_c \hat{\varrho}^c_{\mathbf{q},\text{B}}$ and $\hat{\varrho}^c_{\mathbf{q},\text{B}} = \sum_p e_c \hat{c}^{\dagger}_{\mathbf{p}-\mathbf{q}/2,\sigma} \hat{c}_{\mathbf{p}+\mathbf{q}/2,\sigma}$. In this work only the contribution of the electrons in the plasma is considered. Because of the large mass ratio, the ionic contribution related to the microfield should be treated in a different way. Coming back to the influence term (3.15), the factorization of the interaction Hamiltonian allows us to perform the average over the bath degrees of freedom separately

$$\mathcal{D}^{\text{I}}(t, t_0) = -\frac{1}{\hbar^2} \int_{-\infty}^{0} d\tau \, e^{\varepsilon\tau} \sum_{q,q'} \frac{1}{\epsilon_0^2 q^2 q'^2 \Omega_0^2} \int \frac{d\omega}{2\pi} \int \frac{d\omega'}{2\pi} \, e^{-i(\omega+\omega')(t-t_0)-i\omega'\tau} \tag{3.18}$$

$$\times \left\{ \left[\hat{\varrho}^{\text{I}}_{\mathbf{q},\text{A}}(\omega)\hat{\varrho}^{\text{I}}_{\mathbf{q}',\text{A}}(\omega')\hat{\rho}^{\text{I}}_{\text{A}}(t, t_0) - \hat{\varrho}^{\text{I}}_{\mathbf{q}',\text{A}}(\omega')\hat{\rho}^{\text{I}}_{\text{A}}(t, t_0)\hat{\varrho}^{\text{I}}_{\mathbf{q},\text{A}}(\omega) \right] \langle \hat{\varrho}^{\text{I}}_{-\mathbf{q},\text{B}}(t, t_0)\hat{\varrho}^{\text{I}}_{-\mathbf{q}',\text{B}}(t+\tau, t_0) \rangle_{\text{B}} \right.$$

$$\left. - \left[\hat{\varrho}^{\text{I}}_{\mathbf{q},\text{A}}(\omega)\hat{\rho}^{\text{I}}_{\text{A}}(t, t_0)\hat{\varrho}^{\text{I}}_{\mathbf{q}',\text{A}}(\omega') - \hat{\rho}^{\text{I}}_{\text{A}}(t, t_0)\hat{\varrho}^{\text{I}}_{\mathbf{q}',\text{A}}(\omega')\hat{\varrho}^{\text{I}}_{\mathbf{q},\text{A}}(\omega) \right] \langle \hat{\varrho}^{\text{I}}_{-\mathbf{q}',\text{B}}(t+\tau, t_0)\hat{\varrho}^{\text{I}}_{-\mathbf{q},\text{B}}(t, t_0) \rangle_{\text{B}} \right\}$$

with $\langle \cdots \rangle_B = \mathrm{Tr}_B \{\cdots \hat{\rho}_B\}$. The autocorrelation function $\langle \hat{\varrho}^I_{-\mathbf{q},B}(t, t_0) \hat{\varrho}^I_{-\mathbf{q}',B}(t + \tau, t_0) \rangle_B$ for the charge density is calculated in thermodynamic equilibrium. Because of homogeneity in space and time it is $\propto \delta_{\mathbf{q}',-\mathbf{q}}$ and not depending on the time t as well as t_0. We introduce the Laplace transform of the bath auto-correlation functions which can be also defined as the response function

$$\Gamma_r(\mathbf{q}, \omega) = \frac{1}{\hbar^2} \int_{-\infty}^0 d\tau\, e^{\varepsilon\tau} e^{-i\omega\tau} \langle \hat{\varrho}^I_{-\mathbf{q},B}(t_0, t_0) \hat{\varrho}^I_{\mathbf{q},B}(t_0 + \tau, t_0) \rangle_B. \tag{3.19}$$

The response function $\Gamma_r(\mathbf{q}, \omega)$ is a complex physical quantity which is related to the dynamical structure factor of the plasma or the dielectric function, as shown in the App. A. It can be decomposed into real and imaginary parts,

$$\Gamma_r(\mathbf{q}, \omega) = \frac{1}{2} \gamma_r(\mathbf{q}, \omega) + i S_r(\mathbf{q}, \omega), \tag{3.20}$$

where $\gamma_r(\mathbf{q}, \omega)$ and $S_r(\mathbf{q}, \omega)$ are both real functions. They fulfill the Kramers-Kronig relation and are related to the damping and the spectral line shift, respectively (for details see next subsection).

With the response function (3.19), we find that the influence term (3.15) can be rewritten as

$$\mathcal{D}^I(t, t_0) = -\sum_q \frac{1}{\epsilon_0^2 q^4 \Omega_0^2} \int \frac{d\omega}{2\pi} \int \frac{d\omega'}{2\pi} e^{i(\omega'-\omega)(t-t_0)} \Gamma_r(\mathbf{q}, -\omega') \left[\hat{\varrho}^I_{\mathbf{q},A}(\omega), \hat{\varrho}^I_{-\mathbf{q},A}(-\omega') \hat{\rho}^I_A(t, t_0) \right]$$
$$+ \text{h.c.} \tag{3.21}$$

The second contribution of the r.h.s. of Eq. (3.21) is the hermitean conjugate of the first contribution so that $\mathcal{D}^I(t, t_0)$ is a real quantity. Approximations for the response function $\Gamma_r(\mathbf{q}, \omega)$ are obtained from the approximations for the dielectric function such as the random-phase approximation and improvements accounting for collisions.

In a next step we introduce the orthonormal basis of the hydrogen bound states in the Hilbert space of the atomic subsystem to obtain the Pauli equation for population numbers. We use the basis of hydrogen-like states $|\psi_n\rangle$ of the Hamiltonian $\hat{H}_A$. For the charge density operator

$$\hat{\varrho}_{\mathbf{q},A} = \int d^3\bar{r}\, e^{i\mathbf{q}\cdot\bar{\mathbf{r}}} \hat{\varrho}_A(\bar{\mathbf{r}}) = \int d^3\bar{r}\, e^{i\mathbf{q}\cdot\bar{\mathbf{r}}} [e_e \delta(\hat{\mathbf{r}}_e - \bar{\mathbf{r}}) + e_i \delta(\hat{\mathbf{r}}_i - \bar{\mathbf{r}})] = e_e\, e^{i\mathbf{q}\cdot\hat{\mathbf{r}}_e} + e_i\, e^{i\mathbf{q}\cdot\hat{\mathbf{r}}_i}, \tag{3.22}$$

the time dependence in the interaction picture can be written in matrix representation as $(e_e = -e_i)$

$$\hat{\varrho}^I_{\mathbf{q},A}(t, t_0) = e^{\frac{i}{\hbar}\hat{H}_A(t-t_0)} \hat{\varrho}_{\mathbf{q},A}\, e^{-\frac{i}{\hbar}\hat{H}_A(t-t_0)} = \sum_{nn'} e_e \hat{T}_{n'n}\, F_{n'n}(\mathbf{q})\, e^{-i\omega_{nn'}(t-t_0)} \tag{3.23}$$

with

$$\hat{T}_{n'n} = |\psi_{n'}\rangle\langle\psi_n|, \tag{3.24}$$

$$\omega_{nn'} = \frac{E_n - E_{n'}}{\hbar}, \tag{3.25}$$

$$F_{n'n}(\mathbf{q}) = \int d^3\mathbf{r}\, \psi_{n'}^*(\mathbf{r}) \psi_n(\mathbf{r})\, (1 - e^{-i\mathbf{q}\cdot\mathbf{r}}), \tag{3.26}$$

in adiabatic approximation $m_e \ll m_i$. Furthermore, the atom is assumed to be localized at $\mathbf{R} = 0$. Performing the Fourier transformation with respect to t we obtain the atomic charge density in Fourier-space

$$\hat{\varrho}_{\mathbf{q},\mathrm{A}}^{\mathrm{I}}(\omega) = \sum_{nn'} e_e \hat{T}_{n'n} \, F_{n'n}(\mathbf{q}) \, 2\pi \, \delta(\omega - \omega_{nn'}). \tag{3.27}$$

With Eq. (3.27) the influence function (3.21) can be represented as

$$\mathcal{D}^{\mathrm{I}}(t,t_0) = - \sum_{nn',mm',\mathbf{q}} e^{-i(\omega_{nn'}+\omega_{mm'})(t-t_0)} K_{mm';n'n}(\mathbf{q},\omega_{mm'})$$
$$\times \left\{ \hat{T}_{n'n}\hat{T}_{m'm}\hat{\rho}_{\mathrm{A}}^{\mathrm{I}}(t,t_0) - \hat{T}_{m'm}\hat{\rho}_{\mathrm{A}}^{\mathrm{I}}(t,t_0)\hat{T}_{n'n} \right\} + \mathrm{h.c.} \tag{3.28}$$

with

$$K_{mm';n'n}(\mathbf{q},\omega) = \frac{e_e^2}{\epsilon_0^2 q^4 \Omega_0^2} \, F_{mm'}^*(\mathbf{q}) F_{n'n}(\mathbf{q}) \, \Gamma_r(\mathbf{q},\omega) \tag{3.29}$$

containing informations about the atomic system, the plasma bath and the interaction between them. In matrix representation the atomic QME (3.14) can be represented as ($|\psi_i\rangle$ - initial state, $|\psi_f\rangle$ - final state)

$$\frac{\partial}{\partial t} \rho_{\mathrm{A},if}^{\mathrm{I}}(t,t_0) = \langle \psi_i | \mathcal{D}^{\mathrm{I}}(t,t_0) | \psi_f \rangle \tag{3.30}$$

with the influence function

$$\langle \psi_i | \mathcal{D}^{\mathrm{I}}(t,t_0) | \psi_f \rangle = - \sum_{mn,\mathbf{q}} \left\{ e^{i\omega_{im}(t-t_0)} K_{mn;in}(\mathbf{q},\omega_{mn}) \, \rho_{\mathrm{A},mf}^{\mathrm{I}}(t,t_0) \right. \tag{3.31}$$
$$+ e^{i\omega_{mf}(t-t_0)} K_{mn;nf}^*(\mathbf{q},\omega_{nf}) \, \rho_{\mathrm{A},im}^{\mathrm{I}}(t,t_0)$$
$$\left. - e^{i(\omega_{im}+\omega_{nf})(t-t_0)} \left[K_{mi;fn}(\mathbf{q},\omega_{mi}) + K_{nf;mi}^*(\mathbf{q},\omega_{nf}) \right] \rho_{\mathrm{A},mn}^{\mathrm{I}}(t,t_0) \right\}$$

with the density matrix $\rho_{\mathrm{A},mn}^{\mathrm{I}}(t,t_0) = \langle \psi_m | \hat{\rho}_{\mathrm{A}}^{\mathrm{I}}(t,t_0) | \psi_n \rangle$. The corresponding atomic QME in Schrödinger picture is obtained with $\rho_{\mathrm{A},mn}^{\mathrm{I}}(t,t_0) = e^{i\omega_{mn}(t-t_0)} \rho_{\mathrm{A},mn}(t)$.

Now, we investigate the diagonal elements of the density matrix by setting $i = f$ in the above expression (3.30). This leads to an equation for the population number $P_i(t) = \rho_{\mathrm{A},ii}^{\mathrm{I}}(t,t_0) = \rho_{\mathrm{A},ii}(t)$

$$\frac{\partial P_i(t)}{\partial t} = \sum_{n,\mathbf{q}} \left[k_{ni}(\mathbf{q},\omega_{ni}) P_n(t) - k_{in}(\mathbf{q},\omega_{in}) P_i(t) \right]$$
$$- \sum_{n,m\neq i,\mathbf{k}} 2\mathrm{Re}\left[e^{i\omega_{im}(t-t_0)} K_{mn;in}(\mathbf{q},\omega_{mn}) \right] \rho_{\mathrm{A},mi}^{\mathrm{I}}(t,t_0)$$
$$+ \sum_{m>n,\mathbf{q}} 2\mathrm{Re}\left\{ e^{i\omega_{nm}(t-t_0)} \left[K_{ni;mi}^*(\mathbf{q},\omega_{ni}) + K_{mi;in}(\mathbf{q},\omega_{mi}) \right] \right\} \rho_{\mathrm{A},mn}^{\mathrm{I}}(t,t_0) \tag{3.32}$$

with $k_{ab}(\mathbf{q},\omega_{ab}) = 2\,\mathrm{Re}\,K_{ab;ab}(\mathbf{q},\omega_{ab}) = e_e^2 \, |F_{ab}(\mathbf{q})|^2 \, \gamma_r(\mathbf{q},\omega_{ab})/(\epsilon_0^2 q^4 \Omega_0^2)$, where expression (3.20) is used and the indices m and n are interchanged in the derivation. The interaction picture shows a slow time dependence in $\rho_{\mathrm{A},nm}^{\mathrm{I}}(t,t_0)$ owing to the influence of the bath, Eq. (3.14), and a quick time variation due to the factor $e^{i\omega_{nm}(t-t_0)}$ with $\omega_{nm} \neq 0$. The second and third

term oscillate with the characteristic transition frequencies ω_{nm} and ω_{im}, respectively. Subsequently their contributions vanish when averaging over a time interval large in comparison to the inverse of the characteristic transition frequencies, because the population numbers are approximately constant. This is the so-called *Rotating Wave Approximation* (RWA). For the long-term evolution of the reduced system the nondiagonal elements in Eq. (3.32) can be neglected and consequently we obtain a closed rate equation for the population number – the Pauli equation:

$$\frac{\partial P_i(t)}{\partial t} = \sum_{n,\mathbf{q}} \left[k_{ni}(\mathbf{q}, \omega_{ni}) P_n(t) - k_{in}(\mathbf{q}, \omega_{in}) P_i(t) \right]. \tag{3.33}$$

Comparing with the standard form of the Pauli equation $\frac{\partial}{\partial t} P_i(t) = \sum_n [w_{n \to i} P_n(t) - w_{i \to n} P_i(t)]$, we have for the transition rates

$$w_{n \to i} = \sum_{\mathbf{q}} k_{ni}(\mathbf{q}, \omega_{ni}) = \sum_{\mathbf{q}} \frac{e_e^2 |F_{ni}(\mathbf{q})|^2 \gamma_r(\mathbf{q}, \omega_{ni})}{\epsilon_0^2 q^4 \Omega_0^2}, \tag{3.34}$$

$$w_{i \to n} = \sum_{\mathbf{q}} k_{in}(\mathbf{q}, \omega_{in}) = \sum_{\mathbf{q}} \frac{e_e^2 |F_{in}(\mathbf{q})|^2 \gamma_r(\mathbf{q}, \omega_{in})}{\epsilon_0^2 q^4 \Omega_0^2}. \tag{3.35}$$

To derive the Pauli equation we used the RWA which neglects quickly oscillating terms. Also the dependence on the time t_0 where the interaction picture coincides with the Schrödinger picture disappears. The validity of the RWA in the theory of open quantum systems is under discussion. The dynamics is modified if contributions of the right hand side of Eq. (3.32) are dropped. As we will see in next subsection, if the RWA is carried out prematurely, it will be inappropriate to describe the dissipative properties of the relevant atomic system (Rydberg states) and results in erroneous transition rates. Additionally, the nondiagonal elements of Eq. (3.30) are also derived as well as a principle discussion on the validity of the RWA is given.

3.1.4 Rotating wave approximation

In this subsection, we will investigate the influence of the RWA on the dynamics of the reduced system. The neglect of quickly oscillating terms in Eq. (3.32) modifies the dynamics of the system. This procedure depends on the choice of the basis $|\psi_n\rangle$ which defines the diagonal and non-diagonal elements of the density matrix.

In contrast to the expressions given in subsec. 3.1.3, we here consider the result if performing the RWA in an earlier stage. The starting point is the QME (3.14) (interaction picture) with the influence function (3.28). The RWA implies that the explicit dependence on $t - t_0$ disappears so that in Eq. (3.28) only the terms with $m = n'$ and $m' = n$ contribute. We find

$$\hat{\mathcal{D}}^{\mathrm{I}}_{(1)}(t, t_0) = - \sum_{nn',\mathbf{q}} K_{n'n;n'n}(\mathbf{q}, \omega_{n'n}) \left\{ \hat{T}_{n'n'} \hat{\rho}^{\mathrm{I}}_{\mathrm{A}}(t, t_0) - \hat{T}_{nn'} \hat{\rho}^{\mathrm{I}}_{\mathrm{A}}(t, t_0) \hat{T}_{n'n} \right\} + \mathrm{h.c.} \tag{3.36}$$

In addition the explicit dependence on $t - t_0$ disappears for $n' = n$ and $m' = m$ so that

$$\hat{\mathcal{D}}^{\mathrm{I}}_{(2)}(t, t_0) = - \sum_{mn,\mathbf{q}} K_{mm;nn}(\mathbf{q}, \omega_{mm}) \left\{ \hat{T}_{mm} \hat{\rho}^{\mathrm{I}}_{\mathrm{A}}(t, t_0) \delta_{mn} - \hat{T}_{mm} \hat{\rho}^{\mathrm{I}}_{\mathrm{A}}(t, t_0) \hat{T}_{nn} \right\} + \mathrm{h.c.} \tag{3.37}$$

The term $m = n$ in the sum of $\hat{\mathcal{D}}^{\mathrm{I}}_{(2)}$ gives the same contribution as in $\hat{\mathcal{D}}^{\mathrm{I}}_{(1)}$ if $n' = n$. To avoid this double counting, the corresponding contributions in $\hat{\mathcal{D}}^{\mathrm{I}}_{(2)}$ should be substracted.

The correct contribution can be expressed as

$$\hat{\mathcal{D}}^{\mathrm{I}}_{(2)}(t,t_0) = \sum_{n'\neq n,\mathbf{q}} V_{\mathbf{q}}^2 \, F_{nn}(\mathbf{q}) F_{n'n'}^*(\mathbf{q}) \left(\Gamma_r(\mathbf{q},\omega_{n'n'}) + \Gamma_r^*(\mathbf{q},\omega_{n'n'}) \right) \cdot \hat{T}_{n'n'} \hat{\rho}^{\mathrm{I}}_{\mathrm{A}}(t,t_0)\hat{T}_{nn}$$

$$= \sum_{n'\neq n,\mathbf{q}} V_{\mathbf{q}}^2 \, F_{nn}(\mathbf{q}) F_{n'n'}^*(\mathbf{q}) \, \gamma_r(\mathbf{q},0) \cdot \hat{T}_{n'n'} \hat{\rho}^{\mathrm{I}}_{\mathrm{A}}(t,t_0)\hat{T}_{nn}. \tag{3.38}$$

In dipole approximation, this expression yields no contribution because $F_{nn}(\mathbf{q}) = 0$ in dipole approximation. Beyond dipole approximation this term contributes only to the vertex correction. Alltogether, the influence function in RWA follows as

$$\hat{\mathcal{D}}^{\mathrm{I}}_{\mathrm{RWA}}(t,t_0) = \hat{\mathcal{D}}^{\mathrm{I}}_{(1)}(t,t_0) + \hat{\mathcal{D}}^{\mathrm{I}}_{(2)}(t,t_0). \tag{3.39}$$

The influence function $\hat{\mathcal{D}}^{\mathrm{I}}_{(1)}(t,t_0)$ can be transformed into a more transparent form. With the decomposition of the response function $\Gamma_r(\mathbf{k},\omega)$ (3.20), the influence function (3.36) and (3.37) can be rewritten as

$$\hat{\mathcal{D}}^{\mathrm{I}}_{(1)}(t,t_0) = -\sum_{nn',\mathbf{q}} \left\{ \frac{1}{2} k_{n'n}(\mathbf{q},\omega_{n'n}) \left[\{ \hat{T}_{n'n'} \hat{\rho}^{\mathrm{I}}_{\mathrm{A}}(t,t_0) + \hat{\rho}^{\mathrm{I}}_{\mathrm{A}}(t,t_0)\hat{T}_{n'n'} \} - 2\,\hat{T}_{nn'} \hat{\rho}^{\mathrm{I}}_{\mathrm{A}}(t,t_0)\hat{T}_{n'n} \right] \right.$$

$$\left. -i \sum_{nn',\mathbf{q}} V_{\mathbf{q}}^2 F_{n'n}(\mathbf{q}) F_{nn'}(-\mathbf{q}) \, S_r(\mathbf{q},\omega_{n'n}) \left[\hat{T}_{n'n'} \hat{\rho}^{\mathrm{I}}_{\mathrm{A}}(t,t_0) - \hat{\rho}^{\mathrm{I}}_{\mathrm{A}}(t,t_0)\hat{T}_{n'n'} \right] \right\} \tag{3.40}$$

The last term in Eq. (3.40) can be rewritten as commutator describing the reversible Hamiltonian dynamics which in fact represents the line shift of the eigenenergy levels of the atomic system induced by the coupling to the background as known from the coupling to the radiation field. The terms in the first line of the influence function (3.40) are responsible for the transition processes of atoms. Since $F_{nn}(\mathbf{q}) F_{n'n'}^*(\mathbf{q})$ is a complex quantity, the influence function $\hat{\mathcal{D}}^{\mathrm{I}}_{(2)}(t,t_0)$ can be also decomposed into a real part

$$\hat{\mathrm{D}}_{(2)}[\hat{\rho}_{\mathrm{A}}(t)] = \sum_{n'\neq n,\mathbf{q}} V_{\mathbf{q}}^2 \cdot \mathrm{Re}\left\{ F_{nn}(\mathbf{q}) F_{n'n'}^*(\mathbf{q}) \right\} \cdot \gamma_r(\mathbf{q},0) \cdot \hat{T}_{n'n'} \hat{\rho}^{\mathrm{I}}_{\mathrm{A}}(t,t_0)\hat{T}_{nn} \tag{3.41}$$

and an imaginary part

$$\hat{H}^{(2)}_{\mathrm{shift}} = \sum_{n'\neq n,\mathbf{q}} V_{\mathbf{q}}^2 \cdot \mathrm{Im}\left\{ F_{nn}(\mathbf{q}) F_{n'n'}^*(\mathbf{q}) \right\} \cdot \gamma_r(\mathbf{q},0) \cdot \hat{T}_{n'n'} \hat{\rho}^{\mathrm{I}}_{\mathrm{A}}(t,t_0)\hat{T}_{nn}. \tag{3.42}$$

With the relation $\hat{\rho}^{\mathrm{I}}_{\mathrm{A}}(t,t_0) = \mathrm{e}^{i(\hat{H}_{\mathrm{A}}+\hat{H}_{\mathrm{B}})(t-t_0)/\hbar}\, \hat{\rho}_{\mathrm{A}}(t)\, \mathrm{e}^{-i(\hat{H}_{\mathrm{A}}+\hat{H}_{\mathrm{B}})(t-t_0)/\hbar}$, the atomic QME can be transformed back to the Schrödinger picture

$$\frac{\partial \hat{\rho}_{\mathrm{A}}(t)}{\partial t} - \frac{1}{i\hbar}\left[\hat{H}_{\mathrm{A}} + \hat{H}^{(1)}_{\mathrm{shift}} + \hat{H}^{(2)}_{\mathrm{shift}}, \hat{\rho}_{\mathrm{A}}(t) \right] = \hat{\mathrm{D}}_{(1)}[\hat{\rho}_{\mathrm{A}}(t)] + \hat{\mathrm{D}}_{(2)}[\hat{\rho}_{\mathrm{A}}(t)] \tag{3.43}$$

with the shift Hamiltonian operator

$$\hat{H}^{(1)}_{\mathrm{shift}} = \sum_{nn',\mathbf{q}} V_{\mathbf{q}}^2 |F_{n'n}(\mathbf{q})|^2 S_r(\mathbf{q},\omega_{n'n})\hat{T}_{n'n'}, \tag{3.44}$$

which is related the shift of the eigenenergies. The dissipator $\hat{D}_{(1)}[\hat{\rho}_A(t)]$, which is the real part of the influence function $\hat{\mathcal{D}}_{(1)}^I(t, t_0)$, see Eq. (3.40) and is given in Schrödinger picture by

$$\hat{D}_{(1)}[\hat{\rho}_A(t)] = \sum_{nn',\mathbf{q}} k_{n'n}(\mathbf{q}, \omega_{n'n}) \left[\hat{T}_{nn'}\hat{\rho}_A(t)\hat{T}_{n'n} - \frac{1}{2}\left\{\hat{T}_{n'n'}, \hat{\rho}_A(t)\right\}_+\right], \qquad (3.45)$$

where the curly brackets $\{\cdots, \cdots\}_+$ denote the anticommutator. Without the contributions from $\hat{\mathcal{D}}_{(2)}^I[\hat{\rho}_A(t)]$, the QME (3.43) has the Lindblad form. Generally, by performing the RWA here we can render the QME in the Lindblad form in which the terms describing atomic emissions and absorptions can be seperated as shown in Ref. [BP07]. However, we should point out that the neglecting of the term $\hat{\mathcal{D}}_{(2)}^I[\hat{\rho}_A(t)]$ yields an incorrect description of the dissipative system beyond dipole approximation.

We implement the matrix representation of the QME (3.43) in the Schrödinger picture with Eq. (3.13), then the atomic QME in RWA becomes

$$\begin{aligned}
&\frac{\partial \rho_{A,if}(t)}{\partial t} + i\omega_{if}\rho_{A,if}(t) \\
&= -\sum_{n,\mathbf{q}} \left[K_{in;in}(\mathbf{q}, \omega_{in}) + K_{fn;fn}^*(\mathbf{q}, \omega_{fn})\right] \cdot \rho_{A,if}(t) \\
&\quad + \delta_{if} \sum_{n,\mathbf{q}} \left[K_{ni;ni}(\mathbf{q}, \omega_{ni}) + K_{ni;ni}^*(\mathbf{q}, \omega_{ni})\right] \cdot \rho_{A,nn}(t) \\
&\quad + (1 - \delta_{if}) \sum_{\mathbf{q}} \left[K_{ii;ff}(\mathbf{q}, \omega_{ii}) + K_{ff;ii}^*(\mathbf{q}, \omega_{ff})\right] \cdot \rho_{A,if}(t).
\end{aligned} \qquad (3.46)$$

The last contribution comes from $\hat{\mathcal{D}}_{(2)}^I(t, t_0)$, Eq. (3.38).

On the other hand, we can also study the dissipator (3.45) in its matrix representation. The Pauli equation resulting from the diagonal matrix elements of the the dissipator (3.45) is given by

$$\frac{\partial P_i^{(1)}(t)}{\partial t} = \sum_{n,\mathbf{q}} \left\{k_{ni}(\mathbf{q}, \omega_{ni})P_n^{(1)}(t) - k_{in}(\mathbf{q}, \omega_{in})P_i^{(1)}(t)\right\}. \qquad (3.47)$$

This relation coincides with the Pauli equation (3.33) because the contribution $\hat{\mathcal{D}}_{(2)}^I(t, t_0)$ does not affect the behavior of the population numbers given by the diagonal terms of the density matrix. Note that in comparison to the derivation given in this appendix two additional terms occur in Eq. (3.32), which contain nondiagonal matrix elements $\rho_{A,if}(t)$. The neglecting of these additional terms is only valid if the differences of neighbored eigenenergies E_n of the basis $|\psi_n\rangle$ are enough large so that these terms oscillate quite quickly. In the case of Rydberg states, these terms oscillating with frequency ω_{if} are also relevant and cannot be ignored any more.

The nondiagonal matrix elements of the dissipator (3.43), i.e. $\hat{D}_{RWA}[\hat{\rho}_A(t)] = \hat{D}_{(1)}[\hat{\rho}_A(t)] + \hat{D}_{(2)}[\hat{\rho}_A(t)]$, can be represented as

$$\frac{\partial \rho_{A,if}(t)}{\partial t} + i\tilde{\omega}_{if}\,\rho_{A,if}(t) = \langle\psi_i|\hat{D}_{RWA}[\hat{\rho}_A(t)]|\psi_f\rangle = -\frac{1}{2}\left\{d_1 + d_2 + d_3\right\}\rho_{A,if}(t) \qquad (3.48)$$

with the modified transition frequency $\tilde{\omega}_{if}$ due to the shift Hamiltonian in Eq. (3.43). The contributions d_1, d_2 and d_3 are defined similarly as in Eq. (3.79),

$$d_1 = \sum_{\mathbf{q}} V_{\mathbf{q}}^2 \left| F_{ii}(\mathbf{q}) - F_{ff}(-\mathbf{q}) \right|^2 \gamma_r(\mathbf{q}, 0), \tag{3.49}$$

$$d_2 = \sum_{\mathbf{q}} \left\{ k_{if}(\mathbf{q}, \omega_{if}) + k_{fi}(\mathbf{q}, \omega_{fi}) \right\}, \tag{3.50}$$

$$d_3 = \sum_{n \neq i, f} \sum_{\mathbf{q}} \left\{ k_{in}(\mathbf{q}, \omega_{in}) + k_{fn}(\mathbf{q}, \omega_{fn}) \right\}. \tag{3.51}$$

The mixed contribution in d_1 originates from the dissipator $\hat{D}_{(2)}[\hat{\rho}_A(t)]$ (3.41), whereas another two contributions belong to the dissipator $\hat{D}_{(1)}[\hat{\rho}_A(t)]$ (3.45). It can be seen that the expression (3.50) relates directly to the transition rates of the atomic eigenstates comparing with the Pauli equation (3.33) for a given two-levels system transition, which gives a clue to define the transition rates for the Rydberg wave packet via the QME as explained in Sec. 3.2.4.

For the sake of investigating the effect of the RWA we return to the atomic QME (3.30) which reads in the Schrödinger picture

$$\frac{\partial \rho_{A,if}(t)}{\partial t} + i\omega_{if}\rho_{A,if}(t) = \langle \psi_i | \hat{\mathcal{D}}[\hat{\rho}_A(t)] | \psi_f \rangle \tag{3.52}$$

with the influence function [remember $\rho_{A,mn}^{I}(t, t_0) = e^{i\omega_{mn}(t-t_0)}\rho_{A,mn}(t)$]

$$
\begin{aligned}
\langle \psi_i | \hat{\mathcal{D}}[\hat{\rho}_A(t)] | \psi_f \rangle = & - \sum_{mn,\mathbf{q}} \Big\{ K_{mn;in}(\mathbf{q}, \omega_{mn}) \rho_{A,mf}(t) + K_{mn;fn}^*(\mathbf{q}, \omega_{mn}) \rho_{A,im}(t) \\
& - \left[K_{mi;fn}(\mathbf{q}, \omega_{mi}) + K_{nf;mi}^*(\mathbf{q}, \omega_{nf}) \right] \rho_{A,mn}(t) \Big\}.
\end{aligned}
\tag{3.53}
$$

The RWA for the non-diagonal terms means we should set $m = i$ in the first term, $m = f$ in the second term and $m = i$, $n = f$ in the third term of the influence function (3.53). By using the decomposition of the complex response function $\Gamma_r(\mathbf{q}, \omega) = \gamma_r(\mathbf{q}, \omega)/2 + iS_r(\mathbf{q}, \omega)$ we obtain the same expression as Eq. (3.48).

We found that the RWA performed in Eq. (3.28) by neglecting $\hat{\mathcal{D}}_{(2)}^{I}(t, t_0)$ leads to a QME in Lindblad form. However, the term $\hat{\mathcal{D}}_{(2)}^{I}(t, t_0)$ has a significant contribution in some special cases, for example, the vertex correction of the spectral line profiles. On the other hand, if the RWA is performed in the matrix representation, the contribution of $\hat{\mathcal{D}}_{(2)}^{I}(t, t_0)$ can be automatically included in the influence function. If the RWA is carried out prematurely in Eq. (3.36), it will be inappropriate to describe the dissipative properties of the relevant atomic system (Rydberg states) and results in erroneous transition rates.

In principle, the RWA obtained by the removal of terms that oscillate quickly with respect to some characteristic time scales of the system is problematic as pointed out by different authors [Aga71, Aga73, Fle98, FCAH10, MABL13, MM13]. It depends on the choice of the basis $|\psi_n\rangle$ for the representation of the density matrix, and in the case of small energy differences of neighbored eigenenergies E_n the oscillation may become not quick enough compared to the characteristic time scales of the system. In a study of the spontaneous emission of a two-level system, Agarwal found that the RWA gives an incorrect value for environmentally induced frequency shifts with respect to the system frequency [Aga71, Aga73]. Fleischhauer

studied the photodetection without the RWA, finding that for ultrashort pulses, whose length is of the order of the oscillation period, the mean number of photocounts with the RWA and without the RWA are substantially different [Fle98]. Recently, Fleming *et al.* investigated the validity of the RWA in an open quantum system and argued that the quantum state resulting from the RWA is inappropriate for calculating the detailed properties of the state dynamics such as entanglement dynamics [FCAH10]. In Ref. [MABL13], Majenz *et al.* showed that the RWA leads to the lack of important qualitative features of the population dynamics in a special three-level model. Recently, Mäkelä and Möttönen [MM13] discovered that the RWA yields an considerable reduction of non-Markovianity and is problematic if non-Markovian dynamics is of essential relevance.

In this work, irreversible behavior is not produced by the RWA, but already inherent in the solutions of Eqs. (3.14) and (3.15). The source term with $\varepsilon > 0$ in Eq. (2.82) is obtained from phase averaging in the evolution of $\hat{\rho}_{\rm rel}(t)$, see Eq. (1.101) in Ref. [Röp13]. A positive ε is necessary to get $\gamma_r > 0$, Eq. (3.20), which is calculated here in Born approximation. According to Eqs. (3.33) and (3.34), γ_r determines the relaxation rate w of the states of the system A. Averaging over the phases related to t_0 in the interaction picture, all oscillations with $\omega_{nm} > w \propto \gamma_r$ are damped out so that the corresponding contributions tend to zero and can be dropped, see also Eq. (3.40) in Ref. [Röp13]. Consequently, the RWA is obtained.

3.2 Wave packet description for Rydberg states

3.2.1 Wave packets

Within the QME approach, the statistical operator of the reduced system $\hat{\rho}_{\rm A}$ is of interest. The density matrix $\rho_{{\rm A},mn} = \langle m|\hat{\rho}_{\rm A}|n\rangle$ is represented with respect to the states $|n\rangle$ of the reduced system. One possibility is using the orthonormal basis set of energy eigenstates of the unperturbed atom according to the interaction picture. In the case considered here, these are the hydrogen orbitals including the scattering states. The hydrogen orbitals are long-living if the perturbation by the surrounding plasma is weak. Accordingly, the transition rates due to collisions with the plasma are small.

Rydberg atoms, as ubiquitous states formed due to the recombination of electrons and positive ions in laser-produced plasmas [PPR04a, PPR04b], play a significant role for understanding the evolution of expanding plasmas. Some general properties for Rydberg atoms are displayed in Tab. 3.1. Their interaction effects with the plasma particles are comparable or greater than the differences of atomic energy eigenstates E_n for n near a fixed value n_0. On the other hand, the pressure broadening of the Rydberg states is also comparable to the energy difference between adjacent orbitals since it is scaled as n^{-3} with respect to the principal quantum number n. Furthermore, the transition rates are quite large because of the enormous dipole moment ($\langle nl|\mathbf{r}|n\,l\pm 1\rangle \sim n^2$). Consequently, the pure Rydberg state is strongly affected by the plasma environment and has only a short life time. In this case, mixtures of pure Rydberg states should be taken into account. Hence one can look for more robust states that are formed as superposition of energy eigenstates, which might be more stable in the time evolution. For a local interaction such as the Coulomb potential, the position $\mathbf{r}$ of the atomic electron enters the interaction part of the Hamiltonian, and localization is favored because $\mathbf{r}$ commutes with $\hat{H}_{\rm int}$ and is a conserved quantity with respect to this part of the Hamiltonian. Therefore, localized states are more robust with respect to the interaction with the surrounding plasma. In this case, a wave packet description for Rydberg states can be

Property	n-dependence	Na (state $n = 10, l = 2$)
Binding energy	n^{-2}	0.14 eV
Energy between adjacent n states	n^{-3}	0.023 eV
Orbital radius	n^2	147 a_0
Dipole moment $\langle nd|er|nf \rangle$	n^2	143 $e\,a_0$
Polarizability	n^7	0.21 MHz cm^2 V^{-2}
Radiative lifetime	n^3	1.0 μs

Tab. 3.1: Properties of Rydberg atoms: scaling rules (from Ref. [Gal94]). a_0 is the Born radius and e is the elementary charge.

introduced to describe the evolution of the system, in particular transition rates.

In addition, the introduction of the wave packet description may allow us to investigate the boundary between the quantum and classical descriptions of systems. In fact, since the introduction of quantum mechanics many physicists attempted to establish the connections between these descriptions of nature by exhibiting the so-called coherent wave packet. One of the famous examples is the well known coherent state of the linear harmonic oscillator [Gla63] which may be regarded as an excellent example to describe the macroscopic limit of a quantum mechanical system according to the correspondence principle. For the Coulomb problem, e.g. the hydrogen atom, many attempts to construct localized semi-classical solutions of the coherent-state type have been made [Bro73, NS78, BDRG86, ZZF94, MS97]. Note that the hydrogen atom is equivalent to the four-dimensional harmonic oscillator so that coherent wave packets can be introduced accordingly [BDRG86]. Recently, Makowski and Peplowski constructed well-localized two-dimensional wave packets for two different potentials [MP12, MP13] where an excellent quantum-classical correspondence is observed. We use Brown's circular-orbit wave packets [Bro73, GS90] as a quasiclassical representation to describe the highly excited Rydberg states of the hydrogen atom.

3.2.2 Circular Rydberg states

In the present work, we are interested in the extreme-circular Rydberg states where a valence electron of the atom is highly excited to quantum states $l = m = n - 1$. In the case of a hydrogen atom we have

$$\psi_n(\mathbf{r}) = \langle \mathbf{r}|\psi_{n,n-1,n-1}\rangle = c_n \left(\frac{r}{a_{\mathrm{B}}}\right)^{n-1} e^{-r/(na_{\mathrm{B}})} \sin^{n-1}(\theta) e^{i(n-1)\phi}, \qquad (3.54)$$

where $c_n = (2/(na_{\mathrm{B}}))^{3/2}[2n(2n+1)!]^{-1/2}$. Furthermore, in this section we use the abbreviation $\psi_n(\mathbf{r})$ for the circular wave function $\psi_{n,n-1,n-1}(\mathbf{r})$ and use the notation n for the principal quantum number. It can be seen from Eq. (3.54) that the hydrogen electron in this eigenstate is already excellently localized in the radial (r) and polar (θ) direction, see Fig. 3.1.

Besides the above mentioned localized properties, these extreme-circular Rydberg states have also other remarkable properties: long radiative lifetimes, giant magnetic moments, no linear Stark shift, and smallest quadratic Stark shifts [Hez10, ASSR13, And15]. According to the dipole selection rule $\Delta l = 1$, the radiative decay channels of circular Rydberg states are strongly suppressed. As a consequence, transition between adjacent circular states can be

regarded as a two-level quantum system which may be used to realize a two-qubit quantum gate [XZS13].

(a) Localization in radial direction ($n = 69$).
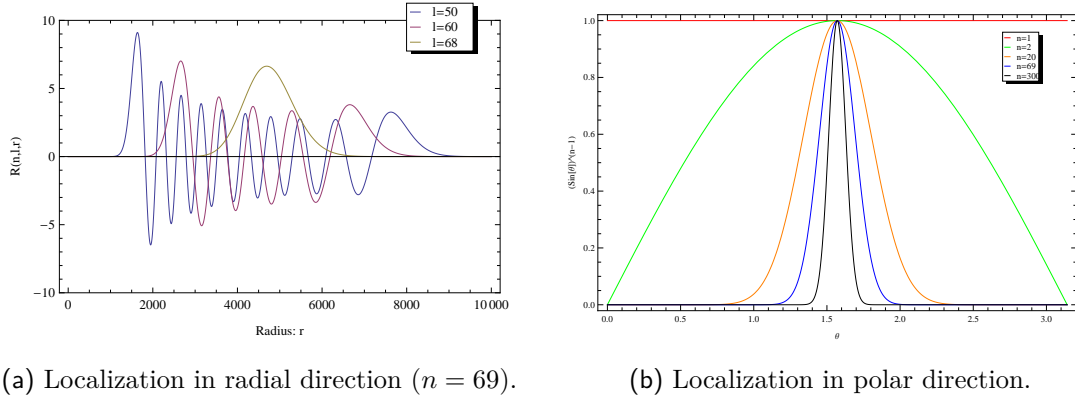

(b) Localization in polar direction.

Abb. 3.1: Localization of the circular wave function [Lin14].

Different methods for creating circular Rydberg atoms have been developed, for example, the adiabatic rapid passage technique [HK83, NBB$^+$93], the crossed-field method [DG88, HGG88], and the adiabatic radio-frequency field technique [MJY86, CCRS93, CLG94]. In addition to the production of circular Rydberg states, special trapping techniques are indispensable for studies and applications of these states. For instance, as recently demonstrated by Anderson *et al.* [ASSR13], a room-temperature magnetic trap for circular Rydberg atoms has been realized. There, circular Rydberg state with $n = 57$ are generated within a sample of 10^7 cold ^{87}Rb atoms via a two-step excitation process with two laser beams. It was possible to observe the center-of-mass and internal-state evolution of circular states. These experiments can be employed to provide a source of long-lived circular state atoms for precision measurements.

3.2.3 Wave packet for circular motion

We now introduce a circular-orbit wave packet of the hydrogen atom as a coherent state constructed from the superposition of circular-orbit eigenfunctions of the hydrogen atom (3.54) with a Gaussian weighting function around a large principal quantum number n_0 [GS90]:

$$|G_{n_0,\phi_0}\rangle = \sum_n \frac{g_{n_0,n}}{\sqrt{\mathcal{N}_{n_0}}} e^{i(n-1)\phi_0} |\psi_n\rangle \tag{3.55}$$

with the Gaussian factor and the normalization factor respectively

$$g_{n_0,n} = \exp\left\{ -\frac{(n-n_0)^2}{4\sigma_{n_0}^2} \right\}, \ \mathcal{N}_{n_0} = \sum_{n=1}^{\infty} \exp\left\{ -\frac{(n-n_0)^2}{2\sigma_{n_0}^2} \right\}, \tag{3.56}$$

where σ_{n_0} is the standard deviation considered as fixed parameter for n_0. Without loss of generality we can put $\phi_0 = 0$ because it fixes, as a phase factor, only the initial position of the wave packet at the azimuthal angle ϕ. We drop ϕ_0 in the following. Due to the superposition with a Gaussian factor, we have also good localization with respect to ϕ in the wave packet description (3.55). The actual Hilbert space $\mathcal{H}_{n,n-1,n-1}$ considered here is only a subspace

of the entire Hilbert space $\mathcal{H}$ of the hydrogen atom. The generalization to the full Hilbert space to include all bound and scattering states could be done straightforwardly.
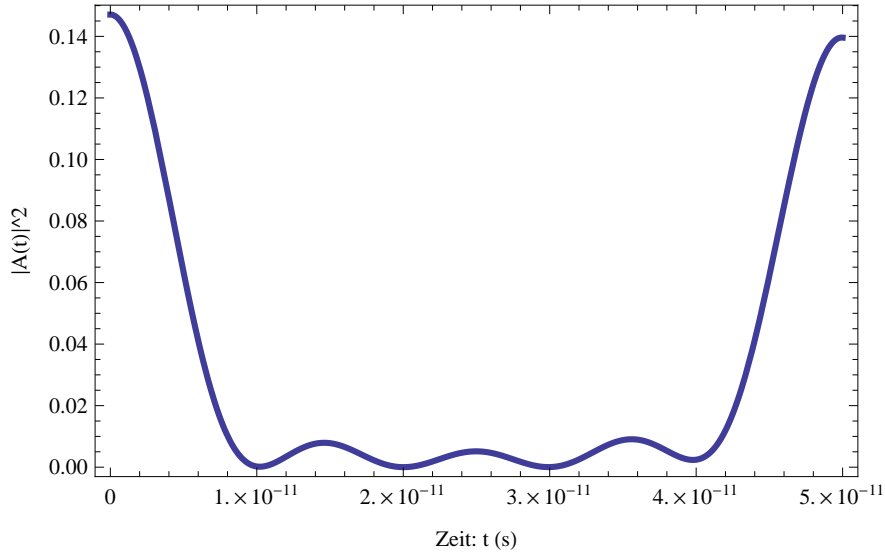
(a) Classical Kepler motion in one Kepler period with frequency ω_{cl}.
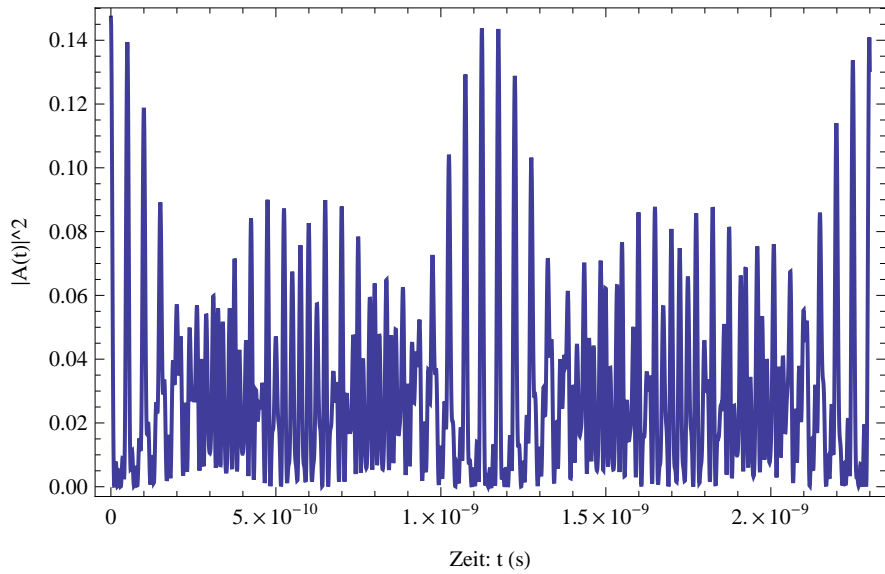
(b) Quantum revival behavior in one revival period with frequency ω_{rev}.

Abb. 3.2: Time evolution of the autocorrelation function $|A(t)|^2$ with $A(t) = \langle G_{n_0}(t)|G_{n_0}(0)\rangle$ around the principal quantum number $n_0 = 69$ [Lin14].

The time-dependent wave packet in the coordinate representation in terms of spherical coordinates is given by

$$\langle \mathbf{r}|G_{n_0}\rangle^t = \sum_n \frac{g_{n_0,n}}{\sqrt{\mathcal{N}_{n_0}}}\, e^{iE_n t/\hbar}\, \psi_n(\mathbf{r}) \tag{3.57}$$

with $E_n = \mathrm{Ry}/n^2$ and $\mathrm{Ry} = 13.6\,eV$. For an appropriate Gaussian factor only the terms with principal quantum number adjacent to n_0 contribute. Therefore we can use the central quantum number n_0 to approximate other states in radial and θ-direction. In addition, for short-term time evolution the energy E_n in the factor $\mathrm{e}^{iE_n t/\hbar}$ in Eq. (3.57) can be expanded around n_0 up to the second order, which relates directly to the quantum revival, see below. The probability distribution of the wave packet can be represented as

$$|\langle \mathbf{r}|G_{n_0}\rangle^t|^2 = \sum_{m,n} c_{n_0}^2 \left(\frac{r}{a_{\mathrm{B}}}\right)^{2n_0-2} \mathrm{e}^{-2r/(n_0 a_{\mathrm{B}})} \sin^{2n_0-2}(\theta) \tag{3.58}$$

$$\times \exp\left\{-(a_1 - i\omega_{\mathrm{rev}}t)(n-n_0)^2 - (a_1 + i\omega_{\mathrm{rev}}t)(m-n_0)^2 + i(\phi - \omega_{\mathrm{cl}}t)(n-m)\right\}$$

with $a_1 = 1/(4\sigma_{n_0}^2)$, $\omega_{\mathrm{cl}} = |E_{n_0}'|/\hbar = 2\mathrm{Ry}/(\hbar n_0^3)$ and $\omega_{\mathrm{rev}} = |E_{n_0}''|/(2\hbar) = 3\mathrm{Ry}/(\hbar n_0^4)$, where E_{n_0}' and E_{n_0}'' are the first and second derivatives of E_n with respect to the main quantum number n at n_0, respectively. As pointed out in [Rob04], ω_{cl} relates to the classical Kepler period $T_{\mathrm{cl}} = 2\pi r_{\mathrm{cl}}/v_{\mathrm{cl}}$ for the Kepler trajectory with $r_{\mathrm{cl}} = n_0^2 a_{\mathrm{B}}$ and $v_{\mathrm{cl}} = \sqrt{\mathrm{Ry}/(m_e n_0^2)}$, and the quantum revival period can be defined by ω_{rev}. To reveal the Kepler motion and the quantum revival behavior, the time evolution of the autocorrelation function $A(t) = \langle G_{n_0}(t)|G_{n_0}(0)\rangle$ is shown in Fig. 3.2.

For highly excited states $|x| \ll n_0$ with $x = n - n_0$ and $|y| \ll n_0$ with $y = m - n_0$, the sum $\sum_{m,n}$ can be replaced by the integral $\int_{-\infty}^{\infty} dx \int_{-\infty}^{\infty} dy$. Integrating over the variables r and θ and performing the integral over x, y yields the probability distribution of the wave packet

$$|G_{n_0}(\phi,t)|^2 \sim \sqrt{\frac{\pi^2}{a_1^2 + (\omega_{\mathrm{rev}}t)^2}} \exp\left[-\frac{\phi_{\mathrm{cl}}^2(t)}{2[a_1^2 + (\omega_{\mathrm{rev}}t)^2]/a_1}\right] \tag{3.59}$$

with $\phi_{\mathrm{cl}}(t) = \phi - \omega_{\mathrm{cl}}t$. From this probability distribution the time-dependent width of the wave packet for a Rydberg electron can be extracted

$$\sigma_{n_0}^\phi(t) = \sqrt{[a_1^2 + (\omega_{\mathrm{rev}}t)^2]/a_1} = \sqrt{\frac{1}{4\sigma_{n_0}^2} + \frac{\sigma_{n_0}^2 (E_{n_0}'' t)^2}{\hbar^2}}. \tag{3.60}$$

For the initial time $t = 0$, we have $\sigma_{n_0}^\phi = 1/(2\sigma_{n_0})$. The expression (3.59) also shows that on such a short time scale the central position of the probability distribution is exactly determined by the Kepler motion. The localized wave packet for the hydrogen atom moves along the classical Keplerian trajectory of the electron and its width broadens. With time evolution the localization of the wave packet is destroyed and interference fringes of different eigenstates are displayed. On a much longer time scale $T_{\mathrm{rev}} = 2\pi/\omega_{\mathrm{rev}}$, the wave packet finally reverses itself, which is the above mentioned quantum revival as indicated in Eq. (3.59).

The dynamics of the wave packet shown above is purely due to quantum mechanical evolution without plasma surroundings. Within a plasma environment, the hydrogen atom undergoes interactions with the plasma particles which results in the shift of the eigenenergy levels, the broadening of plasma spectral lines, the screening of the Coulomb potential, the localization of the hydrogen atom (proton and bound electron), etc. In this work we concentrate on the localization of the bound electron immersed in a plasma environment.

The scattering of the bound electron by free plasma electrons results in the localization of the electron of the hydrogen atom, i.e. the collisions with the plasma tend to localize

the Rydberg electron and to narrow the wave packet. As in the case of free particles in a surrounding environment [JZK⁺03], the spreading of the wave packet competes with the localization effect induced by the plasma environment. The optimum width of a Gaussian wave packet where both effects, localization and quantum diffluence, nearly compensate, describes a state which is nearly stable in time and is denoted as robust state.

In this work we are interested in time scales, which are even smaller than the classical Keplerian periodicity T_{cl}. We assume that on such a short time scale a Rydberg electron behaves like a free electron because of the weak coupling between the electron and the proton. Comparing with the relaxation processes, which describe the inelastic coupling between the internal energy eigenstates and the surrounding environment, the quasiclassical Kepler motion of the wave packet is assumed to be influenced by the elastic scattering of the Rydberg electrons with its surroundings. Similarly as in the case of the quantum Brownian motion of a free particle [JZK⁺03], the equation of motion for the reduced density matrix in space basis can be derived via the collisional decoherence as following.

Following the method represented in the book of Joos *et al.* [JZK⁺03] for the free particles, we study here the weakly bound Rydberg electrons. The reduced density matrix for the Rydberg electron can be derived under the assumptions of recoil-free collisions and elastic scattering

$$\rho(\mathbf{R}_n, \mathbf{R}_n^{'}) \rightarrow \rho(\mathbf{R}_n, \mathbf{R}_n^{'}) \cdot \left\{ 1 + \sum_{\mathbf{k}'} \left[1 - \mathrm{e}^{i(\mathbf{k}-k')\cdot(\mathbf{R}_n - \mathbf{R}_n^{'})} \right] |\langle \mathbf{k}', n | \hat{T} | \mathbf{k}, n \rangle|^2 \right\}, \qquad (3.61)$$

where the T-matrix is given by $\hat{T} = \hat{V} + \hat{V}\hat{G}_0\hat{V} + \hat{V}\hat{G}_0\hat{V}\hat{G}_0\hat{V} + ...$ In the elastic scattering process the principal quantum number n of the Rydberg electron does not change, this means, the Rydberg electron motions along the classical Kepler orbit. For the bound electrons the T-matrix in Born approximation can be represented as

$$\langle \mathbf{k}', n | \hat{T} | \mathbf{k}, n \rangle = V_{\mathbf{q}} \, F_{nn}(\mathbf{q})\delta(E_{\mathbf{k}} - E_{\mathbf{k}'}) \qquad (3.62)$$

with $\mathbf{q} = \mathbf{k} - k'$ and $E_{\mathbf{k}} = \mathbf{k}^2/(2m_e)$. $V_{\mathbf{q}}$ denotes the interaction potential and $F_{nn}(\mathbf{q})$ is diagonal atomic form factor.

In Born approximation we have

$$\begin{aligned}
A \quad &:= \sum_{\mathbf{k}'} \left[1 - \mathrm{e}^{i(\mathbf{k}-k')\cdot(\mathbf{R}_n - \mathbf{R}_n^{'})} \right] |\langle \mathbf{k}', n | \hat{T} | \mathbf{k}, n \rangle|^2 \\
&= \frac{\Omega_0}{(2\pi)^3} \int d^3\mathbf{k}' \left[1 - \mathrm{e}^{i(\mathbf{k}-k')\cdot(\mathbf{R}_n - \mathbf{R}_n^{'})} \right] V_{\mathbf{q}}^2 \, F_{nn}^2(\mathbf{q})\delta^2(E_{\mathbf{k}} - E_{\mathbf{k}'}) \\
&= \frac{\Omega_0 m_e T}{(2\pi\hbar)^3 k} \int_0^{2k} dq \, q V_{\mathbf{q}}^2 \, F_{nn}^2(\mathbf{q}) \left[1 - \mathrm{e}^{i\mathbf{q}\cdot(\mathbf{R}_n - \mathbf{R}_n^{'})} \right].
\end{aligned} \qquad (3.63)$$

In the third line the integrals over k' and ϕ have been carried out and the integral over θ is replaced by $\int_{|k-k'|}^{k+k'} dq$ by using the relation $q^2 = k^2 + k'^2 - 2kk'\cos\theta$. The squared delta function is evaluated by using the Fourier representation of the delta function

$$\begin{aligned}
\delta^2(E_{\mathbf{k}} - E_{\mathbf{k}'}) &= \delta(E_{\mathbf{k}} - E_{\mathbf{k}'}) \cdot \lim_{T\to\infty} \frac{1}{2\pi\hbar} \int_{-T/2}^{T/2} dt \, e^{i(E_{\mathbf{k}} - E_{\mathbf{k}'})t/\hbar} \\
&= \frac{m_e}{\hbar^2 k'} \delta(k - k') \cdot \lim_{T\to\infty} \frac{T}{2\pi\hbar}.
\end{aligned} \qquad (3.64)$$

For a collection of N independent scattering events in plasma, the above expression (3.63) should be multiplied by a factor N. For the momentum distribution $P(\mathbf{q})$ of the plasma environment, the classical Maxwell-Boltzmann distribution is taken. where the momentum distribution $P(\hbar\mathbf{k})$ of the plasma environment, assumed to fulfill Maxwell-Boltzmann distribution $P(\mathbf{q}) = (\frac{\hbar^2}{2\pi m_e k_B T})^{3/2} \exp[-\hbar^2 q^2/(2m_e k_B T)]$ is taken. We find

$$A = \frac{N\Omega_0 T}{\pi(2\pi\hbar)^2} \sqrt{\frac{m_e}{2k_B T}} \int_0^\infty dq\, q V_\mathbf{q}^2\, F_{nn}^2(\mathbf{q})\, \mathrm{e}^{-\hbar^2 q^2/(8m_e k_B T)} \left[1 - \mathrm{e}^{i\mathbf{q}\cdot(\mathbf{R}_n - \mathbf{R}_n')}\right]. \qquad (3.65)$$

For the scattering process described here we have the time evolution of the reduced density matrix (QME) by taking the differential limit of small T

$$\frac{\rho(\mathbf{R}_n, \mathbf{R}_n', T) - \rho(\mathbf{R}_n, \mathbf{R}_n', 0)}{T}$$
$$= \frac{N\Omega_0}{\pi(2\pi\hbar)^2} \sqrt{\frac{m_e}{2k_B T}} \int_0^\infty dq\, q V_\mathbf{q}^2\, F_{nn}^2(\mathbf{q})\, \mathrm{e}^{-\hbar^2 q^2/(8m_e k_B T)} \times \left[1 - \mathrm{e}^{i\mathbf{q}\cdot(\mathbf{R}_n - \mathbf{R}_n')}\right]. \qquad (3.66)$$

To avoid the divergence of the integral in (3.66), the Debye potential [?] can be used. As the next step we can use the long-wavelength limit to evaluate (3.66), i.e. we can expand the exponential function $\mathrm{e}^{i\mathbf{q}\cdot(\mathbf{R}_n - \mathbf{R}_n')}$ up to second order and obtain the QME in the long-wavelength limit

$$\frac{\partial}{\partial t}\rho(\mathbf{R}_n, \mathbf{R}_n', t) = -\frac{N\Omega_0}{\pi(2\pi\hbar)^2} \sqrt{\frac{m_e}{2k_B T}} \int_0^\infty dq\, q V_\mathbf{q}^2\, F_{nn}^2(\mathbf{q})\, \mathrm{e}^{-\hbar^2 q^2/(8m_e k_B T)} \left(\mathbf{q}\cdot(\mathbf{R}_n - \mathbf{R}_n')\right)^2. \qquad (3.67)$$

As shown in Sec. 3.2.3, the Rydberg electron moves along the Kepler orbit, i.e. $\mathbf{R}_n = (n^2 a_\mathrm{B}, \pi/2, \phi)$ and $\mathbf{R}_n' = (n^2 a_\mathrm{B}, \pi/2, \phi')$. This assumption allows us to calculate the term $(\mathbf{q}\cdot(\mathbf{R}_n - \mathbf{R}_n'))^2$ by averaging it over all possible directions $(\mathbf{R}_n - \mathbf{R}_n')$: $(\mathbf{q}\cdot(\mathbf{R}_n - \mathbf{R}_n'))^2 = q^2 \cdot (x - x')^2/3$ with $x = r_\mathrm{cl}\phi$. Then we have

$$\frac{\partial}{\partial t}\rho(x, x', t) = -\Lambda_{R_n} \cdot (x - x')^2 \qquad (3.68)$$

with the localization rate defined by

$$\Lambda_{R_n} = \frac{N\Omega_0}{\pi(2\pi\hbar)^2} \int_0^\infty dq\, \frac{q^4}{3} V_\mathbf{q}^2\, F_{nn}^2(\mathbf{q}) \sqrt{\frac{m_e}{2k_B T q^2}}\, \mathrm{e}^{-\hbar^2 q^2/(8m_e k_B T)}. \qquad (3.69)$$

describing how fast interferences of an entangled system of extension $|x - x'|$ are suppressed. According to [JZK+03], the optimal width of the wave packet is defined by equilibrating the interplay between the spreading of the wave packet and the localization of the wave packet and reads:

$$\sigma_n^\mathrm{cl} = \frac{1}{2}\left(\frac{\hbar}{m_e \Lambda_{R_n}}\right)^{1/4}. \qquad (3.70)$$

As a consequence, an optimal width σ_{n_0} can be calculated using the relation (3.60) for $t = 0$ and the relation $\sigma_{n_0}^\phi = \sigma_{n_0}^\mathrm{cl}/r_\mathrm{cl}$ so that

$$\sigma_{n_0} = \frac{r_\mathrm{cl}}{2\,\sigma_{n_0}^\mathrm{cl}}. \qquad (3.71)$$

For the plasma with temperature $T = 300$K and density $n_{\rm pl} = 10^9\,{\rm cm}^{-3}$, we obtain an optimal width $\sigma_{n_0} = 0.75$ for $n_0 = 13$, which will be shown in the next section to be appropriate to describe the transition rate.

In Table 3.2 we show the dependence of the localization rates on the plasma parameters for different principal quantum numbers. For given temperature and density, the localization rate decreases slightly with the increasing quantum number n_0. At a fixed temperature, the localization rate is raised drastically when the plasma density increases. At the same time, the localization rate shows only a weak dependence on the plasma temperature.

T [K]	$n_{\rm pl}[{\rm cm}^{-3}]$	quantum number n_0			
		10	20	30	40
100	10^9	5.722	5.722	5.722	5.721
	10^{12}	180.3	180.1	180.0	179.7
	10^{15}	5090	4969	4813	4645
1000	10^9	5.722	5.722	5.722	5.722
	10^{12}	180.9	180.8	180.7	180.6
	10^{15}	5619	5549	5474	5399
10000	10^9	5.722	5.722	5.722	5.722
	10^{12}	180.9	180.9	180.9	180.9
	10^{15}	5696	5670	5645	5619

Tab. 3.2: Localization rate Λ_{R_n} (3.69) in units of $[10^{23}\,{\rm cm}^{-2}\,{\rm s}^{-1}]$ for different plasma densities and temperatures.

The transition between descriptions of the bound electron in hydrogen atom by the wave packet and the pure quantum eigenstate may be determined by comparing the optimal width (3.70) with the orbit radius $r_{n_0} = r_{\rm cl} = n_0^2 a_{\rm B}$. For this, a function $b(n_0, n_{\rm pl}, T)$

$$b(n_0) = b(n_0, n_{\rm pl}, T) = \frac{\sigma_{n_0}^{\rm cl}}{r_{n_0}} - 1 \qquad (3.72)$$

can be introduced. For the given electron density $n_{\rm pl}$ and temperature T of the plasma, quantum mechanical descriptions is valid for $b(n_0) > 0$, and for the opposite case $(b(n_0) < 0)$, the wave packet descriptions can be used.

In Fig. 3.3 we show this function for different plasma densities at the given temperature $T = 300$ K. With the increase of the plasma density the principal quantum number $n_{\rm cr}$ at $b(n_{\rm cr}) \approx 0$ characterizing the change from a pure quantum description to a classical description drops drastically.

We discussed the descriptions of the bound electron, in particular the validity of the wave packet description. We have shown that this question is related to the localization of the wave packet if an optimal width of the wave packet is assumed, which also has a dependence on the mass of the localized object as shown in Eq. (3.70). Similar considerations can be made for the free electrons and ions in the plasma, see Refs. [GR06, GR07].

3.2.4 Transition rates

We are interested in a matrix representation of the QME. We use robust states $|i\rangle = |G_{n_i}\rangle$ for the initial state and $|f\rangle = |G_{n_f}\rangle$ for the final state to investigate the atomic transition
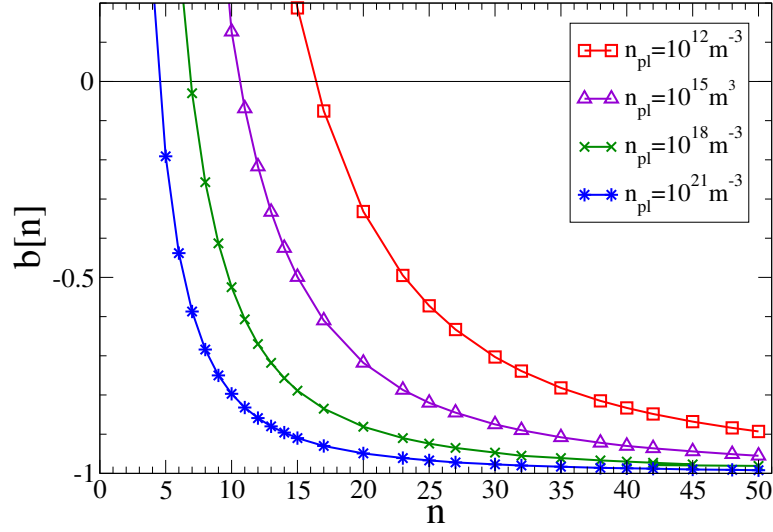
Abb. 3.3: Boundary between classical and quantum mechanical descriptions of the hydrogen electron at $T = 300$ K for different densities.

rates of the Rydberg states. For the reduced Hilbert space $\mathcal{H}_{n,n-1,n-1}$ used to construct the circular-orbit wave packet, there is no completeness relation $\sum_n |n\rangle\langle n| = \hat{1}$ because non-circular orbits are missing. Only if we project on the reduced Hilbert space, this relation can be applied. A more general discussion about the completeness relation in the wave packet case is found in Refs. [Fox99, Kla96]. Therewith the charge density operator in Hilbert space $\mathcal{H}_{n,n-1,n-1}$ is expressed as

$$\hat{\varrho}^{\mathrm{I}}_{\mathbf{q},\mathrm{A}}(t) = \sum_{mn} e_e \, \hat{T}_{mn} \, F_{mn}(\mathbf{q}) e^{i\omega_{mn}t}. \tag{3.73}$$

In Fourier-space the charge density operator reads

$$\hat{\varrho}^{\mathrm{I}}_{\mathbf{q},\mathrm{A}}(\omega) = \sum_{mn} e_e \, \hat{T}_{mn} \, F_{mn}(\mathbf{q}) \, 2\pi\delta(\omega + \omega_{mn}). \tag{3.74}$$

Note that the operators given in this section are all projected on the reduced Hilbert space $\mathcal{H}_{n,n-1,n-1}$. The use of the full Hilbert space is more complex and should be worked out in future investigations.

In the present section, the diffusion of the wave packet with the center quantum number n_0 is of essential interest. The dynamics along the classical trajectory, shown in the previous section, is given by $\phi_{\mathrm{cl}}(t)$. To investigate the diffusion of the wave packet with respect to the quantum number n, we come back to the QME in which the influence function for the wave packet in Hilbert space $\mathcal{H}_{n,n-1,n-1}$ is obtained by inserting the charge density operator (3.74) into equation (3.21)

$$\mathcal{D}^{\mathrm{I}}[\hat{\rho}^{\mathrm{I}}_{\mathrm{A}}(t)] = -\sum_{nn',mm',\mathbf{q}} e^{-i(\omega_{nn'}+\omega_{mm'})(t-t_0)} \, K_{mm';n'n}(\mathbf{q},\omega_{mm'})$$
$$\times \left\{ \hat{T}_{n'n}\hat{T}_{m'm}\hat{\rho}^{\mathrm{I}}_{\mathrm{A}}(t,t_0) - \hat{T}_{m'm}\hat{\rho}^{\mathrm{I}}_{\mathrm{A}}(t,t_0)\hat{T}_{n'n} \right\} + \mathrm{h.c.} \tag{3.75}$$

The influence function in RWA can be represented in matrix representation as

$$\langle f|\mathcal{D}^{\mathrm{I}}[\hat{\rho}_A^{\mathrm{I}}(t)]|i\rangle \quad = \sum_{s,h,\mathbf{q}} \mathcal{G}_{n_f,s}^{n_i,h} \left\{ K_{ss;hh}(\mathbf{q},\omega_{ss}) + K_{hh;ss}^*(\mathbf{q},\omega_{hh}) \right.$$
$$\left. - \sum_n \left\{ K_{sn;sn}(\mathbf{q},\omega_{sn}) + K_{hn;nh}^*(\mathbf{q},\omega_{hn}) \right\} \right\} \rho_{A,sh}^{\mathrm{I}}(t) \tag{3.76}$$

with

$$\mathcal{G}_{n_f,s}^{n_i,h} = \frac{g_{n_f,s} \cdot g_{n_i,h}}{\sqrt{\mathcal{N}_{n_f} \mathcal{N}_{n_i}}}, \tag{3.77}$$

where the g-function is given by Eq. (3.56). After decomposition of the response function $\Gamma_r(\mathbf{q},\omega) = \gamma_r(\mathbf{q},\omega)/2 + iS_r(\mathbf{q},\omega)$, we have the dissipator for the circular wave packet

$$\langle f|\mathrm{D}^{\mathrm{I}}[\hat{\rho}_A^{\mathrm{I}}(t)]|i\rangle = -\frac{1}{2} \sum_{s,h} \mathcal{G}_{n_f,s}^{n_i,h} \left\{ D_1 + D_2 + D_3 \right\} \rho_{A,sh}^{\mathrm{I}}(t) \tag{3.78}$$

with

$$D_1 = \sum_{\mathbf{q}} V_{\mathbf{q}}^2 \left| F_{ss}(\mathbf{q}) - F_{hh}(-\mathbf{q}) \right|^2 \gamma_r(\mathbf{q},0), \tag{3.79}$$

$$D_2 = \sum_{\mathbf{q}} \left\{ k_{hs}(\mathbf{q},\omega_{hs}) + k_{sh}(\mathbf{q},\omega_{sh}) \right\}, \tag{3.80}$$

$$D_3 = \sum_{n\neq s,h} \sum_{\mathbf{q}} \left\{ k_{sn}(\mathbf{q},\omega_{sn}) + k_{hn}(\mathbf{q},\omega_{hn}) \right\}. \tag{3.81}$$

This dissipator, describing the decoherence of the nondiagonal elements of the wave packet, has three different contributions. D_1 originates from the vertex correction and contributes only beyond the dipol approximation. D_3 represents the contributions of all intermediate transitions. The transition between the contributing initial state s and final state h is hidden in D_2 and from which the transition rates for the wave packet can be defined

$$\mathcal{W}_{n_i \to n_f} \quad = \sum_{s,h} \mathcal{G}_{n_f,s}^{n_i,h} \cdot w_{h \to s} \tag{3.82}$$

with the atomic transition rate given in Eq. (3.34).

In collision theory, the T-matrix $\hat{T} = \hat{V} + \hat{V}\hat{G}_0\hat{V} + \hat{V}\hat{G}_0\hat{V}\hat{G}_0\hat{V} + \dots$ is used to calculate the cross sections and the transition rates. Comparison with the Born approximation implemented in the derivation of the QME (3.14) shows that only the first term $\hat{V}$ in T-matrix is taken into account. In order to obtain a better description of the collision effects in plasma, higher-order terms should be evaluated. We use a semiclassical approximation reported in Ref. [BL95] to describe the modification of the transition rate due to the collision effects in plasma, which is given by

$$f(n,\Delta n,\Theta) = \ln\left[1 + \frac{1}{\Delta n\Theta(1 + 2.5n\Theta/\Delta n)}\right] \cdot \left[\ln\left(1 + \frac{1}{\Delta n\Theta}\right)\right]^{-1}, \quad \Theta = \sqrt{\frac{|E_n|}{k_B T}} \tag{3.83}$$

with $\Delta n = n - n'$ and the binding energy E_n for the hydrogen atom. Therefore the modified transition rate for the wave packet description may be written as

$$\mathcal{W}_{n_i \to n_f} = \sum_{s,h} \mathcal{G}_{n_f,s}^{n_i,h} \cdot w_{h \to s} \cdot f(h,|h-s|,\Theta). \tag{3.84}$$

In Fig. 3.4 we show the transition rates calculated from the expression (3.84) for two different values for the width of the hydrogenic wave packet. Comparing with the experimental data of Helium, it can be seen that the transition rates calculated with the wave packet width $\sigma_{n_0} = 0.75$, evaluated using Eq. (3.71) for the given plasma parameters T and n_{pl}, are in best agreement. The agreement reveals the coherent wave packet character of the Rydberg electron.
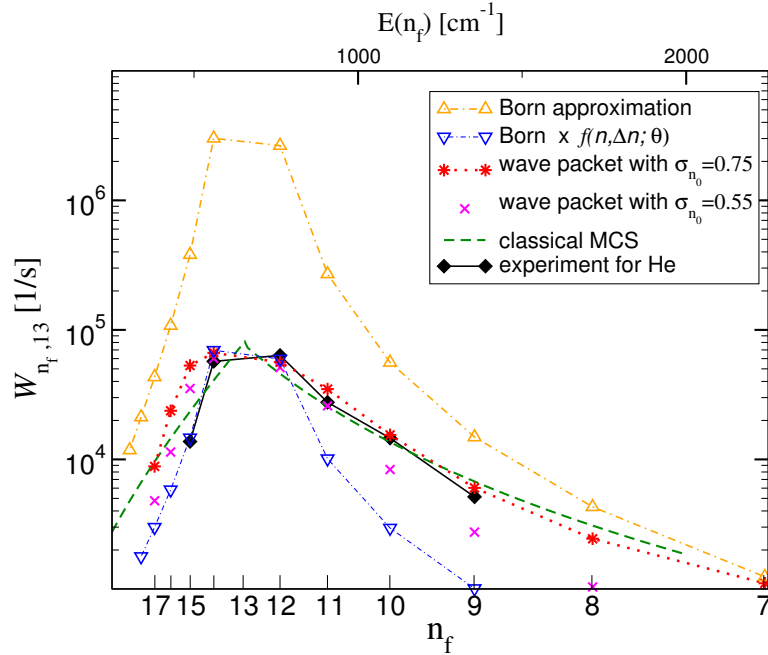

Abb. 3.4: Transition rates of $n_i = 13$ to near n_f states induced at a $T = 300$ K electron plasma with density $n_{\text{pl}} = 10^9 \text{cm}^{-3}$. calculated from the wave packet description with the width $\sigma_{n_0} = 0.55$ and $\sigma_{n_0} = 0.75$ compared to the results from classical Monte-Carlo simulation (MCS) [VS80], the calculation in Born approximation with and without collision effects from Ref. [GR06] and experimental data [DBD79].

The comparison between the results of the classical Monte-Carlo simulation and the experimental data indicates that a classical treatment is more appropriate to calculate the transition rates of the highly excited states. In the classical Monte-Carlo simulation, the highly excited free electron is treated as a point in an 18 dimensional phase space which behaves in accordance with classical laws under the influence of the Coulomb interactions [MK69]. From the quantum mechanical point of view, this treatment is equivalent to represent the electron as an incoherent wave packet with vanishing width.

Another comparison for the transition rates with the initial principal quantum number $n_i = 40$ is shown in Fig. 3.5. From the figure the validity of the wave packet description can be also verified from the agreement between the results of classical Monte-Carlo simulations and the results calculated with the wave packet width $\sigma_{n_0} = 2$.

3.3 Spectral line shapes in plasma in terms of the open quantum system theory

In open quantum system theory one separates a reduced subsystem out from the total quantum system, which includes all relevant observables that one is interested in. The remaining
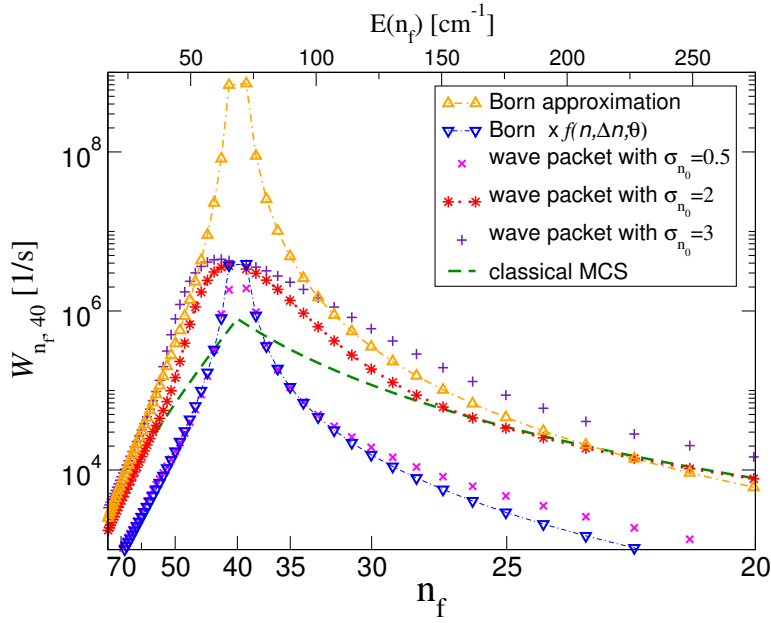
Abb. 3.5: Transition rates of $n_i = 40$ to near n_f states induced by a $T = 20$ K electron plasma with density $n_{\rm pl} = 10^9 {\rm cm}^{-3}$ calculated from the wave packet description with the width $\sigma_{n_0} = 0.5, 2, 3$ compared to the results from classical Monte-Carlo simulation [VS80] (green line) and the results in Born approximation with and without collision effects from Ref. [BL95].

degrees of freedom are treated as irrelevant for the dynamical behavior and are denoted as the observables of the bath. However, the selection of the relevant observables that are appropriate to describe the dynamics of the system depends sensitively on the physical problems that we tackle.

For instance, the degrees of freedom of the emitted photons are irrelevant for the dynamics of the population numbers of the atomic energy eigenstates and therefore can be considered as part of the bath in the derivation of the Pauli equation. This consideration is also applied in the derivation of the natural line width of the spectral line profile [BP07, Röp13]. In contrast, these degrees of freedom are most important for the description of the spectral line profile in a plasma environment where we obtain the spectral line shapes by measuring the energy of the emitted photons. The emitted photons are therefore relevant degrees of freedom. To correctly describe the spectral line shapes via the open quantum system theory, we must extend the reduced system by including the set of the degrees of freedom of the emitted photons. This means that the radiation field together with the atomic system should be considered as the reduced system to be described by the QME, and the surrounding plasma is the bath coupled to the system by Coulomb interaction.

Absorption as well as spontaneous and induced emission coefficients, related by the Einstein relation, are obtained from QED where the transverse part of the Maxwell field

$$\hat{H}_{\rm photon}^{\perp} = \sum_{\mathbf{k},s} \hbar\omega_{\mathbf{k},s}\hat{n}_{\mathbf{k},s} \tag{3.85}$$

is quantized and denoted by the photon modes $|\mathbf{k}, s\rangle$. The frequency $\omega_{\mathbf{k}} = c|\mathbf{k}| = 2\pi c/\lambda$ is the dispersion relation for the frequency as a function of the wave number λ. $\hat{n}_{\mathbf{k},s} = \hat{b}_{\mathbf{k},s}^{\dagger}\hat{b}_{\mathbf{k},s}$ is the

occupation number with the polarization $s = 1, 2$. As mentioned above, the photon field must be treated as part of the reduced system with the Hamiltonian $\hat{H}_S = \hat{H}_A + \hat{H}^\perp_{\text{photon}}$, and the eigenstates will be denoted by the expression $|\tilde{n}\rangle = |\psi_n, N_n(\mathbf{k}, s)\rangle$ containing corresponding quantum numbers for the eigenenergy $\tilde{E}_n = E_n + \sum_{\mathbf{k},s} N_n(\mathbf{k}, s)\,\hbar\omega_{\mathbf{k},s}$ with the occupation number $N_n(\mathbf{k}, s)$ of the mode $|\mathbf{k}, s\rangle$.

Emission and absorption are described by the interaction Hamiltonian, see Eq. (3.5), $\hat{H}^{\text{rad}} = \int d^3\mathbf{r}\, \hat{\mathbf{j}}^\perp_A \cdot \hat{\mathbf{A}}_{\text{ph}} = \int d^3\mathbf{r}\, \hat{\mathbf{d}}_A \cdot \hat{\mathbf{E}}_{\text{ph}}$ after integration by parts with the atomic dipole operator $\hat{\mathbf{d}}_A$. The decomposition of the electric field of the photon subsystem (two polarization vectors $\hat{\mathbf{e}}_{\mathbf{k},s}$) is

$$\hat{\mathbf{E}}_{\text{p}h} = i \sum_{\mathbf{k},s} \sqrt{\frac{\hbar\omega_{\mathbf{k}}}{2\Omega_0}}\, \hat{\mathbf{e}}_{\mathbf{k},s}\,[\hat{b}_{\mathbf{k},s} - \hat{b}^\dagger_{\mathbf{k},s}]. \tag{3.86}$$

For a given measured photon mode $|\bar{\mathbf{k}}, \bar{s}\rangle$ in the experiment, only the mode with $\mathbf{k} = \bar{\mathbf{k}}$ and $s = \bar{s}$ in the Hamiltonian $\hat{H}^{rad}$ contributes. This allows us to introduce a new operator describing emission and absorption

$$\hat{\mathbf{d}}_S = \hat{\mathbf{d}}_A \otimes (\hat{b}_{\bar{\mathbf{k}}} - \hat{b}^\dagger_{\bar{\mathbf{k}}}), \tag{3.87}$$

where the polarization index is suppressed. The initial and final states in this case are given by $|\tilde{i}\rangle = |\psi_i, N_i(\mathbf{k})\rangle$ and $|\tilde{f}\rangle = |\psi_f, N_f(\mathbf{k})\rangle$ with $N_f(\mathbf{k}) = N_i(\mathbf{k}) + \delta_{\mathbf{k},\bar{\mathbf{k}}}$, respectively. This means that for the measured photon mode $\bar{\mathbf{k}}$ the occupation number fulfills $N_f(\bar{\mathbf{k}}) = N_i(\bar{\mathbf{k}}) + 1$, while for all other photon modes their occupation numbers remain unchanged. A shift of the eigenenergy levels is caused by the interaction with the plasma environment via the momentum exchange. Subsequently, this leads to a deviation of the measured transition frequency $\omega_{\bar{\mathbf{k}}}$ from the characteristic transition frequencies $\omega_{nn'}$ between the unperturbed atomic eigenstates $|\psi_n\rangle$. We define the deviation by using the eigenenergies $\tilde{E}_n$ via

$$\Delta\omega_{nn'} = (\tilde{E}_n - \tilde{E}_{n'})/\hbar. \tag{3.88}$$

We use the interaction picture with $\hat{H}_0 = \hat{H}_S + \hat{H}_B$ so that the power spectrum $P(\omega_{\bar{\mathbf{k}}}) = \int_0^\infty e^{-\epsilon t} e^{\pm i\omega_{\bar{\mathbf{k}}} t} \langle \hat{\mathbf{d}}_A \rangle^t dt$ as shown in [BHMV84] in the framework of the linear-response theory can be rewritten as

$$P(\omega_{\bar{\mathbf{k}}}) = \int_0^\infty e^{-\epsilon t} \langle \hat{\mathbf{d}}_S \rangle^t dt = \sum_{if} \mathcal{L}_{i,f}, \tag{3.89}$$

where the photon frequency is absorbed by the new dipole operator $\hat{\mathbf{d}}_S$ of the reduced system (including photons) and

$$\langle \hat{\mathbf{d}}_S \rangle^t = \text{Tr}\{\hat{\rho}_S(t)\hat{\mathbf{d}}_S\} = \sum_{if} \rho^I_{S,fi}(t) \mathbf{d}^I_{S,if}(t) \tag{3.90}$$

with $\rho^I_{S,fi}(t)$ being the solution of the QME in interaction picture (see Eq. (3.95)), and the matrix elements $\mathbf{d}^I_{S,if}(t) = \langle\psi_i|\mathbf{d}_A|\psi_f\rangle e^{-i\Delta\omega_{if}t}$. Consequently, the spectral line shape $\mathcal{L}_{i,f}$ in Eq. (3.95) can be written as

$$\mathcal{L}_{i,f} = \int_0^\infty dt\, e^{-\epsilon t}\, \rho^I_{S,fi}(t) \mathbf{d}^I_{S,if}(t). \tag{3.91}$$

In order to obtain the solution of the QME, a similar reduced charge density operator containing the photon information as in Eq. (3.87) can be introduced for the extended reduced system

$$\hat{\varrho}_{\mathbf{q},\mathrm{S}} = \hat{\varrho}_{\mathbf{q},\mathrm{A}} \otimes (\hat{b}_{\bar{\mathbf{k}}} - \hat{b}_{\bar{\mathbf{k}}}^{\dagger}). \tag{3.92}$$

Using the basis set $|\tilde{n}\rangle$ of the unperturbed reduced system, we obtain the matrix elements of the reduced charge density operator $\hat{\varrho}_{\mathbf{q},\mathrm{S}}^{\mathrm{I}}(t)$ at time t

$$\langle \tilde{n}' | \hat{\varrho}_{\mathbf{q},\mathrm{S}}^{\mathrm{I}}(t) | \tilde{n} \rangle = e_e \, F_{n'n}(\mathbf{q}) \, e^{i\Delta\omega_{n'n}t} \left[\delta_{N_{n'}(\bar{\mathbf{k}}),N_n(\bar{\mathbf{k}})-1} - \delta_{N_{n'}(\bar{\mathbf{k}}),N_n(\bar{\mathbf{k}})+1} \right],$$

where the Kronecker's delta is connected to the atomic emission and absorption with the transition frequency $\omega_{n'n}$. Performing the Fourier transform with respect to the time t, we obtain the reduced charge density operator in Fourier-space

$$\hat{\varrho}_{\mathbf{q},\mathrm{S}}(\omega) = \sum_{n'>n} e_e \, \hat{T}_{n'n}^{-} \cdot F_{n'n}(\mathbf{q}) \, \delta(\omega - \Delta\omega_{n'n}) - \sum_{n'<n} e_e \, \hat{T}_{n'n}^{+} \cdot F_{n'n}(\mathbf{q}) \, \delta(\omega + \Delta\omega_{nn'}) \tag{3.93}$$

with $\hat{T}_{n'n}^{-} = |\tilde{n}'\rangle\langle\tilde{n}| \cdot \delta_{N_{n'}(\bar{\mathbf{k}}),N_n(\bar{\mathbf{k}})-1}$ denoting the one photon absorption and $\hat{T}_{n'n}^{+} = |\tilde{n}'\rangle\langle\tilde{n}| \cdot \delta_{N_{n'}(\bar{\mathbf{k}}),N_n(\bar{\mathbf{k}})+1}$ - the one photon emission. Inserting this expression into the influence function (3.21), we obtain a new influence function including both emission and absorption terms, which can be used as the starting point to derive the spectral line profile. The terms representing the emission processes can be selected by using the matrix element representation $\langle\tilde{f}|\mathcal{D}^{\mathrm{I}}[\hat{\rho}_S(t)]|\tilde{i}\rangle$ with the change of the photon number $\triangle N = N_f(\bar{\mathbf{k}}) - N_i(\bar{\mathbf{k}}) = 1$:

$$\langle\tilde{f}|\mathcal{D}^{\mathrm{I}}[\hat{\rho}_S^{\mathrm{I}}(t)]|\tilde{i}\rangle = -A_1 - A_2 + A_3 + A_4 \tag{3.94}$$

with

$$A_1 = \sum_{n>f,m<n,\mathbf{q}} \exp[i(-\triangle\omega_{nm} + \triangle\omega_{nf})t] \, K_{fn;nm}(\mathbf{q}, \triangle\omega_{nm}) \, \langle\psi_m, \triangle N|\hat{\rho}_S(t)|\psi_i\rangle$$
$$+ \sum_{n<f,m>n,\mathbf{q}} \exp[i(\triangle\omega_{mn} - \triangle\omega_{fn})t] \, K_{fn;nm}(\mathbf{q}, -\triangle\omega_{mn}) \, \langle\psi_m, \triangle N|\hat{\rho}_S(t)|\psi_i\rangle,$$

$$A_2 = \sum_{n>i,m<n,\mathbf{q}} \exp[-i(-\triangle\omega_{nm} + \triangle\omega_{ni})t] \, K_{mn;ni}^{*}(\mathbf{q}, \triangle\omega_{nm}) \, \langle\psi_f, \triangle N|\hat{\rho}_S(t)|\psi_m\rangle$$
$$+ \sum_{n<i,m>n,\mathbf{q}} \exp[-i(\triangle\omega_{mn} - \triangle\omega_{in})t] \, K_{mn;ni}^{*}(\mathbf{q}, \triangle\omega_{nm}) \, \langle\psi_f, \triangle N|\hat{\rho}_S(t)|\psi_m\rangle,$$

$$A_3 = \sum_{i>n,m<f,\mathbf{q}} \exp[i(-\triangle\omega_{fm} + \triangle\omega_{in})t] \, \langle\psi_m, \triangle N|\hat{\rho}_S(t)|\psi_n\rangle$$
$$\times \{K_{ni;fm}(\mathbf{q}, \triangle\omega_{fm}) + K_{mf;in}^{*}(\mathbf{q}, \triangle\omega_{in})\},$$

$$A_4 = \sum_{i<n,m>f,\mathbf{q}} \exp[i(-\triangle\omega_{fm} + \triangle\omega_{in})t] \, \langle\psi_m, \triangle N|\hat{\rho}_S(t)|\psi_n\rangle$$
$$\times \{K_{ni;fm}(\mathbf{q}, -\triangle\omega_{mf}) + K_{mf;in}^{*}(\mathbf{q}, -\triangle\omega_{ni})\}$$

where the indexes m and n are interchanged. These terms can be further simplified in RWA. This means that we can set $m = f$ in A_1, $m = i$ in A_2, and $m = f$, $n = i$ in A_3 and A_4. The QME in RWA becomes

$$\frac{\partial \rho^I_{S,fi}(t)}{\partial t} = -\Gamma^{BS}_{fi}(\omega_{\bar{\mathbf{k}}})\rho^I_{S,fi}(t) + \Gamma^\nu_{fi}\,\rho^I_{S,fi}(t) \tag{3.95}$$

with a coefficient $\Gamma^{BS}_{fi}(\omega_{\bar{\mathbf{k}}})$ describing the shift of the eigenenergy levels and the pressure broadening

$$\Gamma^{BS}_{fi}(\omega_{\bar{\mathbf{k}}}) = \sum_{n,\mathbf{q}} \big\{ K_{nf;fn}(\mathbf{q}, \triangle\omega_{nf}) + K_{nf;fn}(\mathbf{q}, -\triangle\omega_{fn}) \tag{3.96}$$
$$+ K^*_{ni;in}(\mathbf{q}, \triangle\omega_{ni}) + K^*_{ni;in}(\mathbf{q}, -\triangle\omega_{in}) \big\}$$

and a coefficient Γ^V_{fi} describing the vertex correction

$$\Gamma^V_{fi} = \sum_{\mathbf{q}} \big\{ K_{ii;ff}(\mathbf{q}, \triangle\omega_{ff}) + K_{ii;ff}(\mathbf{q}, -\triangle\omega_{ff}) \tag{3.97}$$
$$+ K^*_{ff;ii}(\mathbf{q}, \triangle\omega_{ii}) + K^*_{ff;ii}(\mathbf{q}, -\triangle\omega_{ii}) \big\}.$$

The vertex correction has no dependence on the photon frequency $\omega_{\bar{\mathbf{k}}}$ and contributes only beyond the dipol approximation. Formally integrating the expression (3.95) yields

$$\rho^I_{S,fi}(t) = \rho^I_{S,fi}(0) \cdot e^{-\big\{\Gamma^{BS}_{fi}(\omega_{\bar{\mathbf{k}}}) - \Gamma^V_{fi}\big\}t}. \tag{3.98}$$

Inserting this formal solution into the Eq. (3.91), the line shape function can be expressed as

$$\mathcal{L}(\omega_{\bar{\mathbf{k}}})_{i,f} \quad \propto \frac{1}{\omega_{\bar{\mathbf{k}}} - \omega_{if} + i\epsilon - i\Gamma^{BS}_{if}(\omega_{\bar{\mathbf{k}}}) + i\Gamma^V_{if}}. \tag{3.99}$$

The expression (3.99) coincides with the result of the unified theory for spectral line profiles [KG95], if only the electron contribution (impact approximation) is considered. Note that the unified theory gives the result in Born approximation with respect to the interaction with the surrounding plasma, what corresponds to the Born-Markov approximation for the coupling to the plasma considered as the bath. Strong coupling of the radiator to the perturbing environment has been treated in the Green function approach using a T-matrix approximation, see Ref. [KG95]. The improvement of the Born-Markov approximation for the QME considering strong interactions and the ionic contribution of the plasma environment, given by the microfield distribution.

4. IONIZATION POTENTIAL DEPRESSION IN PLASMAS

A fundamental phenomenon in plasma is the modification of bound state levels as well as of continuum states by the surrounding warm and dense medium. In this chapter, we are interested in the ionization potential depression (IPD) which is relevant for the composition of the plasma, and, accordingly, for the thermodynamic and transport properties. Introducing the ionic dynamical structure factor as the indicator for the ionic microfield, we demonstrate that ionic correlations and fluctuations play a critical role in determining the ionization potential depression. The comparisons with recent experimental measurements and other theoretical approaches are made. The main results of this chapter are published in Phys. Rev. E 96, 013202 (2017).

4.1   Atomic potential and ionization potential depression

When ions or atoms are immersed in a plasma, they experience a special local environment which is substantially different in comparison with that of the isolated case, where only the vacuum fluctuation exists. In addition, the boundary condition for the atomic potential is also drastically changed due to the existence of other plasma particles. In the case of isolated systems, the atomic potential disappears at infinity, i.e. $V(r) \to 0$ for $r \to \infty$, as shown in Fig. 4.1a. In contrast, the atomic potential experienced by a bound electron has a finite negative value at the boundary of ionic system determined by the charge neutrality condition, see Fig. 4.1b.

This change of the local environment results in modifications of the dynamics of the bound electrons. A fundamental related phenomenon is the modification of bound state levels as well as of continuum states (also known as ionization potential depression) due to the surrounding warm and dense medium [KKER86, Gri97, Sal98, Fuj05]. The ionization energy depression (IPD) describes the reduction of the energy needed to liberate a bound electron into the continuum state in plasma in comparison with the case of an isolated ion. In particular, the IPD significantly alters the ionization balance in plasma and therefore strongly modifies the thermodynamic properties and optical properties of the system. This change can be understood as following [Sal98, Fuj05]. Firstly, the original atomic potential exerted by the ion core to the bound electrons is modified by the local instantaneous microfield generated by the surrounding plasma particles, resulting shift and broadening of the bound eigenlevels. Secondly, the boundary condition for the original Coulomb potential, $V(r) \to 0$ for $r \to \infty$, is violated due to the existence of other ions, i.e. the Coulomb potential has a finite negative value at a finite boundary. In the simplest approximation, the IPD in plasma can be expressed in a general form as [Fuj05]

$$\Delta_{\mathrm{IPD}} = \frac{z_i \, e^2}{4\pi\varepsilon_0 R_{\mathrm{cr}}}, \tag{4.1}$$
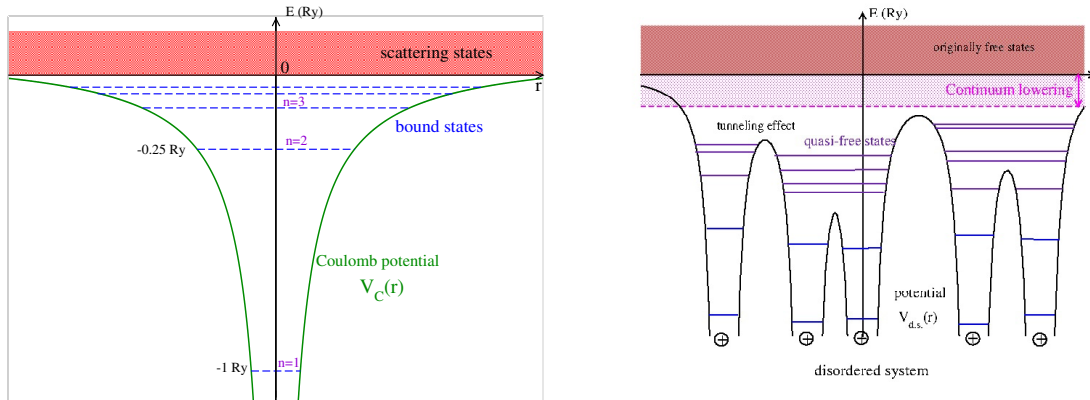
(a) Atomic potential experienced by a bound electron in isolated H atom.

(b) Atomic potential experienced by a bound electron in a plasma environment.

Abb. 4.1: Schematical description of the atomic potential for a bound electron without and with plasma environment

where R_{cr} is some characteristic length in plasma, which describes the geometrical or the dynamical properties of the plasma system. A typical characteristic length describing the geometrical distribution is the average distance between the ions, i.e., the Wigner-Seitz radius $R_{\mathrm{WS}} = (3/(4\pi n_{\mathrm{i}}))^{1/3}$, which leads to the ion sphere model for the IPD. On the other hand, one of the dynamical properties in plasma is the screening effect. In the low density and high temperature limit, the screening is represented by the Debye screening length, so that the Debye-Hückel model for the IPD is obtained. For more complicate cases, for instance in the WDM regime, the IPD can not be described by any such simple model because of the complex structure and dynamical coupling of the plasma.

The shifts both of the continuum edge and of the bound state levels have been discussed for the electron-hole plasma in excited semiconductors [RKK$^+$78, ZKK$^+$78, KKER86, Zim87, KSKB05] some decades ago. Depending on the density and temperature of the electron-hole plasma, excitons are modified by medium effects, and merge with the lowered continuum at the Mott density. Thus, an exciton gas is transformed into an electron-hole liquid. A highly sophisticated theory describing dynamical screening and degeneracy effects by the fermionic plasma constituents had been worked out, explaining precise measurements in excited semiconductors. However, because the ions are heavier compared to the effective mass of holes, a simple transfer of the physics of excited semiconductors to WDM is not possible. The ions remain classical within a large density region, forming strong correlations which are described by the dynamical ionic structure factor (SF) $S_{\mathrm{ii}}(\mathbf{q}, \omega)$ [LRKR17].

4.2 Theoretical models for ionization potential depression

4.2.1 Analytical approaches

The first attempt for the IPD to cover a wide density range was carried out by Ecker and Kröll in 1963 [EK63], which is based on a statistical method in expressing the IPD via the chemical potential. To determine the chemical potential in plasma, the average electrostatic micro-potential at the point of the investigated particle was evaluated. In their work, three

special characteristic radii, i.e. r_{OK}, r_{ic} and r_C, were introduced in order to determine the average electrostatic micro-potential. r_{OK} is the smallest distance from the test particle, above which the Onsager-Kirkwood condition $z_1 z_2 e^2/(4\pi k_B T r_{OK}) \ll 1$ is fulfilled. This condition indicates, in fact, that the particle with charge number z_1 is weakly coupled to another particle with charge number z_2 in the distance r_{OK}. The characteristic length r_{ic} separates the environment of the investigated particle into an individual and a collective region. Then in the domain $r > \max\{r_{OK}, r_{ic}\}$, the potential can be satisfactorily approximated by the Yakuwa potential. The latter-most radius r_C characterizes the largest distance from the test particle, below which the potential can be well approximated by the Coulomb potential. In the intermediate region $r_C < r < \max\{r_{OK}, r_{ic}\}$, the potential distribution is not exactly known but should lie between the above two limited potential distributions. After a detailed analysis, Ecker and Kröll found the expressions for the potential in this region and consequently determined the IPD as following

$$\triangle I_{EK} = \begin{cases} \frac{(Z_{ion}+1)e^2}{4\pi\,\varepsilon_0\,\lambda_D} & \text{if } n < n_{cr} \\ C_{EK}\frac{(Z_{ion}+1)e^2}{4\pi\,\varepsilon_0\,r_{EK}} & \text{if } n \geq n_{cr} \end{cases} \quad \text{with } n_{cr} = \frac{3}{4\pi}\left(\frac{k_B T_e}{Z^2 e^2}\right)^3, n = \frac{N}{V} \qquad (4.2)$$

with the Ecker-Kröll radius $r_{EK} = \sqrt[3]{\frac{3V}{4\pi N}}$ and the total number of particles in plasma $N = N_e + \sum_{z_i} N_{z_i}$. The prefactor C_{EK} is determined by the continuity condition at the critical density. To fit the experimental data with the EK model, Ciricosta $et\ al.$ [CVC$^+$12] found that $C_{EK} = 1$, denoted as modified EK (mEK) model, is most suitable for their measurements. Below the critical density, the expression in Eq. (4.2) is the famous Debye-Hückel (DH) shift and also known as the "polarization term" for the lowering of the ionization potential. In the opposite limit, it is denoted as the "lattice term" for the IPD following the notation introduced by Ecker and Weizel [EW56].

Two years after the publication of EK's work, Stewart and Pyatt developed another approach to calculate the average electrostatic potential distribution around a nucleus located in a plasma environment using a finite-temperature Thomas-Fermi (TF) model [SPJ66]. In calculating the potential distribution via the Poisson equation, the electrons in plasma are described in terms of the non-relativistic Fermi-Dirac statistics whereas the ionic contribution of the neighboring ions to the potential distribution near the test ion is represented by the non-relativistic Maxwell-Boltzmann statistics. Theoretically, the bound and free electrons in the TF theory do not need to be treated differently and could be taken into account consistently. As argued by Stewart and Pyatt in their work, the bound electrons have no contribution to the pressure lowering of the ionization potential because the bound electrons exist already in the isolated system. Therefore, one should isolate the effect of the free electrons and neighboring ions in determining the potential distribution in the TF model. After a lengthy and detailed calculation, Stewart and Pyatt expressed their results for the IPD as

$$\triangle I_{SP} = \frac{3}{2}\frac{(Z_{ion}+1)\,e^2}{4\pi\,\varepsilon_0\,r_{IS}} \cdot \frac{\left[(\kappa_D\,r_{IS})^3 + 1\right]^{2/3} - 1}{(\kappa_D\,r_{IS})^2}, \qquad (4.3)$$

where the total inverse Debye screening length is $\kappa_D = \sqrt{\frac{e^2 \sum_i (z_i^2 + z_i)n_i}{\varepsilon_0 k_B T_e}} = \sqrt{\frac{e^2 n_e (1+z^*)}{\varepsilon_0 k_B T_e}}$ including both ions and electrons with $n_e = \sum_i z_i n_i$ and $z^* = \left(\sum_i z_i^2 n_i\right)/\left(\sum_i z_i n_i\right) = \left(\sum_i z_i^2 n_i\right)/n_e$. The expression (4.3) is actually an interpolation between the DH and Ion-Sphere limits, which

reduces to the DH shift in the case of weakly coupled plasmas whereas for strongly coupled plasma system the IS form, i.e. $\triangle I_{\mathrm{SP}} \rightarrow \triangle I_{\mathrm{IS}} = \frac{3}{2} \frac{(Z_{\mathrm{ion}}+1)\,e^2}{4\pi\,\varepsilon_0\,r_{\mathrm{IS}}}$, can be obtained.

Since then many other attempts to understand the phenomenon of IPD have been made by different authors. Zimmerman and More investigated the Helmholtz free energy in plasmas based on the average atom model and the screened hydrogenic model [ZM80]. The essential problem in their calculation is the determination of the equilibrium populations of the one-electron state in shell $|nl\rangle$ with an effective charge Z_{nl} experienced by the test bound electron. The lowering of the ionization potential Δ_{IPD} is then given by the partial derivative of the Helmholtz free energy over the charge number of the test ion. The average model is more or less a similar model as the IS model, so that a satisfactory description can only be acquired for the case of high density from their calculation. Another calculation was performed by Dharma-wardana and Perrot, where the notation "mobility edge" for the continuum states was introduced based on the so-called neutral pseudoatom model [DwP92]. In plasma, the distinction between the bound discrete states and the continuum states is rather ambiguous because some states around the bound-free limit persistently oscillate between the continuum and the bound levels with the fluctuation of the distribution of the surrounding plasma. Consequently, a sharp definition of the position of the borderline between the discrete and continuum states is extremely difficult and complicate. In other words, we have a mobility edge for the position of the continuum states.

4.2.2   Review of the topic "ionization potential depression" by Crowley

An excellent review on the topic "IPD" can be found in the recent work of Crowley [Cro14], where he pointed out that different definitions for the phenomenon "IPD" are present and should be treated carefully and distinguished in the application to compare the experimental measurements and the theoretical calculations using different models. In general, the ionization is regarded as a quasistatic transition between states of thermodynamic equilibrium. The continuum lowering modeled under this assumption is referred as the thermodynamic IPD. Obviously, the EK and SP models belong to this category. Moreover, in the derivation of these models, the IPD is evaluated in terms of the average electrostatic potential experienced by the electrons in the ion under investigation. This treatment results in the static continuum lowering, since the dynamical influence of the surrounding particles on the test particle, such as the fluctuation of the microfield and dynamical screening, are disregarded.

The discussions above are from the theoretical consideration. In the viewpoint of experiments, photonionization is a dynamical process between plasma microstates, in which the changes of plasma microstates are observed on timescales much smaller than the response from the surrounding plasma to this individual transition. Because of this transition, the initially assumed condition of local thermodynamic equilibrium of plasma system cannot be valid any more. During their propagations in plasma, the photon and the emitted electron exchange energy with their surroundings. This phenomenon is known as relaxation and the exchanged energy is denoted as relaxation energy. Taking into account this relaxation energy yields the spectroscopic ionization potential depression. To analyze the experimental measurement, special care should be taken when applying these definitions of different IPDs. More details can be found in the original paper of Crowley.

4.2.3   Simulation methods

With the development of the computer technique, Monte-Carlo simulations and the molecular dynamical simulations become more and more popular in the scientific researches, in particular in determining the properties of many-body systems in physics. Additionally, numerical approaches based on numerically solving the Schrödinger equation, such as Hartree-Fock calculations [Cra02] and the density functional theory method [Bau13, Red13], are also state-of-the-art modeling methods used in physics, chemistry and material sciences to investigate the properties of electronic structures in many-body systems. After the experiments by Ciricosta *et al.* [CVC+12] and Hoarty *et al.* [HAJ+13a], which renewed the interest on the topic of IPD and suggest that a deeper understanding on this phenomenon is afforded, different numerical approaches, such as classical molecular dynamical simulations [CFT15b, CFT15a], two-step Hatree-Fock calculations [STJ+14], calculations via the density functional theory [VCW14], and Monte-Carlo simulations [Str16] have been performed recently in the investigation of the IPD in plasma.

4.3   Experimental measurements on ionization potential depression

Being a long-standing problem in plasma physics, IPD experiments [HAJ+13a, CVC+12, Ct16, PVC+13, FKP+14, KCK+16] have been performed recently using the new possibility to produce highly excited plasmas at condensed matter densities by intense short-pulse laser irradiation.

### 4.3.1   Measurements of ionization energies of K-shell electrons

The first reliable measurement was performed by Ciricosta *et al.* [CVC+12, Ve12] at the LCLS soft X-ray materials science instrument. In this experiment, targets comprising 1.0μm-thick aluminum foils at solid density were irradiated with 80-fs pulses of X-rays at photon energies in the range $1560 - 1830$ eV (around and above the K-edge of cold Al) at peak intensities exceeding 10^{17} W cm^{-2}. In this conditions the Al sample is isochorically heated to electron temperatures up to 200 eV, depending on the LCLS photon energy. Since the photon energy lies near that ion's K edge and the kinetic energy of free electrons is relatively small in comparison to the photon energy, the main transition mechanism is direct photoionization rather than collisional ionization. Due to the dominated K-shell photoabsorption, a core electron in the K-shell is ejected into the continuum and the K-shell holes are created exclusively by intense, quasi-monochromatic X-ray photons (denoted as K-edge in Subfigure 4.2a). After photoionization, the K-shell holes are filled by two different processes, i.e. the KLL Auger decay and the K$_\alpha$ transition, where the radiative emission accounts only for 3% of the total recombination from the L shell. Subsequently, an X-ray fluorescence spectrum is recorded by means of a flat crystal Bragg spectrometer, as shown in Subfigure 4.2b. The occurrence of K-shell emission is indeed strongly dependent on the energy of the incident photon, which can be therefore regarded as an indicator for the direct measurement of the IPDs, because the threshold value of the photon energy inducing the K-shell holes and subsequent K$_\alpha$ emission in a plasma is reduced in comparison with the K-edge ionization energy of the isolated case. The measured IPD values in different cases are shown in Fig. 4.3, where excellent agreements between the experimental data and the EK model are displayed.
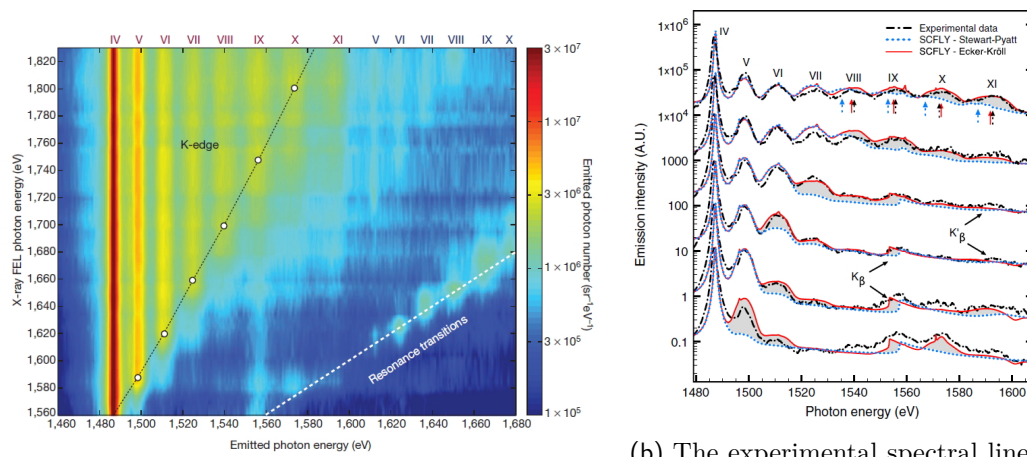
(a) The experimentally detected K-edges for Al at different charge states.

(b) The experimental spectral lines from K-shell by different induced photon energy.

Abb. 4.2: Spectral lines from K-shell in a laser-produced Al plasma, taken from Ref. [Ve12].
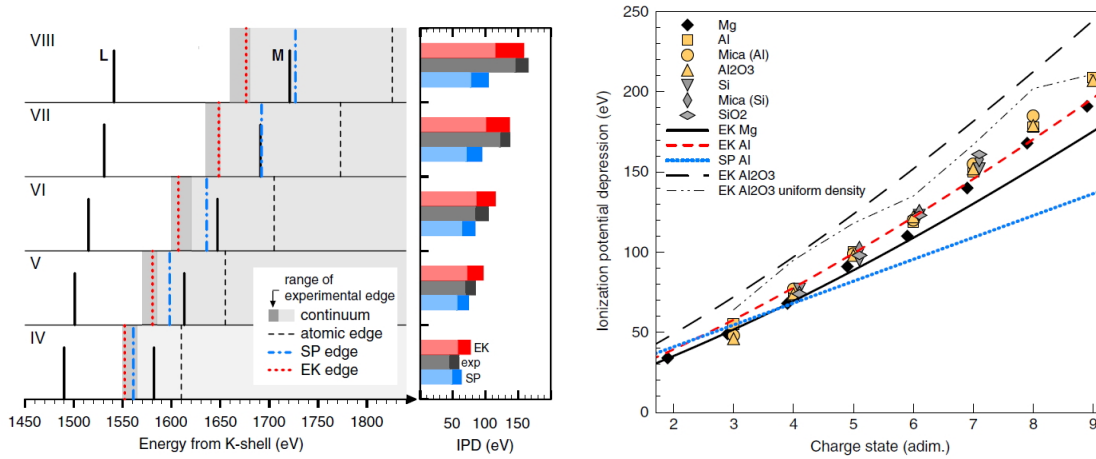
(a) The experimentally detected K edges and the corresponding IPD values for an Al plasma, taken from Ref. [CVC+12].

(b) The experimentally measured IPD values for different compounds, taken from Ref. [Ct16].

Abb. 4.3: Experimental measurements for IPD via the ionization energies of K-shell electrons

4.3.2 Measurements of dissolution of spectral lines

Another experiment on measuring the effect of IPD was carried out by Hoarty *et al.* [HAJ+13a] at the newly commissioned Orion laser in the UK, where the Al sample with density in the range of $1 - 10$ g/cc buried in plastic foils or diamond sheets is compressed and heated to electron temperature between 500 and 700 eV. In this experiment, the disappearance of lines is believed to be attributed to the IPD, but not the broadening of bound states. In these experimental conditions, the hydrogen- and helium-like aluminum ions are abundant and the $n = 1-3$ transitions from these ions are clearly visible at low density, see Subfigure 4.4a. With increasing density as shown in Subfigure 4.4b, the spectral lines are found to be smoothed out at the density of $5.5 - 9$ g/cc. In addition, the peak information of the experimental

lineout can be well reproduced in the FLYCHK code with consideration of the SP model for the reduction of the ionization potential. In contrast to the measurement by Ciricosta *et al.* [CVC$^+$12], this experiment is an indirect measurement for the IPD.
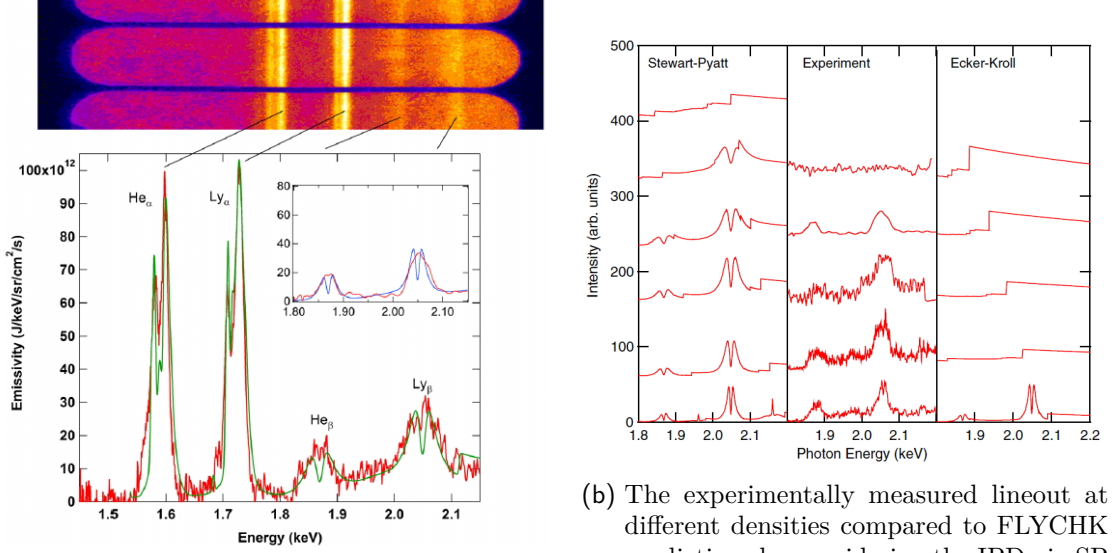
(a) The experimentally detected spectral lines for an Al plasma at 3 g/cc and $T = 700$ eV, taken from Ref. [HAJ$^+$13a].

(b) The experimentally measured lineout at different densities compared to FLYCHK predictions by considering the IPD via SP and EK model. The density of the curves from bottom to top is 1.2, 2.5, 4, 5.5, and 9 g/cc. Taken from Ref. [HAJ$^+$13a].

Abb. 4.4: Experimental measurements for IPD via the Ly$_\beta$ and He$_\beta$ lines

4.3.3 Measurements of bound-free transitions via Thomson scattering

X-ray Thomson scattering (XRTS) spectra have been demonstrated to be a powerful diagnostic tool to measure the electron density and temperature of WDM and highly compressed dense plasmas. The entire spectrum is determined by the total electron structure factor [Chi00, GR09, FKP$^+$14]

$$S_{\text{ee}}^{\text{tot}}(\mathbf{k}, \omega) = \sum_{a,b} \sqrt{x_a x_b} \, |f_a(k) + q_a(k)| \cdot |f_b(k) + q_b(k)| \, S_{ab}(\mathbf{k}, \omega)$$

$$+ Z_{\text{f}} S_{\text{ee}}^0(\mathbf{k}, \omega) + \sum_a Z_a^{\text{c}} x_a \int d\omega' \, S_a^{\text{ce}}(\mathbf{k}, \omega - \omega') \, S_a^{\text{s}}(\mathbf{k}, \omega') \qquad (4.4)$$

where $x_a = n_a / \sum_b n_b$ is the fraction of the ion species a with its density n_a, the number of its core bound electrons Z_a^{c}, atomic form factor $f_a(k)$, and the screening cloud following the motion of the ion a $q_a(k)$. Z_{f} denotes the effective free ionization state which obeys the charge neutrality condition. The first term in Eq. (4.4) given by the partial ion-ion structure factor $S_{ab}(\mathbf{k}, \omega)$ results from elastic scattering of tightly bound electrons (i.e. Rayleigh scattering) and other weakly coupled free electrons that move along with the ions. The second term described by the SF $S_{\text{ee}}^0(\mathbf{k}, \omega)$ represents the Compton scattering for the free electrons that do not follow the ions. The third term, represented by $S_a^{\text{ce}}(\mathbf{k}, \omega - \omega')$ describes the bound-free transitions, which are modulated by the self-motion of the test ion, i.e., $S_a^{\text{s}}(\mathbf{k}, \omega')$.

The XRTS from bound-free transitions under well-characterized electron density n_{e} and temperature T_{e} contains information about the ionization potential depression because it

has a significant influence on the ionization balance [FKP+14, KCK+16]. Therefore, the XRTS technique gives the possibility to have a deeper understanding on the phenomenon "continuum lowering" in plasma and can be used to benchmark different IPD models.

The first application using XRTS to reveal the IPD effect was reported by Fletcher *et al.* [FKP+14]. They found the best-fit to both the elastic and inelastic scattering can be found only with a carbon ionization state of $Z_C = 4$, which means that the L-shell electrons are completely dissolved and have no contribution. In those modelings which neglect the shell structure of the ions, i.e., orbital-free modeling such as the standard Thomas-Fermi model, the mean charge state of the carbon ions is predicated to be $Z_C = 2$, which is inconsistent with the measured ionization state $Z_C = 4$. In other words, the continuum lowering and shell structure must be incorporated in the modeling to analyze the bound-free scattering contribution of the measured XRTS data.

Another recent measurement through the XRTS spectrum was performed by Kraus *et al.* [KCK+16] at the National Ignition Facility, where a CH sphere was irradiated by laser beams with total energy of 1.1 MJ and a peak power of 425 TM and was six time compressed to a density $\rho_{CH} = 6.74$ g/cc with the mean electron temperature $T_e = 86 \pm 20$ eV and the mean charge state of carbon ions $\langle Z_C \rangle = 4.92 \pm 0.15$, while the hydrodynamics simulations predict a mean ionization charge state of $\langle Z_C \rangle = 4.4$ with $\langle T_e \rangle = 109$ eV. A reasonable explanation for this high carbon ionization state is challenging because the simulations incorporating the widely used IPD models, such as EK and SP models, predicate significantly smaller mean charge state with $\langle Z_C \rangle = 4.2$ under the same plasma conditions explored by the experiment. Coincidentally and astonishingly, the prediction by the simulation with DH model results in an excellent agreement with the experimental results because the DH model gives a remarkably larger IPD than other models and consequently a larger mean ionization charge state. However, it is well known that the DH theory works only for the high temperature and low density plasma, i.e., in the classical regime. In other words, although the DH model results in a good agreement with the experiment, the explanation based on it is incredible and questionable. A more general model at the microscopical level is necessary for such extreme states of matter [LRKR17].
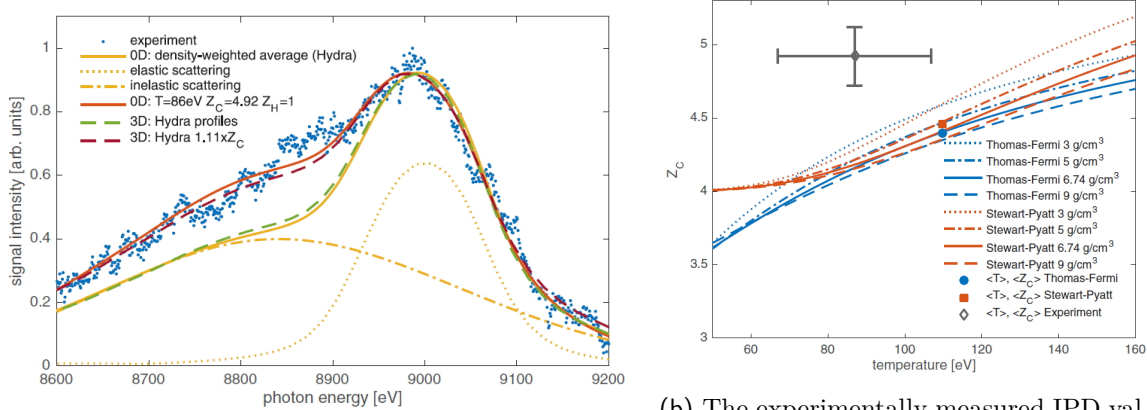
(a) The experimentally measured IPD values for different compounds, taken from Ref. [KCK+16].

(b) The experimentally measured IPD values for different compounds, taken from Ref. [KCK+16].

Abb. 4.5: Inferred mean charge states for carbon ions within different IPD models

4.4 Quantum statistical approach for ionization potential depression in terms of dynamical structure factors

The phenomenon, ionization potential depression, can be better understood within the framework of our quantum statistical approach [KSKB05, KKER86], where the definition of the continuum lowering is more clear and the influence of the plasma environment on the investigated system is simply represented by the quantity "self-energy" as discussed in Chapter II and as detailed in the following.

4.4.1 Continuum lowering and single-particle self-energy in plasmas

To study the properties of the atomic system in plasma, we consider a two-particle system, consisting of an electron (charge $-e$, mass m_e) and an ion (charge $(Z_i + 1)\,e$, mass m_i) embedded in a surrounding plasma. In vacuum, the solution of the Schrödinger equation for the Coulomb interaction is well known. Bound states are found at negative energies, whereas a continuum of scattering states is observed at positive energies. The simple case of the Hydrogen atom ($Z_i = 0$) can be generalized to a two-particle system with total charge $Z_i e$, consisting of a core ion with charge number $Z_i + 1$ and an electron, charge number $Z_e = -1$.

If the two-particle system is embedded in a plasma, bound state energies and wave functions as well as the scattering states are modified. Correspondingly, the Schrödinger equation for the two-particle system has to be amended in order to include the influence of the surrounding plasma. A systematic quantum statistical approach to describe these medium effects is given by the method of thermodynamic Green functions [KSKB05, KKER86]. In particular, the following in-medium Schrödinger equation (usually denoted as Bethe-Salpeter equation) can be derived [ZKK$^+$78, RKK$^+$78, KSKB05, KKER86]:

$$\left\{ E(1) + E(2) + \sum_{\mathbf{q}} \left\{ f(1 + \mathbf{q}) + f(2 - \mathbf{q}) \right\} V_{12}(\mathbf{q}) + \Delta V^{\text{eff}}(1, 2, \mathbf{q}, z) \right\} \psi(1, 2, z)$$

$$+ \sum_{\mathbf{q}} \left\{ \left\{ 1 - f(1) - f(2) \right\} V_{12}(\mathbf{q}) + \Delta V^{\text{eff}}(1, 2, \mathbf{q}, z) \right\} \psi(1 + \mathbf{q}, 2 - \mathbf{q}, z) = \hbar z\, \psi(1, 2, z). \quad (4.5)$$

Neglecting in Eq. (4.5) the medium effect arising from the Fermi functions $f(i)$ as well as the effective interaction $\Delta V^{\text{eff}}(1, 2, \mathbf{q}, z)$, the equation

$$\left[E(1) + E(2) \right] \psi(1, 2, z) + \sum_{\mathbf{q}} V_{12}(\mathbf{q}) \psi(1 + \mathbf{q}, 2 - \mathbf{q}, z) = \hbar z\, \psi(1, 2, z)$$

has eigensolutions $\psi_n(1, 2)$ at energies $\hbar z = E_n$, well known from Hydrogen-like ions. For more complex ions consisting of a nucleus and some bound electrons, a pseudopotential can be introduced to describe the effect of the electrons within the core ion.

The in-medium Schrödinger equation (4.5) describes the influence of the medium according to two effects, Pauli blocking and screening. Pauli blocking is caused by the antisymmetrization of the fermionic wave function. States which are already occupied by the medium are blocked and can not be used for the two-particle system under consideration. The blocking is described by the Fermi distribution function $f(1) = [\exp(\beta(E(1) - \mu(1)) + 1]^{-1}$, with $\beta = 1/(k_B T)$ and $\mu(1)$ denoting the chemical potential of species c_1. The Pauli exclusion principle leads to the Fock shift $\sum_{\mathbf{q}} f(1 + \mathbf{q})\, V_{12}(\mathbf{q})$ in addition to the single particle energy $E(1)$ in Eq. (4.5) (for charge-neutral plasmas, the Hartree term vanishes). Also in the interaction term, the Pauli blocking gives the contribution $-\sum_{\mathbf{q}} f(1) V_{12}(\mathbf{q}) \psi(1 + \mathbf{q}, 2 - \mathbf{q}, z)$.

Both in-medium contributions are caused by the degeneracy of the plasma particles. In the plasmas considered here, electrons may be degenerate because of their small mass m_e. The ions are non-degenerate and can be treated as classical particles.

Considering only the Pauli blocking effects, the effective (non-hermitean) Hamiltonian of Eq. (4.5) remains real and can be symmetrized. The energy eigenvalue problem can be solved, and the bound state energies as well as the edge of continuum states are shifted. At a certain density, the bound states merge with the continuum of scattering states and disappear. Within this approximation, which is essentially a mean-field approximation, a sharp value for the lowering of the continuum edge and for the IPD can be calculated.

Screening of the interaction by the medium is described by the effective interaction

$$\Delta V^{\text{eff}}(1, 2, \mathbf{q}, z) = -V_{12}(\mathbf{q}) \int_{-\infty}^{\infty} \frac{d\omega'}{\pi} \text{Im } \varepsilon^{-1}(q, \omega' + i0) \cdot [n_{\text{B}}(\omega') + 1]$$

$$\times \left(\frac{\hbar}{\hbar z - \hbar\omega' - E(1) - E(2 - \mathbf{q})} + \frac{\hbar}{\hbar z - \hbar\omega' - E(1 + \mathbf{q}) - E(2)} \right). \quad (4.6)$$

We neglected terms $\propto f(1)$, which give corrections in higher orders of the density. $n_{\text{B}}(\omega) = [\exp(\beta\hbar\omega) - 1]^{-1}$ is the Bose distribution function. The dynamical properties of the surrounding plasma are contained in the dielectric function $\varepsilon(q, z)$ to be taken at the real axis, $z = \omega' + i0$. In general, the dielectric function is a complex, frequency dependent quantity, the imaginary part jumps at the real axis. Often the random-phase approximation (RPA) is taken, and in the static limit $\omega \to 0$ the Debye screening is obtained. In this section, we show that this simple approximations have to be improved in a systematic way, which is obtained from the quantum statistical approach.

Including the effective potential, the effective Hamiltonian in the in-medium Schrödinger equation (4.5) becomes complex and frequency dependent. As a consequence, the eigensolutions are no longer stationary states with sharp energy levels which are shifted by the polarisation of the medium, but have a finite life time given by the imaginary part of the effective Hamiltonian. This can be interpreted as collisions with the plasma particles and leads to a broadening of the energy levels. The corresponding quantum statistical approach to plasma line shapes based on the treatment of the polarization function has been worked out [GHR91] and will not be investigated in the present work. As a consequence, sharp level shifts and a sharp shift of the continuum edge is only obtained from a mean-field approximation. Any frequency dependence beyond the mean-field approximation gives imaginary parts and, this way, a broadening of the energy levels.

This problem has been considered also earlier [ZKK+78, SAK95], where both, real part and imaginary part of the energy levels of the in-medium two-particle problem, are calculated. As a consequence, only the spectral function has a unique physical meaning, showing the spectral line profiles and the smooth transition to the continuum. However, we will focus within this work on the shifts that are obtained from the real part of the effective Hamiltonian.

As shown in [KKER86, KSKB05, RKK+78, ZKK+78, SAK95], density effects arise from dynamical screening in the effective potential, expressed by the inverse dielectric function $\varepsilon^{-1}(q, z)$ of the medium in Eq. (4.6). For bound states, Pauli blocking as well as the screening in the self-energy term (ΔV^{eff} in the first square bracket of Eq. (4.5)) and the effective interaction partially compensate each other so that the bound state energy levels are only weakly dependent on the density. In contrast, the energy shift of the continuum states is determined only by the self-energy contribution. In leading order of the density, the medium

modification of the IPD is given by the shift of the edge of continuum states. For a more extended discussion see [KKER86, KSKB05, RKK$^+$78, ZKK$^+$78, SAK95, Zim87].

A standard expression for the dielectric function $\varepsilon(q, z)$ is given in the RPA (see Chapter 2). Here we discuss improvements beyond RPA to evaluate the shift of the continuum edge occurring at $\mathbf{p}_1 = \mathbf{p}_2 = 0$. Under this condition, the two-particle problem for the continuum edge can be reduced to single-particle problem by renaming, e.g., $\hbar z - E(2) = \hbar \omega$ in the last term of (4.6). Then the Eq. (4.6) can be rewritten as

$$\Delta V^{\text{eff}}(1, 2, \mathbf{q}, z)|_{\mathbf{p}_1 = \mathbf{p}_2 = 0} = \Delta V^{\text{eff}}(1, \mathbf{q}, z) + \Delta V^{\text{eff}}(2, \mathbf{q}, z) \tag{4.7}$$

with the contribution from the corresponding single-particle of species c

$$\Delta V^{\text{eff}}(c, \mathbf{q}, \omega) = -V_{12}(\mathbf{q}) \int_{-\infty}^{\infty} \frac{d\omega'}{\pi} \text{Im } \varepsilon^{-1}(q, \omega' + i0) \cdot [n_{\text{B}}(\omega') + 1] \cdot \frac{\hbar}{\hbar\omega - \hbar\omega' - E_c(\mathbf{q})}. \tag{4.8}$$

This expression coincides with the correlation part of the single-particle self-energy $\Sigma_c^{\text{corr}}(1, z)$ described in Chapter 2. In the single-particle picture, the influence of the plasma environment on the properties of the investigated particle is merged in the self-energy $\Sigma_c(1, z)$. It can be represented by Feynman diagrams, in lowest approximation by the diagram (also known as $V^s G$ or GW approximation) with the dressed propagator G and the screened potential V^s

$$\Sigma_c(1, z) = \underbrace{}_{} = \sum_{\mathbf{q}, \omega} G_c(\mathbf{p} - \mathbf{q}, z - \omega) \cdot V^s(\mathbf{q}, \omega) = \Sigma_c^{\text{HF}}(1, z) + \Sigma_c^{\text{corr}}(1, z). \tag{4.9}$$

The Hartree-Fock (HF) contribution for the self-energy reads

$$\Sigma_c^{\text{HF}}(12) = iV_{cc}(12) G_c(12) = -\int \frac{d^3\mathbf{k}}{(2\pi)^3} V_{cc}(k) f_c(\mathbf{p} - \mathbf{k}). \tag{4.10}$$

To derive the last expression, the Matsubara representation is used. For classical plasmas, i.e., in the nondegenerate limit, the HF contribution can be further simplified as

$$\Sigma_c^{\text{HF}}(p) = -\frac{2 Z_c^2 e^2}{\varepsilon_0 (s_c + 1)} n_c \Lambda_c^2 \cdot {}_1F_1\left(1, \frac{3}{2}, -\frac{\beta\hbar^2 p^2}{2m_c}\right). \tag{4.11}$$

It has been investigated elsewhere, see [KKER86, SAK95], and will not be discussed in detail here. The correlation part of the self-energy $\Sigma_c^{\text{corr}}(1, z)$ contains the contribution of the interaction with electrons in plasma, as well as the interaction with ions. We are interested in the real part of the self-energy since it describes the continuum shift

$$\text{Re } \Sigma_c^{\text{corr}}(p, \omega) = -\mathcal{P} \int \frac{d^3\mathbf{q}}{(2\pi)^3} \int \frac{d\omega'}{\pi} V_{cc}(q) \times \text{Im } \varepsilon^{-1}(q, \omega' + i0) \frac{1 + n_{\text{B}}(\omega')}{\omega - \omega' - E_{c, \mathbf{p}+\mathbf{q}}/\hbar} \tag{4.12}$$

with $\mathcal{P}$ denoting the principal value. In the following, the structure factors are introduced as improvements beyond RPA for the dielectric function. Then they are used to evaluate the shift of the continuum edge. Other approaches using semi-empirical assumptions such as the ion sphere model are improved within our approach that is based on a systematic quantum statistical approach as shown in the following.

4.4.2 Dielectric function and dynamical structure factor

The structural properties of plasmas are of essential importance since they provide the basis for a general understanding of different systems in astrophysics, laboratory plasma under normal and extreme conditions, and laser-heated solids and plasmas [GR09, VCW14, Red13, KSKB05]. Additionally, the response of the plasma system to external perturbation are totally determined by the detailed structure of the plasma, i.e., the dynamical SF of the plasma. The dynamical SF is closely related to the density-density correlation function which determines many transport and optical properties, such as stopping power, the equation of state, the spectral lines, and the ionization potential (ionization balance).

In general, the dielectric function is connected to the dynamical structure factor via the fluctuation-dissipation theorem [GR09, KSKB05]

$$S_{\mathrm{ZZ}}(\mathbf{q}, \omega) = \frac{\hbar}{n\pi} \frac{1}{1 - e^{-\hbar\omega/k_{\mathrm{B}}T}} \cdot V^{-1}(q) \cdot \mathrm{Im}\, \varepsilon^{-1}(\mathbf{q}, \omega). \tag{4.13}$$

The dielectric function contains the complete information on the ions and electrons in the interacting systems. Additionally, the dielectric function is connected to the density-density response function $\chi_{cd}(\mathbf{q}, \omega)$ between particles of species c and d via [GR09]

$$\varepsilon^{-1}(\mathbf{q}, \omega) = 1 + \frac{1}{\varepsilon_0\, q^2} \sum_{cd} e_c\, e_d\, \chi_{cd}(\mathbf{q}, \omega), \tag{4.14}$$

which describes the induced density fluctuations of species c due to the influence of an external field on particles of species d. For a two-component plasma system, we have

$$\varepsilon^{-1}(\mathbf{q}, \omega) = 1 + \frac{e^2}{\varepsilon_0\, q^2} \cdot \chi_{ee}(\mathbf{q}, \omega) + \frac{z_i^2\, e^2}{\varepsilon_0\, q^2} \cdot \chi_{ii}(\mathbf{q}, \omega) - \frac{2 z_i e^2}{\varepsilon_0\, q^2} \cdot \chi_{ei}(\mathbf{q}, \omega) \tag{4.15}$$

Taking into account the fact that the dynamical SFs are related to the density-density correlation functions $\langle \delta n_c(\mathbf{r}, t)\delta n_d(0, 0)\rangle$ via Fourier transformation, we can define the partial dynamical SF for different components in plasmas from the density-density response function $\chi_{cd}(\mathbf{q}, \omega)$ as follows [KSKB05]

$$S_{cd}(\mathbf{q}, \omega) = \frac{\hbar}{\pi\,\sqrt{n_c n_d}} \cdot \frac{1}{1 - e^{-\hbar\omega/k_{\mathrm{B}}T}} \cdot \mathrm{Im}\,\chi_{cd}(\mathbf{q}, \omega). \tag{4.16}$$

The dynamical SFs $S_{cd}(\mathbf{q}, \omega)$ characterize the plasma in response to any perturbation. For instance, they have been investigated to describe X-ray Thomson scattering, see Ref. [**?**]. Other plasma properties such as the electrical conductivity are also governed by the dynamical SF.

For a two-component plasma, the imaginary part of the inverse dielectric function can be expressed via the dynamical SFs, see also [Chi00],

$$\mathrm{Im}\, \frac{1}{\varepsilon(\mathbf{q}, \omega + i0)} = \frac{\pi\, e^2}{\hbar \varepsilon_0\, q^2\, (1 + n_{\mathrm{B}}(\omega))} \cdot \left[z_i^2\, n_i S_{\mathrm{ii}}(\mathbf{q}, \omega) - 2 z_i\, \sqrt{n_e n_i} S_{\mathrm{ei}}(\mathbf{q}, \omega) + n_e S_{\mathrm{ee}}(\mathbf{q}, \omega) \right]. \tag{4.17}$$

Comparing this expression to Eq. (5.29), we find that the effective dynamical SF describing the response of all charged species in plasma can be expressed via the sum of contributions from the single component $S_{cc}(\mathbf{q}, \omega)$ and the pair-wise coupling of two different species

$S_{cd}(\mathbf{q}, \omega)$. More exactly, for the two-component plasma (electrons + ions), the total dynamical SF is given by the summation of the ionic SF $S_{ii}(\mathbf{q}, \omega)$, electronic SF $S_{ee}(\mathbf{q}, \omega)$, and the electron-ion coupling $S_{ei}(\mathbf{q}, \omega)$. Moreover, the electronic SF $S_{ee}(\mathbf{q}, \omega)$ in the decomposition of the dynamical SF in Eq. (5.30) can be divided into $S_{ee}^0(q, \omega)$ for fast-moving free electrons and a contribution for the slowly moving free electrons accompanying the ions as shown in Refs [Chi00, GRH$^+$07]

$$S_{ee}(q, \omega) = S_{ee}^0(q, \omega) + \frac{|q_{sc}(k)|^2}{z_i} S_{ii}(q, \omega) \tag{4.18}$$

with the screening function accounting for the screening cloud of electrons

$$q_{sc}(k) = Z \frac{k_{De}^2}{k^2} S_{ee}^0(k). \tag{4.19}$$

In addition, the electron-ion coupling $S_{ei}(\mathbf{q}, \omega)$ can be also expressed via the screening function

$$S_{ei}(q, \omega) = \frac{q_{sc}(k)}{\sqrt{z_i}} S_{ii}(q, \omega). \tag{4.20}$$

Consequently, we have for the total dynamical SF the following form

$$S_{ii}^{ZZ}(k, \omega) = \left(1 - \frac{q_{sc}(k)}{z_i}\right)^2 \cdot S_{ii}(k, \omega). \tag{4.21}$$

Here we focus on the static SF of ions which is given by $S_{ii}^{ZZ}(k) = \int d\omega \, S_{ii}^{ZZ}(k, \omega)$. The simplest model for the static SF of ions is the one-component plasma (OCP) model where the ions are regarded as interacting point charges in a uniform neutralizing background. A further simplification is the mean spherical approximation in which the ion is treated as a positive charged hard sphere of finite diameter σ. This approximation is demonstrated to accurately reproduce experimental data for liquid metals as well as MC simulations, and to be useful to analytically solve the coupled equations (the Ornstein-Zernike equation) [GRH$^+$07].

Alternatively, we can also use the following fit formula for the OCP ionic structure factor [GRH$^+$07] with the introduction of the diameter σ, the packing fraction η, the mean ion distance a_{ii}, and the coupling parameter Γ_{ii} and their compositions

$$\eta = \frac{\pi}{6} n_i \sigma^3, \quad \gamma = \left(\frac{a_{ii}}{\sigma}\right) \Gamma_{ii}, \quad \chi = (24\eta\gamma)^{1/2}. \tag{4.22}$$

Then the OCP ionic structure factor [GRH$^+$07] is expressed as

$$S_{ii}^{OCP}(k) = \frac{1}{1 - C_{ii}(k\sigma)}, \tag{4.23}$$

where the direct correction function reads

$$\begin{aligned}
C_{ii}(q) = \frac{24\eta}{q^6} \cdot \Big\{ & y_0 \, q^3 \, (\sin q - q \cos q) + y_1 \, q^2 \left[2q \sin q - \left(q^2 - 2\right) \cos q - 2\right] \\
& + y_2 \, q \left[\left(3q^2 - 6\right) \sin q - q \left(q^2 - 6\right) \cos q \right] \\
& + y_3 \left[q \left(4q^2 - 24\right) \sin q - \left(q^4 - 12q^2 + 24\right) \cos q + 24 \right] \\
& + y_4 \, q^{-2} \left[6q \left(q^4 - 20q^2 + 120\right) \sin q - \left(q^6 - 30q^4 + 360q^2 - 720\right) \cos q - 720 \right] \\
& - \gamma q^4 \, \cos q \Big\}
\end{aligned} \tag{4.24}$$

with

$$y_0 = -\frac{(1+2\eta)^2}{(1-\eta)^4} + \frac{h_0^2}{4(1-\eta)^2} - \frac{(1+\eta)\,h_0\,\chi}{12\eta} - \frac{(5+\eta^2)\,\chi^2}{60\eta},$$

$$y_1 = 6\eta h_1^2, \qquad y_2 = \chi^2/6, \qquad y_3 = \frac{\eta}{2}\left(y_0 + \chi^2 h_2\right), \qquad y_4 = \eta\chi^2/60 \tag{4.25}$$

and

$$h_0 = \frac{1+2\eta}{1-\eta}\left[1 - \left(1 + \frac{1\,(1-\eta)^3\,\chi}{(1+2\eta)^2}\right)^{1/2}\right], \tag{4.26}$$

$$h_1 = \frac{h_0^2}{24\eta} - \frac{1+\eta/2}{(1-\eta)^2}, \quad h_2 = -\frac{1+\eta-\eta^2/5}{12\eta} - \frac{(1-\eta)\,h_0}{12\eta\chi}.$$

The effective hard-core diameter σ, and therefore the corresponding packing fraction η, is uniquely determined by the solution $h_1 = 0$ because of the continuity of the pair correlation function at the hard sphere boundary.

The fit formula for the OCP ionic SF can reproduce the results for the SF in the low density and high temperature limit, which is known as Debye-Hückel SF

$$S_{\text{ii}}^{\text{DH}}(q) = \frac{q^2}{q^2 + \kappa_{\text{D,i}}^2 r_{\text{WS}}^2}. \tag{4.27}$$

Another well known ion SF is the SF for the average atom model or the ion sphere model, which stems from the Fourier transform of the radial distribution function $g(r) = \Theta(r - r_{\text{WS}})$

$$S_{\text{ii}}^{\text{IS}}(q) = 1 - \frac{1}{q^3} \cdot \{\sin q - q\cos q\}. \tag{4.28}$$

The IS model was developed for a strongly coupled system, in particular for solid state physics. We must be careful with $S_{\text{ii}}^{\text{IS}}(q)$ since the strongly coupled peak near the Wigner-Seitz radius can not be depicted by this SF as shown in Fig. 4.6.

For weakly coupled plasmas, the ionic SF in Fig. 4.6 displays a monotonically increasing behavior as the wave number, which indicates that the ions are randomly distributed in space and form an unordered system. With increasing density and correspondingly increasing ionic coupling parameter, the ionic SF exhibits an oscillatory behavior and shows a strong peak near the Wigner-Seitz radius r_{WS} due to the correlation with the neighboring ions. Such a behavior implies the formation of a lattice-like structure in plasma. For $\Gamma_{\text{ii}} \geq 175 \pm 5$ [Sal98] or $\Gamma_{\text{ii}} \geq 178 \pm 1$ [KG90], the OCP model predicts that the plasma crystallizes and the ions locate in a body-centered cubic lattice. Thereby, a solid state high temperature plasma is generated. In such a strongly coupled plasma, the ionic SF has very slight or no dependence on the temperature.
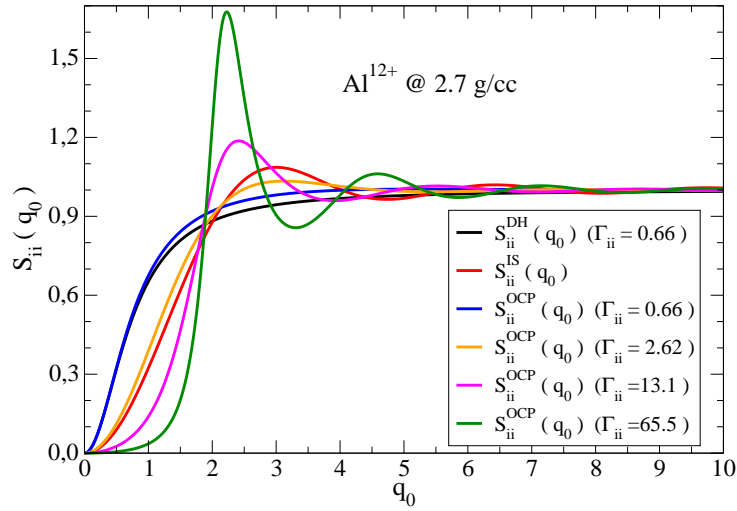
Abb. 4.6: The static SFs for Al^{12+} at solid density and at different temperatures, correspondingly different coupling strength Γ_{ii}.

The discussion above is based on the assumption of the OCP model where the free electrons are treated as a uniformly distributed background and the electron-ion interaction are given by the bare Coulomb potential. Actually, the free electrons form polarized screening clouds around the slowly moving ions. In this case, a screening correction to the electron-ion interaction to be bare Coulomb potential has to the considered. Then a screened ionic SF is constructed from the OCP ion SF as [GRH$^+$07]

$$S_{ii}^{ZZ}(k,\omega) = \left(1 - \frac{q_{sc}(k)}{z_i}\right)^2 \cdot \frac{S_{ii}^{OCP}(k)}{1 + f_v(k) \cdot S_{ii}^{OCP}(k)} \qquad (4.29)$$

with the screening correction to the bare Coulomb potential

$$f_v(k) = -\frac{k_{Di}^2}{k^2} \cos^2\left(\frac{k\sigma}{2}\right) \frac{q_{sc}(k)}{z_i} \qquad (4.30)$$

where the screening correction should be truncated after the first node in order to maintain smooth electron wave functions.

4.4.3 Linear mixing rule for a multi-component plasma

The discussion above based on the description of effective charge is valid for one chemical element. In general, the many-particle system under investigation consists of a mixture of N_{sp} atomic species of charge z_i and mass number A_i with $i = 1, \cdots, N_{sp}$. In chemical picuture every charge state is treated as a new chemical species. The number density of species i is n_i, respectively. The total number density of ions, i.e. the density of the nuclei, and the electron density are, respectively, given by

$$n_n = \sum_i^{N_{sp}} n_i, \quad n_e = \sum_i^{N_{sp}} n_i z_i = \bar{z}\, n_n. \qquad (4.31)$$

For this multi-component system, the effective SF accounting for the response of all species can be approximately expressed by a linear combination of the OCP SF of the single species

$$S_{\text{ii}}^{\text{eff}}(\mathbf{q}) = \sum_{c=1}^{N_{\text{sp}}} x_c \, S_{cc}^{\text{OCP}}(\mathbf{q}). \tag{4.32}$$

This approximation is known as linear mixing rule (LMR) [DG09]. Here x_c is the weight for the corresponding ionic species c. The effective SF has a convergent value in the short wavelength limit, i.e. $S_{\text{ii}}^{\text{eff}}(\mathbf{q} \to \infty) \to 1$. One possible expression for the weight x_c is given by Daligault and Gupta [DG09]

$$x_c = \frac{\langle Z \rangle^{1/3}}{\langle Z^2 \rangle} Z_c^{5/3} \frac{n_c}{n_n} \tag{4.33}$$

or in a simpler approximation by neglecting the charge dependence $x_c = n_c/n_n$ as shown by Chabrier and Ashcroft.

4.4.4   Ionization potential depression in terms of dynamical structure factors

We now discuss the ionic contribution to the correlation shift of the continuum edge, namely, the real part of the self-energy $\text{Re} \, \Sigma_e^{\text{corr}}(0, \omega) + \text{Re} \, \Sigma_i^{\text{corr}}(0, \omega)$. It is expressed as

$$\text{Re} \, \Sigma_c^{\text{corr, ion-ion}}(p = 0, \omega) = \Delta_c^{\text{ion-ion}}(0, \omega) \tag{4.34}$$
$$= -\mathcal{P} \int \frac{d^3\mathbf{q}}{(2\pi)^3} \int \frac{d\omega'}{\pi} \frac{V_{cc}(q)}{\omega - \omega' - E_{c,\mathbf{q}}/\hbar} \frac{\pi Z_i e^2 \, n_e}{\hbar \epsilon_0 \, q^2} S_{\text{ii}}^{\text{ZZ}}(q, \omega').$$

Thus, the ionic contribution to the continuum shift is related to the dynamical SF of the ions. The quasiparticle shift has to be defined self-consistently at $\omega = \Delta_c^{\text{ion-ion}}(0, \omega)$, but this shift is compensated by the energy $E_{c,\mathbf{q}}$ which is shifted, too. Then the ionic contribution $\Delta_c^{\text{ion-ion}}(0, \omega)$ is given by $\Delta_c^{\text{ion-ion}}(0, 0)$, later denoted as $\Delta_c^{\text{ion-ion}}$.

Under WDM conditions considered here, the ions are strongly coupled, so that the SF S_{ii}^{ZZ} should not be always taken in the Debye limit. However, the plasma ions can be treated classically. Therefore, in (4.34), we consider the limit $\hbar \to 0$ in the propagator $1/[-\omega' - \hbar q^2/(2m_c)]$. In addition, the ions move very slowly in comparison to the electrons due to the large ion mass, which indicates that the dynamical SF of ions can be reasonably replaced by the static SF within some approximations. We use the plasmon pole approximation

$$\text{Im} \, \varepsilon_{\text{ion}}^{-1}(q, \omega) = -\frac{\pi \omega_i^2}{2\omega_{q,i}} \{\delta(\omega - \omega_{q,i}) - \delta(\omega + \omega_{q,i})\}, \tag{4.35}$$

where $\omega_i^2 = Z_i^2 n_i e^2/(\epsilon_0 m_i)$ is the ionic plasmon frequency with $\omega_{q,i}^2 = (q^2 \, \omega_i^2) / (\kappa_i^2 \, S_{\text{ii}}^{\text{ZZ}}(q))$ and $\kappa_i^2 = \omega_i^2 m_i/k_B T$ according to the particle number conservation [GRH$^+$07]. Then we find the following approximation

$$S_{\text{ii}}^{\text{ZZ}}(q, \omega) \approx S_{\text{ii}}^{\text{ZZ}}(q) \frac{\delta(\omega - \omega_{q,i}) + \delta(\omega + \omega_{q,i})}{1 + e^{-\hbar\omega/(k_B T)}}. \tag{4.36}$$

The physical meaning of the replacement of the dynamical SF by the static SF in Eq. (4.36) is that the ions are considered to have a fixed distribution in the plasma neglecting temporal fluctuations.

For the ionization process $i_{Z_i} \to e + i_{Z_i+1}$, the IPD can be given by the difference between the self-energy before and that after the ionization of the investigated system, i.e.,

$$\Delta_{\text{IPD}}^{\text{ion}-\text{ion}} = \Delta_i^{\text{ion}-\text{ion}} - (\Delta_e^{\text{ion}-\text{ion}} + \Delta_{i+1}^{\text{ion}-\text{ion}}).$$
(4.37)

Assuming that the ionic structure of the plasma environment does not change during the ionization, we obtain for the IPD

$$\Delta_{\text{IPD}}^{\text{ion}-\text{ion}} = -\frac{(Z_i + 1)e^2}{2\pi^2 \epsilon_0 r_{\text{WS}}} \cdot S(\Gamma_i)$$
(4.38)

with the parameter function

$$S(\Gamma_i) = F(\Gamma_i) \int_0^\infty \frac{dq_0}{q_0^2} S_{\text{ii}}^{\text{ZZ}}(q_0),$$
(4.39)

where $q_0 = q/\left(3\pi^2 n_i\right)^{1/3}$ is the reduced wavenumber. $\Gamma_i = Z_i^2 e^2/(4\pi \epsilon_0 k_B T r_{\text{WS}})$ is the ionic coupling parameter with the Wigner-Seitz radius $r_{\text{WS}} = (4\pi n_i/3)^{-1/3}$. Within the plasmon pole approximation, the function $F(\Gamma_i)$ in the parameter function $S(\Gamma_i)$, i.e., in Eq. (4.39), results from $\omega_{q,i} \sim \kappa_i^{-1}$ as $F(\Gamma_i) = \Gamma_i (12/\pi)^{1/3}$. The screening parameter $\kappa_i^2 \propto 1/(k_B T)$ follows from the linearized Debye theory for classical systems. In this case, we consider the ion-ion SF $S_{\text{ii}}^{\text{DH}}(q) = q^2/(q^2 + \kappa_i^2)$ of a OCP. Then, from Eq. (4.38), the DH result for the low density and high temperature limit, $\Delta_{\text{DH}}^i = -(Z_i + 1)e^2 \kappa_i/(4\pi \varepsilon_0)$, is recovered for the ionic contribution to the IPD.

When the coupling parameter becomes larger, the pair correlation function exhibits a peak near r_{WS} when approaching the liquid state, which would be reasonably well described by a Percus-Yevick SF. In other words, the plasma starts to crystallize and forms a periodic structure. In this case for a fixed charge state Z_i, the function $S(\Gamma_i)$ should gradually tend to a constant and a similar formula as in the IS model for the IPD should be obtained. In this strongly coupled regime, the frequency $\omega_{q,i}$ is determined by r_{WS}, as discussed, e.g., in Ref. [KG90]. Consequently, the parameter κ_i^2 occuring in $\omega_{q,i}$ should be replaced by a more general expression $\tilde{\kappa}_i^2(\Gamma_i)$ depending on the parameter Γ_i. For instance, the non-linear Debye theory which avoids negative densities of the screening cloud, gives the implicit relation [KKER86]

$$\int_0^\infty dx \cdot x^2 \left\{1 - \exp\left[-\frac{\Gamma_i}{x} \cdot \exp\left(-\tilde{\kappa}_i(\Gamma_i) r_{\text{WS}} x\right)\right]\right\} = \frac{1}{3}.$$
(4.40)

In this work, we introduce the following approximation

$$F(\Gamma_i) = \sqrt[3]{\frac{4}{9\pi}} r_{\text{WS}}^2 \tilde{\kappa}_i^2(\Gamma_i) = \frac{3\Gamma_i}{\sqrt{(9\pi/4)^{2/3} + 3\Gamma_i}}$$
(4.41)

to interpolate between the weak and strong coupling limit. Note that the parameter function $S(\Gamma_i)$ has a slight dependence on the charge number Z_i at a fixed temperature and a fixed density. The validity of this interpolation formula is shown in Fig. 4.7. It can be seen that in the range of Γ_i up to 100 the deviation of our interpolated expression with respect to solutions of Eq. (4.40) is less than 1%.
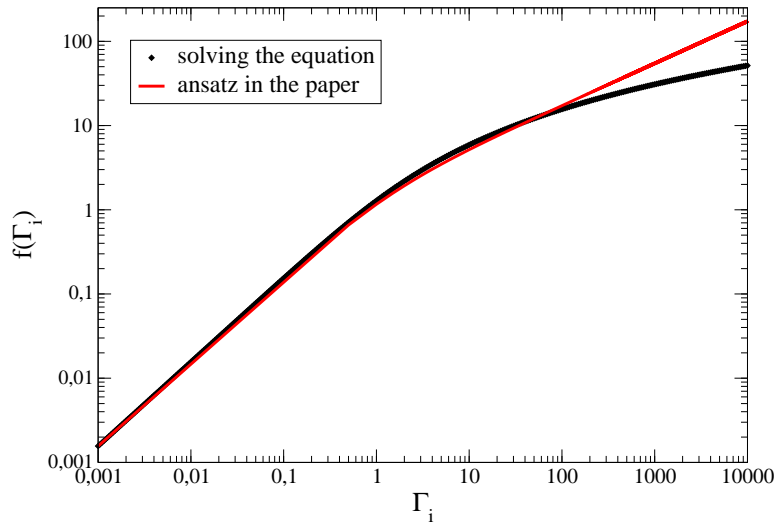
Abb. 4.7: The validity of the interpolation (4.41) with respect to the coupling parameter Γ_i. The black points are calculated by numerically solving the equation (4.40).
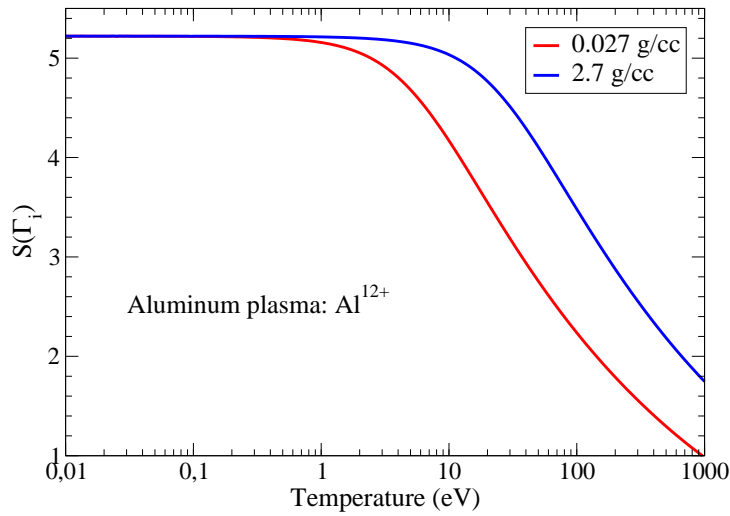
Abb. 4.8: The dependence of the parameter function $S(\Gamma_i)$ on the coupling parameter Γ_i via different temperatures at two different densities.

It can be seen from Fig. 4.8 that the parameter function $S(\Gamma_i)$ tends to a constant which has no dependence on the density because of the crystallization of ions in the low-temperature limit. This conclusion coincides with the results from the ion sphere model in solid state physics. With increasing temperature at a fixed density, the plasma system becomes weakly coupled and a transition to the DH theory can be found in the high-temperature limit.

In the following, we use the expression (4.38) together with Eq. (4.41) and the ionic SF reported in Ref. [GRH$^+$07] to evaluate the ionic contribution to the IPD in a plasma. At

first, a model calculation is performed to compare our approach with other theoretical models. After that, detailed investigations for different experimental measurements and comparisons of our results with other theoretical approaches and experimental predictions are shown.
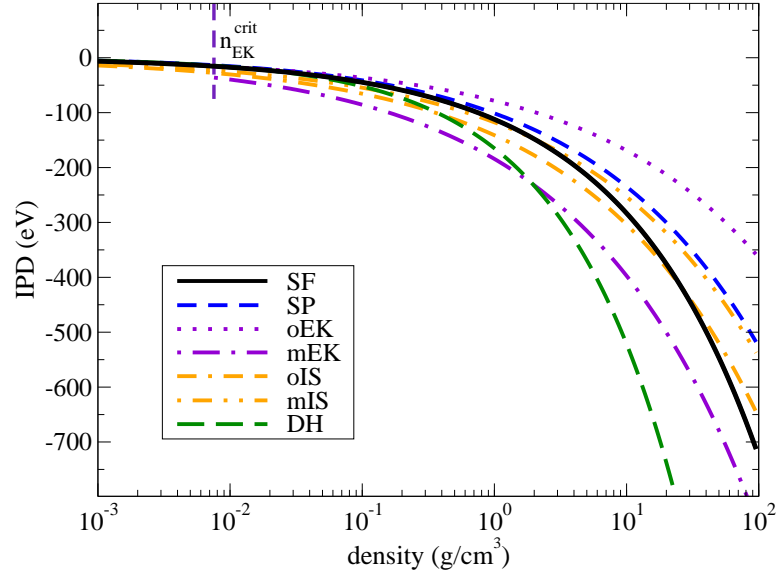
Abb. 4.9: Comparisons of the IPDs predicted by different models for Al^{11+} at 600 eV, as function of the density.

Fig. 4.9 shows the comparisons for the IPD calculated using different models. From Fig. 4.9, it can been seen that the IPD from SP [SPJ66], original EK (oEK) [EK63] and our result are in good agreement with the DH shift in the low density region. Above the critical density $n_{\mathrm{EK,crit}} = 3/(4\pi) \cdot (4\pi\varepsilon_0 k_B T/(Z^2 e^2))^3$ with the nuclear charge Ze, the underestimation of the IPD by the SP model and the overestimation by the modified EK (mEK) model [CVC+12] can be seen in comparison to the original IS (oIS) model [ZM80]. Note that, with increasing density, corresponding to increasing coupling parameter Γ_i ($\Gamma_i = 0.16$ for the denisty 0.001 g/cm^3 and $\Gamma_i = 7.28$ for the denisty 100 g/cm^3), our result shows, on one hand, a transition between SP at low densities (weakly and moderately coupled) and mEK at large densities (strongly coupled), and, on the other hand, a good agreement with the oIS model in the intermediate density region.

The approach, presented in this work, shows a close connection of the IPD to the detailed structure of the plasma system. As a general theory, the expression (4.38) should work within the valid range of the fluctuation-dissipation theorem for both equilibrium and non-equilibrium systems described by the exact SF of the quantum many-body system. Once the SF is known from other methods, for instance, the simulations or the Thomson scattering measurements, the IPD can be directly evaluated. In this work, the local thermodynamic equilibrium is assumed for the calculation. Further investigations are needed to describe non-equilibrium situations, for instance, after irradiations by strong short-pulse laser beams.

4.4.5   Comparisons to other approaches and experimental measurements

A: Comparison to experimental measurements by Hoarty *et al.*

We now discuss our results with respect to recent experiments. The investigated density range in the experiments of Hoarty *et al.* [HAJ+13a, HAJ+13b] is 1.2 to 9 g/cm^3 at the electron temperature in the range of 550 to 700 eV. The assumption of local thermodynamic equilibrium is believed to be valid for the high densities [HAJ+13b], which implies the ionic coupling parameter is estimated to be in the range $2 \sim 4$. In this moderate coupling regime, the SP and IS models should result in good agreement with the experiment, as indicated later in the Fig. 4.11. Under the experimental conditions, the screened ionic SFs for different densities are shown in Fig. 4.10, where the ionic SFs are found to be slightly changed with increasing densities during the compression.

The disappearance of Ly$_\beta$ and He$_\beta$ lines in aluminum plasma [HAJ+13a] was measured experimentally to occur at the density somewhere between 5.5 and 9 g/cm^3, which is in reasonable agreement with the predictions by FLYCHK [CCM+05] using the SP model. For this range of densities, the modified IS (mIS) model is most suitable [Cro14]. This agreement is consistent with the predicted spectra for the opacity using the CASSANDRA opacity code with an IS model for the IPD [HAJ+13b], where the dissolution of lines from $n = 3$ levels is indicated to take place between the density of $6 \sim 8$ g/cm^3. Our approach, predicting the critical density between $7 \sim 8$ g/cm^3 for the disappearance of $n = 3$ levels, gives also an excellent agreement with the experimental data and with the predictions by the simulation codes.
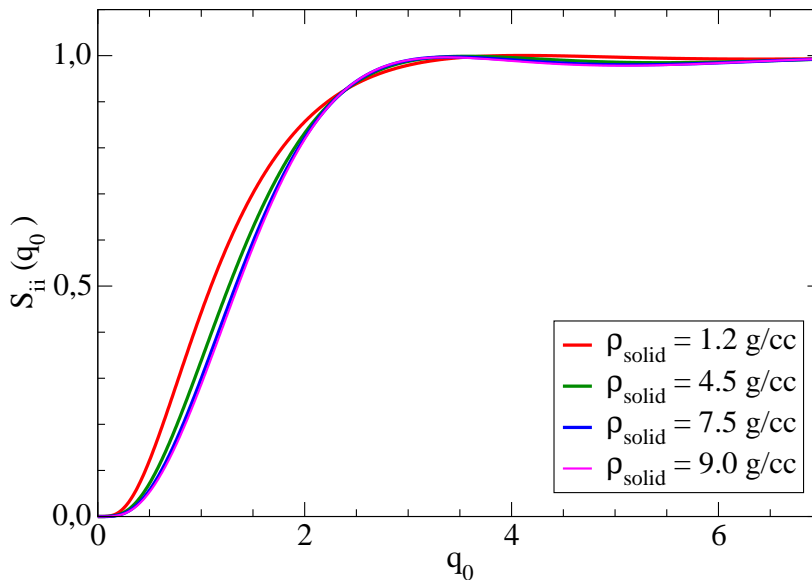

Abb. 4.10: Screened ionic SF for the Al^{11+} at temperature $T = 700$ eV and at different densities.
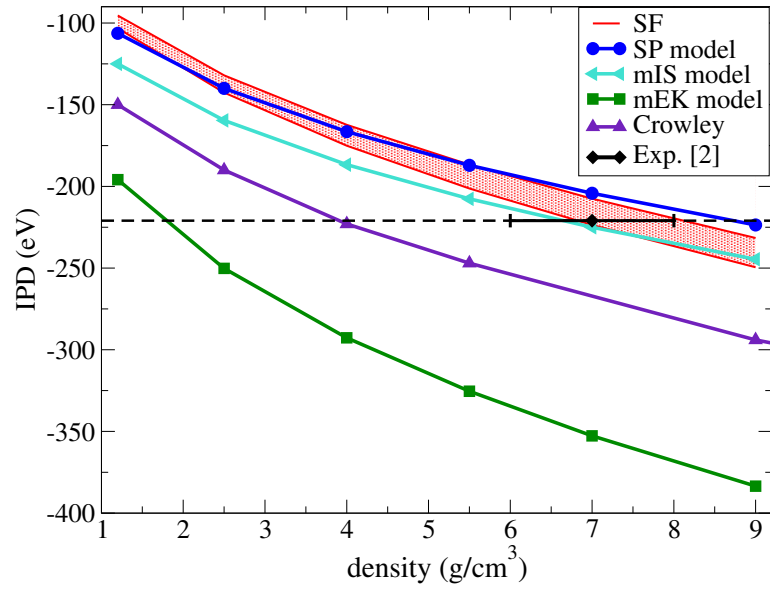
Abb. 4.11: The experimental value is given where the He$_\beta$ line fades out [HAJ$^+$13a]. The corresponding results are different for different models. Our calculation (the red region) shows the results for the electron temperature in the range of 550 to 700 eV.

B: Comparison to experimental measurements by Ciricosta *et al.*

The fact, that the agreement of our results changes gradually from the SP model to the mEK model with increasing coupling parameter, gives a reasonably well explanation for the other experiment. Using FEL [CVC$^+$12, Ct16], the aluminum sample at solid density is isochorically heated to electron temperatures up to 200 eV, indicating a strongly coupled plasma as shown in the Fig. 4.12. The screened ionic SFs at solid density and at different temperatures for diverse charge states are shown. The dash-dotted lines represent the SF for different charge states at same density (solid density) and at same temperature (50 eV), where a clear distinction is found. The LCLS pulse duration in this experiment was estimated to be less than 80 fs, which means that the spatial distribution of ions are more or less the same regardless of different charge states. Obviously, the assumption of same temperature for different charge states are invalid which can be also demonstrated by the ionization balance: higher charged states can only exist at higher temperature for a fixed density.

Additionally, the ionic plasma frequency $\omega_{\rm pl}^{\rm ion}$ in this laser-produced plasma is found to be in the order of 10^{14}/s. In contrast, the response of the electrons to the laser field is much faster and can be described by the electron frequency $\omega_{\rm pl}^{\rm el} \sim 10^{16}$/s. In comparison to the laser pulse, the electrons have enough time to exchange energy between each other and with the laser field and are isochorically heated to a high temperature. Because of the large mass of the ions, the response of the ionic subsystem to the external fluctuation is so slow that the ions in the plasma are weakly excited by the photons and by fast moving electrons, which implies that the ions are colder than the electrons. Of essential importance in the measurement is that the IPD for distinct charge states, inferred from the triggering energy of the photoionization, is measured at different time stages. This fact indicates that the ions are heated with the time evolution and the local thermodynamic equilibrium condition might

be achieved.
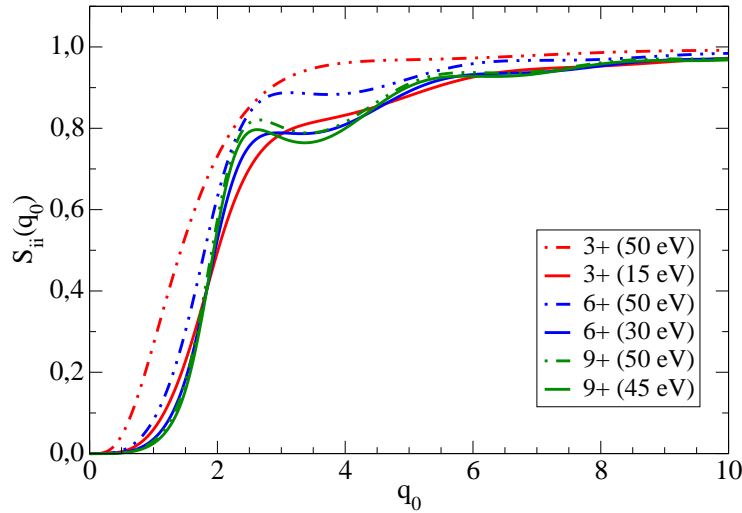
Abb. 4.12: The screened ionic SFs at solid density and at different temperatures for diverse charge states.
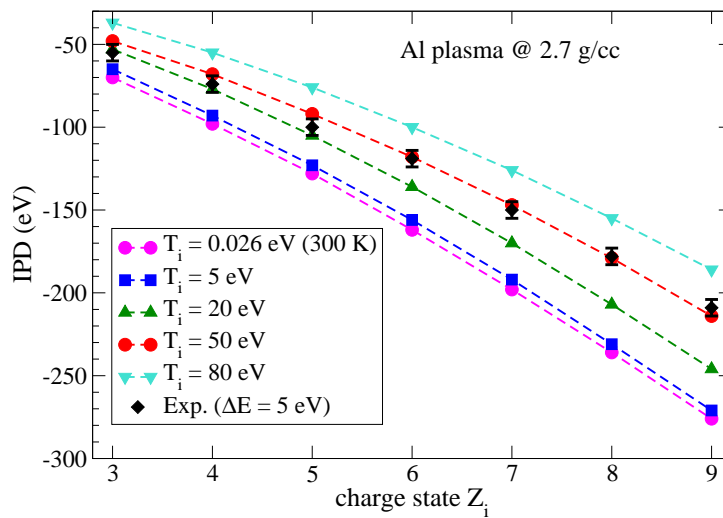
Abb. 4.13: Comparisons of the IPDs for an aluminum plasma at solid density 2.7 g/cm^3. (Lines to guide the eye)

Therefore, we make the following assumption: for different charge states, we have correspondingly different ion temperature. To reveal the validity of this assumption, we show at first the calculated IPD values for different charge states at the same temperature in Fig. 4.13.

As we can see, the experimentally measured IPD values for low charge states $Z_i = 3 \sim 5$ can be reproduced with the ion temperature $T_i = 20$ eV. However, the IPD values for higher charge states can only be obtained with a much higher temperature $T_i = 50$ eV. According to this fact, we assume the ion temperature for different charge states as $T_i(Z_i) = 5 \cdot Z_i$ eV. The results from our approach and the comparisons to the experimental data and other approaches are shown in Fig. 4.14. As discussed by Ciricosta *et al.*, the direct measurement of the IPD in aluminum plasma for different charge states can more reasonably be explained by the mEK model. Our approach can also reproduce the experimental data, see Fig. 4.14.
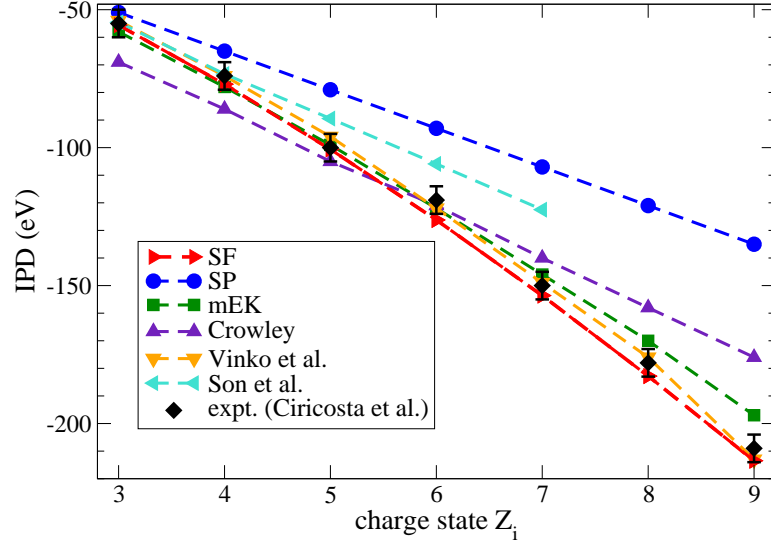
Abb. 4.14: Comparisons of the IPDs predicted by different models and the experimental results [CVC$^+$12, Ct16] for an aluminum plasma at solid density 2.7 g/cm^3. (Lines to guide the eye)

C: Comparison to experimental measurements by Kraus *et al.*

The application of the simple IPD models to a mixture of different ions is problematic as displayed by a recent measurements on a CH mixture at the NIF [KCK$^+$16]. The measured mean charge state can not be explained by either the SP or the mEK models, as shown in Tab. 4.1. Although the DH shift is inappropriate under the experimental conditions because of the strong coupling of the carbon ions ($\Gamma_C \sim 4$), it results in larger IPDs and therefore gives a more reasonable agreement with the experiment than all other models.

This fact can be attributed to the deficiency to account for the strong correlation and fluctuation effects in these models. For the CH mixture, the influence of a different chemical species, the protons from the fully ionized hydrogen, on the properties of the carbon ions is described by an additional electron density in the SP and EK models. In our approach, this effect can be consistently taken into account by the ionic SF, which includes the response of all charged particles in the plasma. We applied the linear mixing rule [DG09] for a multi-component plasma SF. Under the experimental conditions [KCK$^+$16], the carbon ions are strongly coupled while the protons are weakly correlated. The effective SF accounting for both carbon ions and protons reads

$$S_{ii}^{\text{eff}}(q_0) = x\, S_{\text{CC}}^{\text{ZZ}}(q_0) + (1 - x)\, S_{\text{HH}}^{\text{DH}}(q_0). \tag{4.42}$$

Exemplarily, we have taken for our calculation the total SF of $0.75\,S_{\mathrm{CC}}^{\mathrm{ZZ}}(q_0) + 0.25\,S_{\mathrm{HH}}^{\mathrm{DH}}(q_0)$ as shown in Fig. 4.15. Taking into account the influence of the protons, the SF for each wavenumber are moved to a higer value with respect to the SF of carbons. Within this approach, our estimate for the mean charge of 4.79 yields a close match with the experiment 4.92 ± 0.15 [KCK^{+}16]. The SF of the protons modifies the structure of the integrand in Eq. (4.39) leading to higher IPD values for the carbon ions, and therefore push the carbon ions to a higher charge states.

charge model	C^{3+}	C^{4+}	C^{5+}	mean charge
DH	261.3	326.7	392.0	4.91
SP	91.7	108.3	123.9	4.18
IS	103.2	119.7	135.2	4.21
mEK	116.0	145.0	174.0	4.24
SF ($x = 0.75$)	237.3	296.6	355.9	4.79
SF ($x = 1$)	99.0	123.7	148.4	4.19
Exp.				4.92 ± 0.15

Tab. 4.1: IPDs in eV and mean charge for CH mixture at density 6.74 g/cm^3 and $T = 86$ eV [KCK^{+}16]. The ionization energies for different charge states are $\mathrm{I}\,[C^{3+}] = 64.5$ eV, $\mathrm{I}\,[C^{4+}] = 392.1$ eV, $\mathrm{I}\,[C^{5+}] = 490.0$ eV. We have taken in our calculation for the effective SF, i.e., $S_{\mathrm{ii}}^{\mathrm{ZZ}}(q_0) = x\,S_{\mathrm{CC}}^{\mathrm{ZZ}}(q_0) + (1 - x)\,S_{\mathrm{HH}}^{\mathrm{DH}}(q_0)$, the value $x = 1$ and $x = 0.75$, without and with the influence of protons, respectively.
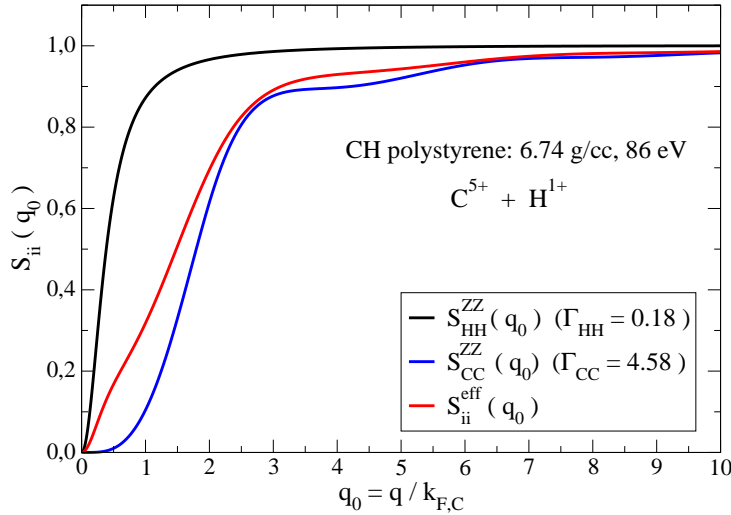
Abb. 4.15: Effective SF according to the linear mixing rule for CH mixture.

To complete our discussion, the dependence of the IPD values on the weight x_{C} in Fig. 4.16, where a linear relation is observed for different charge states. In our consideration, the weight is selected via the form $x_{\mathrm{C}} = \frac{m_{\mathrm{C}}}{m_{\mathrm{C}} + m_{\mathrm{H}}} \cdot \frac{Z_{\mathrm{C}}}{Z_{\mathrm{C}} + Z_{\mathrm{H}}}$. For charge state $Z_{\mathrm{C}} = 4$ and

$Z_C = 5$, we have $x_C = 73.8\%$ and $x_C = 76.9\%$, respectively. Hence, it is reasonable to take $x_C = 75\%$ for calculating the mean charge state in Tab. 4.1.

Calculations for a pure C plasma at the same conditions (same ionic density of carbon and same temperature), lead to the mean ionization degree of 4.2. For the CH plasma, the asymmetry of the charges and masses of protons and carbon ions lead to strong fluctuations and hence significantly enhance the ionization. Future discussions on experiments with pure C targets may test this effect.
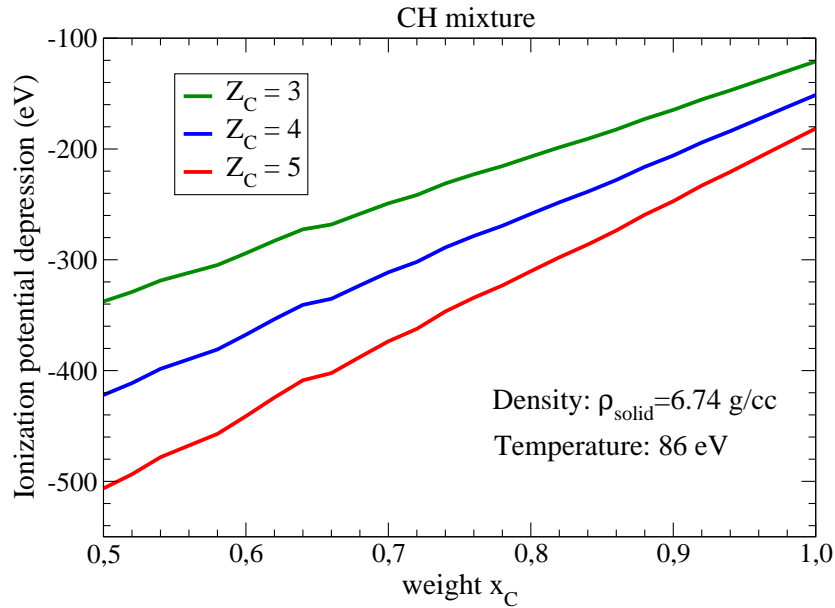
Abb. 4.16: Dependence of the IPD values on the weight of the carbon x_C in the total effective SF.

4.5   Plasma composition and coupled Saha equations

To understand the thermodynamic, optical, and transport properties of plasmas, the detailed knowledge of the charge state distribution is of essential importance. The charge state distribution can be calculated from basic principles, for example, from minimizing the Helmholtz free energy F [Sal98]. In general, conditions of the local thermodynamic equilibrium (LTE) are assumed, where the rates of collisional processes related to depopulations and their inverse processes, namely, recombination, are equal. The Helmholtz free energy F is related to the chemical potential via $\mu_c = \partial F / \partial n_c$. Under LTE conditions, the following relation (also known as the law of mass action) [Red13, KCK$^+$16]

$$\mu_{i+1} + \mu_e = \mu_i \tag{4.43}$$

is fulfilled for a chemical reaction between two involved charge states $i + 1$ and i

$$Z_{i+1}\, e + e \rightleftarrows Z_i\, e. \tag{4.44}$$

The chemical potential includes an ideal part derived from the ideal gases and an additional contribution accounting for the interaction between the plasma particles. The ideal part of

the chemical potential of the species c reads [KSKB05, Red13, KKER86, KCK$^+$16]

$$\beta\mu_c^{\mathrm{id}} = \ln\left(\frac{n_c\Lambda_c^3}{g_c}\right) \tag{4.45}$$

with the thermal wavelength Λ_c, the partial particle density n_c and the statistical weight g_c. This expression is only valid for non-degenerate cases. In the low temperature limit, electron degeneracy must be included in the chemical potential μ_e. Generally, the chemical potential of non-interacting electron gases can be obtained via Fermi integrals [KSKB05, Zim87] or by interpolation between the non-degenerate and the fully degenerate limits [Zim87, KSKB05, Red13].

For the statistical weight g_i of ions, the internal partition function determined by the ionization energies should be considered [Red13]. In other words, the ionization energy has to be taken into account [KCK$^+$16]

$$\beta\mu_i = \beta\mu_i^{\mathrm{id}} + \beta I_i^{\mathrm{eff}} \tag{4.46}$$

with the effective ionization potential for the ion with charge state

$$I_i^{\mathrm{eff}} = I_i - I_i^{\mathrm{IPD}} \tag{4.47}$$

where I_i is the unperturbed ionization energy and I_i^{IPD} describes the ionization potential depression in plasmas. Inserting Eqs. (4.45) and (4.46) into Eq. (4.43), we arrive at the following expression [KSKB05, Red13, KCK$^+$16]

$$\frac{n_{i+1}}{n_i} = \frac{g_{i+1}}{g_i}\,\exp\left(-\beta I_i^{\mathrm{eff}} - \beta\mu_e\right). \tag{4.48}$$

The densities of the higher ionization states with respect to a reference state can be reduced by assuming successive ionization over a sequence of this Saha equation. Then the so-called coupled Saha equations are obtained. To solve the coupled Saha equation system, the following conservation laws have to be obeyed. The first one is the conservation of total ion number

$$n_{\mathrm{sample}} = \sum_i n_i, \tag{4.49}$$

where n_{sample} is the nucleus number density of an atomic species under study. The sum runs over all possible charge states. The second conservation rule is given by the charge neutrality

$$n_e = \sum_i n_i\,z_i. \tag{4.50}$$

The distribution of charge states predicted by the Saha equation (4.48) depends strongly on the IPD model used for the effective ionization energy. In Fig. 4.17, we show the predicted mean charge of a CH plasma with respect to different densities and temperatures by solving the coupled Saha equations considering different IPD models. In comparison to the experimental results by Kraus $et\ al.$ [KCK$^+$16], the influence of the protons in the plasma on the mean charge state of the carbon ions is evidentially revealed.
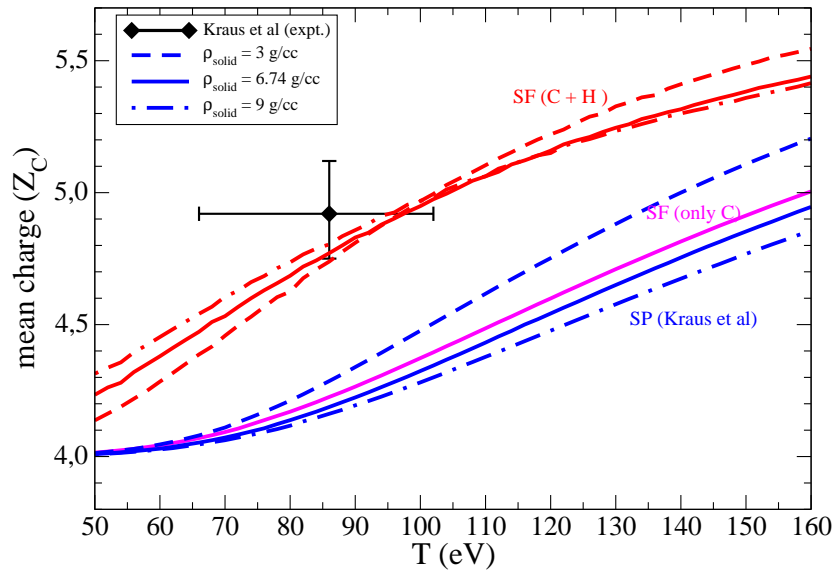
Abb. 4.17: Mean charge of a CH plasma with respect to different densities and temperatures predicted by different models.

Summary

We treated the in-medium two-particle problem (4.5) within a quasiparticle approach and obtained the contribution of the shift of the continuum edge to the IPD. Our approach is based on a Born approximation for the interaction of the two-particle system with the plasma ions. The internal structure and dynamics of the plasma is described by the dielectric function which contains the polarization function $\Pi(\mathbf{q}, \omega)$. Improving the RPA expression for the polarization function, two-particle correlations are included, see also [RD79]. In particular, the ionic dynamical structure factor is taken into account if the cluster decomposition of the polarization function is considered, here the two-ion distribution. Similar approaches have been used for optical spectra [GHR91] where also a cluster decomposition of the polarization function has been considered.

Starting from the general expression (4.9), we obtain a rather simple formula (4.38) for the IPD containing the ionic static structure factor. We emphasize that this result could now be improved by systematically removing some of the approximations for the dynamical SF (4.36). In particular, the plasmon pole approximation in handling the dynamical SF is a model assumption which can be improved, e.g., by numerical simulations. Finally, an advantage of our quantum statistical approach is that any degeneracy effect can be taken into account in a systematic way, which becomes of interest at increasing densities.

A more serious problem is the use of the quasiparticle approximation. Within a sophisticated Green function approach, the quasiparticle propagators are replaced by spectral functions, see, e.g., [For09], which describe also the finite life time of the quasiparticle excitations. This leads to the fact that the energy gaps between the optical lines describing bound state transitions are washed out (Inglis-Teller effect [IT39]). We will continue this discussion in details in the next Chapter.

5. OPTICAL SPECTRA IN PLASMAS

The phenomenon of disappearance of spectral lines in dense plasmas due to the IPD effects is investigated within a more general approach. In this chapter we discuss the following question: what is the reasonable description for the disappearance of the peak structures (spectral lines) in the optical spectra of plasmas? A commonly accepted physical mechanism is the Inglis-Teller (IT) effect resulting from the line merging of highly excited levels. Another mechanism leading to the disappearance of spectral lines is the pressure ionization that describes the truncation of the principal quantum numbers in a medium. The latter effect has been already extensively discussed in the previous chapter. Thus we concentrate on the line merging due to the IT effect, which is closely related to the width and broadening of the energy levels. Similar to the method used in the previous chapter, the quantum statistical approach based on the GF technique is utilized.

5.1 Line dissolution: Inglis-Teller effect versus continuum lowering

To analyze the spectra emitted from plasmas, two spectroscopic effects, i.e. line merging due to IT effect [IT39] and line disappearance because of pressure ionization (also known as IPD and continuum lowering) [SPJ66, EK63], have to be considered carefully and comprehensively. Both effects arise from the deformation of the ionic potential by the plasma fields as well as collisions and have been used for plasma diagnostics [NMG+98, EK63, SPJ66, GHR91]. Generally, pressure ionization is derived from an quasi-static ionic microfield, from which a sharp cutoff for the highest existing principal quantum number can be defined [IT39, NMG+98, KKER86]. Alternatively, the time-dependent effect with considering the fluctuating microfields accounts for the line broadening and line merging and is denoted as Inglis-Teller effect [IT39]. This effect is also known as pressure broadening or the Stark broadening. For correctly reproducing the experimental spectra, a good Stark broadening model should be used in conjunction with the pressure ionization models. Until nowadays, both effects are extensively and well investigated using different models [IT39, NMG+98, EK63, SPJ66, GHR91, KG95, OWGR07, OWR11, DwP92]. However, all these models are unable to describe both effects at the same time. In other words, a systematical and consistent theory is indispensable to account simultaneously for both effects.

In the previous chapter, we have demonstrated that our approach, i.e., the quantum statistical approach based on the GF technique, displays an excellent agreement with different experimental measurements under different plasma conditions. Unlike other models without taking into account the structures of particle correlations, we have introduced the structure factor in calculating the IPD values. Another important feature of our approach is that the time-dependent effect leading to the broadening of the continuum edge can also be described via the imaginary part of the self-energy, as pointed out in our paper [LRKR17].

The IT effect is usually described by the Stark broadening model. The Stark broadening is studied in detail since the elaboration of the quantum mechanics for hydrogen atoms [Sch68].

The relevant physical quantity is the electric field. More generally, the so-called microfield comes into play, if the investigated system is immersed in an environment, in our case, the plasma [GHR91, D'y98, BM59, DwP86, Uns48, Hol19, OWR11]. Therefore, one task that we have to tackle is to find the corresponding microfield distribution for the plasma under a particular condition.

Depending on the plasma density and temperature, the competition of the pressure ionization and the IT effect leads to three consequences: a) the effect of pressure ionization is hidden by the line merging which occurs at lower principal quantum numbers [NMG+98, WKP72]; b) the continuum lowering is so large that the lines disappear before they are subject to broadening sufficient to merge them [HAJ+13a]; c) both effects lead to comparable highest existing principal quantum numbers for the upper level of the emitted lines [OWGR07]. We address again, the aim of the present investigation is to obtain a systematical and consistent theory to explain both the continuum lowering and the IT effect.

5.1.1 Continuum lowering: energy shift and microfield

An important progress for understanding the modification of the atomic potential in a plasma was performed by Unsöld [Uns48]. In his well-known perturbing ion model, Unsöld investigated how the atomic potential well experienced by a confined bound electron is changed by a homogeneous electric field and the nearest neighbor ion. He gave a visualized but simple picture within the framework of classical physics. His fundamental idea is to determine a critical distance at which the binding energy is compensated by the critical electric field produced in plasmas by the nearest perturbing ion. In other words, a critical microfield F_{crit} can be introduced for the corresponding bound state at its classical turning point of the orbit. For hydrogen plasma, the corresponding limit of the radius r_{crit} can be given in terms of the principle quantum number n_{crit} [Uns48]

$$r_{\mathrm{crit}} = n_{\mathrm{crit}}^2 a_0 \tag{5.1}$$

with the Bohr radius a_0.

To ascertain the critical microfield (electric field) F_{crit}, different approximations can be used. The simplest approximation for the microfield is the Holtsmark distribution, where correlation between plasma ions is neglected. More advanced treatments take into account the influence of the interaction between charges, for instance the Hooper distribution. According to D'yachkov [D'y98], the determination of this critical value of the microfield is a rather difficult problem and the uniform field approximation for one-electron atoms and the nearest neighbor approximation for many-electron atoms can be applied. The probability distribution of finding the nearest neighbor ion leads to the following expression for the critical principal quantum number in a plasma [Uns48]

$$n_{\mathrm{crit}} = \frac{1}{6\,a_0} \left(\frac{4\pi n_{\mathrm{e}}}{3} \right)^{-1/3}. \tag{5.2}$$

Therefore, the shift of the continuum edge or the amount of the pressure ionization is characterized by the absolute value of the binding energy at the critical quantum number n_{crit}. Consequently, the continuum lowering can be expressed as

$$\Delta_{\mathrm{ion}} = -\frac{13.6\ \mathrm{eV}}{n_{\mathrm{crit}}^2} = -13.6 \cdot 6a_0 \cdot \left(\frac{4\pi n_{\mathrm{e}}}{3} \right)^{1/3}. \tag{5.3}$$

The simple but elegant analysis on the pressure ionization can be improved in different ways. For example, Fisher and Maron studied the interrelations between characteristic distances on the atomic scale [FM00], where the electron states in plasma are classified into three types: free (with energies $E > 0$), bound (with energies $E < 0$ and trapped only to a single ion), and collectivized (with energies $E < 0$ and confined by the potential wells of two or more ions). In their theory, different effects such as tunneling, screening, and Stark effect are included. Here, we will not discuss the details in great depth.

An alternative approach to describe electrons in the Coulomb potential of the random distributed ions is known from the impurity problem. There exists a mobility edge, where the bound electron becomes itinerant [DwP92]. This approach can be considered as more fundamental in comparison with the simple models for the ion distribution, such as the ion sphere model.

In Fig. 5.1a we show the positions of the continuum edge in hydrogen plasmas predicted by the microfield model, the IS model, and SP model. These results will be discussed in conjunction with the IT effect in the next section.

5.1.2 Inglis-Teller effect: Stark broadening and microfield

It is well known that the degenerate sublevels of energy levels are destroyed due to presence of an external electric field. From the viewpoint of optical spectroscopy, the spectral lines of ions and atoms are split into several components because of the interaction with other charged particles. To investigate the Stark effect in hydrogen-like systems, the parabolic coordinates are generally used. Quantization in the parabolic coordinates leads to the parabolic quantum numbers $|n_1, n_2, m\rangle$ with the principal quantum number [Sch68]

$$n = n_1 + n_2 + |m| + 1, \quad n_1, n_2 = 0, 1, \cdots, n - 1. \tag{5.4}$$

For details see Appendix D. If the external electric field can be regarded as a perturbation, the first- and second-order Stark effects can be derived [SVY81, Gün95]. Obviously, the first-order effect is linear in the perturbing electric field, while the second-order effect is quadratic in the field. Therefore, the first- and second-order Stark effects are also denoted as linear and quadratic Stark effect, respectively. Under certain circumstances, the inhomogeneity of the microfield also contributes significantly to the total Stark effect [SVY81, Gün95]. This contribution is described by the quadrupole interaction between the investigated atomic system and the microfield. To simplify the calculations, we only consider the linear Stark effect.

The linear Stark effect for hydrogen due to the ionic contribution, i.e., the displacement of the level energy $\Sigma_n^{l.s.}$, is given in the parabolic coordinates as [Sch68, SVY81, Gün95]

$$\Sigma_n^{l.s.} = \frac{3}{2} n(n_2 - n_1) \, e a_B \, F, \tag{5.5}$$

where F is the strength of the external electric field experienced by the atomic system under study. Since the ions are randomly distributed in plasmas, the microfield distribution for the electric field F can be introduced. This distribution is responsible for the pressure broadening (or the Stark broadening) of spectral lines. The expression (5.5) gives a variation of the linear Stark effect $\Sigma_n^{l.s.}$ between the limits $\pm (3/2) \, n(n-1) e a_B F$. For highly excited states, the broadenings of the adjacent levels are so large, that their wavefunctions overlap with each other. Consequently, the spectral lines from these levels merge into a continuum [IT39,

OWGR07, OWR11, D'y16]. This is the Inglis-Teller effect mentioned above. Quantitatively, the limited principal quantum number $n_{\max}$ of the uppermost quantum state for the Inglis-Teller effect is given by [IT39, Sal98, Fuj05, Gri97]

$$n_{\max}^{15/2} = \frac{z^{9/2}}{8\,n_{\mathrm{e}}\,a_0^3\,\bar{z}}. \tag{5.6}$$

To evaluate the Stark broadening, the most probable value of the Holtzmark microfield distribution [Hol19, PCG02] for the electric field F are used by Inglis and Teller [IT39], which is given via the ion density

$$F = 3.7e\,n_{\mathrm{ion}}^{2/3}. \tag{5.7}$$

For hydrogen plasmas, $n_{\mathrm{ion}} = n_{\mathrm{e}}$. Inserting this in the equation (5.5), an estimation for the influence of the plasma environment on the spectral lines can be obtained.

To provide insights in how the pressure ionization and IT effect are quantitatively related, calculations for both effects under different plasma conditions are performed and displayed in Fig. 5.1. The positions of the continuum edge depend strongly on the IPD models, as shown in Fig. 5.1a. In contrast to other models, the positions of the continuum edge predicted by the microfield model are located deeper. Consequently, the resulting cutoff for the highest existing principal quantum number lies closer to the maximum quantum number given by the IT effect. It is difficult to distinguish which effect is responsible for the bound-free transition in the experimental spectra.

The modification of positions of the continuum edge can be directly observed in the emission spectra in plasmas. As shown in Fig. 5.2, the following two features are observed: 1) there is no abrupt discontinuity for the Balmer spectral lines near the continuum edge; 2) the Balmer limit is shifted to larger wavelength in comparison to the isolated case. These phenomena are not unique to Balmer series, but a general phenomenon in many-body physics, for example, in the electron-hole plasma in excited semiconductors [ZKK+78, RKK+78, KKER86]. Another well-known example is that in solar astrophysics spectral lines are visible up to main quantum numbers of about 17 [EKKR85]. For Lyman series, These phenomena are also well studied by Hohne and Zimmermann [HZ82], where no transparency window around the threshold frequency distinguishing the bound-bound and bound-free transitions is displayed in the calculated emission spectra for Lyman series.

5.2 Quantum statistical approach for spectral lines in plasma

The problem of predicting the spectral lines of radiating atoms or ions embedded in a plasma is rather complicate. It is usually simplified by treating the ionic and the electronic subsystem in plasmas as well as the investigated atomic system separately. As already mentioned in chapter 2, the ions are heavier than the electrons, so that the average velocity of the ions is much smaller than the average electron velocity [Duf69, SM10, Gün95, Dem10]. During the radiation, the electrons move significantly while the spatial distribution of plasma ions can be approximately regarded as unchanged. Consequently, the ions may be considered as static and the electrons should be treated dynamically within the binary collision approximation.

Within these treatments, a generally accepted expression for the spectral lines is obtained [Gün95]

$$I(\Delta\omega) \sim \int_0^\infty dF\, W(F) \cdot [\Delta\omega + d_{if}\, F - i\, B(\Delta\omega)]^{-1} \tag{5.8}$$
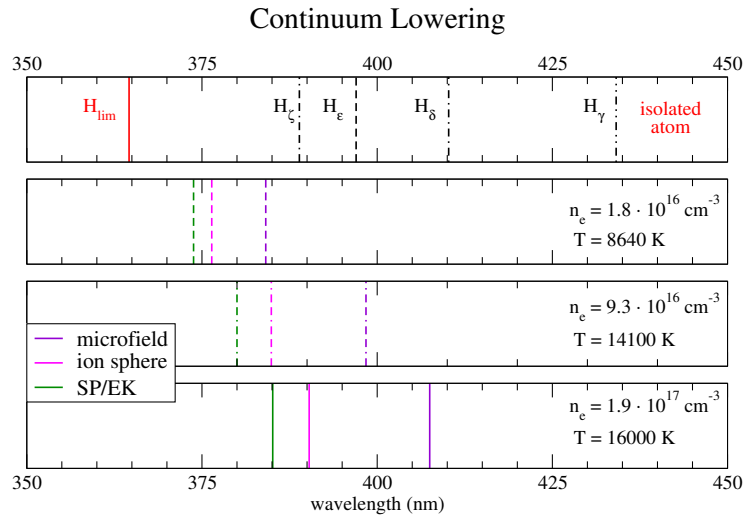
(a) Positions of the continuum edges predicted by different IPD models compared to the isolated lines. The corresponding expressions for the ion-sphere, SP, and EK model for the predictions are given in the previous chapter. The predictions according to the microfield is based on the expression (5.3).
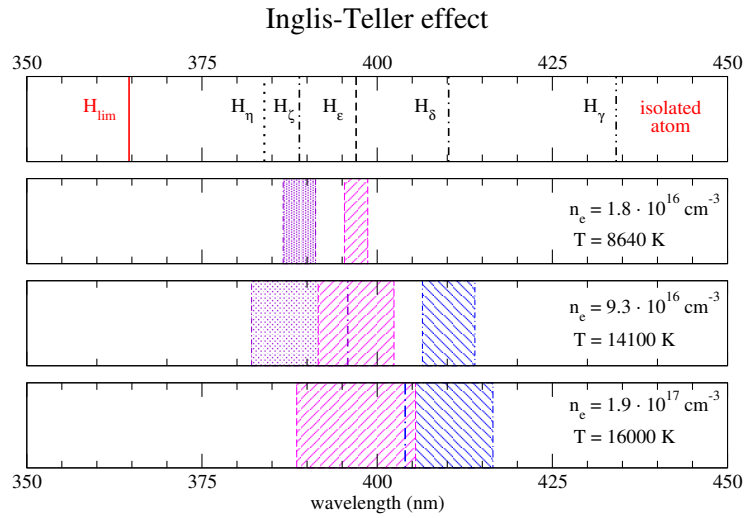
(b) Line merging because of the Stark broadening in comparison to the isolated lines. The predictions are performed according to the expressions (5.5) and (5.7).

Abb. 5.1: Predictions of line dissolution due to the effect of the continuum lowering and the Inglis-Teller effect for different plasma conditions.

where $d_{if} = \langle i|\mathbf{d}|f\rangle$ is the atomic dipole element and $\Delta\omega = \omega - \omega_{if}$ the frequency difference between the emitted photons and the unperturbed transition frequency for the initial state $|i\rangle$ and the final state $|f\rangle$. The positive ions contribute to the broadening through the static Stark effect. However, the contribution of the free electrons to the broadening is by means of
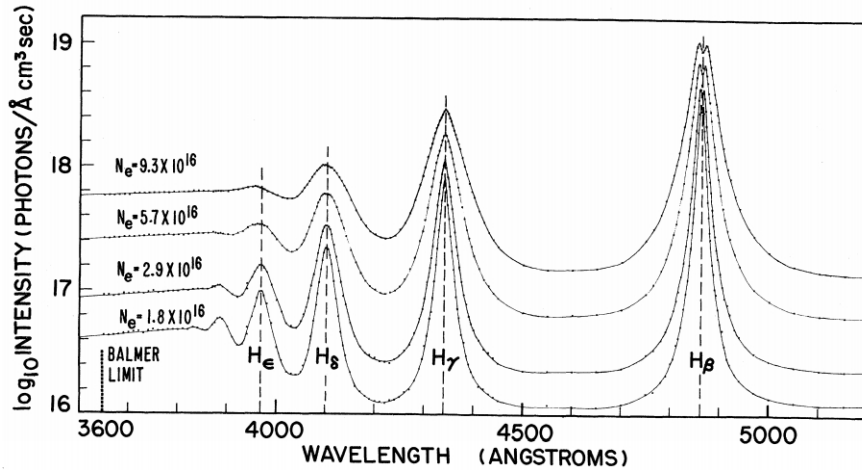
(a) Hydrogen spectra of Balmer series from $3600 - 5200$ Å [WKP72]. The four spectra are selected from different radial positions of the same run in experiment, which represent emissions under different densities and temperatures.
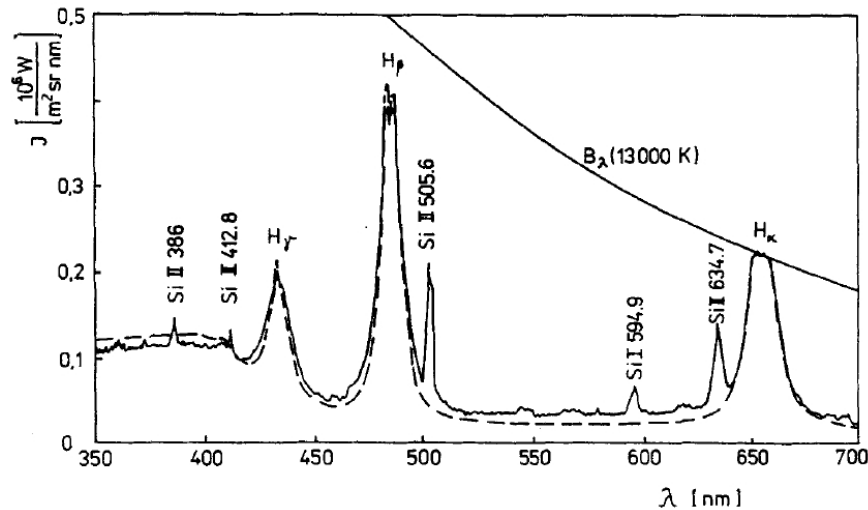
(b) Spectral intensity distribution in the Balmer spectrum of a hydrogen plasma between $350 - 700$ nm [RGS86]. The solid line represents the experimentally recorded spectrum. The dash line describes the theoretical results calculated with a cut-off Coulomb potential approach [RGS86].

Abb. 5.2: Balmer spectra in hydrogen plasmas recorded in different experiments, where no abrupt discontinuity between the bound-free and free-free transitions is observed. The IT effect and the IPD effect are both responsible for this continuity near the continuum edge.

the static Stark effect for low temperatures and via collisions at high temperatures [Duf69, Gün95]. In this formulation the ionic contribution is subdivided into a static and a dynamical component. The static contribution is included by the microfield field distribution $W(F)$,

while the dynamical contribution is described by the operator $B(\Delta\omega)$. The assumptions performed in deriving Eq. (5.8) are unsatisfied for high density plasma since strong collision effects, dynamically screening effects, and degeneracy effects are not considered [Gün95]. Furthermore, the perturbation theory is also problematic for high density plasmas. More importantly, the continuum lowering is not taken into account, which has a strong influence on the emission lines from the highly excited states.

5.2.1 Microfield: autocorrelation function

The total electric microfield $\mathbf{F}$ experienced by a test particle located at $\mathbf{R} = 0$ is evidently represented as the sum of all plasma ion $\mathbf{F}_{\mathrm{ion}}$ and electron fields $\mathbf{F}_{\mathrm{el}}$ under the condition of vector additivity, which can be decomposed into slow $\mathbf{F}_{\mathrm{slow}}$ and fast $\mathbf{F}_{\mathrm{fast}}$ microfield components [Dem10]

$$\mathbf{F} = \sum_i^\infty \mathbf{F}_i = \mathbf{F}_{\mathrm{el}} + \mathbf{F}_{\mathrm{ion}} = \mathbf{F}_{\mathrm{fast}} + \mathbf{F}_{\mathrm{slow}}. \tag{5.9}$$

Obviously, the fast component $\mathbf{F}_{\mathrm{fast}}$ is not equivalent to the electron microfield. Part of the free electrons in plasmas establish a screening cloud around the slowly moving ions. This is also the reason why one should introduce the effective single particle fields in the APEX approximation with adjustable parameters [IRS$^+$00] and in other numerical simulations [DwP86, PCG02, SM10].

The first essentially important quantity for spectral lines is the static microfield distribution $W(F)$, which concentrates only on the slow microfield component $\mathbf{F}_{\mathrm{slow}}$ [Dem10, Gün95]. Actually, in Eq. (5.8) only the slow component of the microfield $\mathbf{F}_{\mathrm{slow}}$ is involved. The fast part of the microfield $\mathbf{F}_{\mathrm{fast}}$ is described by the operator $B(\Delta\omega)$. A number of papers on the study of various physical processes related to microfield characteristics and its effect on medium properties are published. An excellent review on the status of microfield notion can be found in the paper by Demura [Dem10]. In the isotropic case, an elegant expression can be derived for the microfield field distribution [Dem10, PCG02]

$$W(\beta) = \frac{2\beta}{\pi} \int_0^\infty dk \cdot k \, \sin(k\beta) \, A(k) \tag{5.10}$$

with the normalization condition

$$\int_0^\infty d\beta W(\beta) = 1, \tag{5.11}$$

where $\beta = F/F_0$ with $F_0 = 2\pi(4/15)^{2/3} e \, z_i \, n_i^{2/3}$ is the reduced dimensionless microfield value. $A(k)$ is the characteristic function, which reads for an isotropic ideal plasma as

$$A(k) = \exp(-k^{3/2}). \tag{5.12}$$

This is the so-called Holtsmark distribution [Hol19]. It can also be derived for interacting systems, for example, using the Baranger-Mozer cluster expansion [BM59].

Another central quantity to calculate the spectral line shapes is the autocorrelation functions. One of these correlation functions is the electric field autocorrelation function. For example, the field autocorrelation function is directly related to problems of collisional transport and determination of plasma conductivity [Dem10]. Introducing the charge density of

the total plasma

$$\rho(\mathbf{r}, t) = \sum_c e_c n_c(\mathbf{r}, t) = \left(\sum_{\text{all ion species}} e_i n_i(\mathbf{r}, t) \right) - e n_e(\mathbf{r}, t), \tag{5.13}$$

the time-dependent total electric field is described by

$$\mathbf{F}(t) = \int d^3 \mathbf{r} \cdot \frac{\mathbf{r}}{r^3} \, \rho(\mathbf{r}, t). \tag{5.14}$$

Consequently, the field autocorrelation function can be expressed in terms of the charge density autocorrelation function [Duf69]

$$\langle\, \mathbf{F} \cdot \mathbf{F}(t) \,\rangle = \int d^3 \mathbf{r} \int d^3 \mathbf{r}' \cdot \frac{\mathbf{r} \cdot \mathbf{r}'}{r^3 \, r'^3} \cdot \langle\, \rho(\mathbf{r}) \, \rho(\mathbf{r}', t) \,\rangle. \tag{5.15}$$

It is always more convenient to handle the physical quantities in the Fourier representation. Evidently, this correlation function contains the ion-ion correlation, the electron-electron coupling, and the electron-ion interaction. Before detailed discussing these contributions, we first introduce the retarded field autocorrelation function via the Fourier transform

$$\mathrm{C}^{\mathrm{ret}}(\omega) = \int_{-\infty}^{\infty} dt e^{i \omega t} \langle\, \mathbf{F} \cdot \mathbf{F}(t) \,\rangle \, \theta(t) \tag{5.16}$$

and the retarded charge density autocorrelation function in Fourier space

$$\mathcal{C}^{\mathrm{ret}}(\mathbf{k}, \omega) = \int d^3 \mathbf{r} \int dt \, e^{i(\omega t + \mathbf{k} \cdot \mathbf{r})} \langle\, \rho \, \rho(\mathbf{r}, t) \,\rangle \, \theta(t), \tag{5.17}$$

where $\theta(t)$ is the Heaviside step function. Inserting the Eqs. (5.15) and (5.17) into the expression (5.16), the following relation can be achieved [Duf69]

$$\mathrm{C}^{\mathrm{ret}}(\omega) = (4\pi)^2 \int \frac{d^3 \mathbf{k}}{(2\pi)^3} \, k^{-2} \cdot \mathcal{C}^{\mathrm{ret}}(\mathbf{k}, \omega). \tag{5.18}$$

This correlation function is closely related to the plasma structure factor $S(\mathbf{k}, \omega)$, which will be discussed in the subsection 5.2.3.

5.2.2   Self-energy for bound states: microfield

Within the framework of quantum statistical theory, the influence of both electrons and ions are considered via the effective potential. Theoretically, the degeneracy effects and the phase-space occupation (i.e. Pauli blocking) can also be consistently taken into account. Because of different dynamical time scales of ions and electrons, the static microfield ansatz can be also introduced as discussed by Günter [Gün95]. Subsequently, the pressure-broadened line profile is expressed as

$$I^{\mathrm{pr}}(\omega) = \mathrm{Im} \int_0^{\infty} dF \cdot W(F) \cdot \mathcal{L}(\omega, F) \tag{5.19}$$

with the profile function [Gün95, OWGR07, OWR11, LOZ$^+$14]

$$\mathcal{L}(\omega, F) = \sum_{ii'ff'} \frac{\omega^4}{8\pi^3 c^3} \exp\left(-\frac{\hbar\omega}{k_{\mathrm{B}} T} \right) \cdot \langle i|\mathbf{r}|f\rangle \langle f'|\mathbf{r}|i'\rangle$$
$$\times \langle i'|\langle f'| \left[\hbar\omega - \hbar\omega_{if} - \Sigma_{if}(\omega, F) + i\Gamma_{if}^{\mathrm{v}} \right]^{-1} |i\rangle|f\rangle \tag{5.20}$$

with the self-energy for the initial i and final f states

$$\Sigma_{if}(\omega, F) = \text{Re} \left\{ \Sigma_i(\omega, F) - \Sigma_f(\omega, F) \right\} + i\text{Im} \left\{ \Sigma_i(\omega, F) + \Sigma_f(\omega, F) \right\}. \tag{5.21}$$

Following the discussion at the beginning of this section, the total self-energy $\Sigma_n(\omega, F)$ due to both the ions and the electrons of the plasma can be approximately decomposed into a frequency-independent ionic part and an frequency-dependent electronic part which is however independent of the ionic microfield [Gün95, LOZ$^+$14]

$$\Sigma_n(\omega, F) = \Sigma_n^{\text{el}}(\omega) + \Sigma_n^{\text{ion}}(F). \tag{5.22}$$

In dynamically screened Born approximation, the electronic self-energy is given by

$$\Sigma_n^{\text{el}}(\omega) = \int \frac{d^3\mathbf{q}}{(2\pi\hbar)^3} V(q) \sum_\alpha \left| M_{n\alpha}^0(\mathbf{q}) \right|^2 \int_{-\infty}^\infty \frac{d\omega}{\pi} \frac{[1 + n_{\text{B}}(\omega)] \cdot \text{Im} \, \epsilon_{\text{ee}}^{-1}(\mathbf{q}, \omega + i0)}{E_n - E_\alpha - (\hbar\omega + i0)}. \tag{5.23}$$

In the non-degenerate case, the Bose distribution can be replaced by the Maxwell-Boltzmann distribution. Additionally, the dielectric function is treated in the random phase approximation. The ionic self-energy is then described by the Stark effect, for example, by the linear Stark effect

$$\Sigma_n^{\text{ion,l.s.}} = \frac{3}{2} n(n_2 - n_1) \, e a_{\text{B}} \, F. \tag{5.24}$$

This is the standard treatment within the Green's function approach to calculate the spectral lines. The improvement to account for strong collisions has also been developed. Using this approach, the line profiles emitted from hydrogen, helium, and hydrogen-like plasmas are extensively investigated for the purpose of plasma diagnostics [GHR91, Gün95, OGWR06, OWGR07, OWR11, LOZ$^+$14, Oma07, Lor14].

In Eq. (5.26) the integral domain for the microfield distribution $W(F)$ is taken from 0 to ∞. For the emissions from low quantum levels, this procedure does not produce too large errors. However, the energy levels of the bound states are perturbed by the microfield strength and the higher series of transition will disappear, when the microfield strength approaches a certain threshold value [Uns48, D'y98, D'y16, OWGR07, OWR11]. This means that the upper limit of the integral in Eq. has to be truncated due to the dissolution of the discrete upper levels of the permitted transitions. As discussed in Sec 5.1.1, the potential experienced by the atomic electron, which is composed of the sum of the Coulomb potential due to the ionic core of charge Z and the perturbing electric field, exhibits a saddle point above which no bound state can exist. Within the microfield model [RGS86, D'y98, OWR11], a dissolution factor can be introduced [D'y98, OWR11]

$$j(\omega) = \int_0^{F_{\text{crit}}} W(F) dF. \tag{5.25}$$

The remaining important problem in the calculations is the determination of the critical microfield F_{crit}, for which two models can be used: uniform field for one-electron atoms with $F_{\text{crit}} = E^2/(4e^3)$ and nearest neighbor approximations for many-electron atoms with $F_{\text{crit}} = E^2/(16e^3)$ [D'y98]. Here E denotes the ionization energy of the investigated state in an unperturbed atom. Then the line profile covering all bound-bound and bound-free transitions can be expressed as [D'y16]

$$I(\omega) = \text{Im} \int_0^{F_{\text{crit}}} dF \cdot W(F) \cdot \mathcal{L}(\omega, F) + \int_{F_{\text{crit}}}^\infty dF \cdot W(F) \cdot \mathcal{L}_{\text{cont}}(\omega, F), \tag{5.26}$$

where $\mathcal{L}_{\mathrm{cont}}(\omega, F)$ is the line profile function for the bound-free and free-free emissions. We will not go into the details on determining the critical microfield F_{crit} and on deriving the emission coefficients related to the continuum states. In the following, we will discuss the possibility whether we can calculate the spectral line shapes in terms of the dynamical and static structure factors as we have done for the ionization potential depression [LRKR17].

5.2.3 Self-energy for bound states: structure factor

In the original GF formalism derived by Röpke *et al.* for spectral lines [RSK81, HRSZ86], no microfield ansatz is necessary to evaluate the shift and broadening of spectral lines. The influence of the plasma in the two-particle states induced by free electrons and plasma ions is consistently included in the Bethe-Salpeter equation for the two-particle GF. The essential physical quantity is the dielectric function as the sum of electron polarization and ion polarization. In the random-phase approximation, the total dielectric function is well-known [Duf69, RSK81]. The main task within the GF formalism is to calculate the two-particle self-energy [RSK81, Gün95]

$$\Sigma_{n\mathbf{P}} = \int \frac{d^3\mathbf{q}}{(2\pi)^3} \int \frac{d\hbar\omega}{\pi} \, V(q) \sum_{n'} \frac{(1 + n_{\mathrm{B}}(\omega) \, \mathrm{Im} \, \varepsilon^{-1}(\mathbf{q}, \omega + i0))}{E^0_{n\mathbf{P}} - E^0_{n'\mathbf{P}-\mathbf{q}} - \hbar\omega} \cdot |M_{nn'}(\mathbf{q})|^2 \,, \qquad (5.27)$$

where $E^0_{n\mathbf{P}}$ is the total energy of the two-particle state and $M_{nn'}(\mathbf{q})$ is the transition matrix element with the momentum transfer $\mathbf{q}$.

Actually, the dielectric function, the dynamical SF, and the field autocorrelation function are tightly related. For example, the field autocorrelation function is connected to the symmetrized correlation function of the longitudinal microfield fluctuations via $\langle \delta\mathbf{E}\delta\mathbf{E} \rangle_{\mathbf{q},\omega} = 2\pi(Z_i^2 e^2/q^2)S_{\mathrm{ii}}(\mathbf{q}, \omega)$ [KSKB05]. This is the reason why we can use different formalisms to describe the same physics. This fact is reflected by the study on the IPD effect in plasma. In the present work, the possibility using the SF and the microfield model to calculate the IPD is shown in the previous chapter and in this chapter, respectively. As in the theroy of Thomson scattering and in the theroy for IPD, we introduce the dynamical struture factor to investigate the spectral line profile in plasma.

We rewrite the expressions for the dynamical SF

$$S(\mathbf{q}, \omega) = \int d^3\mathbf{r} \int dt \, e^{i(\omega\, t + \mathbf{q}\cdot\mathbf{r})} \langle \, \rho\, \rho(\mathbf{r}, t) \, \rangle \qquad (5.28)$$

and for the dielectric function

$$S(\mathbf{q}, \omega) = \frac{\hbar}{n\pi} \frac{1}{1 - e^{-\hbar\omega/k_{\mathrm{B}}T}} \cdot V^{-1}(q) \cdot \mathrm{Im} \, \varepsilon^{-1}(\mathbf{q}, \omega) \qquad (5.29)$$

or in a more explicit form

$$\mathrm{Im} \, \frac{1}{\varepsilon(\mathbf{q}, \omega + i0)} = \frac{\pi \, e^2 \, (1 + n_{\mathrm{B}}(\omega))^{-1}}{\hbar\varepsilon_0 \, q^2} \cdot \left[z_i^2 \, n_i S_{\mathrm{ii}}(\mathbf{q}, \omega) - 2z_i \, \sqrt{n_e n_i} S_{\mathrm{ei}}(\mathbf{q}, \omega) + n_e S_{\mathrm{ee}}(\mathbf{q}, \omega) \right].$$
$$(5.30)$$

Evidently, the electron and ion contributions to the inverse dielectric function $\varepsilon^{-1}(\mathbf{q}, \omega + i0)$ are not additive. Reminding the relation between the field autocorrelation function and the charge-density autocorrelation function, the connection between the field autocorrelation function and the dynamical SF can be established.

5.2.3.1 Electronic contribution

The electronic contribution is described by the last term of Eq. (5.30), i.e. $S_{ee}(\mathbf{q},\omega)$ and is generally described in the RPA. To account for degeneracy effects, we follow the idea of Arista and Brandt [AB84], where the electronic dielectric function $\epsilon_{ee}(\mathbf{q},\omega + i0)$ can be calculated by an anylytical expression

$$\epsilon_{ee}(\mathbf{q},\omega + i0) = \epsilon_1(\mathbf{q},\omega + i0) + i\epsilon_2(\mathbf{q},\omega + i0) \qquad (5.31)$$

with the following expressions

$$\epsilon_1(\mathbf{q},\omega + i0) = \mathrm{Re}\,\epsilon_{ee}(\mathbf{q},\omega + i0) = 1 + \frac{\chi_0^2\,\theta}{4z^3} \cdot \left\{ g(u+z) - g(u-z) \right\}, \qquad (5.32)$$

$$\epsilon_2(\mathbf{q},\omega + i0) = \mathrm{Im}\,\epsilon_{ee}(\mathbf{q},\omega + i0) = \frac{\pi\chi_0^2\,\theta}{8z^3} \cdot \ln\left\{ \frac{1 + \exp\left[\eta - (u-z)^2/\theta\right]}{1 + \exp\left[\eta - (u+z)^2/\theta\right]} \right\}, \qquad (5.33)$$

where θ is the degeneracy parameter of the plasma electrons. Other reduced parameters are given as $\chi_0^2 = 1/\left(\pi a_0 k_{F,e}\right)$, $u = \omega/\left(k v_{F,e}\right)$ and $z = k/(2k_{F,e})$ with the Fermi wave number of the electron $k_{F,e} = m_e v_{F,e}/\hbar$. Then the imaginary part of the inverse electronic dielectric function, which is related to the dynamical structure factor of free electrons, can be expressed by

$$S_{ee}(\mathbf{q},\omega) \sim I_{ee}(\mathbf{q},\omega + i0) = \mathrm{Im}\,\frac{-1}{\epsilon_{ee}(\mathbf{q},\omega + i0)} = \frac{\epsilon_2(\mathbf{q},\omega + i0)}{(\epsilon_1(\mathbf{q},\omega + i0))^2 + (\epsilon_2(\mathbf{q},\omega + i0))^2}. \qquad (5.34)$$

This expression is also known as energy-loss function, which is the crucial quantity determining the spectrum of excitations in the plasma in terms of the momentum transfer $\hbar\mathbf{q}$ and of the energy transfer $\hbar\omega$. It's impossible to find an exact analytical expression for the energy-loss function $I_{ee}(\mathbf{q},\omega + i0)$ which can, however, be evaluated approximately in various limiting cases.

Generally, the following three limiting cases are interesting for the experiments of light or particle scattering in plasma: (a) low-frequency behavior of the plasma indicated by $u \ll 1$ for all z values; (b) the single-particle ridge in the region of high frequencies and short wavelength with $u \cong z \gg 1$; and (c) the plasma resonance domain at high frequencies and long wavelength limit, i.e. $u \gg 1 \gg z$, which describes the collective excitations of the free electrons.

In the low-frequency limit case (a), the energy-loss function can be approximated as [AB84]

$$I_{ee}^{l.f.}(\mathbf{q},\omega + i0) \approx \frac{2m_e^2 e^2 q\omega}{\hbar^3\left(k^2 + k_s^2\right)^2} \cdot \left\{ 1 + \exp\left[\frac{\hbar^2 k^2}{8m_e k_B T} - \eta\right] \right\}^{-1} \qquad (5.35)$$

where the screening constant can be expressed approximately as $k_s^2 \approx k_{TF}^2/\left(1 + 9\theta^2/4\right)^{1/2}$ with the Thomas-Fermi screening length $k_{TF}^2 = \sqrt{3}\,\omega_{pl,e}/v_{F,e}$ or given approximately as $k_s^{-4} = k_{TF}^{-4} + \kappa_{D,e}^{-4}$.

The single-particle ridge, case (b), describes short-range excitations of individual electrons in the plasma, whose existence is a pure quantum feature and has no correspondence in the classical or semi-classical treatments of the dielectric function. From the condition $u \cong z$, it

can be seen that $\hbar\omega = \hbar^2 q^2/(2\,m_e)$, $\epsilon_1(\mathbf{q}, \omega + i0) \approx 1 + \mathcal{O}\left(k_{\mathrm{F,e}}/k\right)^4$, and $\epsilon_2(\mathbf{q}, \omega + i0) \ll 1$, so that the energy-loss function can given approximately as [AB84]

$$I_{\mathrm{ee}}^{\mathrm{s.p.}}(\mathbf{q}, \omega + i0) \approx \epsilon_2(\mathbf{q}, \omega + i0) = \frac{\pi \chi_0^2\, \theta}{8 z^3} \cdot \ln \left\{ \frac{1 + \exp\left[\eta - (u-z)^2/\theta\right]}{1 + \exp\left[\eta - (u+z)^2/\theta\right]} \right\}. \qquad (5.36)$$

The collective resonance of the plasma, which describes the modes of collective motion of the electrons, is determined by the condition $\epsilon_{\mathrm{ee}}(\mathbf{q}, \omega + i0) = 0$. For example, the famous phenomenon of "Landau damping" can be explained by this collective resonance behavior of free electrons in plasma. The resonance frequency is given by the dispersion relation [AB84]

$$\omega_q^2 \cong \omega_{\mathrm{pl,e}}^2 + \langle v^2 \rangle q^2, \quad \text{with} \quad \langle v^2 \rangle = \frac{3}{2}\, v_{\mathrm{F,e}}^2\, \theta^{5/2}\, F_{3/2}(\eta) \approx \frac{3}{5} v_{\mathrm{F,e}}^2 \cdot \left(1 + 25\theta^2/4\right)^{1/2}, \qquad (5.37)$$

and the corresponding energy-loss function is

$$I_{\mathrm{ee}}^{\mathrm{p.r.}}(\mathbf{q}, \omega + i0) \approx \frac{\omega_q^4\, \epsilon_2(\mathbf{q}, \omega + i0)}{\left(\omega^2 - \omega_q^2\right)^2 + \omega_q^4\, \epsilon_2^2(\mathbf{q}, \omega + i0)}. \qquad (5.38)$$

Obviously, for transitions with $\Delta n = 0$, the approximate expression (5.35) can be used. For the optical transitions with $\Delta n \neq 0$, the approximation (5.36) for the inverse electronic dielectric function can be performed.

5.2.3.2 Ionic contribution

Theoretically, the final results can be obtained for calculating the spectral lines by inserting Eq. (5.30) into the expression (5.27), where the ionic contribution is included in the ionic dynamical SF $S_{\mathrm{ii}}(\mathbf{q}, \omega)$. But this procedure does not lead to satisfying results since the unperturbed level energy $E_{n\mathbf{P}}^0$ and the unperturbed wavefunction in the transition matrix element $M_{nn'}(\mathbf{q})$ are applied. In the microfield formalism the perturbation of the plasma environment on the eigenenergies is removed by the microfield ansatz [GHR91, Gün95]

$$E_{n\mathbf{P}} = E_{n\mathbf{P}}^0 + C(\beta), \qquad (5.39)$$

where $C(\beta)$ is related to the microfield distribution $W(\beta)$ in terms of the dipole interaction.

For the single-particle problem, the shift in the self-consistently defined self-energy is compensated by the eigenenergy shift [LRKR17]. In analogy to the case of single-particle problem, the following self consistent relation for the two-particle eigenenergy has to be solved

$$E_{n\mathbf{P}} = E_{n\mathbf{P}}^0 + \mathrm{Re}\,\Sigma_{n\mathbf{P}; E_{n\mathbf{P}}}. \qquad (5.40)$$

The current assignment is to reveal the implicit connection between the perturbed eigenenergy and the SF, which is rather difficult and complicate and still under investigation. In the next subsection we will show how this approach woks in calculating spectra line shapes in dense plasmas.

5.2.4 Spectral lines in plasmas

To investigate the optical spectra within the quantum statistical approach, we should return to the two-particle problem, which is described by the atomic polarization function (i.e. the second term in the cluster decomposition of the polarization function) [RKK$^+$78, KKER86]. The pressure-broadened line profile is then given by [GHR91, Gün95, OWR11]

$$
\mathcal{L}(\omega) = \sum_{ii'ff'} \frac{\omega^4}{8\pi^3 c^3} e^{-\frac{\hbar\omega}{k_{\mathrm{B}}T}} \langle i|\mathbf{r}|f\rangle \langle f'|\mathbf{r}|i'\rangle \cdot \langle i'|\langle f'| \left[\hbar\omega - \hbar\omega_{if} - \Sigma_{if}(\omega) + i\Gamma_{if}^{\mathrm{v}}\right]^{-1} |i\rangle|f\rangle
$$

(5.41)

with the SE for the initial i and final f states

$$
\Sigma_{if}(\omega) = \mathrm{Re}\left\{\Sigma_i(\omega) - \Sigma_f(\omega)\right\} + i\mathrm{Im}\left\{\Sigma_i(\omega) + \Sigma_f(\omega)\right\}
$$

(5.42)

and the vertex correction

$$
\Gamma_{if}^{\mathrm{v}} = -\int \frac{d^3\mathbf{p}}{(2\pi)^3} \int \frac{d^3\mathbf{q}}{(2\pi)^3} f_{\mathrm{e}}(E_{\mathbf{p}}) V^2(q) M_{ii}^0(\mathbf{q}) M_{ff}^0(-\mathbf{q}) \delta\left(\frac{\hbar^2 \mathbf{p}\cdot\mathbf{q}}{m_{\mathrm{e}}}\right)
$$

(5.43)

where the unperturbed transition matrix elements are given by [OWR11]

$$
M_{n\alpha}^0(\mathbf{q}) = i\left\{Z\delta_{n\alpha} - \int d^3\mathbf{r}\, \psi_n^*(\mathbf{r})\, e^{i\mathbf{q}\cdot\mathbf{r}}\, \psi_\alpha(\mathbf{r})\right\}.
$$

(5.44)

Evidently, the shift of transition energy is given by the difference of real parts of the SE for the initial i and final f states, whereas the broadening of spectral lines is determined by the imaginary parts of the SE for the initial i and final f states as well as the vertex correction Γ_{if}^{v}. Because of different dynamical time scales of ions and electrons, the electronic contribution is usually calculated in the impact approximation and the ionic contribution is described within the quasi-static approximation [GHR91, Gri97].

Introducing the microfield ansatz [GHR91], the total SE $\Sigma_n(\omega, F)$ can be approximately decomposed into a frequency-independent ionic part determined by the microfield strength F and an only frequency-dependent electronic part (for details see section 2.2.3.2). In this work, we deal with the problem in a different way by treating the plasma electrons and ions at the same level, i.e. directly via the DF. The RPA DF for the non-degenerate case reads [KKER86, Red97]

$$
\epsilon_{\mathrm{RPA}}(\mathbf{q},\omega) = 1 + \frac{K}{2Q^3}\left\{\sqrt{2}\left[D(x_1^+) - D(x_1^-)\right] + \sqrt{2/\gamma}\left[D(x_2^+) - D(x_2^-)\right]\right.
$$

$$
\left. -i\left\{\sqrt{\pi/2}\left[e^{-(x_1^+)^2} - e^{-(x_1^-)^2}\right] + \sqrt{\pi/(2\gamma)}\left[e^{-(x_2^+)^2} - e^{-(x_2^-)^2}\right]\right\}\right\}
$$

(5.45)

with the abbreviations

$$
Q = \frac{\hbar q}{(m_{\mathrm{e}}\, k_{\mathrm{B}}T)^{1/2}}, \qquad K = \frac{(1+z^2)\hbar^2 n_{\mathrm{e}} e^2}{m_{\mathrm{e}}\, \varepsilon_0\, (k_{\mathrm{B}}T)^2}, \qquad \gamma = \frac{m_{\mathrm{e}}}{m_{\mathrm{ion}}}
$$

$$
x_1^\pm = \sqrt{\frac{1}{2}\left[\frac{\omega}{q}\left(\frac{m_{\mathrm{e}}}{k_{\mathrm{B}}T}\right) \pm \frac{Q}{2}\right]}, \qquad x_2^\pm = \sqrt{\frac{1}{2\gamma}\left[\frac{\omega}{q}\left(\frac{m_{\mathrm{e}}}{k_{\mathrm{B}}T}\right) \pm \gamma\frac{Q}{2}\right]},
$$

(5.46)

where $D(x) = \exp\left(-x^2\right) \int_0^x dt \, \exp\left(-t^2\right)$ is the Dawson integral. Inserting this expression into the single-particle self-energy discussed in the last chapter, an expression for the IPD can be obtained, which is the Debye shift for the IPD in the low density case and is equivalent to the expression (4.38). Then we have for the SE of bound two-particle states with the following expression [RD79]

$$\Sigma_n(\omega) = \int \frac{d^3\mathbf{q}}{(2\pi\hbar)^3} V(q) \sum_\alpha \left| M^0_{n\alpha}(\mathbf{q}) \right|^2 \int_{-\infty}^{\infty} \frac{d\omega}{\pi} \frac{[1 + n_{\mathrm{B}}(\omega)] \cdot \mathrm{Im}\, \epsilon_{\mathrm{RPA}}^{-1}(\mathbf{q}, \omega + i0)}{E_n - E_\alpha - (\hbar\omega + i0)}, \quad (5.47)$$

which is the SE in dynamically screened Born approximation with the RPA DF. Accounting for the thermal motion of the plasma ions, which results in the Doppler broadening, the full line profile is given by a convolution [Gri97]

$$I^{\mathrm{total}}(\Delta\omega) = \frac{c}{\omega_0} \sqrt{\frac{m_{\mathrm{ion}}}{2\pi k_{\mathrm{B}} T}} \int_{-\infty}^{\infty} d\Delta\omega' \cdot I^{\mathrm{pr}}(\Delta\omega') \cdot \exp\left\{ -\frac{m_{\mathrm{ion}} c^2}{2 k_{\mathrm{B}} T} \left(\frac{\Delta\omega - \Delta\omega'}{\omega_0 + \Delta\omega'} \right)^2 \right\}. \quad (5.48)$$
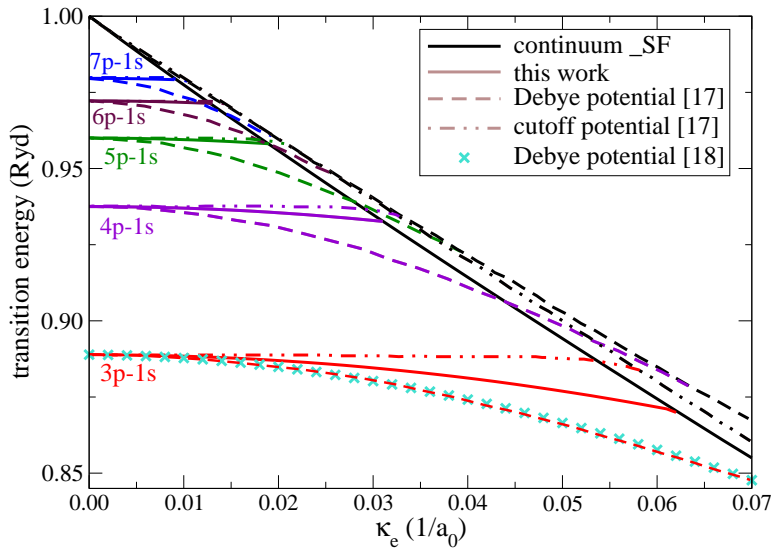
Abb. 5.3: Transition energy for the Lyman series $\hbar\omega = E_{n\mathrm{p}} - E_{1\mathrm{s}}$ and the threshold energy for the bound-free transition $\hbar\omega_{\mathrm{th}} = V(\infty) - E_{1\mathrm{s}}$ with respect to the inverse Debye length of electrons κ_{e}. The solid lines represent the results of this work. The dashed lines and the dotted-dashed lines describe the numerical results of the Schrödinger equation with a Debye potential [HZ82, QWWQ09] and a cutoff potential [HZ82], respectively. The cross points are also calculated with Debye potential [QWWQ09].

The interaction of a radiating particles with the plasma environment results in both shift and broadening of the eigenlevels of a two-particle state. At first, we concentrate on the shifts of both the bound states and the free states. In the present work, we calculate the IPD and the shift of bound states via Eq. (4.38) and Eq. (5.47), respectively. Comparison of our results for the transition energies and bound-free threshold energies and the results predicted by other theoretical approaches is shown is Fig. 5.3.

The positions of emission line centers are determined by the transition energies. One of the commonly used theoretical approaches is to solve the Schrödinger equation with a
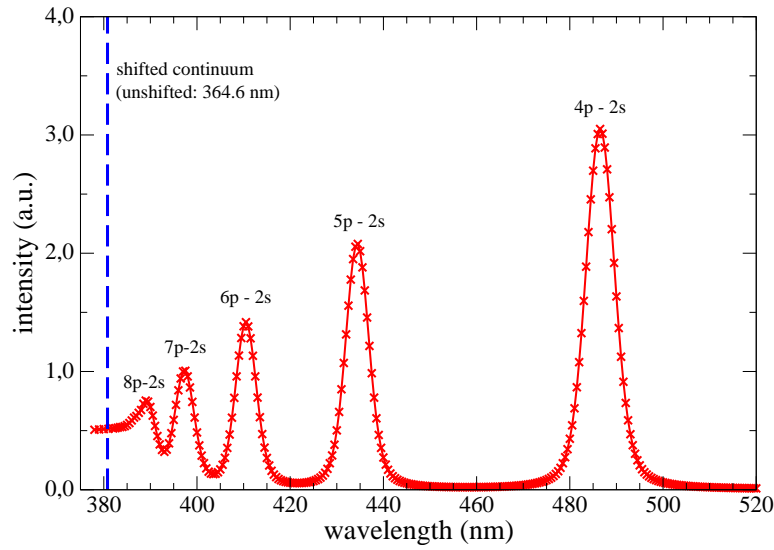
Abb. 5.4: Optical spectra of a plasma at the electron density $n_e = 2.1 \cdot 10^{17}\,\text{cm}^{-3}$ and temperature $T_e = 1.02$ eV calculated within RPA (5.47). Gaussian broadening with FWHM of 0.002 Ryd is considered in the calculation. Both ITE and IPD are systematically calculated from the quantum statistical approach. A continuum background [OWR11] is considered.

pseudo-potential [HZ82, QWWQ09] for eigenenergies and the corresponding wave functions. Numerical solutions have been obtained using the Debye potential [HZ82, QWWQ09] or the cutoff potential [HZ82, RGS86] as the pseudo-potential. From Fig. 5.3, it is seen that the line center positions derived from the cutoff potentials are almost unchanged in comparison to the pure Coulomb case. In contrast, the Debye potential predicts a strong modification for the transition energy, in particular for relatively high densities ($\kappa_e = \sqrt{n_e e^2/(\varepsilon_0 k_B T)} \geq 0.02/a_0$). However, this result is in strong contradiction to the experimental measurements, where the positions of line centers are only slightly shifted [RGS86]. In the Debye model, the shifts do not separately depend on density and temperature but only on the screening parameter κ_e.

The optical spectra of the Balmer series calculated within RPA combined with a continuum background due to Bremsstrahlung are displayed in Fig. 5.4. For the given plasma conditions ($n_e = 2.1 \cdot 10^{17}\,\text{cm}^{-3}$, $T_e = 1.02$ eV), the IPD value is about 0.138 eV, which means that the energy levels appear only up to $n = 9$ and the Balmer limit is shifted from 364.6 nm to 380.8 nm. Another feature of the predicted line shape (i.e. ITE) is the formation of quasi-continuum states, i.e. the band structure, starting from the energy level $n = 6$. Moreover, the transition peak from $9p \rightarrow 2s$ is washed out due to the broadening. In summary, to calculate the spectra in the whole wavelength range, the first step is to determine the highest existing quantum state from the IPD theory. The second step is to calculate the line shape up to the highest energy level predicted by the IPD theory. Actually, the optical spectra of Balmer series under these conditions were experimentally measured by Goto *et al.* [GMK10], where the disappearance of the transition peaks is observed already starting from a lower principal quantum number $n = 6$. The reason for this disagreement arises from the fact that the ionic contribution to the broadening is excessively underestimated by RPA. Comparing the experimentally measured line broadening of H_α line with the RPA result, it is shown that the RPA result is only 25% of the experimental value.

The line merging due to the broadening does not have a simple relation to the shift of the continuum edge. Generally, both effects have to be considered carefully and comprehensively for correctly reproducing the experimental spectra. For weakly coupled and non-degenerate plasmas, the line merging occurs at lower principal quantum numbers in comparison to the IPD effect as shown in Fig. 5.4 and measured in laser produced plasmas [HAJ+13a, NMG+98]. Recently, the optical spectra in highly charged aluminum plasmas are observed, where the continuum lowering is so large that the lines disappear before they are subject to broadening sufficient to merge them [HAJ+13a]. Therefore, it is of relevance to develop an accurate spectral line theory using the systematic quantum statistical approach, since spectroscopic methods are the most reliable tool to analyze density and temperature conditions.

5.3 Further work

We have shown that both effects, IPD and ITE, have to be considered to explain the disappearance of spectral lines. The synthetic spectra and the transition energies are systematically described using a consistent quantum statistical approach within the simplest RPA. The Debye results for both IPD and optical transitions are obtained. Of course, the Debye model is very simple and the ionic contributions are strongly underestimated. For the hydrogen plasmas, the ion contribution is more important. The RPA is not satisfied and has to be improved. The underestimation might be rendered by using the ionic structure factor to calculate the line broadening and shift like in the case for the IPD when going beyond the RPA [LRKR17]. Additionally, the electron contribution can be improved by introducing the T matrix describing strong collisions. Furthermore, photon re-absorption plays an important role for the transport of radiation in a plasma, which has a strong influence on the transitions from the low quantum numbers [OWR11]. This has to be taken into account in calculating the line shapes. For higher levels, the transition rates may be better described via semi-classical description, for example using wave-packet states for the electrons [LGRR16].

In the context of new experimental facilities exploring warm dense matter [HAJ+13a, CVC+12, KCK+16, NMG+98], strongly coupled and nearly degenerate Coulomb systems can be produced. A detailed description of the spectrum emitted from such systems in equilibrium and non-equilibrium conditions is still a challenging problem. As shown in this work, the quantum statistical approach based on thermodynamic Green's function technique provides a possibility to understand the many-body systems under such extreme conditions.

For further works, we are aiming to find out a consistent description for both single- and two-particle problem in terms of the SFs at the same time. Additionally, how to realize the application of our approach, i.e. thermodynamical GF technique, to inner-shell transitions, for example, the K_α spectral lines [Sen10, Che14] deserves further extensive investigation. Some preliminary results see Appendix E.

Stark broadening parameters of H-like He-like carbon systems are of interest for hot and dense stars, as well as for the diagnostics of laser-produced plasmas [Oma07]. To reveal conditions of extreme pressure ionization and line merging in spectroscopic observations, time- and space-resolved extreme ultraviolet spectra of carbon plasmas were recorded and analyzed in detail [NMG+98]. Obviously, a detailed description of the spectrum emitted by such an expanding plasma in non-equilibrium is a challenging problem. It is of great interest and of relevance to develop an accurate spectral line theory, since spectroscopic methods are the most reliable tool to analyze density and temperature conditions [Sal98, Fuj05]. The most interesting and most important feature of these spectra is that a dip in the spectrum

near the series limit for the DH case is shown in the numerical simulation. This is caused by an overestimation of the continuum lowering, leaving no merged bound-bound transitions to contribute to the spectrum in that region [NMG+98].
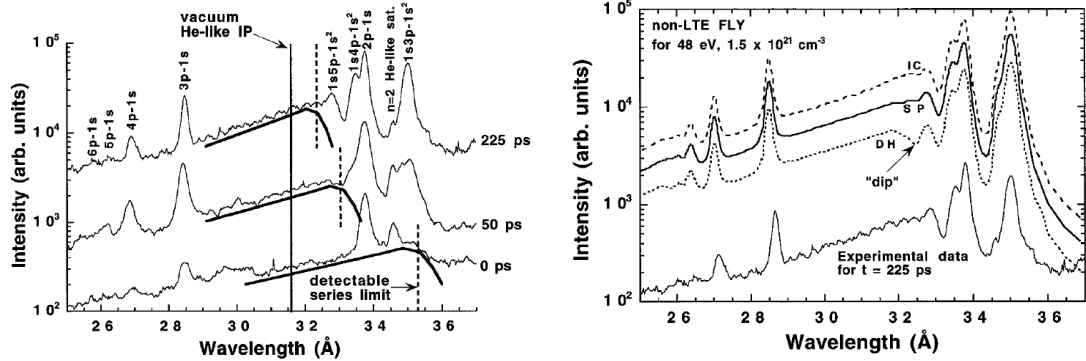
(a) Lineouts from the time-resolved spectra taken at time points. The He-like $np1s - 1s^2 (n > 3)$ and H-like $np - 1s$ line emissions are identified. The free-bound continuum and the detectable series limit are drawn on each lineout.

(b) Comparison of a lineout at $t = 225$ ps and non-LTE FLY simulations at 48 eV and $1.5e + 21$ cm^{-3}. To account for the continuum lowering effect, three different models, i.e. IS, SP, and DH model, are used for comparison in simulations.

Abb. 5.5: Pressure ionization and line merging in strongly coupled carbon plasmas [NMG+98].

6. CONCLUSION AND OUTLOOK

To study the optical properties in plasmas, two different theories, i.e., the quantum master equation approach and the thermodynamic Green's function technique, are introduced in the present investigation. Within the Born-Markov approximation, the QME for an atom interacting with the charged particles of a plasma environment has been derived, where the influence function of the plasma environment is determined by the dynamical structure factor of the plasma. Alternatively to the QME approach, the thermodynamic Green's function technique within the framework of the quantum statistical theory has been applied to investigate the continuum lowering, the ionization potential depression, and the modifications of spectral lines in dense plasmas.

The Rydberg atoms considered in the present work are an interesting object to describe the transition from the quantum micro-world to the macroscopic classical world where new properties such as trajectories emerge [Joo03, Goc07, Gal94, Hez10, Sch07, Rob04]. A main advantage of the QME for a hydrogen Rydberg atom surrounded by a plasma is the use of robust states instead of the pure hydrogen eigenenergy states [Goc07, LGRR16]. Generally, the Rydberg states are assumed to be described quasi-classically. Here we provide an explanation for this treatment. The treatment of localization due to the interaction with the surrounding environment allows the transition to classical physics and the very efficient use of classical descriptions.

Introducing the Brown circular-orbit wave packets [Bro73, GS90] as the optimized robust states for the bound Rydberg electrons, the transition rates were calculated. Comparing with experiments [DBD79] and MCS results [VS80], it turns out that the use of robust wave packets gives a better agreement with measured data and classical calculations than the approach using pure hydrogen energy eigenstates. The wave packet is constructed from the superposition of different quantum states and is characterized by an average quantum number n_0. On the other side, it is well known that the low-lying bound states are more appropriately described by the quantum number. Therefore, a critical quantum number n_{cr} is introduced to represent the transition between descriptions of the bound electron in hydrogen atoms by the wave packet and the pure quantum eigenstate.

As another example for the use of the atomic master equation, the spectral line shape for transitions at low quantum numbers has been derived. The equivalence with a quantum statistical approach to profiles of spectral lines [Gün95] has been shown. After decoupling the ion and electron subsystems of the plasma environment, only the electron contribution to the spectral line shape has been considered (impact approximation). The standard description of the interaction with the plasma ions is the ionic microfield. The ionic structure factor and the corresponding pair distribution function determine the microfield distribution [DwP86]. A superposition of the Stark shift in the ionic microfield and the electron contribution in impact approximation lead to the line profiles as derived from the unified theory [Gün95].

A fundamental issue in the theory of open quantum systems is that the subdivision of the total system into the reduced system and the bath is arbitrary and can be changed [Wei99,

BP07, Goc07, Röp13]. Degrees of freedom of the bath which are strongly coupled to the reduced system may be incorporated into the reduced system, so that the bath contains only weakly coupled degrees of freedom, which may be treated in the Born-Markov approximation. Various approximations, in particular the Born-Markov approximation and the rotating-wave approximation, performed in the present work can be improved in future work, see also Ref. [ZMR97, BP07]. Furthermore, the electrons in atoms and the plasma electrons must be antisymmetric so that exchange terms will occur. With respect to radiation processes, it is in general not the single electron which emits radiation but the whole reduced system which couples to the radiation field [KKER86]. Another interesting application of this aspect is the treatment of radiation from many-electron atoms, for instance the K_α radiation [Sen10].

Another interest and important feature for an atom immersed in a plasma is that the existence of the plasma environment also leads to a reduction of the bound electron binding energy because of the screening effects in the plasma [KKER86, Sal98, Fuj05, KSKB05]. This means there is a maximum principal quantum number $n_{\max}$ under a certain plasma condition, above which the continuum states for electrons can be defined. From the quantum Brownian motion [Joo03, Goc07] we know that a wave packet description constructed from plane-wave states can be applied for free particles moving in a bath. Moreover, no abrupt jump between the bound states and continuum ones is observed in spectroscopic measurements. Therefore, it would be of interest to investigate whether a wave-packet description might be more suitable near the continuum edge for both bound and free states, if we extend the definition of the wave packet to include the continuum states. The remaining question is how we can determine the maximum principal quantum number $n_{\max}$, i.e. the position of the continuum edge. Within the QME approach, this question is rather difficult to solve. As shown in this investigation, the Green's function technique is more convenient to understand problems related to the continuum edge [LRKR17].

As mentioned above, the thermodynamic Green's function technique is also a powerful tool for investigation of the spectral lines in dense plasmas. This approach has been successfully applied for hydrogen, helium, and hydrogen-like ionic spectral lines [Gün95, Oma07, Lor14], where the ionic contribution is described by the microfield. Different from this treatment, we have introduced the structure factor as the indicator for the ionic correlations and fluctuations. In fact, both the microfield distribution and the structure factor are related to the pair distribution function [DwP86, KSKB05]. With the help of the structure factor, the in-medium two-particle problems, i.e. the ionization potential depression and the emission spectral lines in a dense plasma, are investigated using the thermodynamic GF technique.

With respect to the IPD effect in the plasma, we demonstrated that ionic correlations and fluctuations play a critical role in determining the IPD. The simple but elegant expression for the IPD shown in chapter 4 has many advantages in comparison with other phenomenological models, such as the SP [SPJ66], EK [EK63] and IS [ZM80] models, as well as the numerical simulations [CFT15a, STJ+14, VCW14, Str16]. On one hand, the traditional phenomenological expressions for the IPD are generally restricted in a certain plasma regime, as verified by different experimental observations [NMG+98, HAJ+13a, CVC+12, Ct16, KCK+16]. On the other hand, detailed structures, for example, the spatial distribution of the ions in matters, can not be considered in these approaches. Additionally, the numerical simulations are time consuming, although the numerical simulations are nowadays extremely popular and have excellent ability for studying the detailed structures and properties of materials. Therefore, such kind of approaches are inconvenient and even awkward for simulation codes such as FLYCHK [CCM+05] which model plasmas under extreme conditions. Distinctly good agree-

ments are seen with various experimental measurements for Al plasma and for CH mixture. In particular, for mixtures of different ions with large mass and charge asymmetry, the experimental results can not be explained by any phenomenological models [KCK$^+$16], since those models could not include the influence of different ions at the same level. Our model has the ability to take into account this feature through the structure factor under the assumption of linear mixing rule, and provides a reasonable and good explanation for the experimental observations. As proposed, it would be of interest to perform experiments with pure substances like C. Compared to the large IPD seen in CH experiments, a lower IPD is expected for a pure C plasma.

Our approach is based on a Born approximation for the interaction of the two-particle system with the plasma ions, which can be improved in different ways. Firstly, the MW approximation for the self-energy is employed. This can be replaced by a more advanced treatment, i.e., the GWΓ-approximation [KKER86, SL13]. Secondly, the Born approximation has to be completed accounting for multiple interaction. Taking into account the strong collisions and multi-particle interaction, the so-called T-matrix approximation [KKER86, Röp13] can be performed. Thirdly, more details of the ionic subsystem may be incorporated, in particular, the relaxation of the ionic subsystem and collective excitations (plasmons, phonons) can be treated. Our model in terms of the ionic static structure factor could be improved by systematically removing again some of the approximations for the dynamical SF [VDTG12, WSGR17]. In particular, the plasmon pole approximation in handling the dynamical SF is a model assumption which can be improved, e.g., by numerical simulations. Finally, an advantage of our quantum statistical approach is that any degeneracy effect can be taken into account in a systematic way, which becomes of interest at increasing densities.

A more serious problem is the use of the quasiparticle approximation. Within a sophisticated Green function approach, the quasiparticle propagators are replaced by spectral functions, see, e.g., Refs. [KKER86, For09], which describe also the finite life time of the quasiparticle excitations. This leads to the fact that the energy gaps between the optical lines describing bound-state transitions are washed out [NMG$^+$98, OWR11]. According to our knowledge, there exists no unified quantum mechanical theory for this phenomenon. We have shown that both effects, IPD and ITE, have to be considered to explain the disappearance of spectral lines. The synthetic spectra and the transition energies are systematically described using a consistent quantum statistical approach within the simplest RPA. The Debye results for both IPD and optical transitions are obtained. Of course, the Debye model is very simple and the ionic contributions are strongly underestimated. In order to better understand and describe such spectra from plasmas observed in nature and laboratory systems, a consistent and systematic quantum statistical theory is indispensable.

APPENDIX

A. DYNAMICAL STRUCTURE FACTOR AND RESPONSE FUNCTION

The response function γ_r is the real part of the Laplace transform of the density-density correlation function. With the eigenstates $|\phi_n\rangle$ of the bath, $(\hat{H}_{\mathrm{B}} - \sum_c \mu_c \hat{N}_c)|\phi_n\rangle = B_n|\phi_n\rangle$, the spectral density of the density-density correlation function follows as [Röp13, LGRR16]

$$I(\mathbf{q}, \omega) = \frac{1}{e_e^2} \sum_{n,m} \frac{e^{-\beta B_n}}{\sum_{n'} e^{-\beta B_{n'}}} \langle\phi_n|\hat{\varrho}_{-\mathbf{q},\mathrm{B}}|\phi_m\rangle\langle\phi_m|\hat{\varrho}_{\mathbf{q},\mathrm{B}}|\phi_n\rangle 2\pi\,\delta(\omega - B_n/\hbar + B_m/\hbar). \quad \text{(A.1)}$$

The spectral density is the Fourier transform of the density autocorrelation function,

$$\langle\hat{\varrho}_{-\mathbf{q},\mathrm{B}}(\tau)\hat{\varrho}_{\mathbf{q},\mathrm{B}}(0)\rangle_{\mathrm{B}} = e_e^2 \int_{-\infty}^{\infty} \frac{d\omega}{2\pi} I(\mathbf{q},\omega) e^{i\omega\tau}. \quad \text{(A.2)}$$

We find [LGRR16]

$$\Gamma_r(\mathbf{q},\omega) = \frac{e_e^2}{2\hbar^2} I(\mathbf{q},-\omega) + i\mathcal{P}\frac{e_e^2}{\hbar^2} \int_{-\infty}^{\infty} \frac{d\omega'}{2\pi} I(\mathbf{q},-\omega')\frac{1}{\omega - \omega'}, \quad \text{(A.3)}$$

where $\mathcal{P}$ denotes the principal value of the integral.

Now we can use the fluctuation-dissipation theorem

$$\gamma_r(\mathbf{q},\omega) = \frac{e_e^2}{\hbar^2} I(\mathbf{q},-\omega) \quad \text{(A.4)}$$

and have for $S_r(\mathbf{q},\omega)$, which determines the Lamb shift, the Kramers-Kronig relation

$$S_r(\mathbf{q},\omega) = \mathcal{P}\frac{e_e^2}{\hbar^2} \int_{-\infty}^{\infty} \frac{d\omega'}{2\pi} I(\mathbf{q},-\omega')\frac{1}{\omega - \omega'} = \mathcal{P}\int_{-\infty}^{\infty} \frac{d\omega'}{2\pi} 2\gamma_r(\mathbf{q},\omega')\frac{1}{\omega - \omega'}. \quad \text{(A.5)}$$

The response function can be related to the dynamical structure factor (DSF) of the bath which is defined via the Fourier transform of the correlation function of the density fluctuation [HM86]

$$S_{\mathrm{B}}(\mathbf{q},\omega) = \frac{1}{2\pi n_{\mathrm{pl}}\Omega_0 e_e^2} \int_{-\infty}^{\infty} d\tau\, \mathrm{e}^{i\omega\tau} \langle\delta\hat{\varrho}_{\mathbf{q},\mathrm{B}}(\tau)\delta\hat{\varrho}_{-\mathbf{q},\mathrm{B}}(0)\rangle_B, \quad \text{(A.6)}$$

where n_{pl} is the electron density in plasma and $\delta\hat{\varrho}_{\mathbf{q},\mathrm{B}}(\tau) = \hat{\varrho}_{\mathbf{q},\mathrm{B}}(\tau) - \langle\hat{\varrho}_{\mathbf{q},\mathrm{B}}(\tau)\rangle_B$ is the density fluctuation of the electrons. Because of the plasma environment in equilibrium, the condition $\langle\hat{\varrho}_{\mathbf{q},\mathrm{B}}(\tau)\rangle_B = e_e n_{pl}\delta_{\mathbf{q},0}$ holds for all times. Then the DSF can be rewritten as

$$\begin{aligned}
S_{\mathrm{B}}(\mathbf{q},\omega) &= \frac{1}{2\pi n_{\mathrm{pl}}\Omega_0 e_e^2} \int_{-\infty}^{\infty} d\tau\, \mathrm{e}^{i\omega\tau} \langle\delta\hat{\varrho}_{\mathbf{q},\mathrm{B}}(\tau)\delta\hat{\varrho}_{-\mathbf{q},\mathrm{B}}(0)\rangle_B \\
&= \frac{1}{2\pi n_{\mathrm{pl}}\Omega_0} I(-\mathbf{q},\omega) + \frac{n_{pl}}{2\pi\Omega_0}\delta(\omega)\delta(\mathbf{q}).
\end{aligned} \quad \text{(A.7)}$$

The last term in the above expression contributes only at $\omega = 0$ and $\mathbf{q} = 0$. For dynamical processes this contribution can be neglected.

It can be seen that the functions $\gamma_r(\mathbf{q}, \omega)$, $S_r(\mathbf{q}, \omega)$, $I(\mathbf{q}, \omega)$ and $S_\mathrm{B}(\mathbf{q}, \omega)$ are all related to the density-density correlation function and connected to each other, which means that we need only one of them to construct the correlation function of the plasma environment. In this work we use the DSF $S_\mathrm{B}(\mathbf{q}, \omega)$ which is directly related to the inverse dielectric function $\epsilon^{-1}(\mathbf{q}, \omega)$ in plasma physics by employing the well-known fluctuation-dissipation theorem [KSKB05]:

$$S_\mathrm{B}(\mathbf{q}, \omega) = \frac{\hbar}{\pi n_\mathrm{pl}} \frac{1}{\mathrm{e}^{\hbar\omega/k_B T} - 1} \frac{\epsilon_0 q^2}{e_e^2} \mathrm{Im}\left\{ \lim_{\varepsilon \to 0^+} \epsilon^{-1}(\mathbf{q}, \omega + i\varepsilon) \right\}. \tag{A.8}$$

The dielectric function can be treated by perturbation theory or numerical simulations as a quantum many-body problem. An analytical approach calculating the dielectric function in context of the linear response theory and the random phase approximation can be found, e.g., in Refs. [KSKB05, Röp13].

B. AUTOCORRELATION FUNCTIONS AND LINE SHAPE FUNCTION

In general, the line shape function is given by the Fourier transform of the dipole-dipole correlation function [Gün95, Fuj05]

$$L(\omega) = \frac{1}{\pi} \text{Re} \left\{ \int_0^\infty \Phi(\tau) \exp\left[-i\left(\omega - \omega_0\right)\tau\right] d\tau \right\}, \tag{B.1}$$

where ω and ω_0 are the transition frequency in plasma and in the isolated system, respectively. The dipole autocorrelation function $\Phi(\tau)$ reads

$$\Phi(\tau) = \text{Tr} \left\{ \mathbf{d} U^\dagger(\tau, 0) \, \mathbf{d} U(\tau, 0) \, \rho \right\}, \tag{B.2}$$

where $\mathbf{d}$ is the dipole operator, $U(\tau, 0)$ the time evolution operator, and ρ is the statistical operator of the radiator.

The canonical current density is generally defined as [Rei05, Röp13]

$$\mathbf{j_k} = \sum_c \mathbf{j}_\mathbf{k}^c = \frac{1}{\Omega_0} \sum_{c,\mathbf{p}} \frac{e_c}{m_c} \hbar \mathbf{p} \, n_{\mathbf{p},\mathbf{k}}^c, \tag{B.3}$$

where the index c denotes the particle species, and $n_{\mathbf{p},\mathbf{k}}^c = a_{\mathbf{p}-\mathbf{k},c}^\dagger a_{\mathbf{p}+\mathbf{k},c}$ is the particle number density. It can be seen that the current-current correlation function can be expressed by the density-density correlation function

$$\langle \mathbf{j}_\mathbf{k}^c; \mathbf{j}_\mathbf{k}^{c'} \rangle_\text{z} = \left(\frac{\hbar}{\Omega_0} \right)^2 \sum_{c,c'} \sum_{\mathbf{p},\mathbf{p}'} \frac{e_c e_{c'}}{m_c m_{c'}} \mathbf{p} \cdot \mathbf{p}' \langle n_{\mathbf{p},\mathbf{k}}^c; n_{\mathbf{p},\mathbf{k}}^{c'} \rangle_\text{z}. \tag{B.4}$$

For optical transitions involving only one bound electron, this expression can be rewritten in a form via the matrix elements

$$\langle \mathbf{j}_{\mu\nu}; \mathbf{j}_{\mu\nu} \rangle_\text{z} = \sum_{\mathbf{p},\mathbf{p}'} \left(\frac{\hbar e}{m_e \Omega_0} \right)^2 \mathbf{p}_{\mu\nu} \cdot \mathbf{p}'_{\mu\nu} \langle n_\mathbf{p}; n_{\mathbf{p}'} \rangle_\text{z}. \tag{B.5}$$

Additionally, the dipole-dipole correlation function can be also reformulated via the density-denisity correlation function

$$\langle \mathbf{d}_{\mu\nu}; \mathbf{d}_{\mu\nu} \rangle_\text{z} = \langle \sum_\mathbf{p} \frac{i\hbar e}{m_e \omega_{\mu\nu} \Omega_0} \mathbf{p}_{\mu\nu} n_\mathbf{p}; \sum_{\mathbf{p}'} \frac{i\hbar e}{m_e \omega_{\mu\nu} \Omega_0} \mathbf{p}'_{\mu\nu} n_{\mathbf{p}'} \rangle_\text{z}$$

$$= -\sum_{\mathbf{p},\mathbf{p}'} \left(\frac{\hbar e}{m_e \omega_{\mu\nu} \Omega_0} \right)^2 \mathbf{p}_{\mu\nu} \cdot \mathbf{p}'_{\mu\nu} \langle n_\mathbf{p}; n_{\mathbf{p}'} \rangle_\text{z}. \tag{B.6}$$

To derive this expression, the relation $\langle\phi_\mu|\hat{\mathbf{r}}|\phi_\nu\rangle = -i\hbar\langle\phi_\mu|\hat{\mathbf{p}}|\phi_\nu\rangle/\left(m_e\omega_{\mu\nu}\right)$ is utilized. Comparing the formula (B.6) with the expression (B.5), we found [Lor14]

$$\langle\,\mathbf{d}_{\mu\nu};\mathbf{d}_{\mu\nu}\,\rangle_{\mathrm{z}} = -\frac{1}{\omega_{\mu\nu}^2}\langle\,\mathbf{j}_{\mu\nu};\mathbf{j}_{\mu\nu}\,\rangle_{\mathrm{z}}. \tag{B.7}$$

Within the framework of the Green's function technique, the line shape function is determined by the polarization function, which can be calculated from equilibrium correlation functions. The longitudinal polarization function is related to the irreducible current-current correlation function via the formula [Rei05, Lor14]

$$\Pi^{\mathrm{long}}(\mathbf{k},\omega) = -i\frac{k^2\beta\Omega_0}{\omega}\langle\,j_{\mathbf{k}}^{\mathrm{long}};\,j_{\mathbf{k}}^{\mathrm{long}}\,\rangle_{\omega+\mathrm{i}\delta}^{\mathrm{irred}} \tag{B.8}$$

with the longitudinal component of the above defined canonical current density $\mathbf{j_k}$.

C. RELATION TO THE UNIFIED THEORY OF SPECTRAL LINE SHAPES

We investigate in this appendix the relationship between the spectral line profile and the response function which relates to the retarted two-time Green's function [ZMR96, ZMR97].

In plasma, if the interacting transition frequency of the reduced atomic system $\omega_{nn'}$ is larger than the plasma frequency $\omega_{\mathrm{pl}} = (\frac{ne^2}{\epsilon_0 m_e})^{1/2}$, the imaginary part of the inverse dielectric function can be approximated as

$$\mathrm{Im}\left\{\epsilon_{\mathrm{long}}^{-1}(\mathbf{k},\omega)\right\} \approx -\mathrm{Im}\left\{\epsilon_{\mathrm{long}}(\mathbf{k},\omega)\right\}. \tag{C.1}$$

In this case follows the relation discussed in the appendix A

$$
\begin{aligned}
\mathcal{L}(\triangle\,\omega) \quad &= \mathrm{Im}\,\varepsilon_{\mathrm{long}}(\mathbf{q},\omega) = \hbar(1 - e^{\hbar\omega/k_B T})\frac{e^2}{\Omega_0\epsilon_0 k^2}\gamma_r(\mathbf{k},\omega) \\
&= (1 - e^{\hbar\omega/k_B T})\frac{2\hbar e^2}{\Omega_0\epsilon_0 k^2}\cdot\mathrm{Re}\left\{\frac{1}{\hbar^2}\int_0^\infty d\tau e^{-\varepsilon\tau}e^{i\omega\tau}\langle\hat{\varrho}_{-\mathbf{k},\mathrm{B}}(\tau)\hat{\varrho}_{\mathbf{k},\mathrm{B}}(0)\rangle_{\mathrm{B}}\right\}. \tag{C.2}
\end{aligned}
$$

We must keep in mind that the above expression implies that it is not a single atom but the plasma as a whole emitting or absorbing radiation. In the present work, we consider a radiating system which consists of a single radiator immersed in a plasma environment. In this case the spectral line shape is related to the Laplace tranform of the dipole correlation function of the atomic emmitter A,

$$\mathcal{L}(\triangle\,\omega) = (1 - e^{\hbar\omega/k_B T})\frac{2\hbar e^2}{\Omega_0\epsilon_0 k^2}\cdot\mathrm{Re}\left\{\frac{1}{\hbar^2}\int_0^\infty d\tau e^{-\varepsilon\tau}e^{i\omega\tau}\langle\hat{\varrho}_{\mathbf{k},\mathrm{A}}^{\mathrm{H}}(\tau)\hat{\varrho}_{-\mathbf{k},\mathrm{A}}^{\mathrm{H}}(0)\rangle\right\}, \tag{C.3}$$

where the trace is performed over both the atomic system and the bath variables. The index H denotes the Heisenberg picture.

In oder to give the Doppler broadening in the case that no density effects are taken into account by neglecting the surrounding plasma we identify the emitting atom

$$\langle\hat{\varrho}_{\mathbf{k},\mathrm{A}}(\tau)\hat{\varrho}_{-\mathbf{k},\mathrm{A}}(0)\rangle_{\mathrm{A}}. \tag{C.4}$$

In zeroth order with respect to the interaction, we simply have after introducing the atomic eigenstates

$$
\begin{aligned}
\mathcal{L}(\triangle\,\omega) &= \frac{e^2(1 - e^{\hbar\omega/k_B T})}{\hbar\Omega_0\epsilon_0 k^2}\mathrm{Re}\left\{\sum_{nn'\mathbf{P}} Z^{-1}e^{-\beta E_{n,\mathbf{P}}}\int_0^\infty d\tau e^{-\varepsilon\tau}e^{i\omega\tau - i\omega_{n'n}\tau}|\langle\psi_{n,\mathbf{P}}|\hat{\varrho}_{\mathbf{k},\mathrm{A}}^0|\psi_{n',\mathbf{P}+k}\rangle|^2\right\} \\
&= \lim_{\delta\to 0}\frac{e^2(1 - e^{\hbar\omega/k_B T})}{\hbar\Omega_0\epsilon_0 k^2}\mathrm{Re}\left\{\sum_{nn'\mathbf{P}} Z_{\mathrm{A}}^{-1}e^{-\beta E_{n,\mathbf{P}}}|\langle\psi_{n,\mathbf{P}}|\hat{\varrho}_{\mathbf{k},\mathrm{A}}^0|\psi_{n',\mathbf{P}+k}\rangle|^2\frac{i}{L_{nn'P}^{(0)}(\mathbf{k},\omega + i\delta)}\right\},
\end{aligned}
\tag{C.5}
$$

with

$$L_{nn'P}^{(0)}(\mathbf{k}, \omega + i\delta) \qquad = \hbar(\omega + i\delta) - \hbar\omega_{nn'} - \frac{\hbar^2\mathbf{k}^2 + 2\hbar^2\mathbf{P}\cdot\mathbf{k}}{2M}. \qquad (C.6)$$

This gives already the Doppler broadening. $\langle\psi_{n,\mathbf{P}}|\hat{\varrho}_{\mathbf{k},A}^0|\psi_{n',\mathbf{P}+k}\rangle$ denotes matrix elements of the charge density operator $\hat{\varrho}_{\mathbf{k},A}^0$.

To investigate the pressure broadening, we introduce the interaction picture where the operators depend on time only via $\hat{H}_0 = \hat{H}_A + \hat{H}_B$ so that

$$\hat{O}^{\mathrm{H}}(t) = e^{(i/\hbar)(\hat{H}_0 + \hat{H}_{\mathrm{int}})t}e^{-(i/\hbar)\hat{H}_0 t}\hat{O}^{\mathrm{I}}(t)e^{(i/\hbar)\hat{H}_0 t}e^{-(i/\hbar)(\hat{H}_0 + \hat{H}_{\mathrm{int}})t}. \qquad (C.7)$$

We apply the Baker-Campbell-Hausdorff-formula for the exponential function for two non-commutating operators $\hat{A}$ and $\hat{B}$ [ZMR96, ZMR97, Röp13]

$$e^{-\hat{A}}e^{\hat{A}+\hat{B}} = 1 + \int_0^1 dx e^{-x\hat{A}}\hat{B}e^{x(\hat{A}+\hat{B})}$$
$$\approx 1 + \int_0^1 dx e^{-x\hat{A}}\hat{B}e^{x\hat{A}}[1 + \int_0^x d\lambda e^{-\lambda\hat{A}}\hat{B}e^{\lambda\hat{A}}]; \qquad (C.8)$$
$$e^{\hat{A}+\hat{B}}e^{-\hat{A}} = 1 + \int_0^1 dx e^{x(\hat{A}+\hat{B})}\hat{B}e^{-x\hat{A}}$$
$$\approx 1 + \int_0^1 dx[1 + \int_0^x d\lambda e^{\lambda\hat{A}}\hat{B}e^{-\lambda\hat{A}}]e^{x\hat{A}}\hat{B}e^{-x\hat{A}}. \qquad (C.9)$$

With these expressions the time dependence of the operator $\hat{\varrho}_{\mathbf{k},A}(t)$ in Heisenberg picture with $\hat{A} = i\hat{H}_0 t/\hbar = i(\hat{H}_A + \hat{H}_B)t/\hbar$ and $\hat{B} = i\hat{H}_{\mathrm{int}}t/\hbar$ is calculated up to the second-order terms in $\hat{H}_{int}$

$$\hat{\varrho}_{\mathbf{k},A}^{\mathrm{H}}(t) \quad = \left(1 + \frac{i}{\hbar}\int_0^t dt_1\hat{H}_{\mathrm{int}}^{\mathrm{I}}(t_1) - \frac{1}{\hbar^2}\int_0^t dt_1\int_0^{t_1} dt_2\hat{H}_{\mathrm{int}}^{\mathrm{I}}(t_2)\hat{H}_{\mathrm{int}}^{\mathrm{I}}(t_1)\right)\hat{\varrho}_{\mathbf{k},A}^{\mathrm{I}}(t)$$
$$\times\left(1 - \frac{i}{\hbar}\int_0^t dt_1\hat{H}_{\mathrm{int}}^{\mathrm{I}}(t_1) - \frac{1}{\hbar^2}\int_0^t dt_1\int_0^{t_1} dt_2\hat{H}_{\mathrm{int}}^{\mathrm{I}}(t_1)\hat{H}_{\mathrm{int}}^{\mathrm{I}}(t_2)\right) \quad (C.10)$$

where we have neglected the higher order terms in $\hat{H}_{\mathrm{int}}$. The first-order terms vanish because of the commutation $[\hat{H}_{\mathrm{int}}^{\mathrm{I}}(t_1), \hat{\varrho}_{\mathbf{k},A}^{\mathrm{I}}(t)] = 0$.

In the zeroth order the above expression yields the natural line profile:

$$\int_0^\infty d\tau e^{-\epsilon\tau}e^{i\omega\tau}\langle\hat{\varrho}_{\mathbf{k},A}^{\mathrm{H}}(\tau)\hat{\varrho}_{-\mathbf{k},A}^{\mathrm{H}}(0)\rangle \quad = \sum_{i,j}\frac{e^{-\beta E_i}}{Z_A}|\langle\psi_i|\hat{\varrho}_{\mathbf{k},A}^0|\psi_j\rangle|^2\int_0^\infty d\tau e^{(i\omega+i\omega_{ij}-\epsilon)\tau}$$
$$= \sum_{i,j}\frac{e^{-\beta E_i}}{Z_A}|\langle\psi_i|\hat{\varrho}_{\mathbf{k},A}^0|\psi_j\rangle|^2\frac{i}{\omega + \omega_{ij} + i\epsilon}. \qquad (C.11)$$

Going up to second order with respect to the interaction we have to perform the trace of the correlation function also over the bath variables. We have three contributions to the

Laplace transform (C.3) in the second order:

$$\mathcal{L}^{(2)}(\Delta\omega) \quad \propto \mathrm{Re}\frac{1}{\hbar^4}\int_0^\infty d\tau e^{-\varepsilon\tau}e^{i\omega\tau}\left\{\int_0^\tau dt_1\int_0^{t_1}dt_2\langle\hat{H}_{\mathrm{int}}^{\mathrm{I}}(t_2)\hat{H}_{\mathrm{int}}^{\mathrm{I}}(t_1)\hat{\varrho}_{-\mathbf{k},\mathrm{A}}^{\mathrm{I}}(\tau)\hat{\varrho}_{\mathbf{k},\mathrm{A}}\rangle\right.$$

$$+\int_0^\tau dt_1\int_0^{t_1}dt_2\langle\hat{\varrho}_{-\mathbf{k},\mathrm{A}}^{\mathrm{I}}(\tau)\hat{H}_{\mathrm{int}}^{\mathrm{I}}(t_1)\hat{H}_{\mathrm{int}}^{\mathrm{I}}(t_2)\hat{\varrho}_{\mathbf{k},\mathrm{A}}\rangle \tag{C.12}$$

$$\left.-\int_0^\tau dt_1\int_0^\tau dt_2\langle\hat{H}_{\mathrm{int}}^{\mathrm{I}}(t_1)\hat{\varrho}_{-\mathbf{k},\mathrm{A}}^{\mathrm{I}}(\tau)\hat{H}_{\mathrm{int}}^{\mathrm{I}}(t_2)\hat{\varrho}_{\mathbf{k},\mathrm{A}}\rangle\right\}\ .$$

To perform the integration over time we introduce the atomic eigenstates $|i\rangle$, the Hilbert space of the bath variables is separated and the trace $\langle\ldots\rangle_\mathrm{B}$ is performed independently. The matrix elements of the following operators in the atomic Hilbert subspace arise

$$\hat{\mathcal{L}}^{(2,1)} = -\frac{1}{\hbar^4}\int_0^\infty d\tau e^{-\varepsilon\tau}e^{i\omega\tau}\sum_{\mathbf{k}_1\mathbf{k}_2}\int_0^\tau dt_1\int_0^{t_1}dt_2\frac{1}{\epsilon_0^2\mathbf{k}_1^2\mathbf{k}_2^2} \tag{C.13}$$

$$\times\hat{\varrho}_{\mathbf{k}_1,\mathrm{A}}^{\mathrm{I}}(t_2)\hat{\varrho}_{\mathbf{k}_2,\mathrm{A}}^{\mathrm{I}}(t_1)\hat{\varrho}_{\mathbf{k},\mathrm{A}}^{\mathrm{I}}(\tau)\hat{\varrho}_{-\mathbf{k},\mathrm{A}}^{\mathrm{I}}\langle\hat{\varrho}_{-\mathbf{k}_1,\mathrm{B}}^{\mathrm{I}}(t_2)\hat{\varrho}_{-\mathbf{k}_2,\mathrm{B}}^{\mathrm{I}}(t_1)\rangle_\mathrm{B},$$

$$\hat{\mathcal{L}}^{(2,2)} = -\frac{1}{\hbar^4}\int_0^\infty d\tau e^{-\varepsilon\tau}e^{i\omega\tau}\sum_{\mathbf{k}_1\mathbf{k}_2}\int_0^\tau dt_1\int_0^{t_1}dt_2\frac{1}{\epsilon_0^2\mathbf{k}_1^2\mathbf{k}_2^2} \tag{C.14}$$

$$\times\hat{\varrho}_{\mathbf{k},\mathrm{A}}^{\mathrm{I}}(\tau)\hat{\varrho}_{\mathbf{k}_1,\mathrm{A}}^{\mathrm{I}}(t_1)\hat{\varrho}_{\mathbf{k}_2,\mathrm{A}}^{\mathrm{I}}(t_2)\hat{\varrho}_{-\mathbf{k},\mathrm{A}}^{\mathrm{I}}\langle\hat{\varrho}_{-\mathbf{k}_1,\mathrm{B}}^{\mathrm{I}}(t_1)\hat{\varrho}_{-\mathbf{k}_2,\mathrm{B}}^{\mathrm{I}}(t_2)\rangle_\mathrm{B},$$

$$\hat{\mathcal{L}}^{(2,3)} = \frac{1}{\hbar^4}\int_0^\infty d\tau e^{-\varepsilon\tau}e^{i\omega\tau}\sum_{\mathbf{k}_1\mathbf{k}_2}\int_0^\tau dt_1\int_0^\tau dt_2\frac{1}{\epsilon_0^2\mathbf{k}_1^2\mathbf{k}_2^2} \tag{C.15}$$

$$\times\hat{\varrho}_{\mathbf{k}_1,\mathrm{A}}^{\mathrm{I}}(t_1)\hat{\varrho}_{\mathbf{k},\mathrm{A}}^{\mathrm{I}}(\tau)\hat{\varrho}_{\mathbf{k}_2,\mathrm{A}}^{\mathrm{I}}(t_2)\hat{\varrho}_{-\mathbf{k},\mathrm{A}}^{\mathrm{I}}\langle\hat{\varrho}_{-\mathbf{k}_1,\mathrm{B}}^{\mathrm{I}}(t_1)\hat{\varrho}_{-\mathbf{k}_2,\mathrm{B}}^{\mathrm{I}}(t_2)\rangle_\mathrm{B}.$$

The trace over the atomic system has the form $Z_\mathrm{A}^{-1}\sum_i e^{-\beta E_i}\mathcal{L}_{i,i}$ with $\mathcal{L}_{i,j} = \langle i|\hat{\mathcal{L}}|j\rangle$. with the matrix elements (atomic form factors) $F_{ij}(\mathbf{k})e^{i\omega_{ij}t} = \langle i|\hat{\varrho}_{\mathbf{k},\mathrm{A}}^{\mathrm{I}}(t)|j\rangle$ after writing the time dependence in the interaction picture using the eigenstates of the atomic system $|i\rangle$ we have

$$\mathcal{L}_{i,i}^{(2,1)} = -\frac{1}{\hbar^4}\sum_{\mathbf{k}_1}\frac{1}{\epsilon_0^2\mathbf{k}_1^4}\sum_{jmn}\int_0^\infty d\tau e^{-\varepsilon\tau}e^{i\omega\tau}\int_0^\tau dt_1\int_0^{t_1}dt_2$$

$$\times F_{ij}(\mathbf{k}_1)e^{i\omega_{ij}t_2}F_{jm}(-\mathbf{k}_1)e^{i\omega_{jm}t_1}F_{mn}(\mathbf{k})e^{i\omega_{mn}\tau}F_{ni}(-\mathbf{k})\langle\hat{\varrho}_{-\mathbf{k}_1,\mathrm{B}}^{\mathrm{I}}(-\tau_1)\hat{\varrho}_{\mathbf{k}_1,\mathrm{B}}\rangle_\mathrm{B}, \tag{C.16}$$

where we used $\mathbf{k}_1 = -\mathbf{k}_2$ because of the homogeneity of the bath and $t_1 - t_2 = \tau_1$ because of the equilibrium of the bath. In this work we only show the derivation for $\mathcal{L}_{i,i}^{(2,1)}$. Similar treatments can be performed for $\mathcal{L}_{i,i}^{(2,2)}$ and $\mathcal{L}_{i,i}^{(2,3)}$.

Now we can perform the integrals over the time variables. After integration by parts, we have for $\mathcal{L}_{i,i}^{(2,1)}$ with $t_2 = t_1 - \tau_1$

$$\int_0^\infty d\tau e^{-\varepsilon\tau}e^{i\omega\tau}\int_0^\tau dt_1\int_0^{t_1}dt_2 e^{i\omega_{ij}t_2}e^{i\omega_{jm}t_1}e^{i\omega_{mn}\tau}\langle\hat{\varrho}_{-\mathbf{k}_1,\mathrm{B}}^{\mathrm{I}}(-\tau_1)\hat{\varrho}_{\mathbf{k}_1,\mathrm{B}}\rangle_\mathrm{B}$$

$$= \int_0^\infty d\tau e^{-\varepsilon\tau}e^{i(\omega+\omega_{mn})\tau}\int_0^\tau dt_1 e^{i\omega_{im}t_1}\int_0^{t_1}d\tau_1 e^{-i\omega_{ij}\tau_1}\langle\hat{\varrho}_{-\mathbf{k}_1,\mathrm{B}}^{\mathrm{I}}(-\tau_1)\hat{\varrho}_{\mathbf{k}_1,\mathrm{B}}\rangle_\mathrm{B}$$

$$= \frac{1}{\omega+\omega_{mn}+i\varepsilon}\frac{1}{\omega+\omega_{in}+i\varepsilon}\int_0^\infty d\tau e^{-\varepsilon\tau}e^{i(\omega+\omega_{jn})\tau}\langle\hat{\varrho}_{-\mathbf{k}_1,\mathrm{B}}^{\mathrm{I}}(-\tau)\hat{\varrho}_{\mathbf{k}_1,\mathrm{B}}\rangle_\mathrm{B}\ . \tag{C.17}$$

This expression can be further simplified using the RWA by setting $m = i$ for $\mathcal{L}_{i,i}^{(2,1)}$. Using the definition of Gamma function $\Gamma_r(\mathbf{k}, \omega)$ we obtain

$$\mathcal{L}_{i,i}^{(2,1)} = -\frac{1}{\hbar^2} \sum_{\mathbf{k}_1} \frac{1}{\epsilon_0^2 \mathbf{k}_1^4} \sum_{jn} \frac{|F_{ij}(\mathbf{k}_1)|^2 |F_{in}(\mathbf{k})|^2}{(\omega + \omega_{in} + i\varepsilon)^2} \Gamma_r^*(\mathbf{k}_1, \omega_{nj} - \omega). \tag{C.18}$$

Similarly for $\mathcal{L}^{(2,2)}$ and $\mathcal{L}^{(2,3)}$ we find

$$\mathcal{L}_{i,i}^{(2,2)} = -\frac{1}{\hbar^2} \sum_{\mathbf{k}_1} \frac{1}{\epsilon_0^2 \mathbf{k}_1^4} \sum_{mn} \frac{|F_{nm}(\mathbf{k}_1)|^2 |F_{in}(\mathbf{k})|^2}{(\omega + \omega_{in} + i\varepsilon)^2} \Gamma_r(\mathbf{k}_1, \omega_{im} + \omega), \tag{C.19}$$

$$\mathcal{L}_{i,i}^{(2,3)} = \frac{1}{\hbar^2} \sum_{\mathbf{k}_1} \frac{1}{\epsilon_0^2 \mathbf{k}_1^4} \sum_{n} \frac{F_{ii}(\mathbf{k}_1) F_{nn}(-\mathbf{k}_1) |F_{in}(\mathbf{k})|^2}{(\omega + \omega_{in} + i\varepsilon)^2} \Big(\Gamma_r(\mathbf{k}_1, \omega_{in} + \omega) + \Gamma_r^*(\mathbf{k}_1, \omega_{ni} - \omega) \Big).$$

Then we have the spectral line profile

$$\mathcal{L}^{(2)}(\triangle \omega) = \frac{2e^2(1 - e^{\hbar\omega/k_B T})}{\hbar \Omega_0 \epsilon_0 k^2} \sum_{i,n} \frac{e^{-\beta E_i}}{Z_A} \frac{i|F_{in}(\mathbf{k})|^2}{\omega + \omega_{in} + i\varepsilon} \cdot \frac{1}{\omega + \omega_{in} + i\epsilon + i\Gamma_{in}^{\mathrm{BS}} - i\Gamma_{in}^{\nu}} \tag{C.20}$$

with the vertex correction coefficient Γ_{ij}^{ν} and the broadening and energy-shift coefficient $\Gamma_{in}^{\mathrm{BS}}$

$$\Gamma_{in}^{\nu} = \frac{1}{\hbar^2} \sum_{\mathbf{k}_1} \frac{1}{\epsilon_0^2 \mathbf{k}_1^4} F_{ii}(\mathbf{k}_1) F_{nn}(-\mathbf{k}_1) \Big(\Gamma_r(\mathbf{k}_1, \omega_{in} + \omega) + \Gamma_r^*(\mathbf{k}_1, \omega_{ni} - \omega) \Big), \tag{C.21}$$

$$\Gamma_{in}^{\mathrm{BS}} = \frac{1}{\hbar^2} \sum_{\mathbf{k}_1} \frac{1}{\epsilon_0^2 \mathbf{k}_1^4} \sum_{j} \Big(|F_{ij}(\mathbf{k}_1)|^2 \Gamma_r^*(\mathbf{k}_1, \omega_{nj} - \omega) + |F_{nj}(\mathbf{k}_1)|^2 \Gamma_r(\mathbf{k}_1, \omega_{ij} + \omega) \Big), \tag{C.22}$$

where the trick $1 + x = \frac{1}{1-x}$ is used for the derivation of $\mathcal{L}^{(2)}(\triangle \omega)$.

D. PARABOLIC COORDINATES AND STARK EFFECTS

The solution of the problem of motion in a centrally symmetric field in terms of spherical coordinates (r, θ, ϕ) is generally useful. This is already shown in investigating the properties of hydrogen atoms, where the bound electron moves in a spherically symmetric Coulomb field. Another possibility to such symmetric Coulomb field is to separate the variables in terms of parabolic coordinates (ξ, η, ϕ), which is defined with respect to the Cartesian coordinate system (x, y, z) via [Sch68, LL85]

$$\xi = r + z, \quad \eta = r - z, \quad \phi = \tan^{-1}(y/x) \qquad \text{with} \quad r = \sqrt{x^2 + y^2 + z^2}, \qquad (D.1)$$

where ξ and η takes values from 0 to ∞ and ϕ from 0 to 2π. For hydrogen atoms, solving the Schrödinger equation

$$-i\hbar \frac{\partial}{\partial t} \psi(r, t) = H_0 \psi(r, t) = E\psi(r, t) \quad H_0 = -\frac{\hbar^2}{2\mu} \nabla_r^2 - \frac{e^2}{4\pi\varepsilon_0\, r} \qquad (D.2)$$

in parabolic coordinates, the following normalized wave functions are obtained

$$\psi_{n_1 n_2 m}(\xi, \eta, \phi) = \frac{\sqrt{2}}{n^2} f_{n_1 m}(\xi/(na_0)) \, f_{n_2 m}(\eta/(na_0)) \, \frac{e^{im\phi}}{\sqrt{2\pi}} \qquad (D.3)$$

with

$$f_{pm}(\rho) = \frac{1}{m!} \sqrt{\frac{(p + |m|)!}{p!}} \, F(-p, |m| + 1, \rho) \, e^{-\rho/2} \, \rho^{|m|/2}, \qquad (D.4)$$

where $F(-p, |m| + 1, \rho)$ is the confluent hypergeometric function, n_1 and n_2 the parabolic quantum numbers and m the magnetic quantum number. They connect to the principle quantum number via

$$n = n_1 + n_2 + |m| + 1. \qquad (D.5)$$

Obviously, the possible values of the quantum number $|m|$ for a given n run from 0 to $n - 1$. For fixed n and $|m|$, n_1 takes values from 0 to $n - |m| - 1$. Introducing the following notations

$$\mu_1 = (m + n_1 - n_2)/2, \quad \mu_2 = (m - n_1 + n_2)/2, \qquad (D.6)$$

the wave functions in the parabolic coordinates for the state $|n_1 n_2 m\rangle$, or equivalently $|n\mu_1\mu_2\rangle$, can be transformed to those in the spherical coordinates which is represented in terms of the quantum numbers $|nlm\rangle$ [LL85]

$$\psi_{nlm} = \sum_{\mu_1 + \mu_2} \langle lm|\mu_1\mu_2\rangle \, \psi_{n\mu_1\mu_2} \qquad (D.7)$$

or conversely

$$\psi_{n\mu_1\mu_2} = \sum_{l=0}^{n-1} \langle l, \mu_1 + \mu_2 | \mu_1 \mu_2 \rangle \, \psi_{nlm} \tag{D.8}$$

with the overlapping coefficients $\langle lm | \mu_1 \mu_2 \rangle$.

In the case that an atom is placed in an external electric field $\mathcal{E}$ with the perturbation Hamiltonian

$$H' = -e\,\mathcal{E}\,z = -e\,\mathcal{E}\,r\cos\theta, \tag{D.9}$$

it is more convenient to use the parabolic coordinates, since the polarization axis is in a certain direction in space, here in the direction of positive z.

Because of the perturbation of the external electric field, the energy levels of the hydrogen atoms are altered, which is generally known as Stark effect. This modification of the energy levels is determined via the perturbation theory up to the second order. The displacement of the energy levels of the level E_n is given by the form

$$\Delta E_n = -\frac{1}{2}\alpha_{ik}^{(n)}\mathcal{E}_i\mathcal{E}_k \tag{D.10}$$

with the atomic polarizability tensor of rank two $\alpha_{ik}^{(n)}$. To understand the Stark effect, the matrix elements for transitions $n_1 n_2 m \to n_1' n_2' m'$ with in the same principle quantum number n should be studied. In this case, only the diagonal matrix elements are non-zero and given by

$$\int |\psi_{n_1 n_2 m}|^2 \, \mathcal{E}zdV = \frac{1}{8}\mathcal{E}\int_0^\infty \int_0^\infty \int_0^{2\pi} d\xi d\eta d\phi \, (\xi^2 - \eta^2), |\psi_{n_1 n_2 m}|^2. \tag{D.11}$$

Then the energy displacement for the linear Stark effect (in atomic units) can be obtained

$$\Delta E_n^{(1)} = \frac{3}{2}\mathcal{E}\,n(n_1 - n_2). \tag{D.12}$$

To calculate the quadratic effect, it is not convenient to use ordinary perturbation theory and will not be detailed here. For details, the textbooks in quantum mechanics and atomic physics [Sch68, LL85, SVY81] are recommended.

E. MULTI-ELECTRON SYSTEM AND INNER-SHELL TRANSITIONS

In discussing shift and broadening of bound electrons induced by electron scattering, we should treat the ion as a bound system consisting of N electrons each of negative charge $-e$ and mass m, and a nucleus of positive charge $+Ze$ and mass M. Within the independent-particle approximation (IPA), each bound electron is considered to move in an effective central potential representing the Coulomb interaction with the nucleus and the $(N-1)$ other electrons. In other words, an effective composite system of two interacting particles can be taken into account and the so-called *screened hydrogenic model* (SHM) [FBR08] can be applied.

The effective charge, which is seen by the radiative electron belonging to the k subshell of a given configuration $\{(n_1 l_1)^{g_1} \cdots (n_k l_k)^{g_k} \cdots (n_{k_{\max}} l_{k_{\max}})^{g_{k_{\max}}}\}$, is given by [FBR08]

$$Z_k = Z - \sum_{k'}^{k_{\max}} \sigma_{kk'} \cdot (g_{k'} - \delta_{kk'}), \tag{E.1}$$

where $\sigma_{kk'}$ and $\delta_{kk'}$ are respectively a screening coefficient and the Kronecker symbol. The coefficients $\sigma_{kk'}$, describing screening of the k subshell by the k' subshell ($k < k'$ for outer screening effect and $k > k'$ for inner screening), are constants that are independent of the ion. g_k is the integer population of the k subshell varying from 0 to $2(2l_k + 1)$ with $\sum_{k=1}^{k_{\max}} g_k = N$.

Tab. E.1: Screening constants $\sigma_{kk'}$ of the screened hydrogenic model [FBR08]

$k' \diagdown k$	$1s$	$2s$	$2p$	$3s$	$3p$	$3d$	$4s$	$4p$	$4d$	$4f$
$1s$	0.3100	0.0135	0.0003	0.0000	0.0000	0.0000	0.0000	0.0000	0.0000	0.0000
$2s$	0.7388	0.3082	0.2522	0.0000	0.0000	0.0000	0.0000	0.0000	0.0000	0.0000
$2p$	0.9461	0.3481	0.3495	0.0392	0.0210	0.0007	0.0097	0.0060	0.0000	0.0000
$3s$	0.9511	0.8511	0.6480	0.3106	0.2496	0.1676	0.0477	0.0245	0.0290	0.0000
$3p$	0.9696	0.8550	0.7916	0.3002	0.3136	0.3226	0.0513	0.0338	0.0392	0.0000
$3d$	0.9987	0.9865	0.9413	0.4847	0.3230	0.3786	0.0743	0.0781	0.0188	0.0224
$4s$	0.9340	0.7502	0.8500	0.6718	0.6068	0.6547	0.2983	0.2881	0.1889	0.1276
$4p$	0.9886	0.9068	0.8899	0.6760	0.6770	0.6543	0.2988	0.3348	0.2663	0.2574
$4d$	0.9988	0.9973	0.9891	0.9856	0.9109	0.7160	0.4474	0.3416	0.3438	0.2737
$4f$	0.9988	0.9983	0.9955	0.9891	0.9280	0.9768	0.5507	0.4388	0.4126	0.3863

Classically, all the electrons and the nucleus are regarded as point charges and their spatial distributions are described by the Dirac-delta functions. This description is not valid from the viewpoint of quantum mechanics where each of the atomic electrons is being characterized by

an extended charge distribution. The charge distribution is generally scaled by the hydrogenic wave function [Sch68, FBR08]

$$R_{nl}(Z_{nl}, r) = \left(\frac{2Z_{nl}}{n}\right)^{3/2} \sqrt{\frac{(n-l-1)!}{2n\,(n+l)!}} \left(\frac{2Z_{nl}r}{n}\right)^l \exp\left[-\frac{Z_{nl}r}{n}\right] L_{n-l-1}^{2l+1}(\frac{2Z_{nl}r}{n}) \qquad \text{(E.2)}$$

Based on the SHM, an effective two-particle description is introduced within this chemical model for the the A-particle GF. In the ladder approximation, the A-particle GF satisfies the Bethe-Salpeter equation [SRS90, RSSN98, Röp13]

$$G_A(1\cdots A; 1'\cdots A'; z_A) = G_A^0(1\cdots A; z_A) \cdot \prod_{i=1}^{A} \delta_{ii'} \qquad \text{(E.3)}$$
$$+ \sum_{1''\cdots A''} G_A^0(1\cdots A; z_A) \cdot V_A(1\cdots A; 1''\cdots A'') \cdot G_A(1''\cdots A''; 1'\cdots A'; z_A)$$

with the interaction $V_A(1\cdots A; 1'\cdots A') = \sum_{i<j} V(ij; i'j') \cdot \prod_{k\neq i,j} \delta_{kk'}$. The unperturbed A-particle GF is given by

$$G_A^0(1\cdots A; z_A) = \frac{\tilde{f}(1)\tilde{f}(2)\cdots\tilde{f}(A) - f(1)f(2)\cdots f(3)}{z_A - \varepsilon(1,\cdots,A)} = \frac{f(1)f(2)\cdots f(3) \times g_A^{-1}(1,\cdots,A)}{z_A - \varepsilon(1,\cdots,A)}$$
$$\text{(E.4)}$$

with the following shorthand notations

$$\tilde{f}(n) = 1 - f(n), \quad \varepsilon(1,\cdots,A) = \sum_{i=1}^{A} \varepsilon_i = \sum_{i=1}^{A} (E_i - \mu_i), \qquad \text{(E.5)}$$

$$g_A(1,\cdots,A) = \left\{\exp\left[\beta \cdot \varepsilon(1,\cdots,A)\right] + (-1)^{A-1}\right\}^{-1} \qquad \text{(E.6)}$$

The composite A particles can be decomposed into an Ath optical electron involved in the transition and a rest atomic core $\beta = (1,\cdots A-1)$ in the frozen orbital approximation. Then the effective two-particle GF can be expressed as

$$G_2^{\text{eff}}(1, \beta) = G_1^0(A)\,G_\beta^0 + G_1^0\,G_\beta^0\,V_A^{\text{MF}}\,G_2^{\text{eff}}(1, \beta) \qquad \text{(E.7)}$$

with the effective mean field potential V_A^{MF}.

The discussion displayed in the present section gives a possibility to calculate the K_α lines in plasmas via the GF technique. Before we consider the specific physical systems, there are still a lot of other problems that have to be solved. For example, how can we build the effective two-particle vertex function to replace the transition matrix element $M_{nn'}(\mathbf{q})$? How can we handle the relaxation of other bound electrons during the transition?

BIBLIOGRAPHY

[AB84]   Néstor R. Arista and Werner Brandt. Dielectric response of quantum plasmas in thermal equilibrium. *Phys. Rev. A*, 29:1471–1480, Mar 1984.

[Aga71]   G. S. Agarwal. Rotating-wave approximation and spontaneous emission. *Phys. Rev. A*, 4:1778–1781, Nov 1971.

[Aga73]   G. S. Agarwal. Rotating-wave approximation and spontaneous emission. *Phys. Rev. A*, 7:1195–1197, Mar 1973.

[And15]   D. A. Anderson. *Rydberg molecules and circular Rydberg states in cold atom clouds.* Dissertation, University of Michigan, 2015.

[ASSR13]   D. A. Anderson, A. Schwarzkopf, R. E. Sapiro, and G. Raithel. Production and trapping of cold circular Rydberg atoms. *Phys. Rev. A*, 88:031401, Sep 2013.

[Bau13]   D. Bauer. *Vorlesungsskript: Quantentheorie für Fortgeschrittene.* Universität Rostock, 2013.

[BDRG86]   D. Bhaumik, B. Dutta-Roy, and G. Ghosh. Classical limit of the hydrogen atom. *J. Phys. A: Math. Gen.*, 19:1355–1364, 1986.

[BHMV84]   J. Bretön, A. Hardisson, F. Mauricio, and S. Velasco. Relaxation of quantum systems weakly coupled to a bath. ii. Formal analysis of the total-time-ordering-cumulant and partial-time-ordering-cumulant spectral line shapes. *Phys. Rev. A*, 30:553–559, Jul 1984.

[BL95]   I. L. Beigman and V. S. Lebedev. Collision theory of Rydberg atoms with neutral and charged particles. *Phys. Rep.*, 250:95–328, 1995.

[BM59]   Michel Baranger and Bernard Mozer. Electric field distributions in an ionized gas. *Phys. Rev.*, 115:521–525, Aug 1959.

[BP07]   H. P. Breuer and F Petruccione. *The theory of open quantum systems.* Clarendon Press, Oxford, 2007.

[Bro73]   L. S. Brown. Classical limit of the hydrogen atom. *Am. J. Phys.*, pages 525–530, 1973.

[CCM+05]   H.-K. Chung, M.H. Chen, W.L. Morgan, Y. Ralchenko, and R.W. Lee. Fly-chk: Generalized population kinetics and spectral model for rapid spectroscopic analysis for all elements. *High Energy Density Physics*, 1(1):3 – 12, 2005.

[CCRS93] L. Chen, M. Cheret, F. Roussel, and G. Spiess. New scheme for producing circular orbital states in combined RF and static fields. *Journal of Physics B: Atomic, Molecular and Optical Physics*, 26(15):L437, 1993.

[CFT15a] A. Calisti, S. Ferri, and B. Talin. Ionization potential depression for non equilibrated aluminum plasmas. *Journal of Physics B: Atomic, Molecular and Optical Physics*, 48(22):224003, 2015.

[CFT15b] A. Calisti, S. Ferri, and B. Talin. Ionization potential depression in hot dense plasmas through a pure classical model. *Contrib. Plasma Phys.*, 55(5):360–365, 2015.

[Che14]   Yiling Chen. *Plasma Diagnostics Applying K-Line Emission Profiles of Si and Ar*. Dissertation, Universität Rostock, 2014.

[Chi00]   Junzo Chihara. Interaction of photons with plasmas and liquid metals - photoabsorption and scattering. *Journal of Physics: Condensed Matter*, 12(3):231, 2000.

[CLG94]   C. H. Cheng, C. Y. Lee, and T. F. Gallagher. Production of circular Rydberg states with circularly polarized microwave fields. *Phys. Rev. Lett.*, 73:3078–3081, Dec 1994.

[Cra02]   Christopher J. Cramer. *Essentials of computational chemistry: theories and models*. Wiley, Chichester, 2002.

[Cro14]   B.J.B. Crowley. Continuum lowering - a new perspective. *High Energy Density Physics*, 13:84 – 102, 2014.

[Ct16]   O. Ciricosta *et al.* Measurements of continuum lowering in solid-density plasmas created from elements and compounds. *Nat. Commun.*, 7:11713, 2016.

[CVC+12] O. Ciricosta, S. M. Vinko, H.-K. Chung, B.-I. Cho, C. R. D. Brown, T. Burian, J. Chalupsky, K. Engelhorn, R. W. Falcone, C. Graves, V. Hajkova, A. Higginbotham, L. Juha, J. Krzywinski, H. J. Lee, M. Messerschmidt, C. D. Murphy, Y. Ping, D. S. Rackstraw, A. Scherz, W. Schlotter, S. Toleikis, J. J. Turner, L. Vysin, T. Wang, B. Wu, U. Zastrau, D. Zhu, R. W. Lee, P. Heimann, B. Nagler, and J. S. Wark. Direct measurements of the ionization potential depression in a dense plasma. *Phys. Rev. Lett.*, 109:065002, Aug 2012.

[DBD77]   J. F. Delpech, J. Boulmer, and F. Devos. Transitions between Rydberg levels of helium induced by electron collisions. *Phys. Rev. Lett.*, 39:1400–1403, 1977.

[DBD79]   F. Devos, J. Boulmer, and J. F. Delpech. Transitions between Rydberg levels of helium induced by electron and neutral collisions. *J. Phys. (Paris)*, 40:215, 1979.

[Dem10]   A. V. Demura. Physical models of plasma microfield. *International Journal of Spectroscopy*, 2010:Article ID 671073, 2010.

[DG88]   D. Delande and J. C. Gay. A new method for producing circular Rydberg states. *Europhysics Letter*, 5(4):303, 1988.

[DG09]   J. Daligault and S. Gupta. Electron-ion scattering in dense multi-component plasmas: Application to the outer crust of an accreting neutron star. *The Astrophysical Journal*, 703(1):994, 2009.

[DKMS05]   A. Dinklage, T. Klinger, G. Marx, and L. Schweikhard. *Plasma Physics: Confinement, Transport and Collective Effects.* Springer-Verlag, Berlin Heidelberg, 2005.

[Duf69]   James W. Dufty. Charge-density fluctuations in spectral line broadening. *Phys. Rev.*, 187:305–313, Nov 1969.

[DwP86]   M. W. C. Dharma-wardana and F. Perrot. Electric microfield distributions in plasmas of arbitrary degeneracy and density. *Phys. Rev. A*, 33:3303–3313, May 1986.

[DwP92]   M. W. C. Dharma-wardana and F. Perrot. Level shifts, continuum lowering, and the mobility edge in dense plasmas. *Phys. Rev. A*, 45:5883–5896, Apr 1992.

[D'y98]   L.G. D'yachkov. Approximation for the probabilities of the realization of atomic bound states in a plasma. *Journal of Quantitative Spectroscopy and Radiative Transfer*, 59(1):65 – 69, 1998.

[D'y16]   L. G. D'yachkov. Smooth transition from spectral lines to a continuum in dense hydrogen plasma. *High Temperature*, 54(1):5–10, Jan 2016.

[EK63]   G. Ecker and W. Kröll. Lowering of the ionization energy for a plasma in thermodynamic equilibrium. *Physics of Fluids*, 6(1):62–69, 1963.

[EKKR85]   W. Ebeling, W. D. Kraeft, D. Kremp, and G. Röpke. Energy levels in hydrogen plasmas and the Planck-Larkin partition function - A comment. *Astrophysical J.*, 290:24, 1985.

[EW56]   G. Ecker and W. Weizel. Zustandssumme und effektive Ionisierungsspannung eines Atoms im Inneren des Plasmas. *Annalen der Physik*, 452(2-3):126–140, 1956.

[FBR08]   G. Faussurier, C. Blancard, and P. Renaudin. Equation of state of dense plasmas using a screened-hydrogenic model with l-splitting. *High Energy Density Physics*, 4(3):114 – 123, 2008.

[FCAH10]   Chris Fleming, N. I. Cummings, Charis Anastopoulos, and B. L. Hu. The rotating-wave approximation: consistency and applicability from an open quantum system analysis. *Journal of Physics A: Mathematical and Theoretical*, 43(40):405304, 2010.

[FH65]   R. Feynman and A. Hibbs. *Quantum mechanics and integrals*. McGraw-Hill, New York, 1965.

[FKP+14]   L. B. Fletcher, A. L. Kritcher, A. Pak, T. Ma, T. Döppner, C. Fortmann, L. Divol, O. S. Jones, O. L. Landen, H. A. Scott, J. Vorberger, D. A. Chapman, D. O. Gericke, B. A. Mattern, G. T. Seidler, G. Gregori, R. W. Falcone, and S. H. Glenzer. Observations of continuum depression in warm dense matter with x-ray thomson scattering. *Phys. Rev. Lett.*, 112:145004, Apr 2014.

[Fle98]   Michael Fleischhauer. Quantum-theory of photodetection without the rotat-
            ing wave approximation. *Journal of Physics A: Mathematical and General*,
            31(2):453, 1998.

[FM00]   D.V. Fisher and Y. Maron. Effective statistical weights of bound states in
            plasmas. *The European Physical Journal D - Atomic, Molecular, Optical and
            Plasma Physics*, 18(1):93–111, 200.

[For09]   C. Fortmann. Single-particle spectral function for the classical one-component
            plasma. *Phys. Rev. E*, 79:016404, Jan 2009.

[Fox99]   Ronald F. Fox. Generalized coherent states. *Phys. Rev. A*, 59:3241–3255, May
            1999.

[Fuj05]   T. Fujimoto. *Plasma Spectroscopy*. Clarendon Press, New York, 2005.

[GAH+16]   P. Grünwald, M. Aßmann, J. Heckötter, D. Fröhlich, M. Bayer, H. Stolz, and
            S. Scheel. Signatures of quantum coherences in Rydberg excitons. *Phys. Rev.
            Lett.*, 117:133003, Sep 2016.

[Gal94]   T. F. Gallagher. *Rydberg Atoms*. Cambridge University Press, Cambridge, 1994.

[GGL06]   G. Gregori, S. H. Glenzer, and O. L. Landen. Generalized x-ray scattering cross
            section from nonequilibrium plasmas. *Phys. Rev. E*, 74:026402, Aug 2006.

[GHR91]   S. Günter, L. Hitzschke, and G. Röpke. Hydrogen spectral lines with the inclu-
            sion of dense-plasma effects. *Phys. Rev. A*, 44:6834–6844, Nov 1991.

[Gla63]   Roy J. Glauber. Coherent and incoherent states of the radiation field. *Phys. Rev.*,
            131:2766–2788, 1963.

[GMI+09]   Yu.N. Gnedin, A.A. Mihajlov, Lj.M. Ignjatovic, N.M. Sakan, V.A. Sreckovic,
            M.Yu. Zakharov, N.N. Bezuglov, and A.N. Klycharev. Rydberg atoms in astro-
            physics. *New Astronomy Reviews*, 53(7):259 – 265, 2009. Proceedings of the VII
            Serbian Cdonference on Spectral Line Shapes (VII SCSLSA) held in Zrenjanin,
            Serbia June 15th-19th 2009.

[GMK10]   M. Goto, S. Morita, and M. Koubiti. Spectroscopic study of a carbon pellet
            ablation cloud. *Journal of Physics B: Atomic, Molecular and Optical Physics*,
            43(14):144023, 2010.

[Goc07]   Christian Gocke. *Dekohärenz in offenen Quantensystemen am Beispiel eines
            Rydbergatoms im Plasma*. Dissertation, Universität Rostock, 2007.

[GR06]   C. Gocke and G. Röpke. Electron scattering and dephasing rate of Rydberg
            atoms in a plasma. *J. Phys. A: Math. Gen.*, 39:4587–4594, 2006.

[GR07]   C. Gocke and G. Röpke. Localization of coherent wave packets in plasmas due
            to decoherence. *Contrib. Plasma Phys.*, 47:291–296, 2007.

[GR09]   Siegfried H. Glenzer and Ronald Redmer. X-ray thomson scattering in high
            energy density plasmas. *Rev. Mod. Phys.*, 81:1625–1663, Dec 2009.

[GRH+07]   G. Gregori, A. Ravasio, A. Höll, S.H. Glenzer, and S.J. Rose. Derivation of the static structure factor in strongly coupled non-equilibrium plasmas for x-ray scattering studies. *High Energy Density Physics*, 3(1):99–108, 2007.

[Gri97]   H. R. Griem. *Principles of Plasma Spectroscopy.* Cambridge University Press, Cambridge, 1997.

[GS90]   Z. D. Gaeta and C. R. Stroud. Classical and quantum-mechanical dynamics of a quasiclassical state of the hydrogen atom. *Phys. Rev.*, A 42:6308, 1990.

[Gün95]   S. Günter. *Optische Eigenschaften dichter Plasmen.* Habilitationsschrift, Universität Rostock, 1995.

[HAJ+13a]   D. J. Hoarty, P. Allan, S. F. James, C. R. D. Brown, L. M. R. Hobbs, M. P. Hill, J. W. O. Harris, J. Morton, M. G. Brookes, R. Shepherd, J. Dunn, H. Chen, E. Von Marley, P. Beiersdorfer, H. K. Chung, R. W. Lee, G. Brown, and J. Emig. Observations of the effect of ionization-potential depression in hot dense plasma. *Phys. Rev. Lett.*, 110:265003, Jun 2013.

[HAJ+13b]   D.J. Hoarty, P. Allan, S.F. James, C.R.D. Brown, L.M.R. Hobbs, M.P. Hill, J.W.O. Harris, J. Morton, M.G. Brookes, R. Shepherd, J. Dunn, H. Chen, E. Von Marley, P. Beiersdorfer, H.K. Chung, R.W. Lee, G. Brown, and J. Emig. The first data from the orion laser; measurements of the spectrum of hot, dense aluminium. *High Energy Density Physics*, 9(4):661 – 671, 2013.

[Hez10]   B. Hezel. *Interaction-induced stabilization of ultracold Rydberg atoms in a Ioffe-Pritchard trap.* Dissertation, University of Heidelberg, 2010.

[HGG88]   J. Hare, M. Gross, and P. Goy. Circular atoms prepared by a new method of crossed electric and magnetic fields. *Phys. Rev. Lett.*, 61:1938–1941, Oct 1988.

[HK83]   Randall G. Hulet and Daniel Kleppner. Rydberg atoms in "circular" states. *Phys. Rev. Lett.*, 51:1430–1433, Oct 1983.

[HM86]   Jean Pierre Hansen and Ian R. McDonald. *Theory of simple liquids.* Acad. Press, London, 2. edition, 1986.

[Hol19]   J. Holtsmark. Über die Verbreiterung von Spektrallinien. *Annalen der Physik*, 58:577, 1919.

[Hoo68]   C. F. Hooper. Low-frequency component electric microfield distributions in plasmas. *Phys. Rev.*, 165:215–222, Jan 1968.

[HRSZ86]   L. Hitzchke, G. Röpke, T. Seifert, and R. Zimmermann. Green's function approach to the electron shift and broadening of spectral lines in non-ideal plasmas. *Journal of Physics B: Atomic and Molecular Physics*, 19(16):2443, 1986.

[HZ82]   F. E. Höhne and R. Zimmermann. Oscillator strengths in dense hydrogen plasma-no 'transparency window'. *Journal of Physics B: Atomic and Molecular Physics*, 15(15):2551, 1982.

[IMM03]   Intravaia, F., Maniscalco, S., and Messina, A. Comparison between the rotating wave and Feynman-Vernon system-reservoir couplings in the non-Markovian regime. *Eur. Phys. J. B*, 32(1):97–107, 2003.

[IRS⁺00]   C.A. Iglesias, F.J. Rogers, R. Shepherd, A. Bar-Shalom, M.S. Murillo, D.P. Kilcrease, A. Calisti, and R.W. Lee. Fast electric microfield distribution calculations in extreme matter conditions. *Journal of Quantitative Spectroscopy and Radiative Transfer*, 65(1):303 – 315, 2000.

[IT39]   D. R. Inglis and E. Teller. Ionic depression of series limits in one-electron spectra. *Astrophys. J.*, 90:439, 1939.

[Joo03]   E. Joos. Decoherence through interaction with the environment. In *Decoherence and the Appearance of a Classical World in Quantum Theory* [JZK⁺03], chapter 3.

[JZK⁺03]   E. Joos, H. D. Zeh, C. Kiefer, D. Giulini, J. Kupsch, and I. O. Stamatescu. *Decoherence and the Appearance of a Classical World in Quantum Theory*. Springer, Berlin, 2. edition, 2003.

[KCK⁺16]   D. Kraus, D. A. Chapman, A. L. Kritcher, R. A. Baggott, B. Bachmann, G. W. Collins, S. H. Glenzer, J. A. Hawreliak, D. H. Kalantar, O. L. Landen, T. Ma, S. Le Pape, J. Nilsen, D. C. Swift, P. Neumayer, R. W. Falcone, D. O. Gericke, and T. Döppner. X-ray scattering measurements on imploding ch spheres at the national ignition facility. *Phys. Rev. E*, 94:011202, Jul 2016.

[KFS⁺14]   T. Kazimierczuk, D. Fröhlich, S. Scheel, H. Stolz, and M. Bayer. Giant Rydberg excitons in the copper oxide Cu_2o. *Nature*, 514:343–347, 2014.

[KG90]   G. Kalman and K. I. Golden. Response function and plasmon dispersion for strongly coupled Coulomb liquids. *Phys. Rev. A*, 41:5516–5527, May 1990.

[KG95]   A. Könies and S. Günter. Quantum-mechanical treatment of strong electron-atom collision contributions to the shift and width of hydrogen lines. *Phys. Rev.*, E 52:6658–6663, 1995.

[KKER86]   W. D. Kraeft, D. Kremp, W. Ebeling, and G. Röpke. *Quantum Statistics of Charged Particle Systems*. Plenum Press, New York, 1986.

[Kla96]   John R. Klauder. Coherent states for the hydrogen atom. *Journal of Physics A: Mathematical and General*, 29(12):L293, 1996.

[KSKB05]   D. Kremp, M. Schlanges, W. D. Kraeft, and T. Bornath. *Quantum statistics of nonideal plasmas*. Springer, Berlin, 2005.

[LBMW03]   D. Leibfried, R. Blatt, C. Monroe, and D. Wineland. Quantum dynamics of single trapped ions. *Rev. Mod. Phys.*, 75:281–324, 2003.

[LFC⁺01]   M. D. Lukin, M. Fleischhauer, R. Cote, L. M. Duan, D. Jaksch, J. I. Cirac, and P. Zoller. Dipole blockade and quantum information processing in mesoscopic atomic ensembles. *Phys. Rev. Lett.*, 87:037901, 2001.

[LGRR16]   Chengliang Lin, Christian Gocke, Gerd Röpke, and Heidi Reinholz. Transition rates for a Rydberg atom surrounded by a plasma. *Phys. Rev. A*, 93:042711, Apr 2016.

[Lin14]   Chengliang Lin. *Rydbergatome im dichten Plasma: Dekohärenz und Quantenmastergleichung.* Master thesis, Universität Rostock, 2014.

[LL85]   L. D. Landau and E. M. Lifschitz. *Lehrbuch der Theoretischen Physik III: Quantenmechanik.* Akademie Verlag, Berlin, 1985.

[Lor14]   Sonja Lorenzen. *Quantum-statistical approach to pressure broadening of Lyman lines in hydrogen-like plasmas.* Dissertation, Universität Rostock, 2014.

[LOZ⁺14]   Sonja Lorenzen, Banaz Omar, Mark C. Zammit, Dmitry V. Fursa, and Igor Bray. Plasma pressure broadening for few-electron emitters including strong electron collisions within a quantum-statistical theory. *Phys. Rev. E*, 89:023106, Feb 2014.

[LRKR17]   Chengliang Lin, Gerd Röpke, Wolf-Dietrich Kraeft, and Heidi Reinholz. Ionization-potential depression and dynamical structure factor in dense plasmas. *Phys. Rev. E*, 96:013202, Jul 2017.

[MABL13]   Christian Majenz, Tameem Albash, Heinz-Peter Breuer, and Daniel A. Lidar. Coarse graining can beat the rotating-wave approximation in quantum markovian master equations. *Phys. Rev. A*, 88:012103, Jul 2013.

[MJY86]   W. A. Molander, C. R. Stroud Jr., and J. A. Yeazell. Excitation of high angular momentum Rydberg states. *Journal of Physics B: Atomic and Molecular Physics*, 19(12):L461, 1986.

[MK69]   P. Mansbach and J. Keck. Monte Carlo trajectory calculations of atomic excitation and ionization by thermal electrons. *Phys. Rev.*, 181:275–289, 1969.

[MM13]   H. Mäkelä and M. Möttönen. Effects of the rotating-wave and secular approximations on non-markovianity. *Phys. Rev. A*, 88:052111, Nov 2013.

[MP12]   Adam J. Makowski and Piotr Peplowski. Zero-energy wave packets that follow classical orbits. *Phys. Rev. A*, 86:042117, Oct 2012.

[MP13]   Adam J. Makowski and Piotr Peplowski. Dynamics of zero-energy nonspreading non-gaussian wave packets for a class of central potentials. *Annals of Physics*, 337:25–33, 2013.

[MS97]   Pushan Majumdar and H. S. Sharatchandra. Coherent states for the hydrogen atom. *Phys. Rev. A*, 56:R3322–R3325, Nov 1997.

[NBB⁺93]   P. Nussenzveig, F. Bernardot, M. Brune, J. Hare, J. M. Raimond, S. Haroche, and W. Gawlik. Preparation of high-principal-quantum-number "circular" states of rubidium. *Phys. Rev. A*, 48:3991–3994, Nov 1993.

[NMG⁺98]   M. Nantel, G. Ma, S. Gu, C. Y. Côté, J. Itatani, and D. Umstadter. Pressure ionization and line merging in strongly coupled plasmas produced by 100-fs laser pulses. *Phys. Rev. Lett.*, 80:4442–4445, May 1998.

[Nol17]   W Nolting. *Quantum mechanics - basics.* Cham: Springer, Berlin, 2017.

[NS78]   Michael Martin Nieto and L. M. Simmons. Coherent states for general potentials. *Phys. Rev. Lett.*, 41:207–210, Jul 1978.

[OGWR06]   Banaz Omar, Sibylle Günter, August Wierling, and Gerd Röpke. Neutral helium spectral lines in dense plasmas. *Phys. Rev. E*, 73:056405, May 2006.

[Oma07]   Banaz Omar. *Spectral Line Broadening of He I and He-like Ions in Dense Plasmas.* Dissertation, Universität Rostock, 2007.

[OWGR07]   B. Omar, A. Wierling, S. Günter, and G. Röpke. Hydrogen Balmer spectrum from a high-pressure arc discharge: Revisited. *Contrib. Plasma Phys.*, 47:315, 2007.

[OWR11]   B. Omar, A. Wierling, and G. Röpke. Diagnostics of high-pressure arc plasmas by hydrogen Balmer spectra. *Contrib. Plasma Phys.*, 51:22, 2011.

[PCG02]   Alexander Y. Potekhin, Gilles Chabrier, and Dominique Gilles. Electric microfield distributions in electron-ion plasmas. *Phys. Rev. E*, 65:036412, Mar 2002.

[PPR04a]   T. Pohl, T. Pattard, and J. M. Rost. Kinetic modeling and molecular dynamics simulation of ultracold neutral plasmas including ionic correlations. *Phys. Rev.*, A 70:033416, 2004.

[PPR04b]   T. Pohl, T. Pattard, and J. M. Rost. Plasma formation from ultracold Rydberg gases. *Phys. Rev.*, A 68:010703, 2004.

[PVC$^+$13] Thomas R. Preston, Sam M. Vinko, Orlando Ciricosta, Hyun-Kyung Chung, Richard W. Lee, and Justin S. Wark. The effects of ionization potential depression on the spectra emitted by hot dense aluminium plasmas. *High Energy Density Physics*, 9(2):258 – 263, 2013.

[QWWQ09] Y. Qi, Y. Wu, J. Wang, and Y. Qu. The generalized oscillator strengths of hydrogenlike ions in Debye plasmas. *Physics of Plasmas*, 16:023502, 2009.

[RD79]   G. Röpke and R. Der. The influence of two-particle states (excitons) on the dielectric function of the electron-hole plasma. *Phys. Status Solidi B*, 92:501, 1979.

[Red97]   Ronald Redmer. Physical properties of dense, low-temperature plasmas. *Physics Reports*, 282(2):35 – 157, 1997.

[Red13]   R. Redmer. *Vorlesungsskript: Einführung in die Plasma- und Astrophysil.* Universität Rostock, 2013.

[Rei05]   H. Reinholz. Dielectric and optical properties of dense plasmas. *Ann. Phys. Fr.*, 30(4-5):1–187, 2005.

[RGS86]   R. Radtke, K. Günther, and R. Spanke. Study of the Balmer spectrum of hydrogen from a high-pressure arc discharge. ii. Comparison of experiment and theory. *Beiträge aus der Plasmaphysik*, 26(2):151–158, 1986.

[RKK+78]   G. Röpke, K. Kilimann, D. Kremp, W.-D. Kraeft, and R. Zimmerman. The influence of dynamical effects on the two-particle states (excitons) in the electron-hole plasma. *phys. stat. sol. (b)*, 88:K59–K63, 1978.

[RM09]   G. Röpke and Winkel M. *Green's functions technique for statistical ensembles: lecture notes.* Universtät Rostock, Rostock, 2009.

[Rob04]   R.W. Robinett. Quantum wave packet revivals. *Physics Reports*, 392(1):1 – 119, 2004.

[Röp13]   G. Röpke. *Nonequilibrium Statistical Physics.* Wiley, Weinheim, 2013.

[RSK81]   G. Röpke, T. Seifert, and K. Kilimann. A Green's function approach to the shift of spectral lines in dense plasmas. *Annalen der Physik*, 493(6):381–395, 1981.

[RSSN98]   G. Röpke, A. Schnell, P. Schuck, and P. Nozières. Four-particle condensate in strongly coupled Fermion systems. *Phys. Rev. Lett.*, 80:3177–3180, Apr 1998.

[SAK95]   J. Seidel, S. Arndt, and W. D. Kraeft. Energy spectrum of hydrogen atoms in dense plasmas. *Phys. Rev. E*, 52:5387–5400, Nov 1995.

[Sal98]   David Salzmann. *Atomic physics in hot plasmas.* Oxford Univ. Press, New York, 1998.

[Sch68]   L. I. Schiff. *Quantum Mechanics.* McGraw-Hill, New York, 3. edition, 1968.

[Sch07]   M. Schlosshauer. *Decoherence and the Quantum-To-Classical Transition.* Springer, Berlin, 2007.

[Sen10]   Andrea Sengebusch. *Linienprofile von Röntgenübergängen komplexer Atome in dichten Plasmen.* Dissertation, Universität Rostock, 2010.

[SL13]   G. Stefanucci and R. van Leeuwen. *Nonequilibrium many-body theory of quantum system: a modern introduction.* Cambridge University Press, Cambridge, 2013.

[SM10]   E. Stambulchik and Y. Maron. Plasma line broadening and computer simulations: A mini-review. *High Energy Density Physics*, 6(1):9 – 14, 2010.

[SPJ66]   John C. Stewart and Kedar D. Pyatt Jr. Lowering of ionization potentials in plasmas. *Astrophysical Journal*, 144:1203, 1966.

[SRS90]   Martin Schmidt, Gerd Röpke, and Hartmut Schulz. Generalized Beth-Uhlenbeck approach for hot nuclear matter. *Annals of Physics*, 202(1):57 – 99, 1990.

[STJ+14]   Sang-Kil Son, Robert Thiele, Zoltan Jurek, Beata Ziaja, and Robin Santra. Quantum-mechanical calculation of ionization-potential lowering in dense plasmas. *Phys. Rev. X*, 4:031004, Jul 2014.

[Str16]   M. Stransky. Monte Carlo simulations of ionization potential depression in dense plasmas. *Physics of Plasmas*, 23(1):012708, 2016.

[SVY81]   I. I. Sobelman, L. A. Vainshtein, and E. A. Yukov. *Excitation of Atoms and Broadening of Spectral Lines.* Springer, Berlin, 1981.

[Uns48]   A. Unsöld. Zur Berechnung der Zustandsummen für Atome und Ionen in einem
            teilweise ionisierten Gas. *Zeitschrift für Astrophysik*, 24:355, 1948.

[VCW14]   S. M. Vinko, O. Ciricosta, and J. S. Wark. Density functional theory calculations
            of continuum lowering in strongly coupled plasmas. *Nat. Commun.*, 5:3533, 2014.

[VDTG12]   J. Vorberger, Z. Donko, I. M. Tkachenko, and D. O. Gericke. Dynamic ion
            structure factor of warm dense matter. *Phys. Rev. Lett.*, 109:225001, Nov 2012.

[Ve12]   S. M. Vinko *et al.*. Creation and diagnosis of a solid-density plasma with an
            x-ray free-electron laser. *Nature*, 482:59, 2012.

[VS80]   L. Vriens and A. H. M. Smeets. Cross-section and rate formulas for electron-
            impact ionization, excitation, deexcitation, and total depopulation of excited
            atoms. *Phys. Rev.*, A 22:940–951, 1980.

[Wei99]   U. Weiss. *Quantum Dissipative Systems*. World Scientific, Signapore, 2. edition,
            1999.

[Wen86]   Xiao-Gang Wen. *Quantum field theory of many-body systems: from the origin
            of sound to an origin of light and electrons*. Oxford Univ. Press, Oxford, 1986.

[Wik17]   Wikipedia. wikipedia:interaction picture. 2017.

[WKP72]   W. L. Wiese, D. E. Kelleher, and D. R. Paquette. Detailed study of the Stark
            broadening of Balmer lines in a high-density plasma. *Phys. Rev. A*, 6:1132–1153,
            Sep 1972.

[WSGR17]   B. B. L. Witte, M. Shihab, S. H. Glenzer, and R. Redmer. Ab initio simula-
            tions of the dynamic ion structure factor of warm dense lithium. *Phys. Rev. B*,
            95:144105, Apr 2017.

[XZS13]   T. Xia, X. L. Zhang, and M. Saffman. Analysis of a controlled phase gate using
            circular Rydberg states. *Phys. Rev. A*, 88:062337, Dec 2013.

[Zim87]   R. Zimmermann. *Many-particle theory of highly excited semiconductors*. Teub-
            ner, Leipzig, 1987.

[ZKK$^+$78] R. Zimmerman, K. Kilimann, W.-D. Kraeft, D. Kremp, and G. Röpke. Dynam-
            ical screening and self energy of excitons in the electron-hole plasma. *phys. stat.
            sol. (b)*, 90:175–187, 1978.

[ZM80]   G.B. Zimmerman and R.M. More. Pressure ionization in laser-fusion target sim-
            ulation. *Journal of Quantitative Spectroscopy and Radiative Transfer*, 23(5):517
            – 522, 1980.

[ZMR96]   D. Zubarev, V. Morozov, and G. Röpke. *Statistical Mechanics of Nonequilibrium
            Processes*, volume 1. Akademie Verlag, Berlin, 1996.

[ZMR97]   D. Zubarev, V. Morozov, and G. Röpke. *Statistical Mechanics of Nonequilibrium
            Processes*, volume 2. Akademie Verlag, Berlin, 1997.

[ZZF94]   Ivaylo Zlatev, Wei-Min Zhang, and Da Hsuan Feng.   Possibility that schrödinger's conjecture for the hydrogen-atom coherent states is not attainable. *Phys. Rev. A*, 50:R1973–R1975, Sep 1994.

DANKSAGUNG

Hiermit möchte ich all jenen danken, die diese Arbeit möglich gemacht haben. An erster Stelle möchte ich meinen Eltern danken, die mir mein Master- und Promotionsstudium in Deutschland ermöglicht haben. Sie haben mich immer unterstützt und sind sehr zuversichtlich, dass ich mein Promotionsstudium abschließen werde. Außerdem möchte ich mich bei meiner Frau dafür bedanken, dass sie geduldig darauf gewartet hat, dass ich endlich fertig werden.

Ich bedanke mich bei meiner Betreuerin Priv.-Doz. Dr. Heidi Reinholz, die mir die Möglichkeit gegeben hat, in ihrer Arbeitsgruppe meine Masterarbeit sowie meine Dissertation zu schreiben. Ich danke für ihre hilfreichen und fachlichen Hinweise, die dazu geführt haben, meine Arbeit voran zu treiben und mich immer auf wesentliche Kernpunkte zu konzentrieren. Insbesondere bin ich sehr dankbar, viele Gelegenheiten zur Teilnahme an internationalen Tagungen gehabt zu haben. Gleichmaßen gilt mein herzlicher Dank Prof. Dr. Gerd Röpke, der mir stets während meines Master- und Promotionsstudiums nicht nur zu meiner Arbeit sondern auch zu meinem Leben in Deutschland mit gutem Rat zur Seite stand. Ich danke dafür, dass er mich mit der quantenstatistischen Theorie und mit der Theorie der offenen Quantensysteme vertraut machte.

Ich danke natürlich auch für die konstruktiven Diskussionen und die fruchtbare Zusammenarbeit mit Dr. Christian Gocke und Prof. Dr. Wolf-Dietrich Kraeft. Zudem darf ich absolut nicht vergessen, allen Mitgliedern in unserer Arbeitsgruppe zu danken. Explizit möchte ich Dr. Andrea Sengebusch für die fachlichen Diskussionen, das Durchlesen und das Korrigieren meines Manuskripts danken. Der speziellen Dank gilt auch meinem Kollegen, Kommilitonen und Freund, Sebastian Rosmej, mit dem ich interessante Diskussionen über Physik gemacht habe und viele Späße in meiner Freizeit erlebt habe. Auch möchte ich unserer netten Sekretärin, Marina Hertzfeldt, für ihre eifrige Hilfe und ehrlichen Ratschläge danken.

Es ist in China sehr verbreitet, wichtige Dinge dreimal sagen zu müssen. Danke! Danke! Danke!

SELBSTSTÄNDIGKEITSERKLÄRUNG

Ich versichere hiermit an Eides statt, dass ich die vorliegende Arbeit selbstständig angefertigt und ohne fremde Hilfe verfasst habe. Ich habe keine außer den von mir angegebenen Hilfsmitteln und Quellen benutzt. Inhaltlich und wörtlich entnommene Stellen sind als solche kenntlich gemacht.

Rostock, den 12. 10. 2017

Chengliang Lin